Process Monitoring and Chipping Fault Detection in Drilling

by

Davut Otar

A Thesis Submitted to the
Graduate School of Engineering
in Partial Fulfillment of the Requirements for
the Degree of

Master of Science

in

Mechanical Engineering

Koç University

December 2004

Koc University

Graduate School of Sciences and Engineering

This is to certify that I have examined this copy of a master's thesis by

Davut Otar

and have found that it is complete and satisfactory in all respects,
and that any and all revisions required by the final
examining committee has been made.

Committee Members:

İsmail Lazoğlu, Ph. D. (Advisor)

Erdem Alaca, Ph. D.

Muzaffer Erten, Ph. D.

Date: 3/12/04

ABSTRACT

Drilling is one of the most important and fundamental machining process and widely used in automobile, aircraft, home appliance and electronic industries. Chipping is among the important process faults occur commonly in drilling. Chipping has serious adverse effects on the surface finish and dimensional accuracy of the workpiece. Furthermore, chipping may cause tool failure which may lead to part scrappage and/or damage to CNC machines. Therefore, reliable monitoring of chipping fault would be indispensable to benefit from the machining equipment in an optimal way including automated production.

In this project, chipping is induced in various amounts and types to different drills supplied by Arcelik A.S. Extensive numbers of experiments were performed by utilizing the chipped drills under different machining conditions in a CNC machine tool.

Machining forces were obtained from the experiments performed in order to establish monitoring features for different chipping types / amounts in time domain, in frequency domain using Fast Fourier Transform (FFT) and in time-frequency domain using Discrete Wavelet Transform (DWT). Among the chipping types, tip chipping is easily identified in time domain whereas, shank chipping and arbitrary chipping are better monitored in time-frequency domain.

ACKNOWLEDGEMENTS

I would like to express my sincere gratitude and appreciation to my advisor, Dr. Ismail Lazoglu for his expert guidance and mentorship and I would also like to thank Dr. Erdem Alaca and Dr. Muzaffer Erten for reading this dissertation and offering constructive criticism.

For the drilling tools used in the experiments, I would like to thank Arcelik A.S, the supplier of the drills.

I would also like to thank all of my friends, especially to, Faik Can Meral, Harun Dericioglu, Erhan Deniz, Doruk Kayaalp, M.B.S and Burak Öztürk (special thanks for long CMM measurements) for making these two years more pleasant and their presence when I needed.

I am very grateful to Pınar Erkek, for her love, support and patience to me during the M.S period.

And finally, I would like to thank to my family, especially to my mother Remziye Otar and my father Cevdet Otar for their life-long love, for the kind of encouragement and support they have provided me throughout my entire education life, and for their absolute confidence in me. This thesis and my all previous success are dedicated to them.

TABLE OF CONTENTS

LIST OF TABLES

LIST OF FIGURES

NOMENCLATURE

β_0	Helix angle
ψ_c	Chisel edge angle
K	Total tip angle
K_t	Taper angle
β	Lag angle
θ	Angular rotation of drill
Z , $\hat{Z}$	Depth along drill length, calculated depth along drill length
Z', $\hat{Z}'$	Distance along cutting edge, calculated length along cutting edge
R	Radius of drill
w	Chisel width for one cutting edge
f	Frequency
Ψ	Wavelet Base

Chapter 1

INTRODUCTION

Drilling is a machining operation that is used to generate holes in a workpiece by rotary and axial movements of the tool or workpiece. This process is one of the most important and fundamental machining process and is widely used in the automobile, aircraft, home appliance and electronic industries, etc.

Drill wear has a bad effect on the surface finish and dimensional accuracy of the workpiece. Moreover, serious wear can cause drill failure and workpiece damage. Therefore, a reliable diagnosis of drill wear state would be an indispensable for establishing the automation of drilling operation.

The main reasons for the interest for tool wear monitoring can be stated as follows:

- Automated production is possible only if the manufacturing process includes methods for tool wear monitoring. The economical values involved in modern manufacturing are very high because of the high investments in the manufacturing equipment and naturally it would be in the interest of the industry to benefit from the equipment in an optimal way including automated production with high availability.
- Tool wear influences the ability of the hole cutting system to satisfy specified performance characteristics such as quality of the surface finish and the dimensional accuracy of the manufactured parts.
- Due to variations in tool life, optimum tool life can not be utilized without a means for tool wear monitoring. Underusage or overusage can be avoided by scheduling tool change or regrind just in-time.

Drill wear can be categorized into five main wear types as seen in the Figure 1.1. These wear types are chisel wear, crater wear, flank wear, corner wear and edge fracture (chipping). Chisel wear normally occurs due to very high shear and compressive stresses in the flow zone of the tool-workpiece. Crater wear presents possibly on the rake face of the cutting edge and it is due to high temperature conditions along the rake surface. Flank wear can be observed on the two flanks or clearance faces of the lips. Corner wear is mainly due to high friction between the drill and the machined hole walls and occurs on both outside corers of the drill point. Finally chipping shows off itself on the cutting lip by fracture or breakage of the lip of the cutting edge along cutting edge [26].

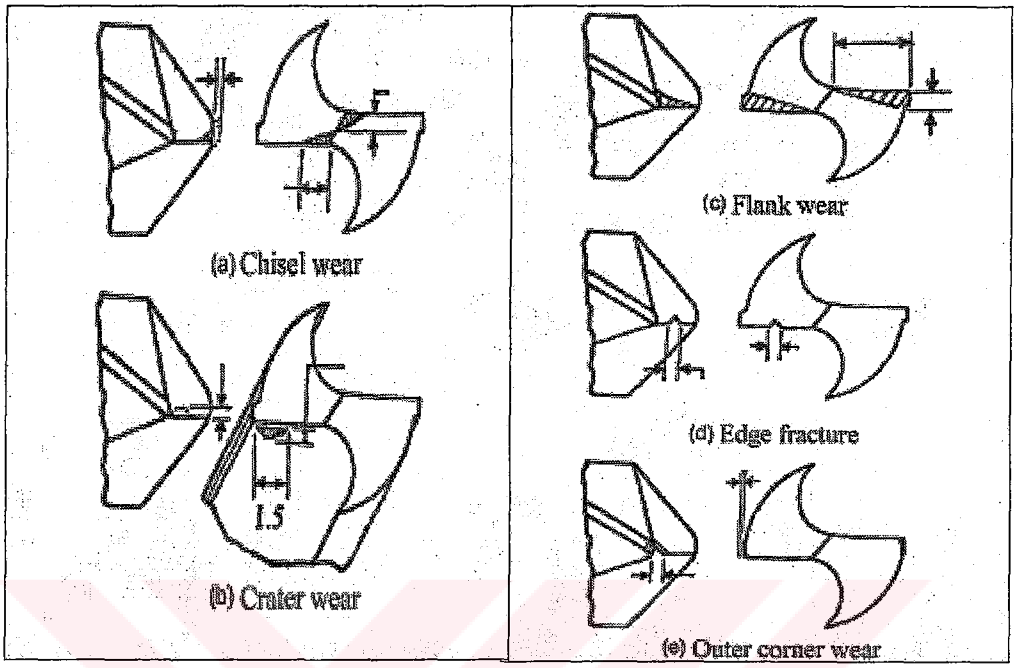

Figure 1.1: Illustration of drill wear types [26].

In this study, chipping as a drill wear type is investigated. Different types of chipping are artificially induced to the drills and the effect of the types of chipping on the cutting forces is monitored. Monitoring features are obtained from the time domain, time-frequency domain and also from frequency domain.

Chapter 2 provides the necessary background and literature review on drilling and drill wear monitoring. The fundamentals of sensor-data acquisition signal processing and feature extraction are thoroughly reviewed.

In Chapter 3, the mechanics of drilling process, typical design parameters of drill and experimental procedure are investigated.

Chapter 4 deals with the time domain monitoring features of chipped tools. How the several types of chipping conditions show off themselves are analyzed in time domain.

Chapter 5 provides the monitoring features obtained from frequency domain and time-frequency domain by utilizing Fast Fourier Transform and Wavelet Transformation respectively.

Chapter 6 summarizes the research conducted in this study and also gives some future recommendations.

Chapter 2

LITERATURE REVIEW

Present monitoring systems contain four components, sensor-data acquisition, signal processing, feature extraction and decision making strategy. The chart [22] below represents typical monitoring system components with possible different alternatives.

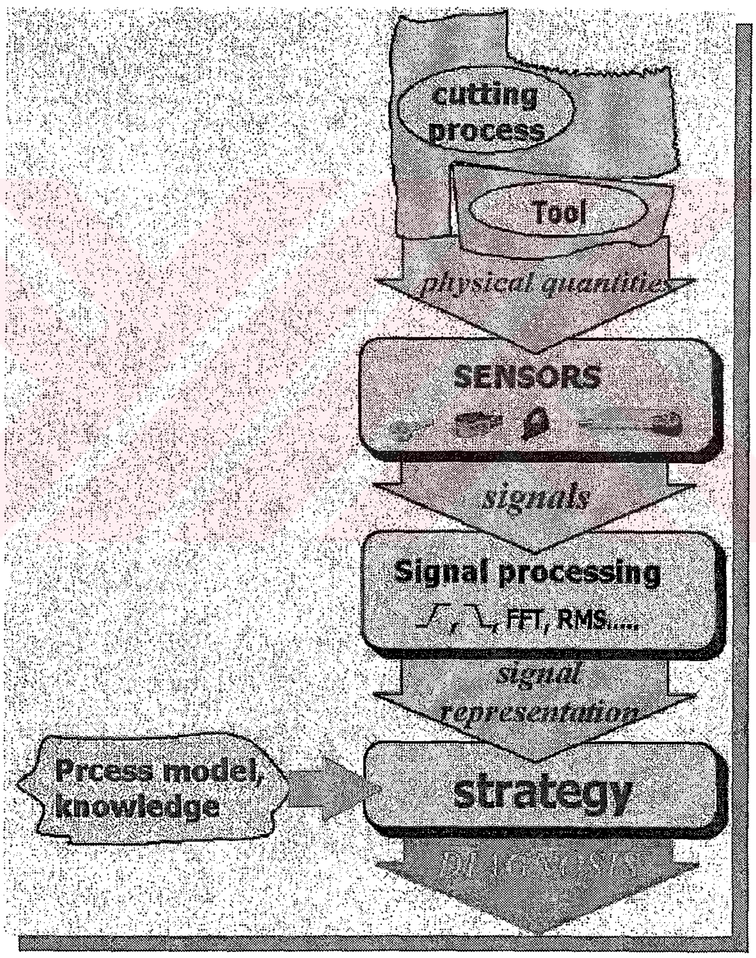

Figure 2.1: Illustration of typical monitoring system components [22]

In principle, the tool wear monitoring methods can be classified in two separate categories by sensor point of view. A distinction is made on the one hand between continuous and intermittent systems and, on the other hand between direct and indirect measuring systems. In the case of continuously measuring systems, the measured variable is available throughout the machining process; intermittently measuring systems record the measured variable only during intervals in the machining process. Direct measuring systems employ the actual quantity of the measured variable, while indirect measuring systems measure suitable auxiliary quantities and deduce the actual quantity via empirically determined correlations. Direct measuring systems possess higher degree accuracy, while indirect methods are less complex and more suitable for practical application. [6, 27]

2.1 MEASURING METHODS

2.1.1 Torque, drift force and feed force

Monitoring forces is a widely used technique in manufacturing processes in order to investigate the development of cutting tool wear. There is almost a direct correlation between cutting forces and tool wear, i.e., cutting forces increase as tool wear increases. This fact can be attributed to the increase of friction between tool and workpiece.

In drilling operation, monitoring torque, drift forces (lateral forces affecting the workpiece) and the feed (thrust) force are widely used. The idea behind monitoring torque, drift force and feed force is that it is expected that these forces change as the tool gradually wears. The thrust force has been used as the only measured signal in [4, 7, and 8]. The simultaneous monitoring of thrust force and torque is more common (see e.g. [2, 7, 12, 13, and 16]).

A drill generally wears at one lip till the height of both lips is equal; this fact is due to slight asymmetricity of a drill in the range of production tolerances [16]. The second lip, which is now sharper, starts cutting. This alternating process continues until neither lip has any more clearance at the margin. In the end the drill sticks into the workpiece and breaks if the cutting process is not stopped. Assuming this kind of wear progress gives reason to monitor the drift forces. In a series of tests [15] no consistent change of feed force or torque was observed but a certain change in the drift forces was recorded. This is again explained as first the cutting edge on one side and then on the other side wears.

In [2] torque and thrust force are measured for tool wear monitoring purposes. It is concluded in this article that: the effects of feed per revolution depth of cut and tool wear on cutting force signals are significant, while the effect of cutting speed on force signals is relatively insignificant. Furthermore, both thrust and torque increase as the flank wear increase and it is also shown that both thrust and torque can be well represented as functions of tool wear and feed per revolution. Finally, tool wear can be properly estimated knowing the thrust force and other cutting parameters.

In reference [7] investigations of three different melts of the material C 1055 were carried. The conclusions drawn are as follows: as the strength of workpiece material increases, or the wear resistance of the tool materials decreases the F=f(VB) lines rise more steeply. This is due to the crater depth increasing faster than the flank wear with higher work material strength values, or to the lower wear resistance of tool materials, respectively. If the increase dF/VB of the line VB=f(F) is plotted as a function of the material hardness, a linear increase of value dF/VB along with rising hardness of the cut material is obtained.

Reference [4] is the investigation of a real time control system to monitor the performance of the twist drills. After a series of drilling experiments conducted in the laboratory, the gradient of the thrust force has been identified to be a suitable process parameter for prediction of drill failure. Besides, experimental evidence emphasizes the correlation between thrust force and outer corner wear; it is suggested that the sharp spikes in the thrust force that are observed under the failure conditions are caused by a macroscopic stick-slip phenomenon.

Also torque, drift and feed force have been measured simultaneously when comparing two different types of coatings (titanium nitride and zirconium nitride). It is concluded that tool wear can be properly estimated knowing the thrust force and other cutting parameters, especially for larger tool wear. Based on tests with different workpiece material hardness, formulas for torque and thrust force have been developed as a function of Brinell hardness of work material, diameter of the drill, feed per revolution, average flank wear and radius at the cutting edge It is concluded that the variation in drill life is significantly influenced by the workpiece hardness. [1]

It is speculated that it could be so that the presence of a few random workpieces with a high hardness may influence the drill life much more than a large number of workpieces with a low hardness. Hence, in an industrial operation, drills may fail very early or after a long time, depending on the occurrence of a few workpieces with a high hardness. This could explain the large variation in drill life observed in industrial conditions. The workpiece hardness also influences the amplitudes of thrust forces and torque occurring in a drilling operation. If the variation in thrust force, on account of changes in flank wear, is to be significant, the variation in workpiece hardness has to be held within 5% of the mean hardness value in order to be able to base the diagnosis of flank wear on the amplitude of thrust force or torque. This is very difficult to achieve in industrial castings. Hence, torque or thrust measurements for monitoring drill wear should be attempted only after a very close tolerance has been obtained in the workpiece hardness. [1]

2.1.2 Spindle motor current, feed drive current and motor power

Spindle motor current is in principle a measure of the same feature as torque, i.e. they both depict how much power is used in the cutting process and they both also advise about the dynamics of cutting. It is fair to claim that torque is a more sensitive way to measure than is the spindle motor current since the torque sensor is located close to the cutting tool and e.g. the dynamics of the electric motor do not influence it to the same extent that they influence the current measurement. However, measuring torque is more complicated than measuring the current of the spindle motor and therefore the measurement of the current has also been widely tested and used [1, 3, 10, and 20]. Similarly, as spindle current corresponds to torque, feed drive current corresponds to the measurement of the thrust force. Again there is a similar difference in the sensitivity of the methods as described above. The feed drive current as an indicator of tool wear and failure has been studied in [3, 10, and 20]. Spindle motor power can be used as a measured variable to monitor the tool wear states as used in ref [1, 3]

The effect of tool wear and cutting parameters on the spindle motor and feed motor current are analyzed in reference [10]. The models regarding the relationship between the current signals and the cutting parameters are established through experimental study and regression analysis. It is found in this study that flank wear state can be more accurately estimated by using feed motor current model than spindle motor current model.

A real-time drill wear estimation method based on spindle motor power consumption during drilling is proposed [11]. A key advantage of employing this method is that progressive drill wear can be estimated quantitatively in real-time. The proposed estimation method estimates the drill wear successfully under various drilling conditions even when feed rate changes during drilling.

In reference [3], variations in the cutting process were detected by sensing the value of the feed motor current/power. On the basis of investigations reported in ref [3], the following conclusions can be made: cutting tool breakage can be very successfully detected by sensing motor-related parameters. Tool wear can be detected by sensing the current variations from servo motors for feed motion. This requires that currents should increase proportionally to the wear rate. In some cases it should be noted that current/power sensing for tool wear detection has a disadvantage common to most indirect techniques, that it requires strict proportionality between wear rate and that change in measured parameters. The motor current measurement is rather sensitive to thermal changes in a machine tool. Especially current measured from the feed drives was seen to be more sensitive than current from the spindle drive.

Both feed drive and spindle current have also been measured in [1]. In these tests it has been possible to compare the measurement of feed current to the measurement of thrust force based on the use of strain gages. It is stated that typically, the strain gage is a better sensor than the feed motor current sensor for wear diagnosis. Nevertheless, the current sensor was used to investigate whether the cost effective and easily implementable current sensors alone would suffice. The reported results in [1] for feed drive current and spindle power together with feed force and torque are quite similar. The measurement results show that all the quantities measured remain at an almost constant level during the entire tool life-time until the hole in which the drill totally fails. It is impossible to successfully apply these measurements as tool-monitoring methods, stopping the machining after the increase in one or several signals above a particular limit value before actual tool failure. However, the measurements can be used for tool-breakage detection where the machining operation is interrupted after tool breakage.

2.2 SIGNAL ANALYSIS

2.2.1 Time domain signal:

The time domain signal is not very informative as such, or at least it is very time consuming to look at the raw signal in graphical format. Evaluation of the changes by measuring only the amplitude of the signal is very complicated. Usually a number of statistical parameters such as root mean square (RMS), arithmetic mean, standard deviation and kurtosis are calculated and these are then used for comparison and diagnosis. [1]

With almost all of the measuring signals the most common parameter to look at is the RMS value. The RMS value contains all the energy in the signal and therefore also all the noise and all the elements that depend on the cutting process. Therefore, it is not the most suitable parameter to look but has still widely used due to the fact that it is easy to produce and understand. Besides, it does actually work when compared to other statistical parameters. In a series of tests in [14] the RMS value was compared to seven other statistical parameters, i.e. arithmetic mean, mean and standard deviation, skewness, kurtosis, maximum and minimum. The comparison showed that the RMS value is usually not the best but it is often one of the four best functioning parameters.

In the tests reported in [17–19], mean value together with the variance torque, feed and drift force have been calculated for all of the holes. No significant changes were actually observed in the mean and the variance of sensor signals. Therefore, it has been concluded that the force sensor signals in the time domain do not show any correlation with drill wear.

Due to the great variation in measured signals, i.e. dynamic behaviors, average values for longer test period are often used in statistical studies. For example, in [6] average values of thrust force and torque are used when developing tool wear models. Average, peak, RMS values and the area of thrust and torque have been used as input features in the diagnostic system described in [15]. These features have been chosen because of their previous successful application for on-line monitoring and diagnosis. Furthermore, these features were justified from the researchers' experimental observations. Mean, peak and standard deviation have been used in the analysis of thrust force and torque signals in [17]. Of the tested statistical parameters, standard deviation proved to be the best indicator of tool wear and it was the indicator that is more closely related to the change in the standard deviation of the hole surface in composite material.

2.2.2 *Fast Fourier Transform (FFT)*

The widely used Fast Fourier transform (FFT) provides a means to find out the frequency content of a measured signal. Assuming the wear influences the frequency contents of the measured signal, FFT then gives an inside view of this process. Although the calculation of the power spectrum is a more sophisticated way of signal analysis than the calculation of many of the statistical parameters in the time domain and thus is a more powerful tool to get rid of noise and disturbances [14], it does suffer from limitations such as [16]: (a) materials such as cast iron are not homogeneous and will affect the amplitude of the vibration measured, which may cause false alarms; (b) tool damage in drilling produces a high level of transient vibrations (spikes) which are largely attenuated by the averaging procedure typically used in spectrum calculations and this makes it difficult to extract a discriminating feature to distinguish the change in the tool conditions; (c) non-uniform hardness of the workpiece material, built up edges, and micro-cracks can also cause false alarms by increasing the vibration amplitude. In order to decrease the adverse risks explained earlier, the trapezoid method has been used to calculate the area of the power spectrum between two frequencies in order to monitor tool wear with vibration [16].

The power spectral density function of torque, drift and feed force have been calculated in [1] for two different types of drill coatings tested (zirconium nitride and titanium nitride). It is concluded that the power content of the axial force and torque is significant over the entire frequency range, whereas the power content of the drift force is band limited. The power spectrum of the drift force changes from a band limited process to a wide band process when the drill is worn. The power content of the high frequencies of the cutting forces (especially the drift force component) increase as the tool approaches failure. This can be used as an index to detect the failure of the cutting tool. Sometimes the number of points in the time domain is kept very small compared to typical values like 2048. If a small number of points is used, calculation of the power spectrum is much faster and also the frequency resolution is lower which is an advantage in the sense that even though the frequency of amplitudes in the spectrum might wander a little, they stay at the same frequency in the power spectrum. Another advantage is that the number of possible features that are used as input for a diagnosis system is in this way limited. In [12] only 256 points in the time domain have been used, which corresponds to a spectrum of 128 points in this case. The somewhat limited 256 points in the time domain have also been used in [17, 24]. The area under the power spectral density function (obtained through the Welsh method) has been studied with success. Averaging of the spectrums over a hole proved to give noisy results but this could be improved by averaging the results over a number of holes. All sensor signals i.e. feed and drift force (strain) and torque gave similar results. Signal-to-noise analysis indicated that the power at frequencies between 50 and 300 Hz have the highest value of signal-to-noise ratio and, hence, are the most reliable frequencies. Comparison of the PSD plots showed that power at each frequency increases with increase in drill wear. Normalized PSD plots of all of the four sensor signals at different states of drill wear were coincident. This indicates that power at all frequencies increases proportionally with an increase in drill wear. Therefore, the change of area under the PSD plots was considered instead of power at one frequency, for integration decreases the error. A number of FFT based functions such as autocorrelation, power spectrum (16 highest amplitudes, harmonics, as well as 1/3 and 1/1 octave bands), cepstrum and liftered spectrum and also two-channel functions such as cross-correlation, cross-spectrum, frequency response as well as some multi-signal frequency response function with more than two channels have been tested for tool wear monitoring in metal cutting including drilling [14]. The normal power spectrum worked well when the analyzed data were fitted to a third order regression curve. Some of the two-channel functions (cross-spectrum, coherence) also proved to work well in drilling. Cepstrum analysis is used to identify a series of harmonics or side bands in the power spectrum and to estimate their relative strength [16].

2.2.3 Wavelet transform

Wavelet transforms have become well known as useful tools for various signal processing applications [20]. Wavelet transform is described as a good solution in the time-frequency domain so that it can extract more information in the time domain at different frequency bands. Both continuous and discrete wavelet transforms are used for tool breakage detection using spindle and feed current signals. The test signals have been shown both in the time domain and after wavelet transform in [20], but no comparison with other methods is given. Hence it is difficult to compare whether what is seen clearly after the wavelet transform could also be seen clearly with some other analysis method, i.e. the benefits of the use of wavelet transform are not apparent.

In [13] the use of wavelet transformations together with neural networks is proposed in order to detect severe damage to micro-drills just before the breakage occurs. The use of wavelets is justified on the basis of the many weaknesses FFT has, the first being fixed resolution. The resolution of an entire frequency spectrum depends on sampling frequency and the number of data points. The second weakness is the representation of the entire spectrum, with the addition of harmonic signals, by assuming that the data window is repeated indefinitely. This assumption causes leakage problems and the transitions cannot be identified in the data window. A third weakness is the considerable noise in the transformations because of the very large degrees of freedom of the system. FFT analysis must be repeated several times and the results must be averaged to obtain smooth output.

In [13], the Daubechies type wavelet system based on an orthonormal base was used. By using wavelets, the thrust force signal of the micro-drill has been simplified. The analysis indicated that the wavelet translation coefficients can represent the characteristics of micro-drilling signals with reasonable accuracy without high frequency components. The transition coefficients of all the normal micro-drills demonstrated similar patterns. The characteristics of the severely damaged micro-drills were found to be totally different. Based on these results, it is suggested that wavelets might be the perfect tool for many applications requiring automated monitoring of manufacturing operations. However, no comparison to FFT or statistical parameters has been made.

Chapter 3

DRILL GEOMETRY, DRILLING PROCESS AND EXPERIMENTAL PROCEDURE

3.1 DRILL GEOMETRY and DRILLING PROCESS

A typical drill has several design parameters such as tip angle, chisel edge angle, chisel edge length, cutting lip length and helix angle. Each one of these parameters affecting the cutting forces and tool wear and drilled hole qualities in various ways.

A twist drill, which is used in drilling holes, is shown in Figures 3.1-3.2. A twist drill has a chisel edge at the bottom and two helical cutting lips with a tip angle (K_t) that meets with the flutes with a helix angle (β_0). The helical flutes do not cut; they are used to evacuate the chips from the drilled hole. The chisel edge has a width of (w) and an edge angle (Ψ_c). The cutting lips have an offset from the drill center due to chisel. The lips expand the hole by removing the material with a constant chip thickness as the drill is fed into the material.

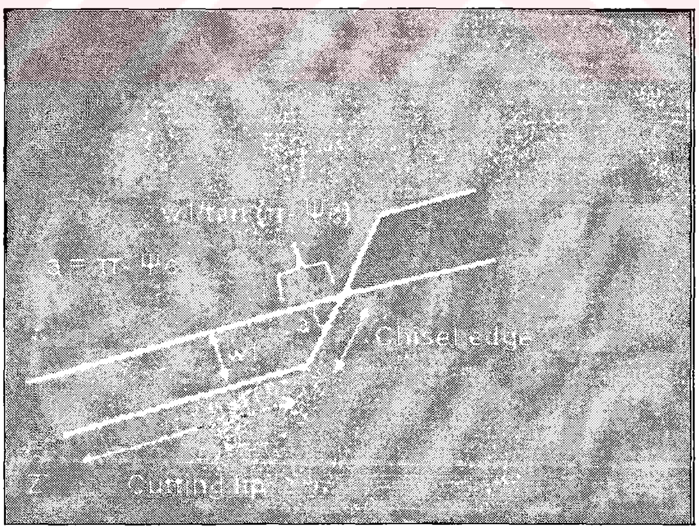

Figure 3.1: Top view of cutting lip and chisel edge for one cutting edge

Some geometrical relationships regarding the drill are as follows:

$$Z = Z' \times \text{Cos}\,(K_t/2) \qquad (3.1)$$

$$\text{Chisel edge projection along cutting edge} = w_1 / \tan(\pi - \Psi_c) \qquad (3.2)$$

$$\text{Chisel edge projection along drill axis} = [w_1 / \tan(\pi - \Psi_c)] \times \text{Cos}(K_t/2) \qquad (3.3)$$

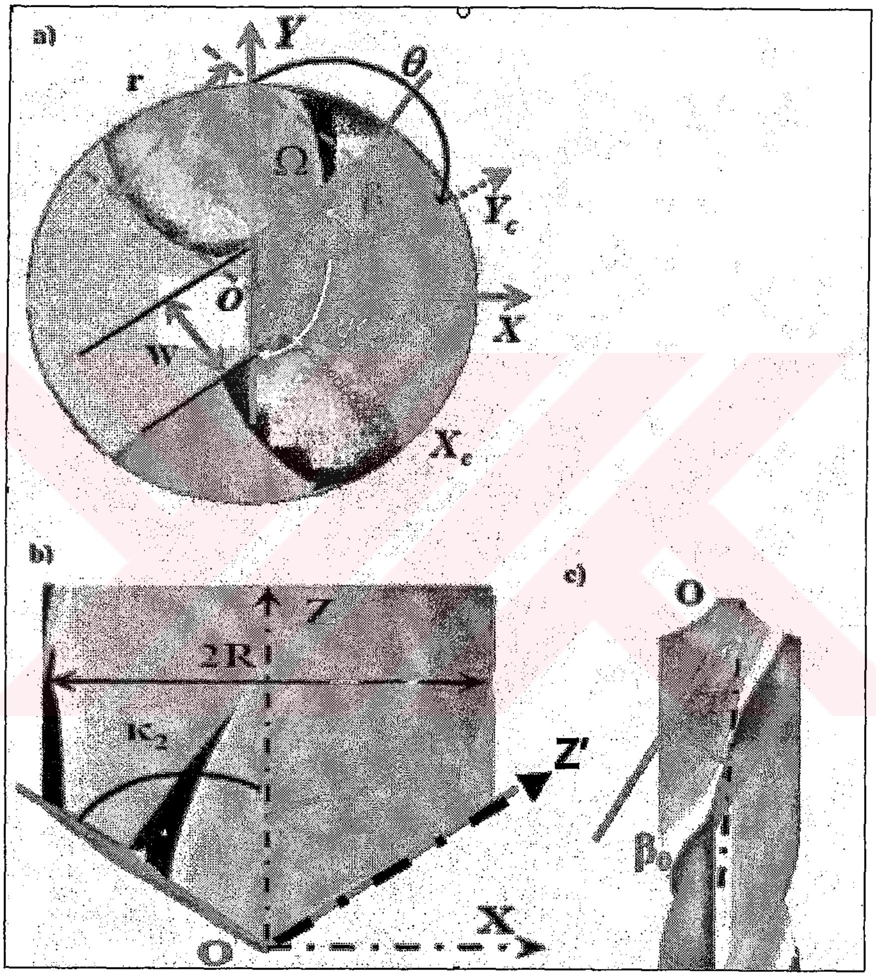

Figure3.2: a) Illustration of the angular relationships, b) Illustration of the point angle, c) Illustration of lag angle

As the drill is fed into the workpiece, firstly chisel edge contacts with the workpiece. After chisel edge fully engaged with the workpiece, cutting edge also contacts with the workpiece. The mechanics of the drill must be analyzed separately for the chisel and cutting lip regions. Because, cutting mechanisms are different for the chisel edge and cutting lip regions. Due to relatively low cutting speed, the chisel edge extrudes into the workpiece material and contributes substantially to the thrust force. The cutting lips, on the other hand, cut out the material with shearing mechanism and produce the minority of the drilling thrust but majority of drilling torque due to relatively higher radius and local cutting speed. The drill geometry has a complicated effect on the cutting forces. In addition to that, the cutting forces depend on the tool and workpiece material properties and machining conditions. The cutting forces are the main reason of the problems related to drilling in manufacturing such as tool wear, form and surface errors, etc. [23].

In general the drills have two cutting edges, the geometrical parameters related to the cutting edges are generally assumed to be the same. However, in reality due to inaccuracies in manufacturing of the tools, the drill design parameters of each cutting edge may be different from the other, this phenomena is the reason of the drift forces in drilling. Therefore the design parameters should be treated separately for each cutting edge.

Cutting forces in drilling has some unique features special to drilling process. As the drill is fed into the workpiece all the cutting force components (F_x, F_y and F_z) increase, this increase in cutting force components continues until the chisel edge is fully engaged with the workpiece after which forces are nearly constant or have little increase until the drill is fully engaged with the workpiece. After full engagement, all the cutting forces are almost constant. This can be viewed in Figure 3.3-3.4 in detail. In Section I only chisel edge cuts, in Section II chisel edge and cutting edge cut till the full engagement of the drill, in Section III drill has fully contacted with the workpiece.

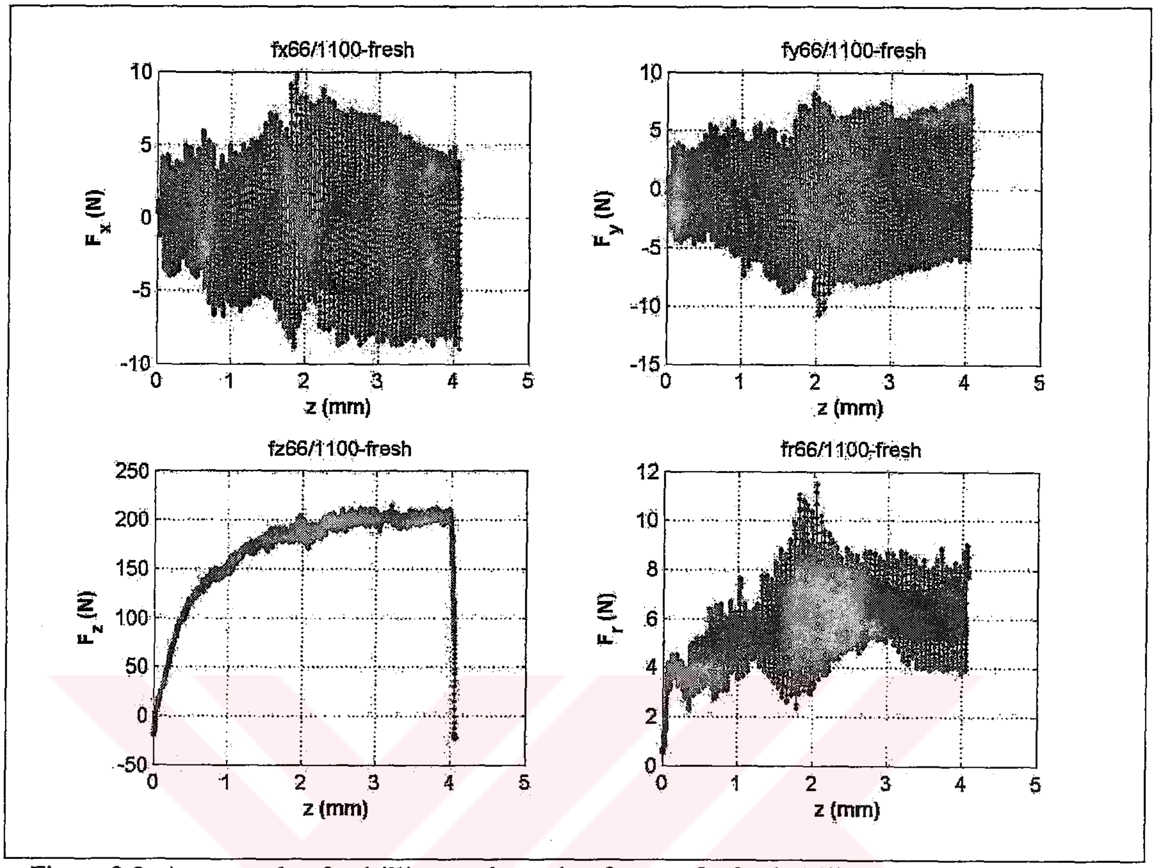

Figure 3.3: An example of a drilling test's cutting forces of a fresh drill for cutting conditions 1100 [rpm] spindle speed and 66 [mm/min] feed rate.

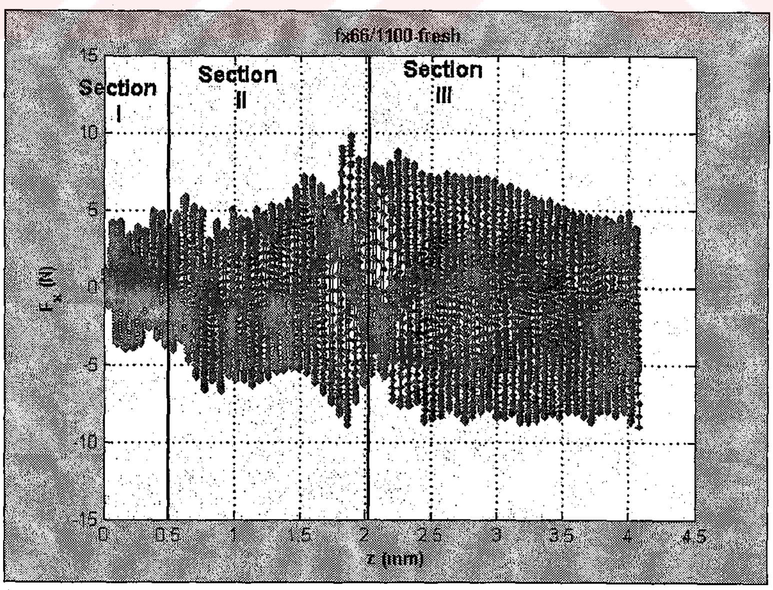

Figure 3.4: Illustration of cutting force in X direction of a fresh drill for spindle speed of 1100 [rpm] and feed rate 66 [mm/min]

3.2 EXPERIMENTAL PROCEDURE

Illustration of experimental setup is shown in the Figure3.5. The experiments were performed on Mazak FJV-200 UHS Vertical Machining Center (VMC) with 25000 rpm spindle motor, +/- 2.5 micron sensitivity and, +/- 0.7 micron repeatability. The drills used had 7.7 mm nominal diameter, 8 mm shank diameter, 90 mm projection length. The workpiece materials were aluminum blocks (Al7039) of size 250x170x38 [mm]. Kistler 3-component dynamometer (Model 9257B) and a charge amplifier have been used to measure cutting forces. The 3-component dynamometer has been fixed to the machine table using fixtures and the aluminum block was attached to the dynamometer using four 8M screws as seen in Figure 3.7.

The cutting forces are sensed by the piezoelectric transducer in the dynamometer and an electric charge output is the outcome of this process. This electric charge is later taken by the charge amplifier and converted into voltage output. The sensitivity values for the three channels (x, y and z) in the amplifier were -7.87, -7.90, and -3.69 pC/N respectively. Subsequently, through use of a proper data acquisition card, NI PCI DAQ Card with 200 kS/s sampling rate, 16 SE/8 DI analog input and +/-10 V analog input, and software, the voltage output is displayed and recorded as cutting forces in Newton. Displaying and recording of the data was done by Cutpro as seen in the Figure3.8.

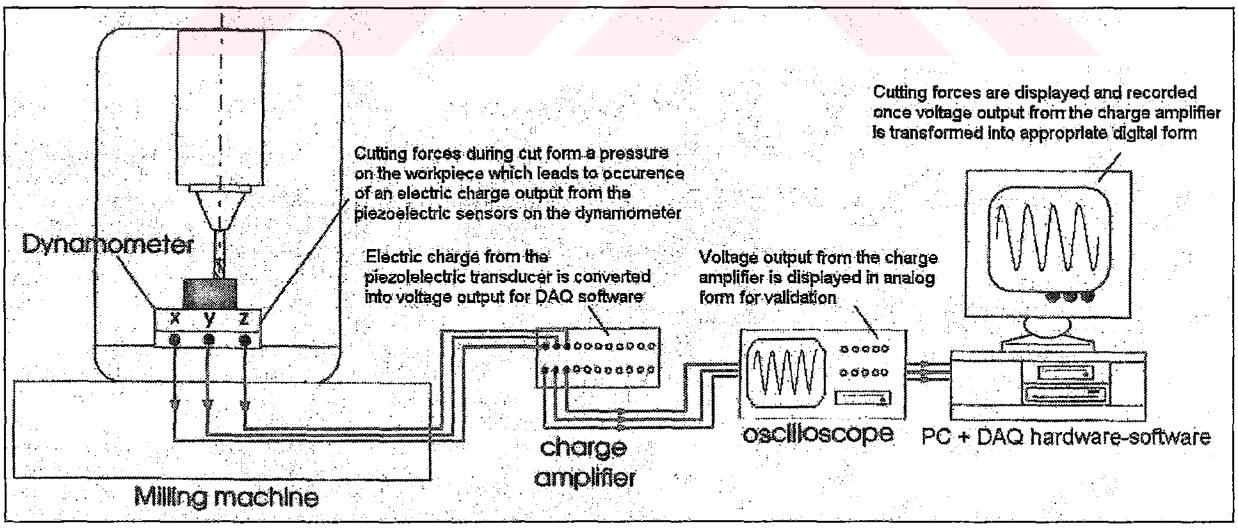

Figure 3.5: Detailed illustration of the experimental setup for measurement of cutting forces;

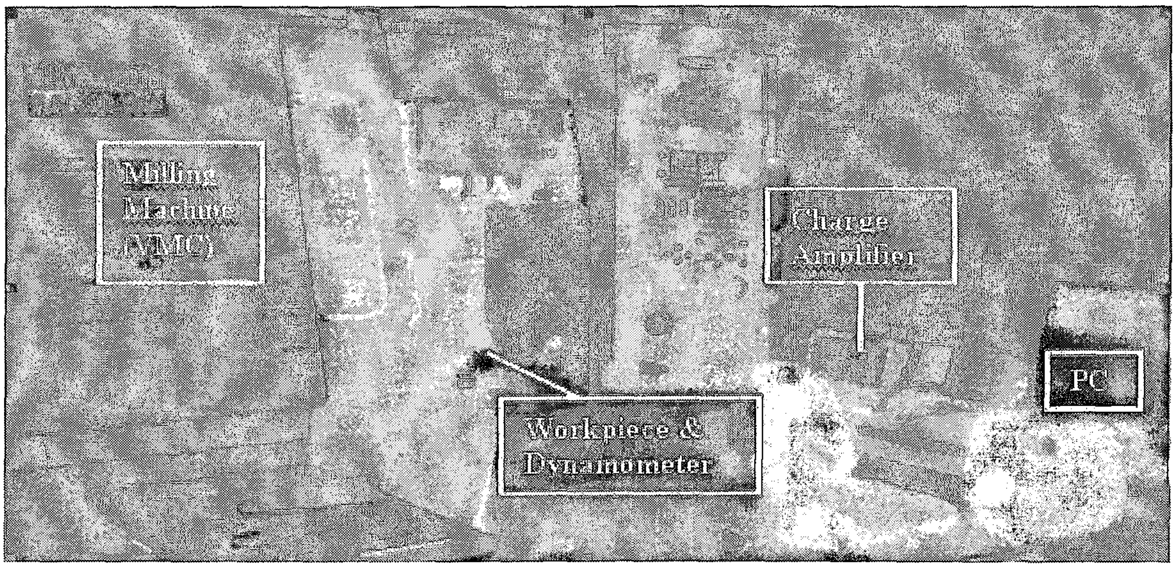

Figure 3.6: Actual experimental setup for measurement of cutting forces

Figure 3.7: Detailed illustration of actual experimental set-up

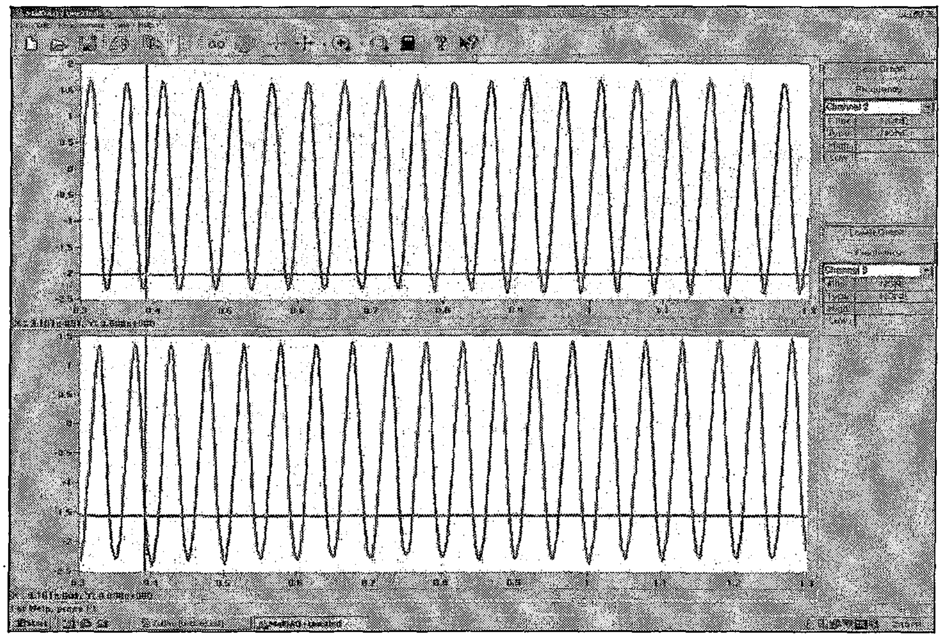

Figure 3.8: Sample output screen in CutPro for cutting forces

3.3 Chipped Drills and Dimensional Measurement Results

Different type of chippings are artificially introduced to different drills and experiments are conducted for four types of chipping conditions; SHANK1, SHANK2, TIP1, TIP2, and ARB. These conditions are classified according to the place of the chipping present. For SHANK1 and SHANK2 the chipping is beginning from the outer corner of the cutting edge, for TIP1, TIP2 the chipping is beginning from the point where chisel edge ends and meets with cutting lip. Furthermore, with these chipping cases experiments were conducted. In order to see the effect of spindle speed and feed rate, experiments of all type of chipping cases were performed for spindle speeds 550/1100/2200 [rpm] and for feed rates 54/66/88/110/132 [mm/min].

Abbreviations used for chipping cases include;

SHANK1: Shank chipping with a chipping amount 1.2 mm.
SHANK2: Shank chipping with a chipping amount 2.2 mm.
TIP1: Tip chipping with a chipping amount 1.1 mm.
TIP2: Tip chipping with a chipping amount 2.1 mm.
ARB: Arbitrarily given chipping as 1.1 mm with arbitrary location.

The tables below are constructed to present some geometrical quantities for the drill types used. Table 3.1 is for design parameters for drills like drill diameter, taper angle, chisel edge width and amount of chipping. Table 3.2 is prepared to give full engagement depth of the drills used and the projection of full engagement depth along the cutting edge (Z′) as seen in the Figure 3.9. Tables 3.3-3.4 are for detailed geometrical details. It gives where the chipping starts and ends, where the chisel edge begins along the drill axis (Z) and also along the cutting edge axis (Z′)

Table 3.1: The parameters related to the geometry of the drill types used

Tool Type	**Amount of Chipping (mm)**	**Drill Diameter (mm)**	**κ_{t1}(unchipped)/ κ_{t2}(chipped) (degree)**	**w_1/w_2 [mm]**
TIP1	1.12	7.697	58.8/59.0	0.91/0.92/
TIP2	2.1	7.698	58.2/ 58.9	0.92/0.91
SHANK1	1.2	7.700	58.9/58.9	0.95/0.94
SHANK2	2.2	7.700	58.9/58.9	0.93/0.94
ARB	1.1	7.701	58.9/58.8	0.96/0.95

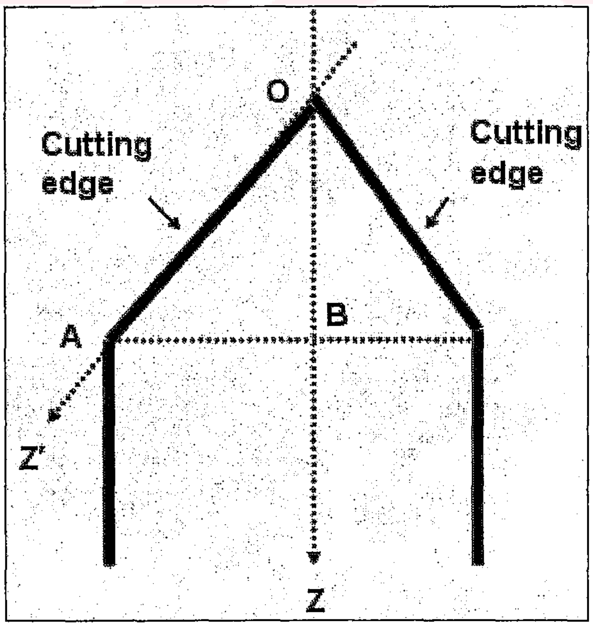

Figure 3.9: Front view of a typical drill restated

Table 3.2: Full engagement lengths along cutting edge (Z′) and along drill axis (Z).

Tool Type	Z'_{OA} [mm]	Z_{OB} [mm]
TIP1	4.49	2.32
TIP2	4.51	2.35
SHANK1	4.50	2.32
SHANK2	4.50	2.32
ARB	4.50	2.32

Table3.3: The chipping details of different type of drills used along drill axis

		Z [mm] at Which		
Tool Type	**CHISEL EDGE HEIGHT [mm]**	**CHIPPING STARTS**	**CHIPPING ENDS**	**ΔZ, CHIPPING HEIGHT [mm]**
TIP1	0.52	0.52	1.10	0.58
TIP2	0.48	0.48	1.57	1.09
SHANK1	0.51	1.69	2.32	0.63
SHANK2	0.50	1.18	2.32	1.14
ARB	0.49	1.034	1.65	1.616

Table3.4: The chipping details of different type of drills used along cutting edge

		Z′ [mm] at Which		
Tool Type	**CHISEL EDGE LENGHT [mm]**	**CHIPPING STARTS**	**CHIPPING ENDS**	**Δ Z′, CHIPPING LENGTH [mm]**
TIP1	1.01	1.01	2.13	1.12
TIP2	0.92	0.92	3.01	2.09
SHANK1	0.99	3.27	4.49	1.22
SHANK2	0.97	2.28	4.49	2.21
ARB	0.95	2.00	3.19	1.19

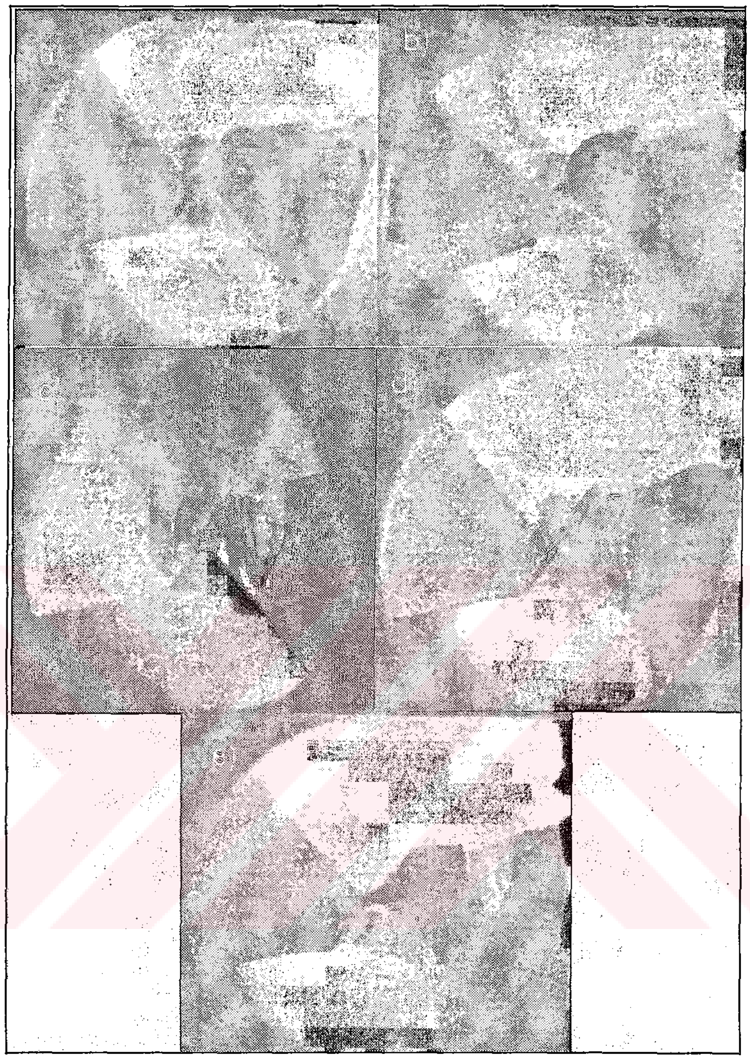

Figure 3.10: Top views of a) SHANK1, b) SHANK2, c) TIP1, d) TIP2, e) ARB

Chapter 4

TIME DOMAIN ANALYSIS

4.1 Introduction

This chapter is dedicated to obtain monitoring features of drills by analyzing the time domain data of cutting force components (F_x, F_y and F_z,). The analysis in this chapter will be performed for tip and shank chipping cases for each feed rate/spindle speed conditions specified in Table 4.1.

Table 4.1: Spindle Speed and Feed Rate Conditions used

Spindle Speed [rpm]	550 1100 2200				
Feed Rate [mm/min]	44	66	88	110	132

The chipping cases investigated in this chapter are tip chipping and shank shipping. From these, tip chipping is the one that includes edge fracture starting from the end of the chisel edge and lying along the cutting edge. On the other hand, shank chipping has a property that it ends at the point where the cutting flute and shank of the drill meet and lying along the cutting edge. These two types of chipping cases will be investigated separately, because each one has different cutting geometry hence each chipping configuration shows different type of force pattern.

4.2 Tip Chipping Cases

4.2.1 TIP1 Chipping

The chipping in the tip section has special geometry. This geometry is better viewed in Figure 4.1. Geometrically, this type of drill consists of three separate regions starting from the tip of the drill: chisel edge cutting region, chipped portion and unchipped portion. These separate regions show themselves in the cutting force data in the time domain as will be discussed below.

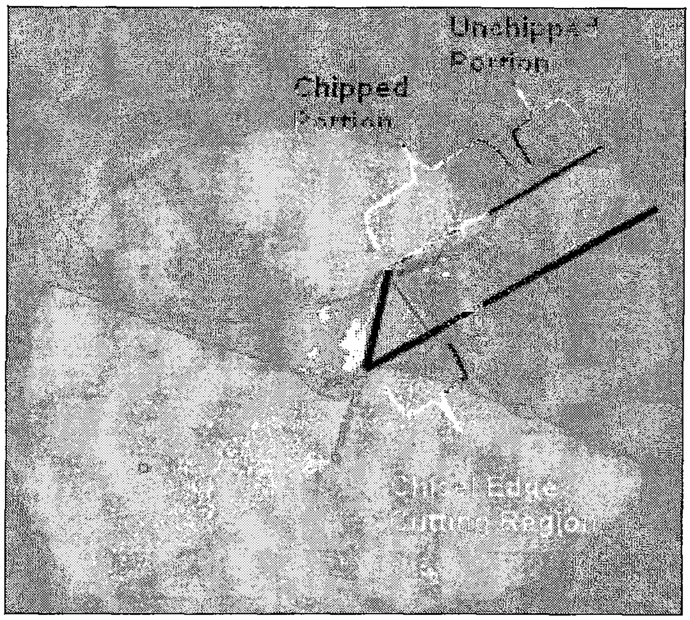

Figure 4.1: Illustration of a drill with a tip chipping induced

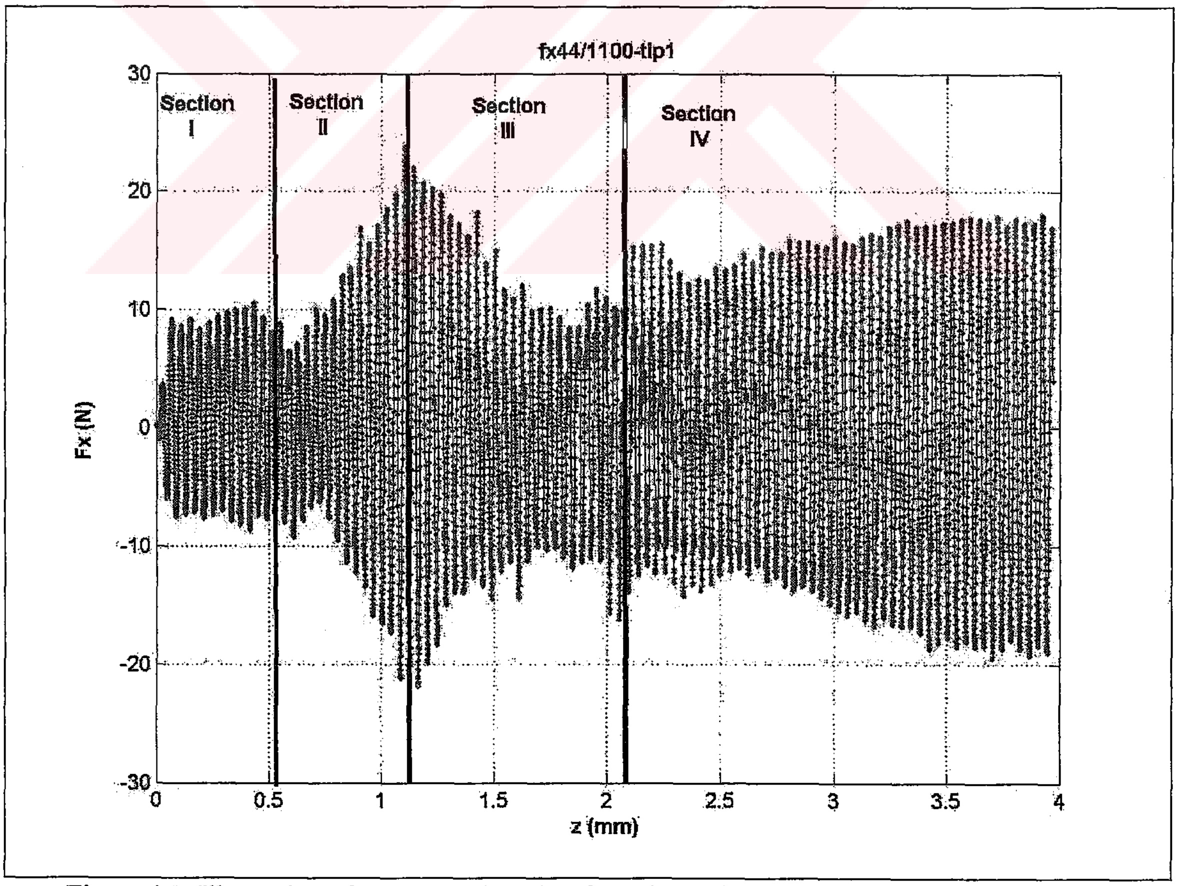

Figure 4.2: Illustration of a measured cutting force in X directions of a TIP1 drill for spindle speed 1100 of [rpm] and feed rate of 44[mm/min].

Cutting force in X direction can be analyzed in four sections in time domain as it can be seen in the Figure 4.2;

- Section I: This portion can be called as chisel edge portion because in this portion only the chisel edge of the drill cuts. Geometrically speaking, at the end of Section I, the chisel edge ends cutting edge starts to cut.
- Section II: In this section, effect of chipping can be observed. Geometrically, as the chisel edge ends cutting lips start to cut. There is an increasing force pattern in this section. The increase in the cutting force amplitude is due to the fact that one flute is cutting the other flute cannot due to chipping, therefore fresh flute has to cut the other flute's chip load as well. End of Section II is useful because it determines the end of chipping portion in the time domain which can be used to calculate the amount of chipping if tip chipping is encountered. The calculation is done as follows. The time at which cutting force reaches maximum is obtained, then time is converted to instantaneous depth by using simple formula;

$$\text{Instantaneous Depth [mm]} = \text{feed rate [mm/min]} \times \text{time [sec]}/60 \qquad (4.1)$$

Then, the depth at which cutting force reaches maximum is projected along the cutting edge by using formula;

$$\text{Instantaneous Distance Along Cutting Edge [mm]} = \text{Depth [mm]} \times \text{Cos}(K_t/2) \qquad (4.2)$$

Then, chisel edge length is already known for this TIP1 drill from Chapter 3. Therefore, the chisel edge length is projected along the cutting edge again using the Eq. 4.2. Finally, difference between projected lengths gives the amount of chipping present. The analysis is rather simple because the start point of the chipping is already fixed to the end of chisel edge.

- Section III: After chipping portion is passed, chipped cutting edge's unchipped part begin cutting as the drill is fed into the workpiece. In this portion, cutting force that reaches maximum in chipping portion tends to decrease till the end of Section III which is the point where the cutting edge meets with the shank of the drill. This is called as full engagement in the machining.
- Section IV: After full engagement occurs, if the cutting depth is larger than full engagement depth, a force pattern similar to Section IV is observed. In this portion cutting force is steadily increasing.

The figures below are the experimental results of the TIP1 chipping case. The figures are plotted for all cutting force components (F_x, F_y, F_z and F_r) and spindle speeds 550 [rpm], 1100 [rpm] and 2200 [rpm], respectively. Each spindle speed configuration includes feed rates 44-66-88-110-132 [mm/min]. Moreover, sampling frequency of the DAQ system is 2000 Hz. Monitoring features for TIP1 case are obtained by analyzing the figures below.

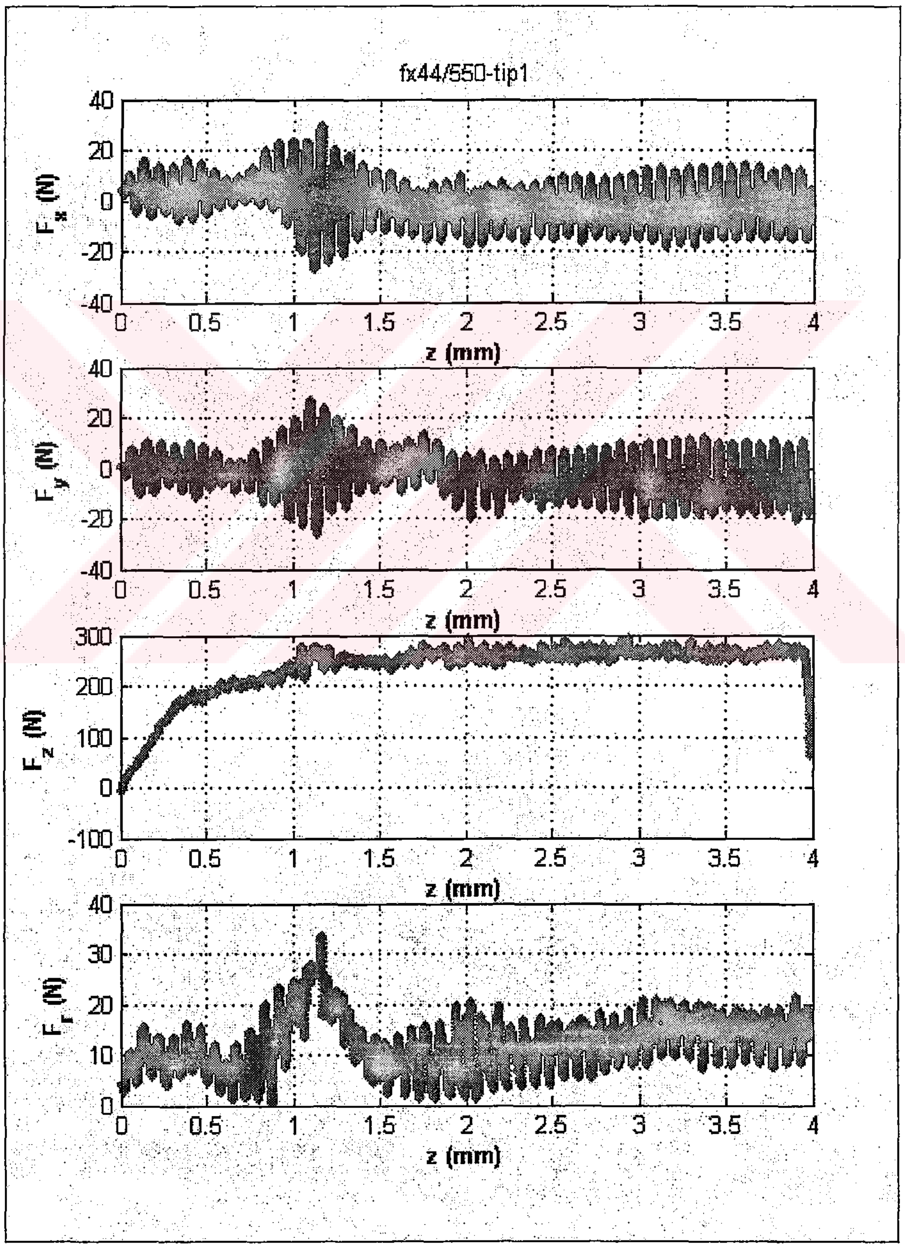

Figure 4.3: Illustration of a measured cutting forces in X, Y, Z and Radial directions of a TIP1 drill for spindle speed of 550[rpm] and feed rate of 44[mm/min].

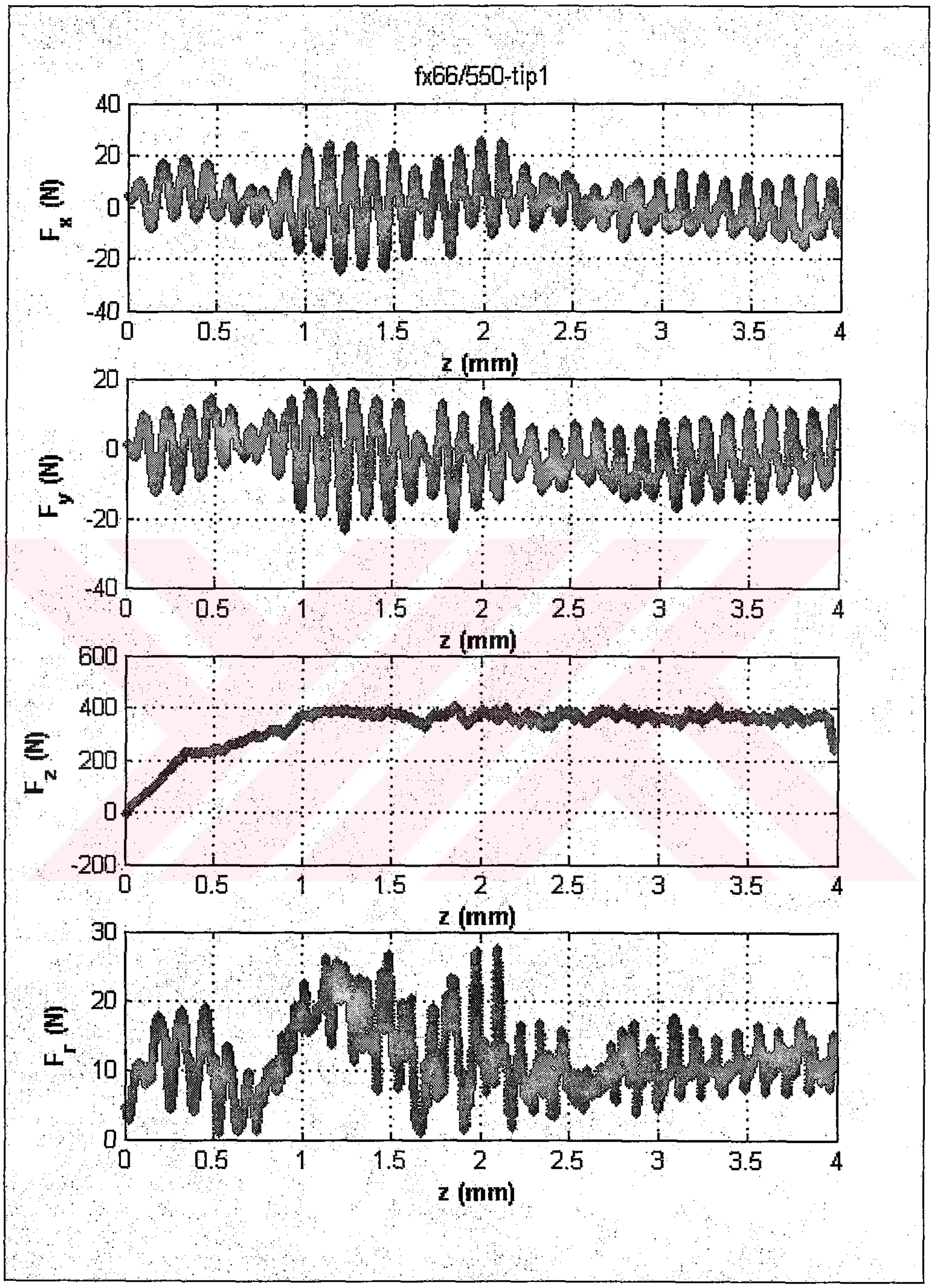

Figure 4.4: Illustration of a measured cutting forces in X, Y, Z and radial directions of a TIP1 drill for spindle speed of 550 [rpm] and feed rate of 66 [mm/min].

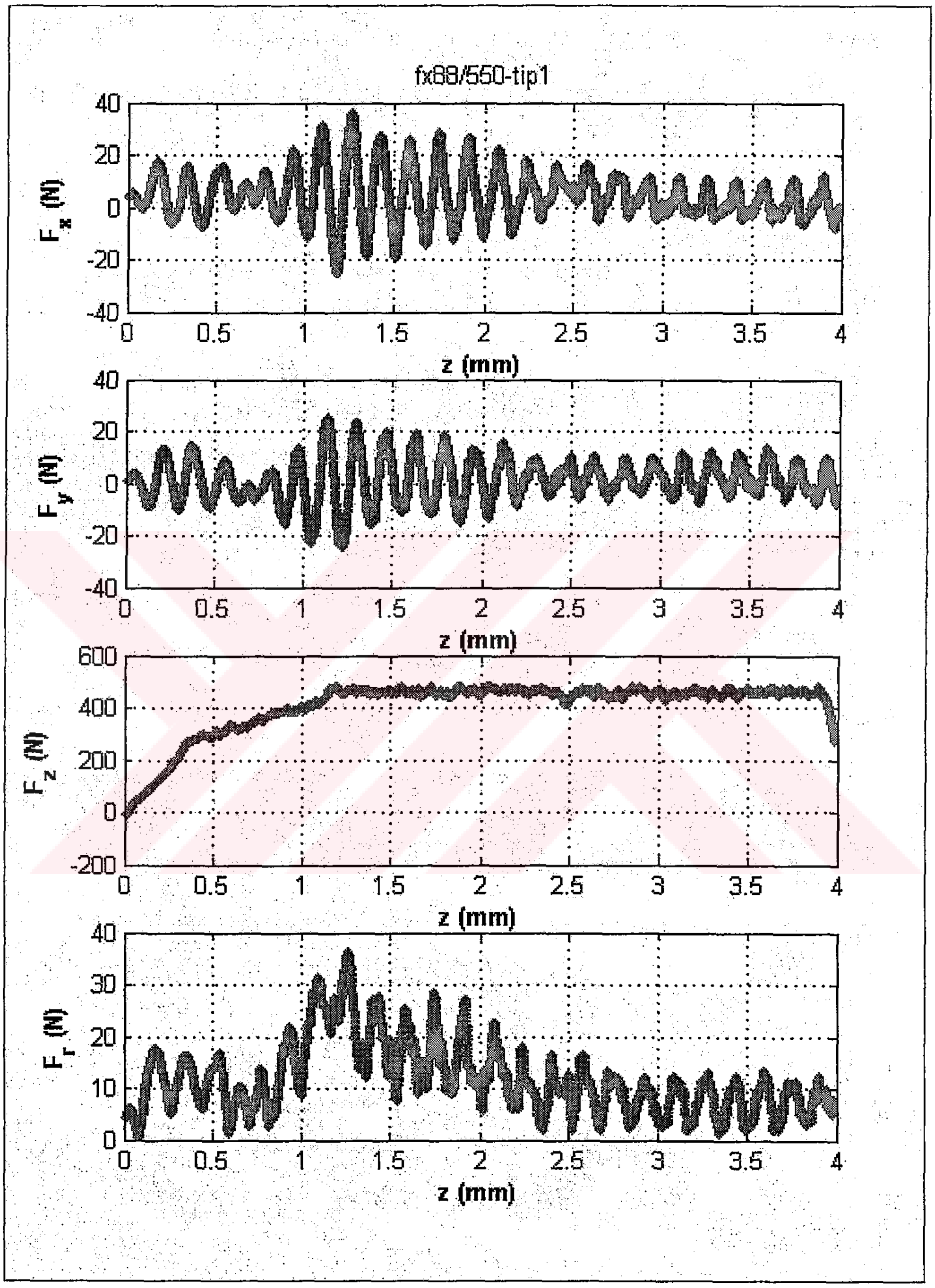

Figure 4.5: Illustration of a measured cutting forces in X, Y, Z and radial directions of a TIP1 drill for spindle speed of 550 [rpm] and feed rate of 88 [mm/min].

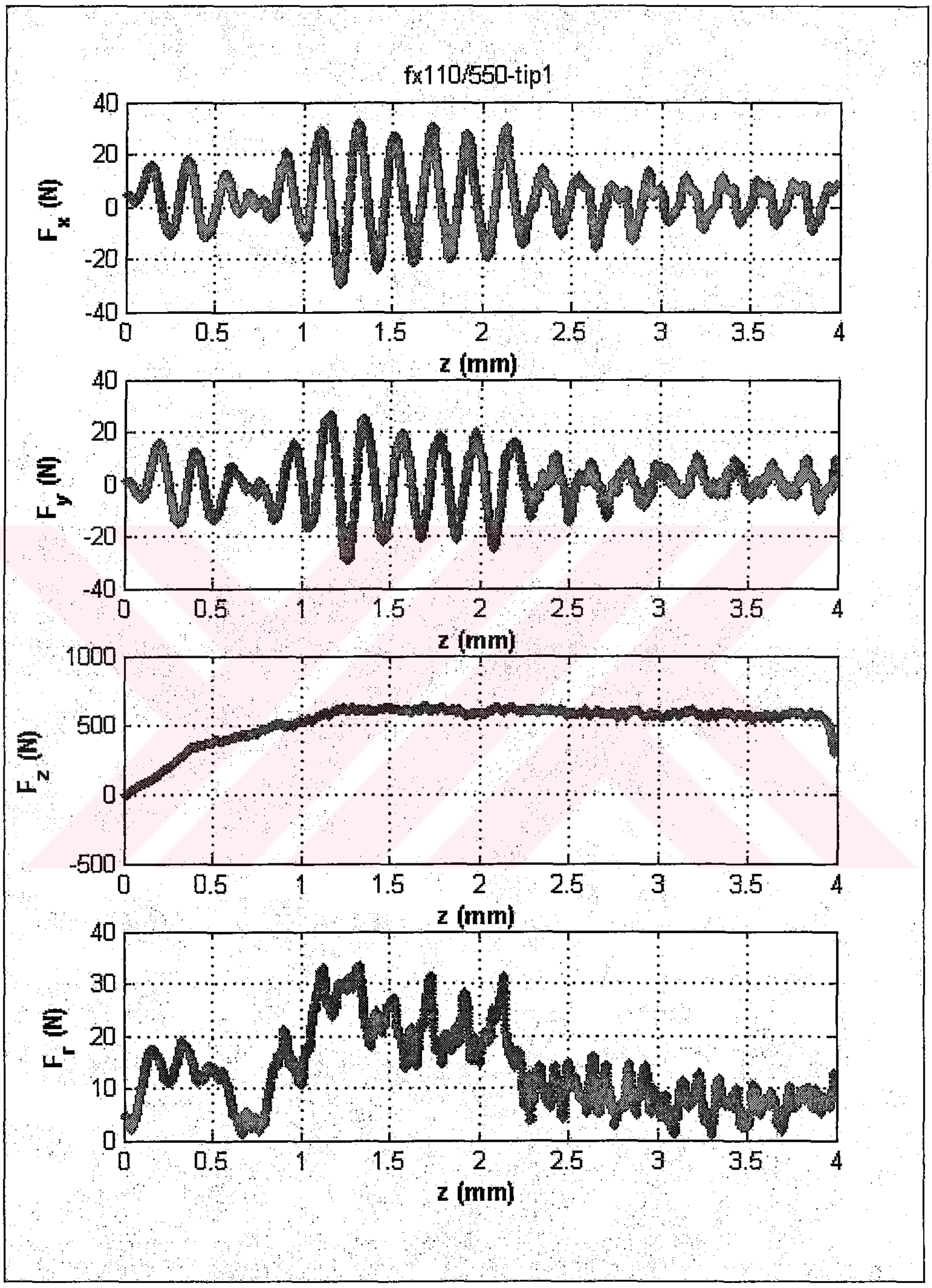

Figure 4.6: Illustration of a measured cutting forces in X, Y, Z and radial directions of a TIP1 drill for spindle speed of 550 [rpm] and feed rate of 110 [mm/min].

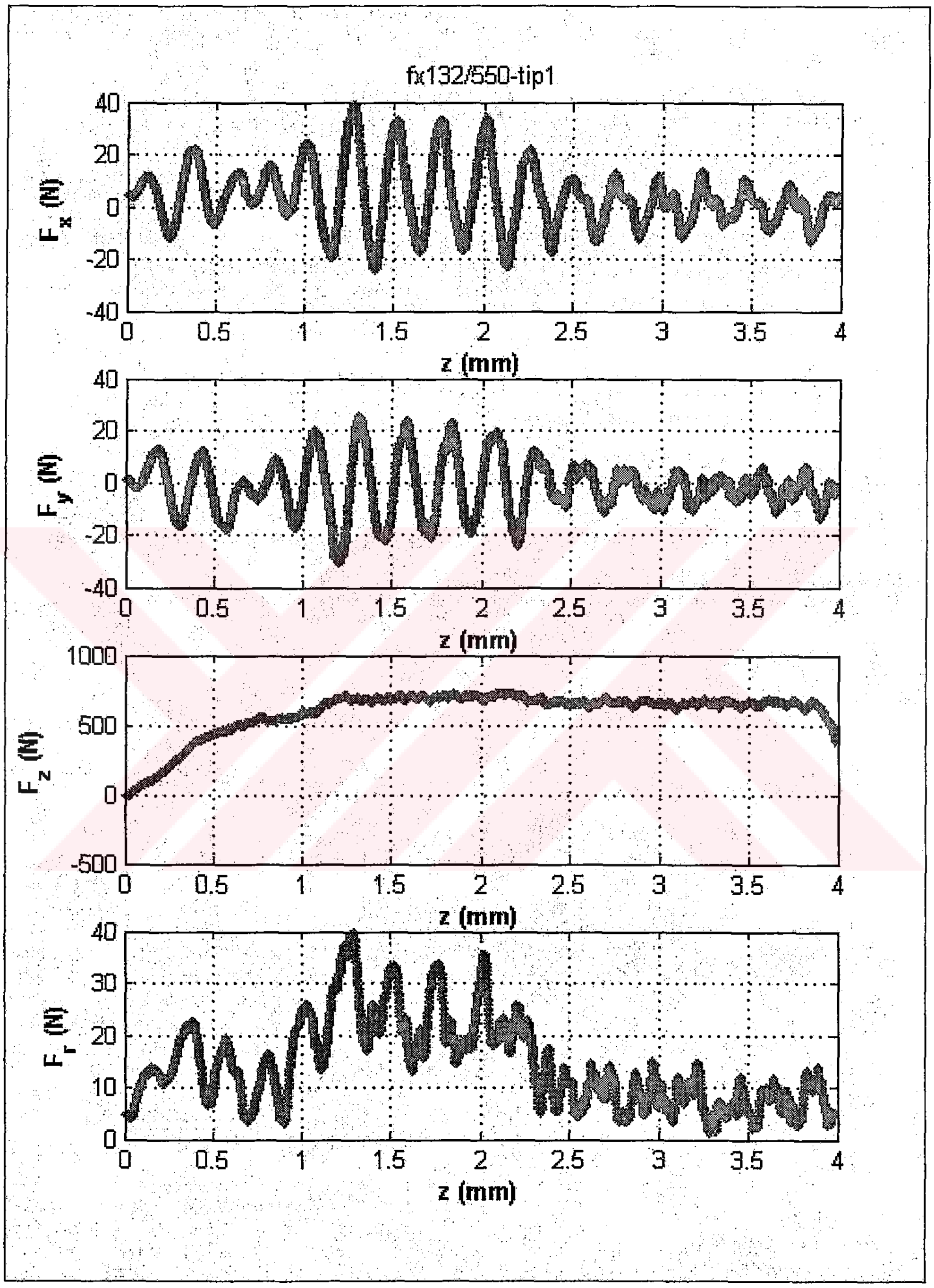

Figure 4.7: Illustration of a measured cutting forces in X, Y, Z and radial directions of a TIP1 drill for spindle speed of 550 [rpm] and feed rate 132 [mm/min].

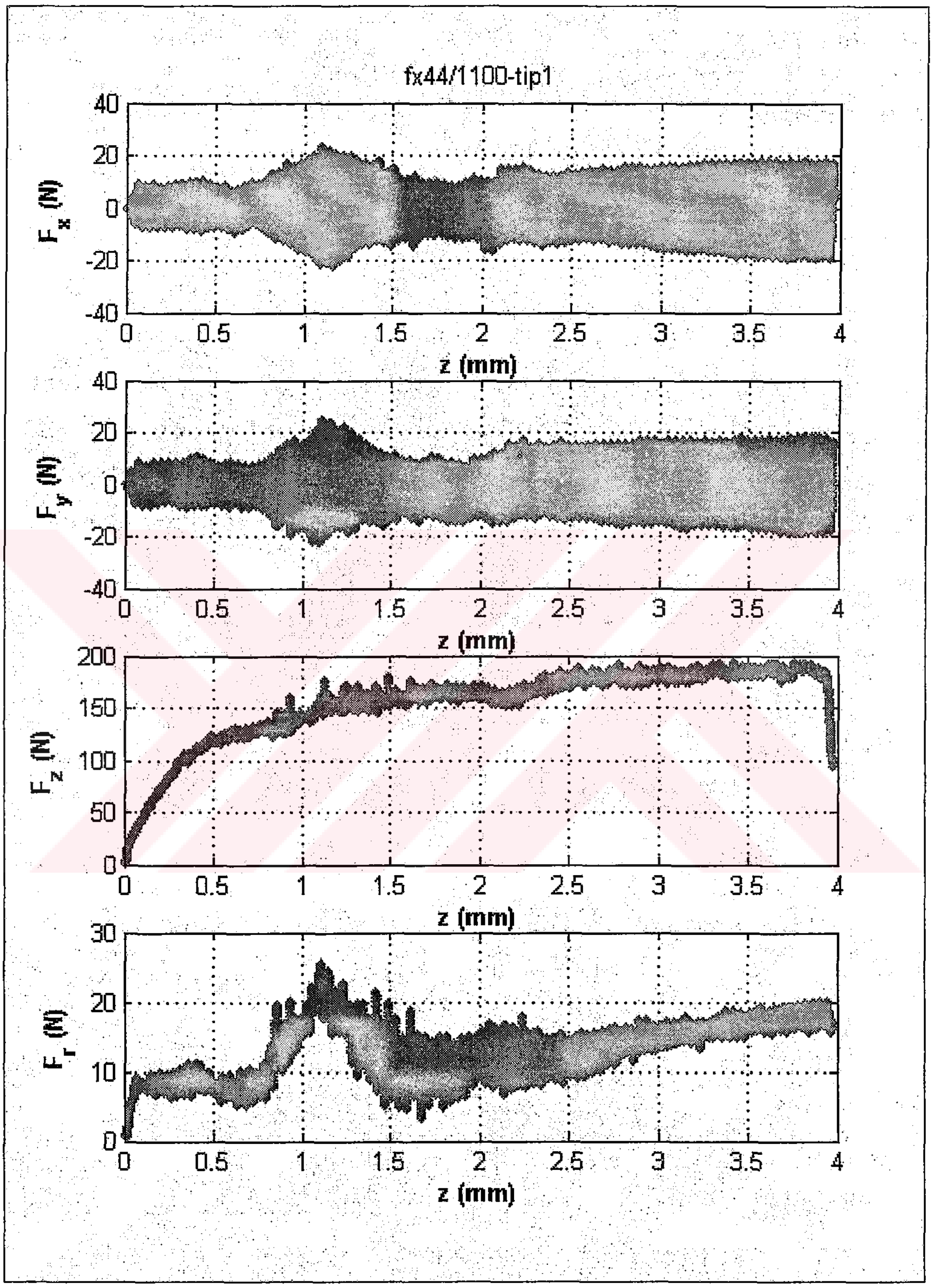

Figure 4.8: Illustration of a measured cutting forces in X, Y, Z and radial directions of a TIP1 drill for spindle speed of 1100 [rpm] and feed rate 44 [mm/min].

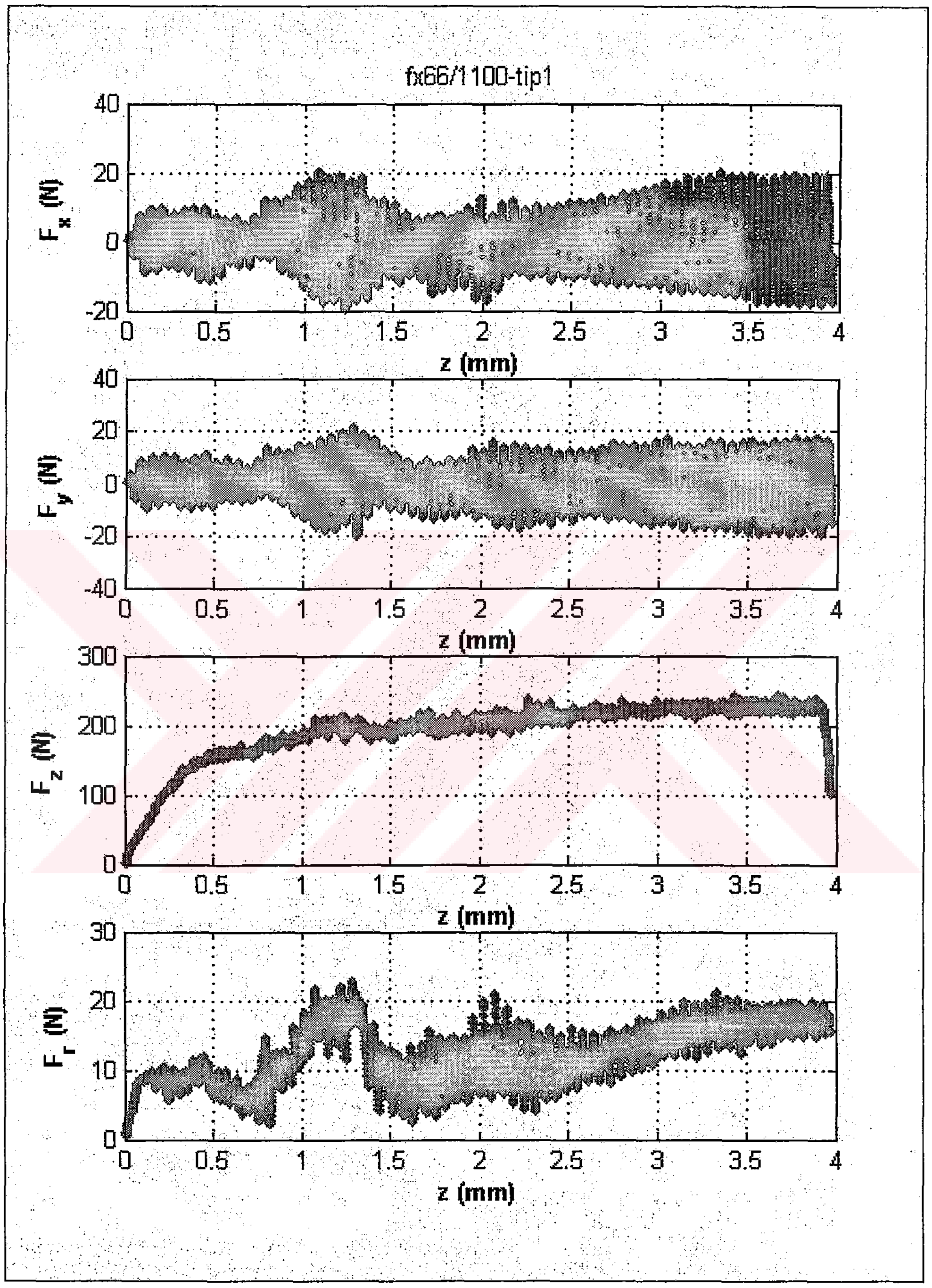

Figure 4.9: Illustration of a measured cutting forces in X, Y, Z and radial directions of a TIP1 drill for spindle speed of 1100 [rpm] and feed rate 66[mm/min].

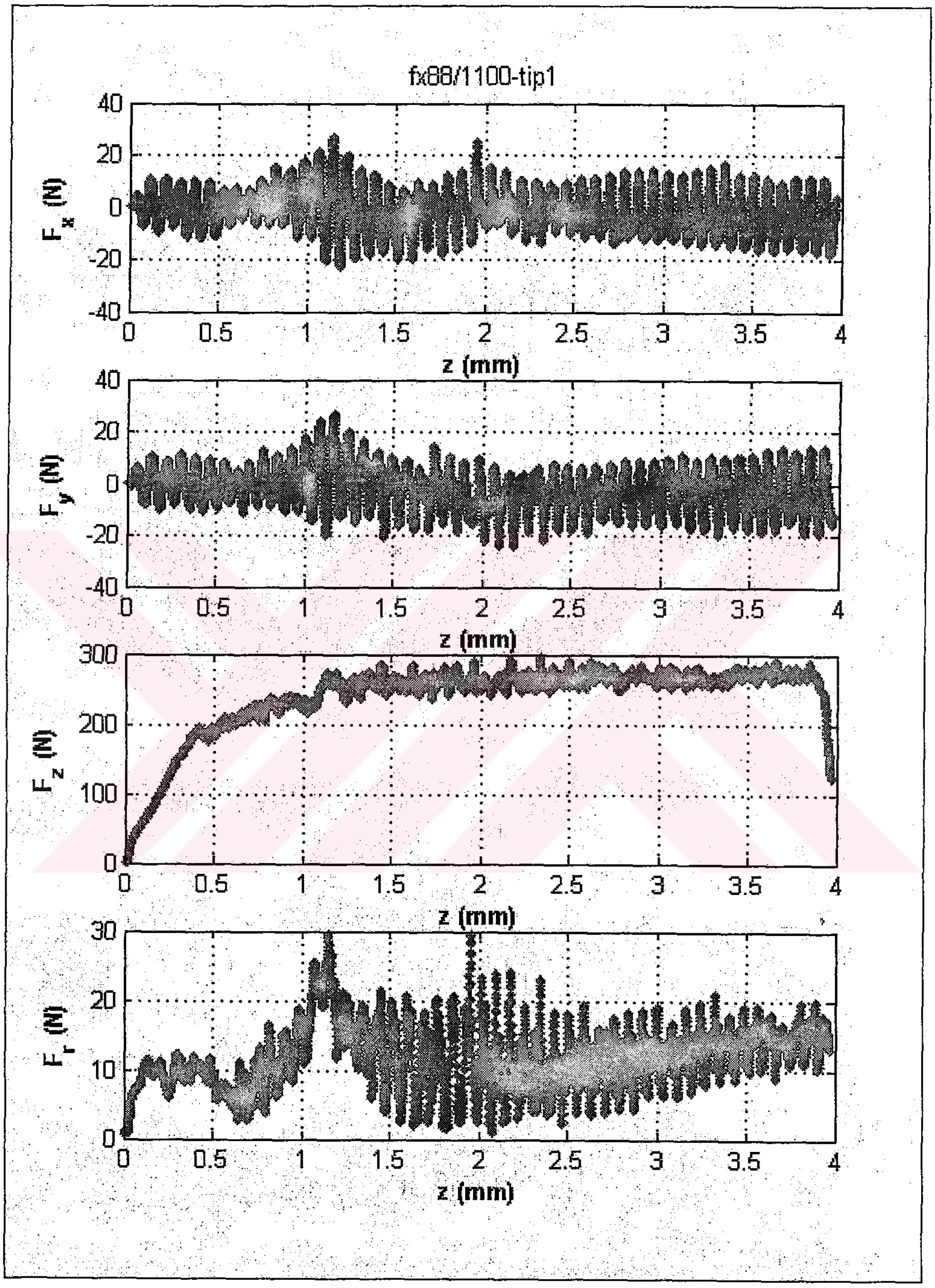

Figure 4.10: Illustration of a measured cutting forces in X, Y, Z and Radial directions of a TIP1 drill for spindle speed of 1100 [rpm] and feed rate 88 [mm/min].

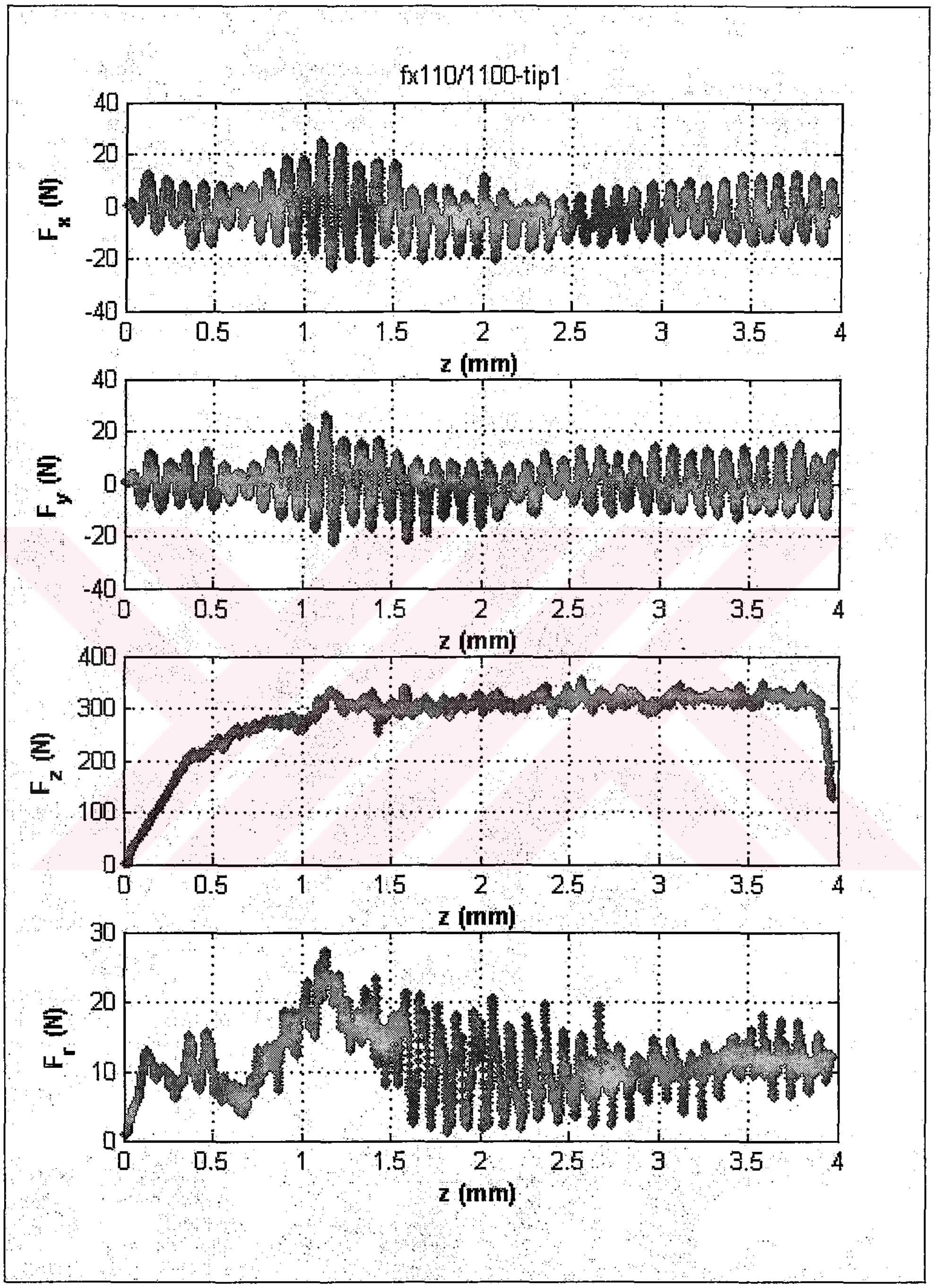

Figure 4.11: Illustration of a measured cutting forces in X, Y, Z and Radial directions of a TIP1 drill for spindle speed of 1100 [rpm] and feed rate 110 [mm/min].

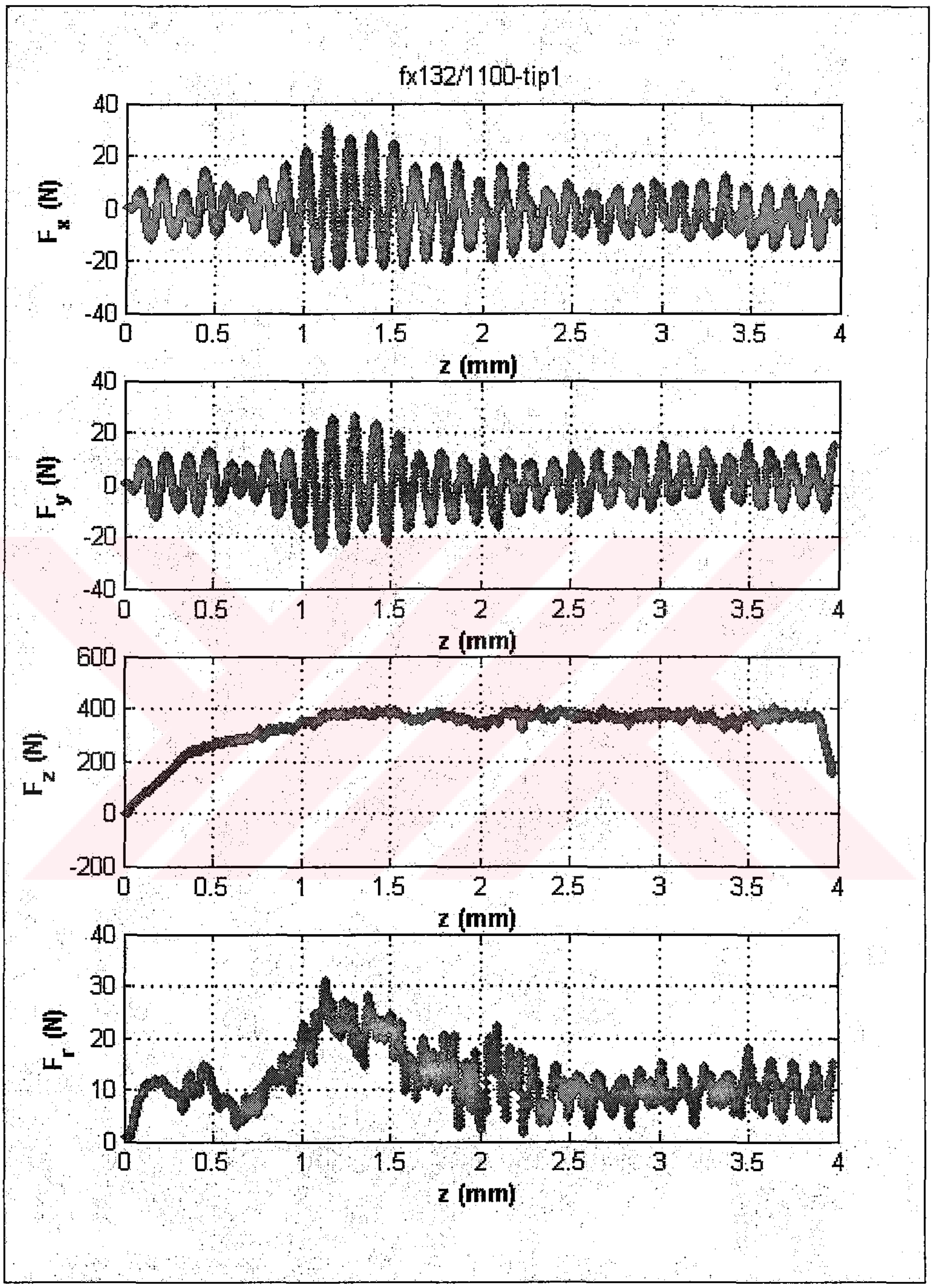

Figure 4.12: Illustration of a measured cutting forces in X, Y, Z and Radial directions of a TIP1 drill for spindle speed of 1100 [rpm] and feed rate 132 [mm/min].

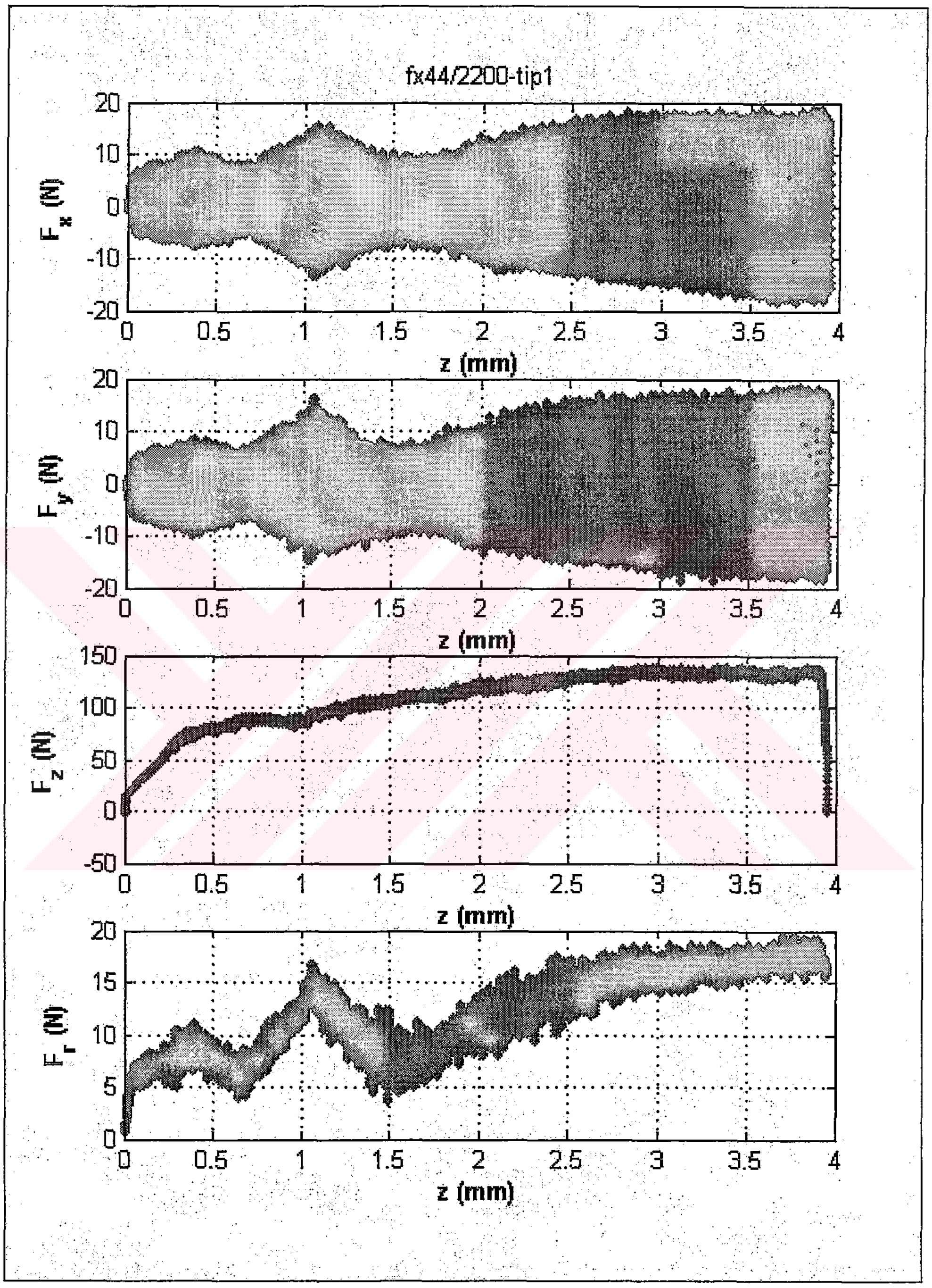

Figure 4.13: Illustration of a measured cutting forces in X, Y, Z and Radial directions of a TIP1 drill for spindle speed of 2200 [rpm] and feed rate 44 [mm/min].

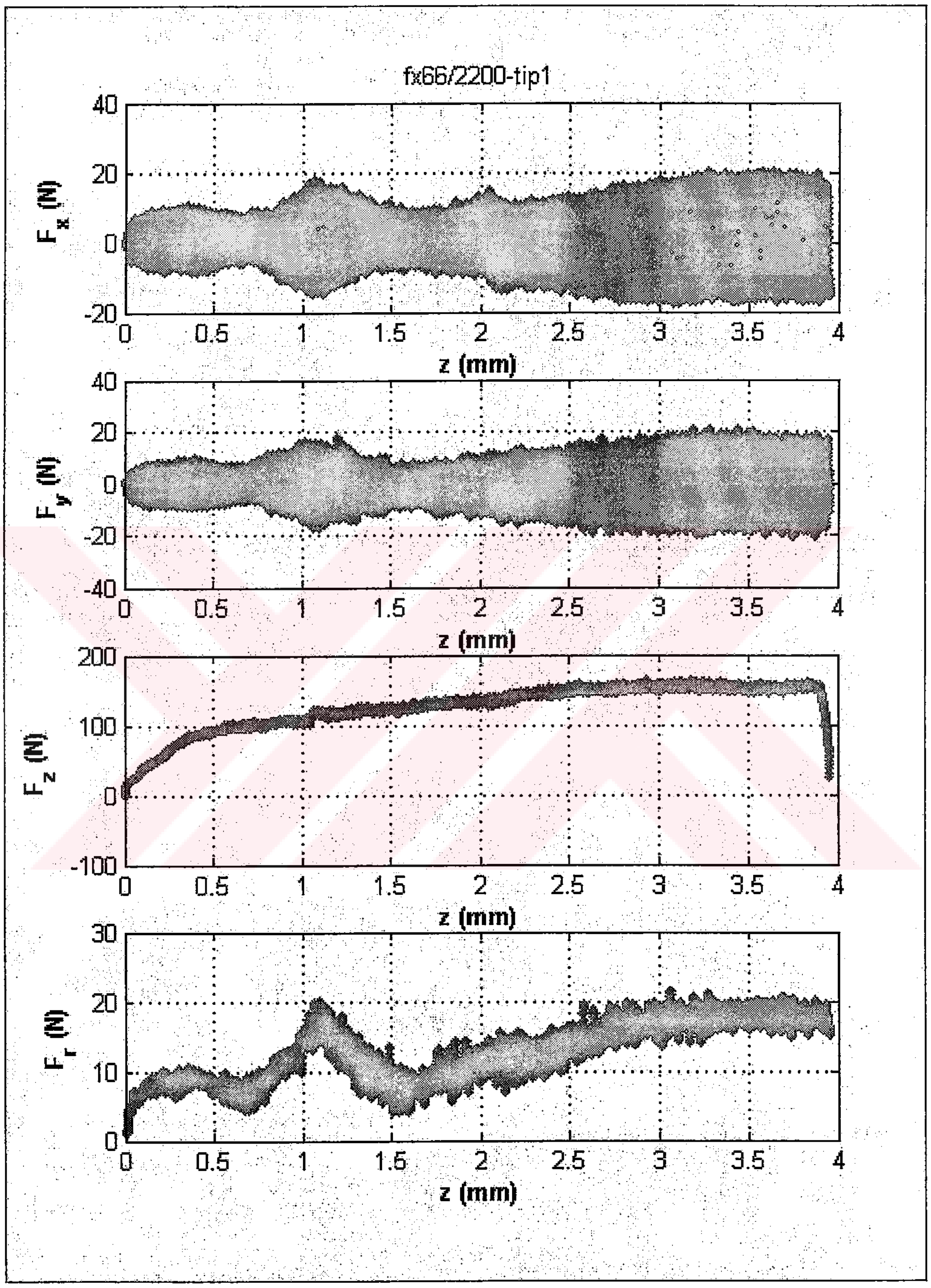

Figure 4.14: Illustration of a measured cutting forces in X, Y, Z and Radial directions of a TIP1 drill for spindle speed of 2200 [rpm] and feed rate 66 [mm/min].

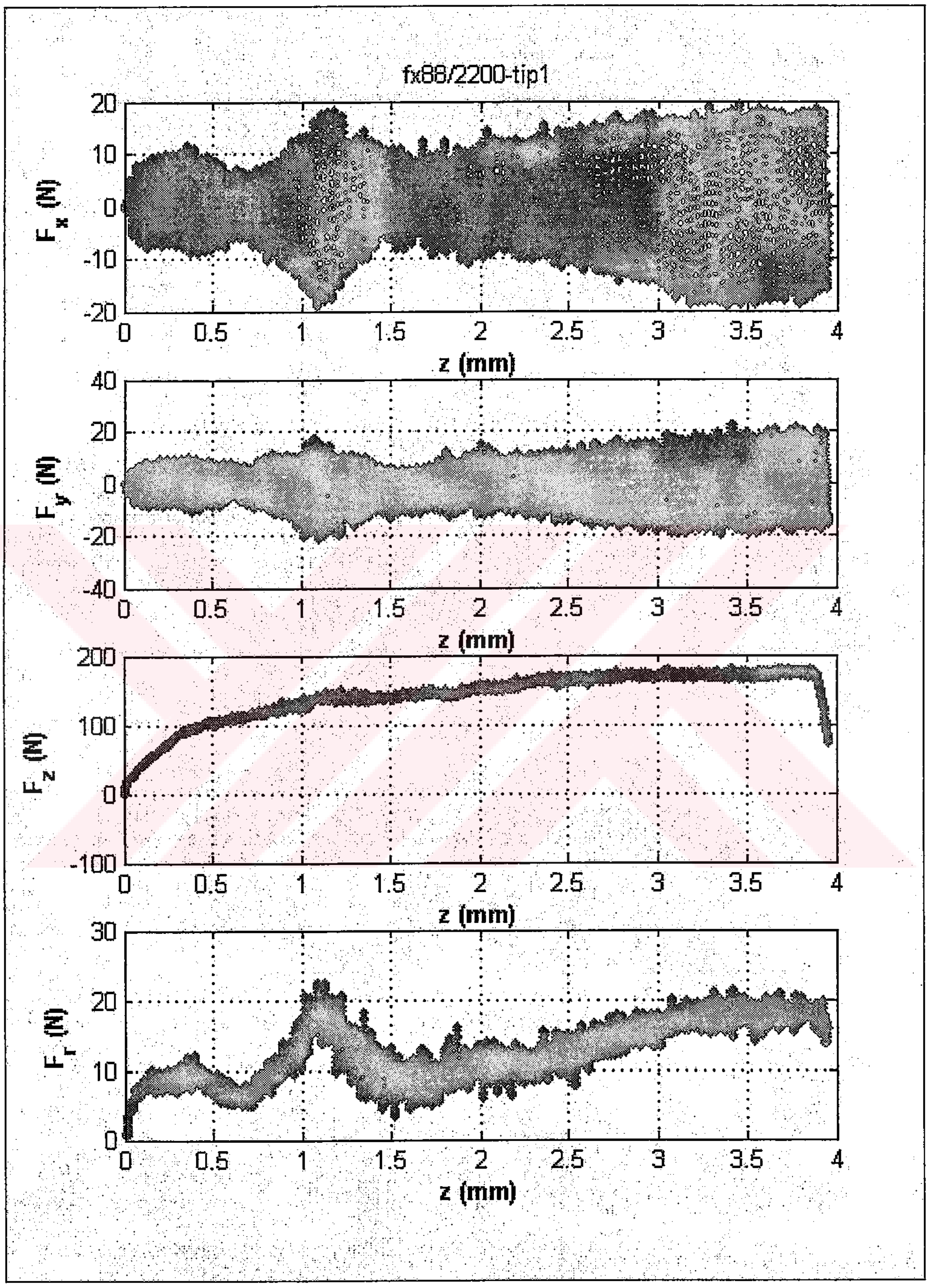

Figure 4.15: Illustration of a measured cutting forces in X, Y, Z and Radial directions of a TIP1 drill for spindle speed of 2200 [rpm] and feed rate 88 [mm/min].

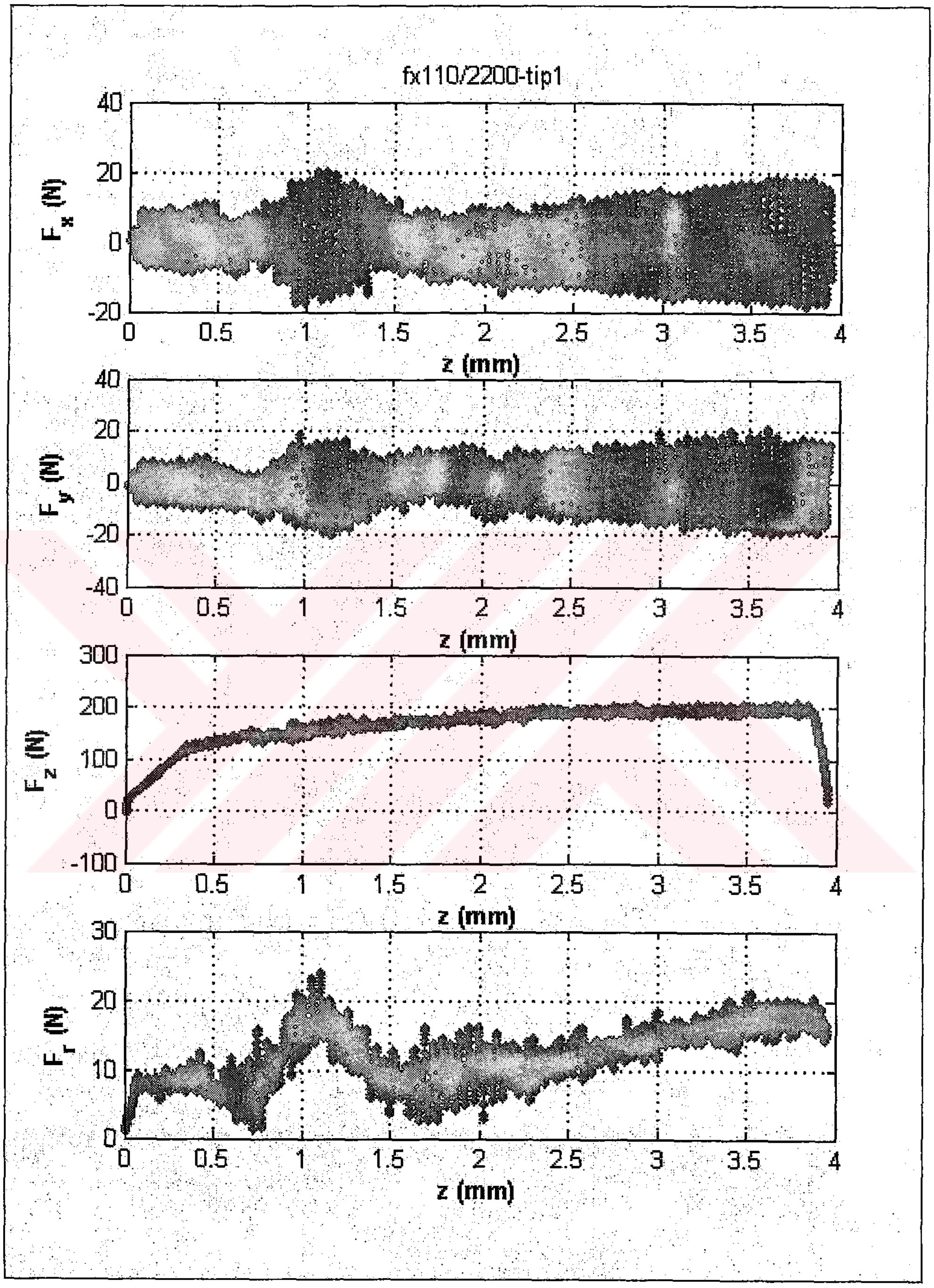

Figure 4.16: Illustration of a measured cutting forces in X, Y, Z and Radial directions of a TIP1 drill for spindle speed of 2200 [rpm] and feed rate 110 [mm/min].

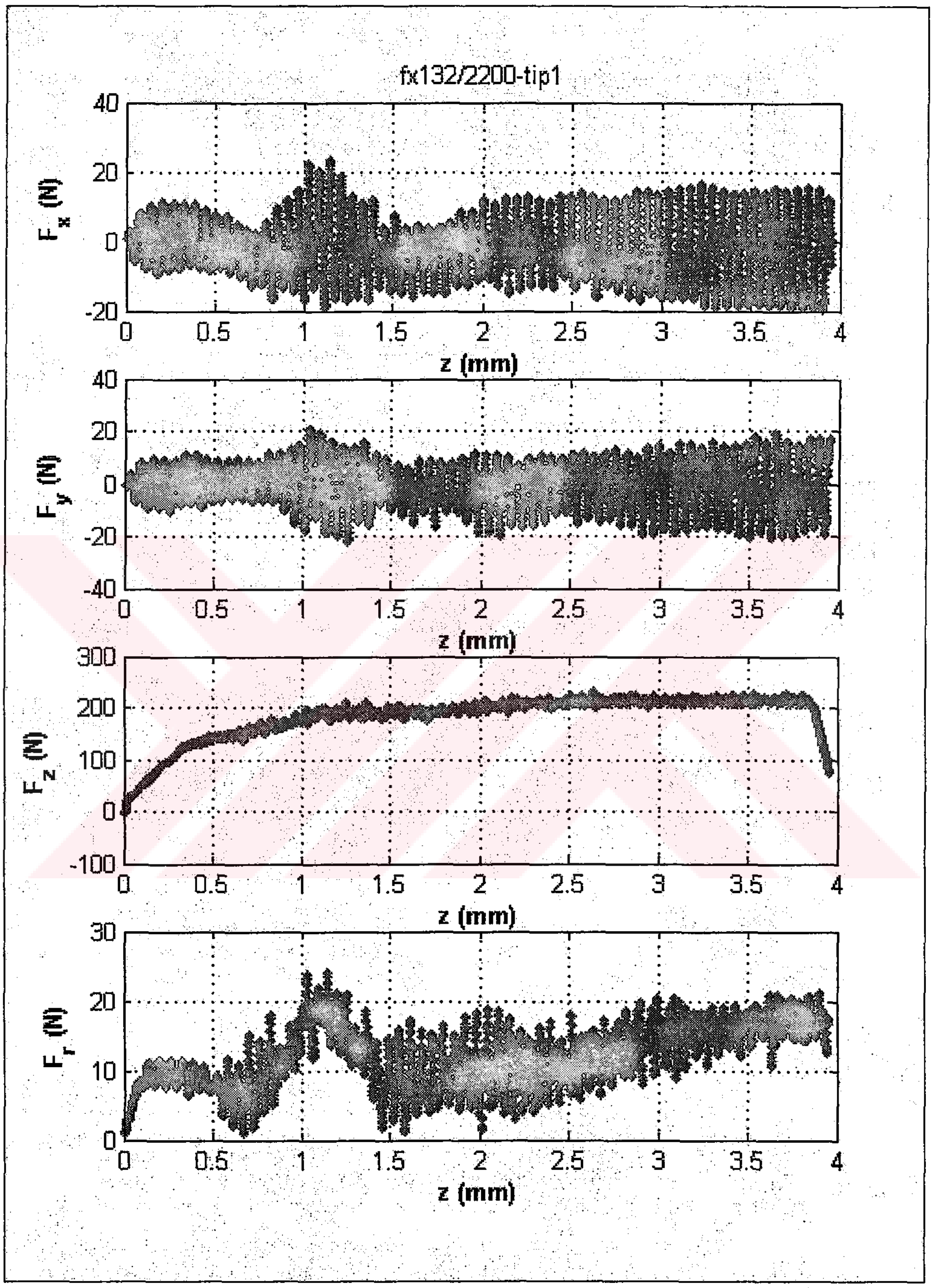

Figure 4.17: Illustration of a measured cutting forces in X, Y, Z and Radial directions of a TIP1 drill for spindle speed of 2200 [rpm] and feed rate 132 [mm/min].

Table 4.2: The time, instantaneous depth $\hat{Z}$, $\hat{Z'}$ at which F_x reaches maximum and calculated chipping amount for TIP1 drill, spindle speed 550 [rpm].

Feed Rate [mm/min]	Time [sec]	$\hat{Z}$ [mm]	$\hat{Z'}$ [mm]	Chipping Calculated [mm]	True Chipping [mm]
44	1.586	1.163	2.254	1.244	1.12
66	1.091	1.200	2.324	1.314	1.12
88	0.859	1.260	2.441	1.431	1.12
110	0.660	1.210	2.344	1.334	1.12
132	0.577	1.270	2.460	1.450	1.12

Table 4.3: The time, instantaneous depth $\hat{Z}$, $\hat{Z'}$ at which F_x reaches maximum and calculated chipping amount for TIP1 drill, spindle speed of 1100 [rpm].

Feed Rate [mm/min]	Time [sec]	$\hat{Z}$ [mm]	$\hat{Z'}$ [mm]	Chipping Calculated [mm]	True Chipping [mm]
44	1.502	1.101	2.133	1.123	1.12
66	0.984	1.083	2.097	1.087	1.12
88	0.783	1.149	2.225	1.215	1.12
110	0.601	1.101	2.133	1.123	1.12
132	0.517	1.138	2.204	1.194	1.12

Table 4.4: The time, instantaneous depth $\hat{Z}$, $\hat{Z'}$ at which F_x reaches maximum and calculated chipping amount for TIP1 drill, spindle speed of 2200 [rpm].

Feed Rate [mm/min]	Time [sec]	$\hat{Z}$ [mm]	$\hat{Z'}$ [mm]	Chipping Calculated [mm]	True Chipping [mm]
44	1.469	1.077	2.086	1.076	1.12
66	0.974	1.071	2.075	1.065	1.12
88	0.741	1.087	2.106	1.096	1.12
110	0.581	1.065	2.063	1.053	1.12
132	0.505	1.110	2.150	1.140	1.12

Table 4.5: Percent Error (%) in chipping amount for spindle speed of 550/1100/2200 [rpm] of TIP1 drill.

Feed Rate [mm/min]	Tip1/550	Tip1/1100	Tip1/2200
44	11.0	0.3	3.9
66	17.4	3.0	5.0
88	27.7	8.5	2.2
110	19.1	0.3	6.0
132	29.5	6.6	1.8

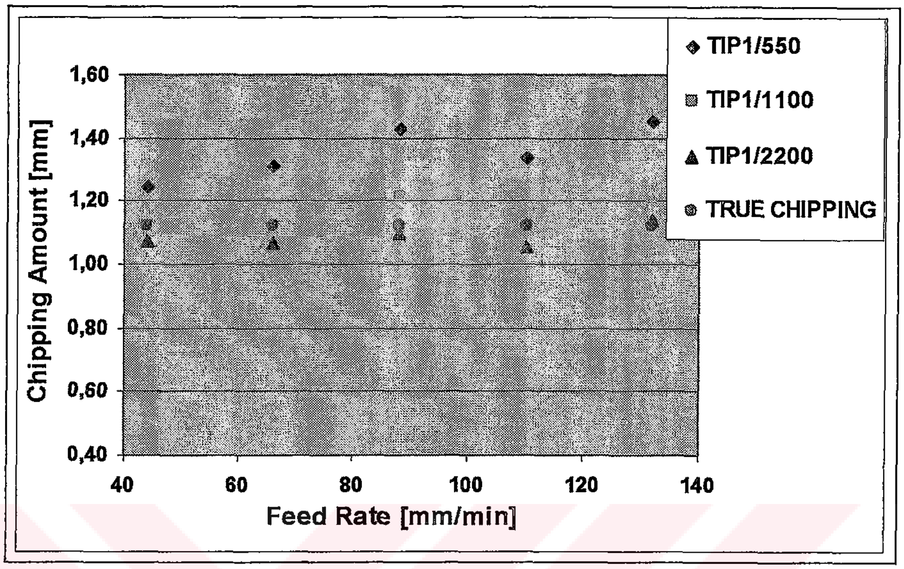

Figure 4.18: Comparison of chipping amount of TIP1 Drill, for spindle speeds 550/1100/2200 [rpm]

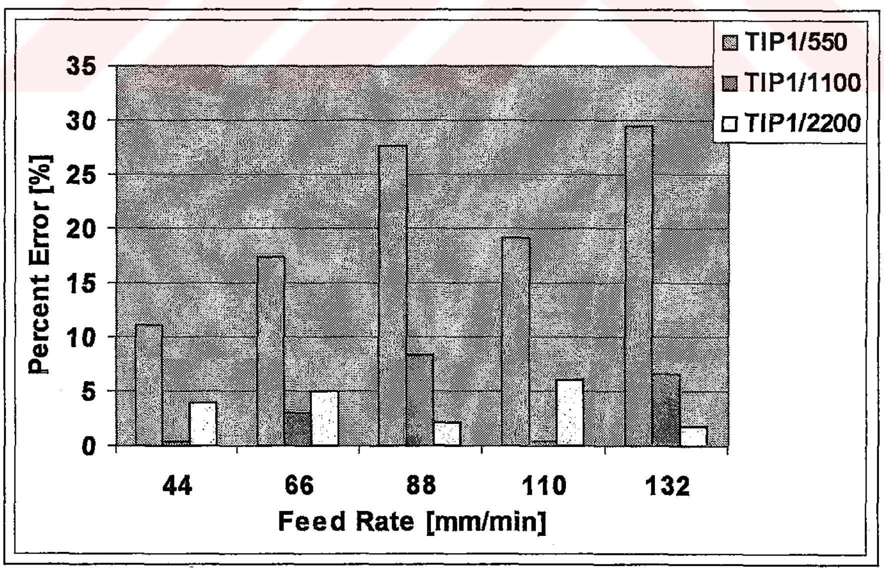

Figure 4.19: Comparison of percent error on chipping length of TIP1 Drill for spindle speeds 550/1100/2200 [rpm]

4.2.2 TIP2 Chipping

TIP2 chipping is the same as TIP1 case only difference is the amount of chipping present in these two cases. The geometry of the drill is the same with the one shown in the Figure 4.1. Cutting force in x directions can be analyzed in three sections.

- Section I: Same properties as Tip1 chipping case. Geometrically speaking, at the end of section I the chisel edge ends.
- Section II: Same regime as Section II in Tip1 chipping case. This section is due to the chipping. Geometrically as the chisel edge ends, cutting lips start to cut. The increase in the cutting force amplitude is due to the fact that when one flute is cutting the other cannot due to chipping therefore fresh flute has to cut the other flute's chip load. End of Section II is useful because it gives the end of chipping portion in the time domain which can be used to calculate the amount of chipping if tip chipping is encountered. Same calculations as mentioned in Tip 1 chipping section apply for this case.
- Section III: After chipped portion is passed, unchipped portion of chipped cutting flute starts cutting, therefore cutting forces shows a decreasing pattern in this section.

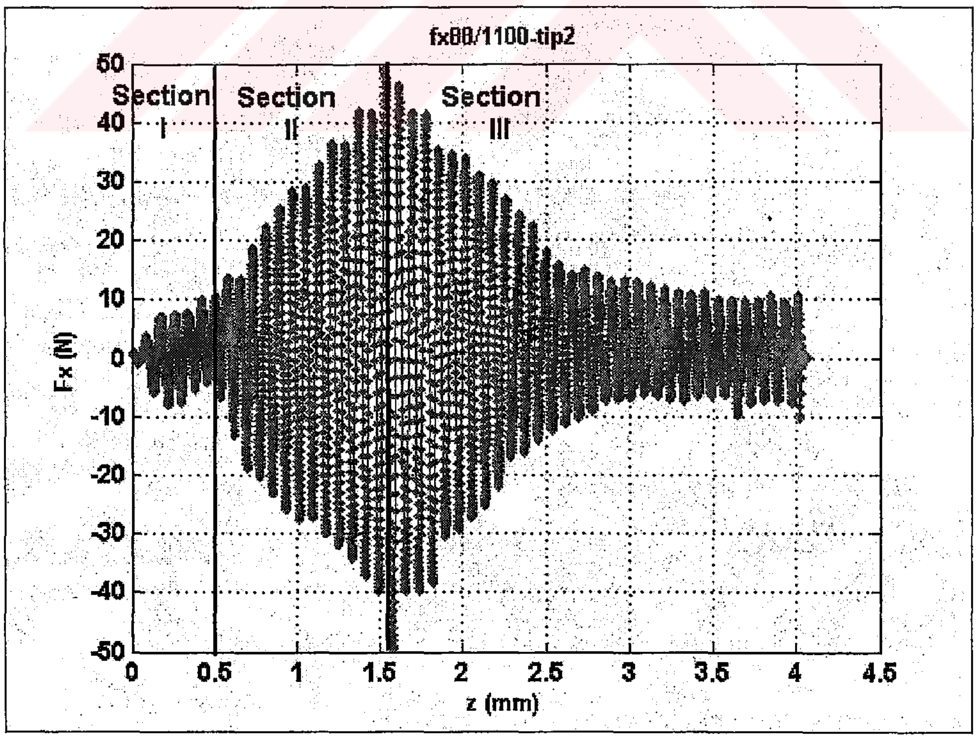

Figure 4.20: Illustration of a measured cutting force in X direction of a TIP2 drill for spindle speed of 1100 [rpm] and feed rate of 88[mm/min].

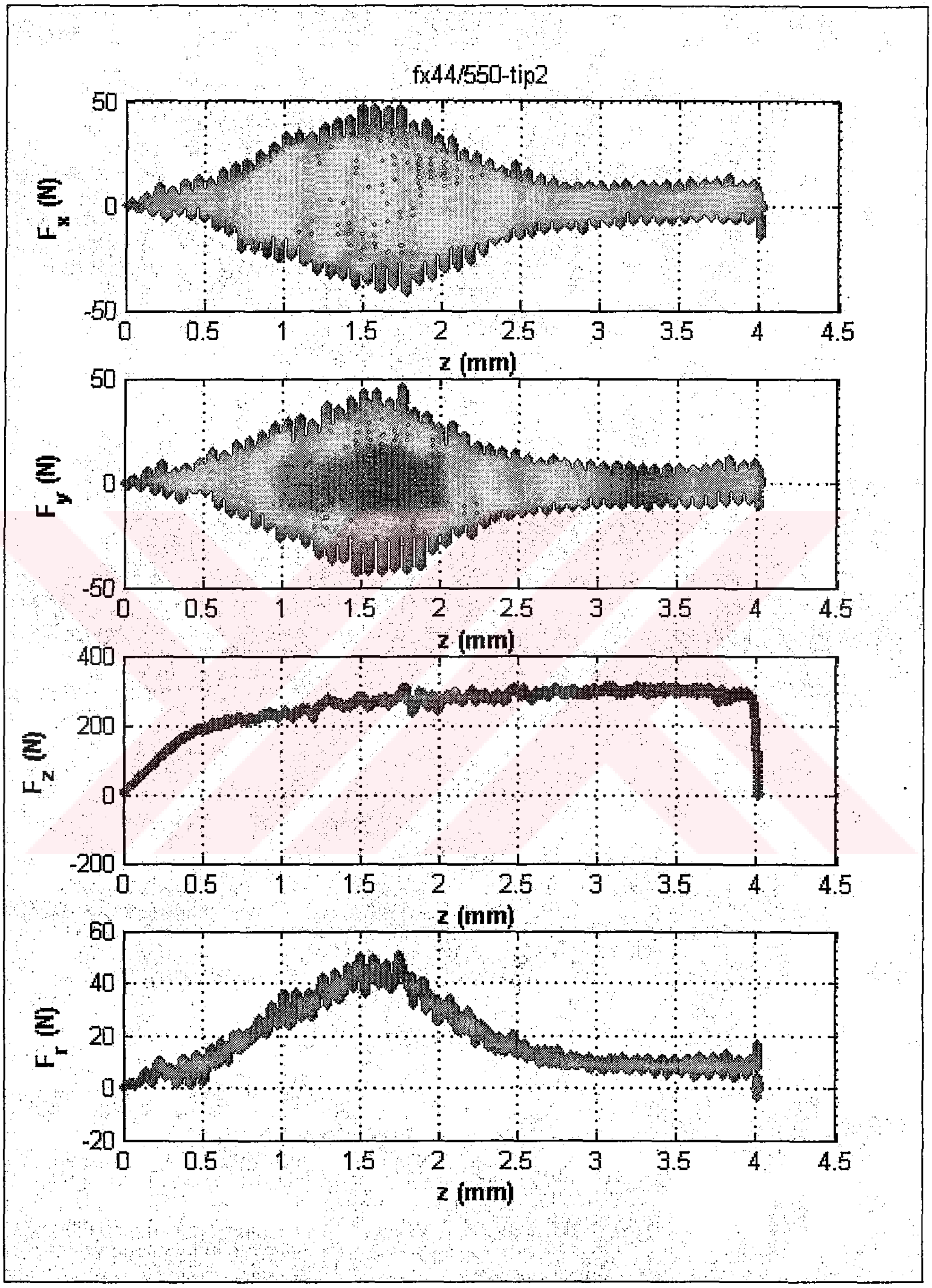

Figure 4.21: Illustration of a measured cutting forces in X, Y, Z and Radial directions of a TIP2 drill for spindle speed of 550 [rpm] and feed rate of 44[mm/min].

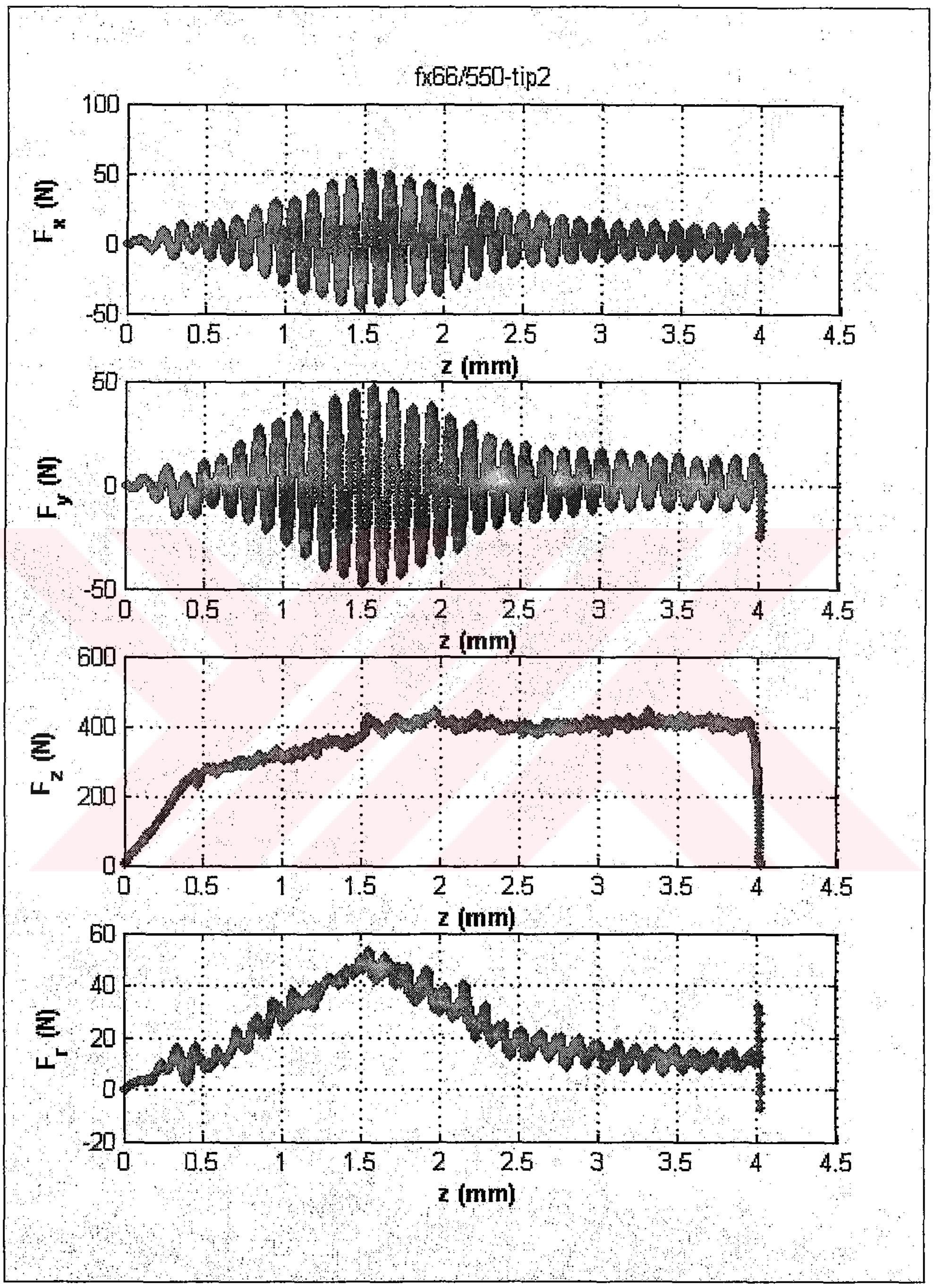

Figure 4.22: Illustration of a measured cutting forces in X, Y, Z and Radial directions of a TIP2 drill for spindle speed of 550 [rpm] and feed rate of 66[mm/min].

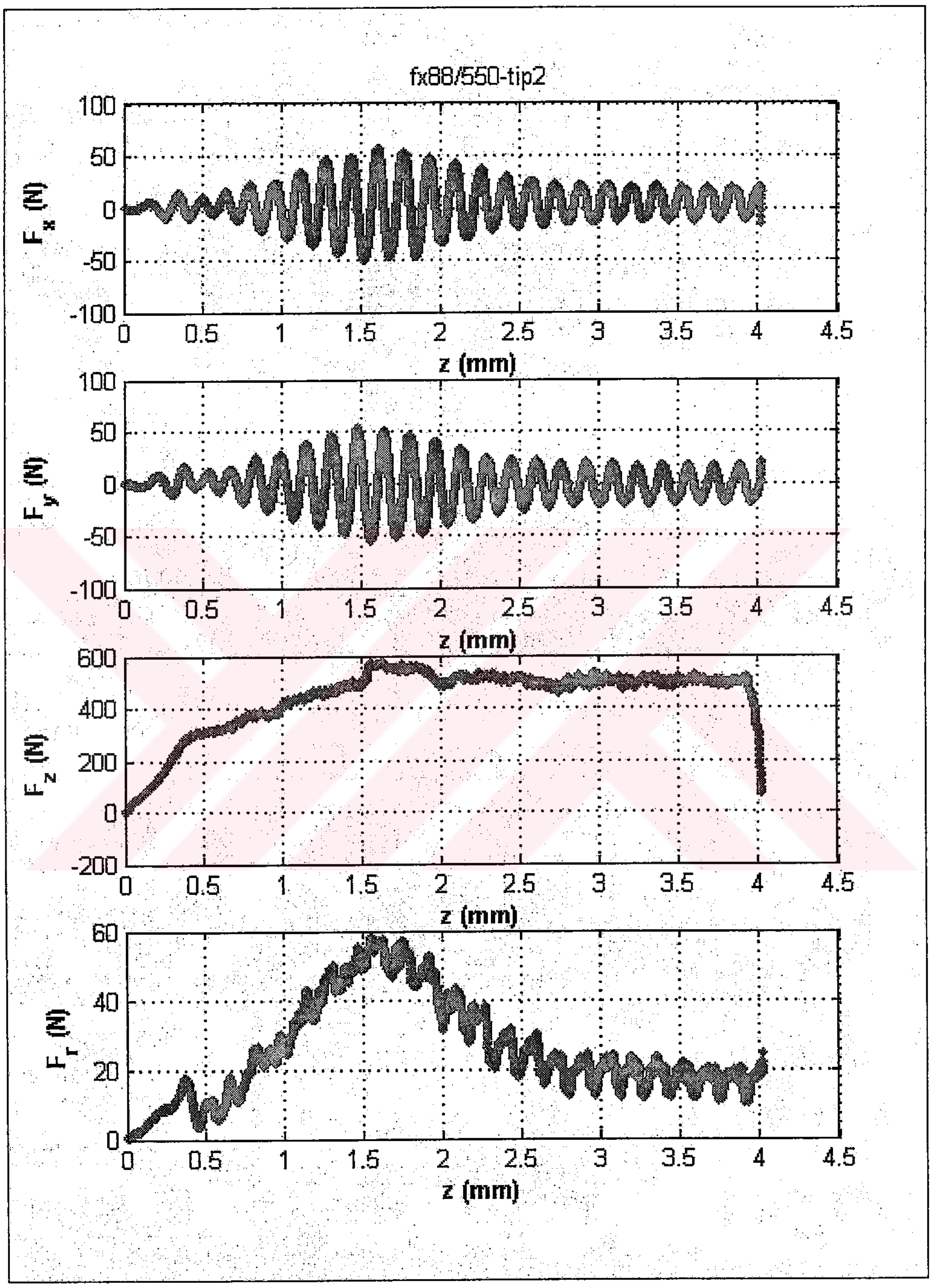

Figure 4.23: Illustration of a measured cutting forces in X, Y, Z and Radial directions of a TIP2 drill for spindle speed of 550 [rpm] and feed rate of 88[mm/min].

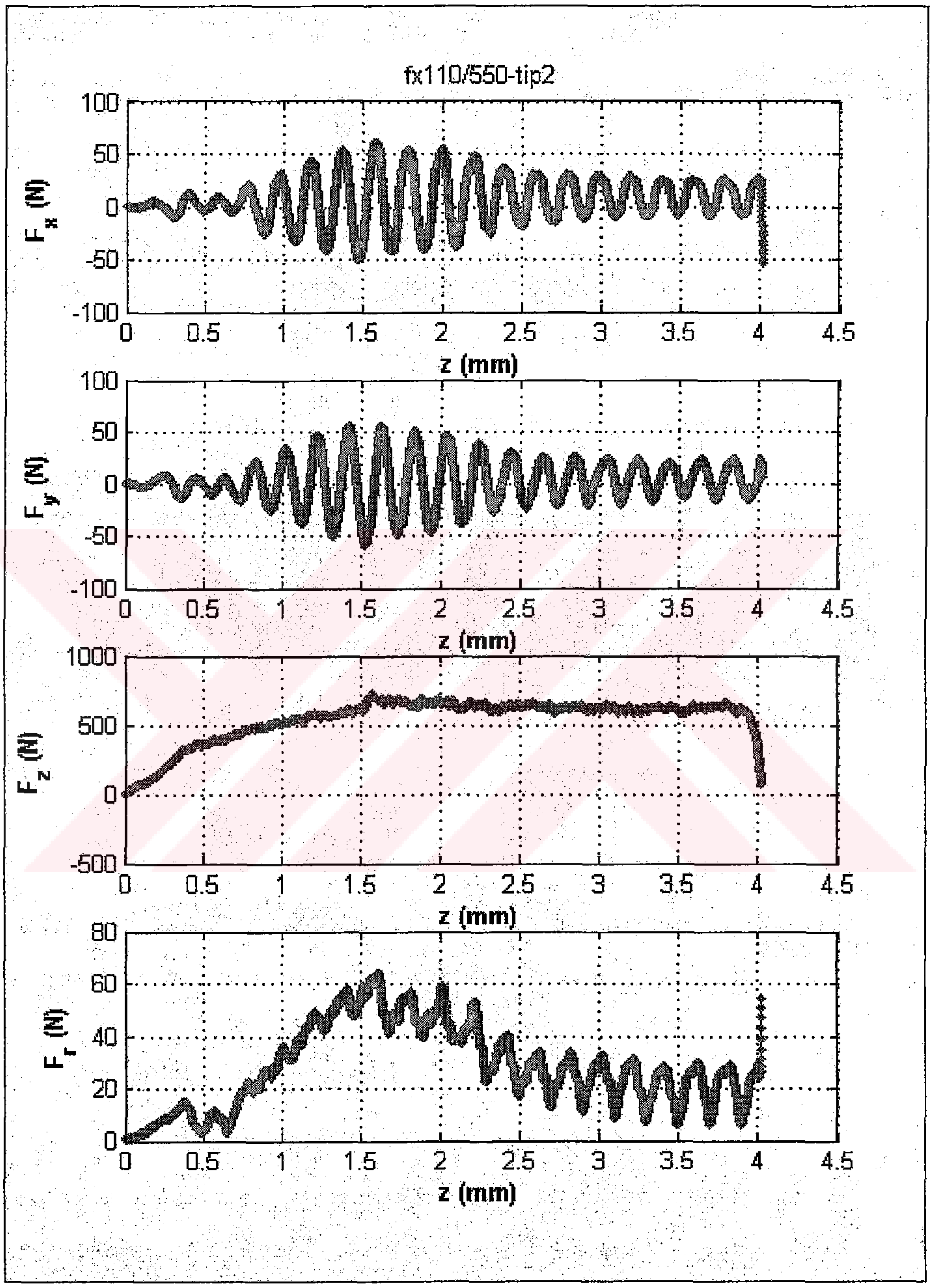

Figure 4.24: Illustration of a measured cutting forces in X, Y, Z and Radial directions of a TIP2 drill for spindle speed of 550 [rpm] and feed rate of 110[mm/min].

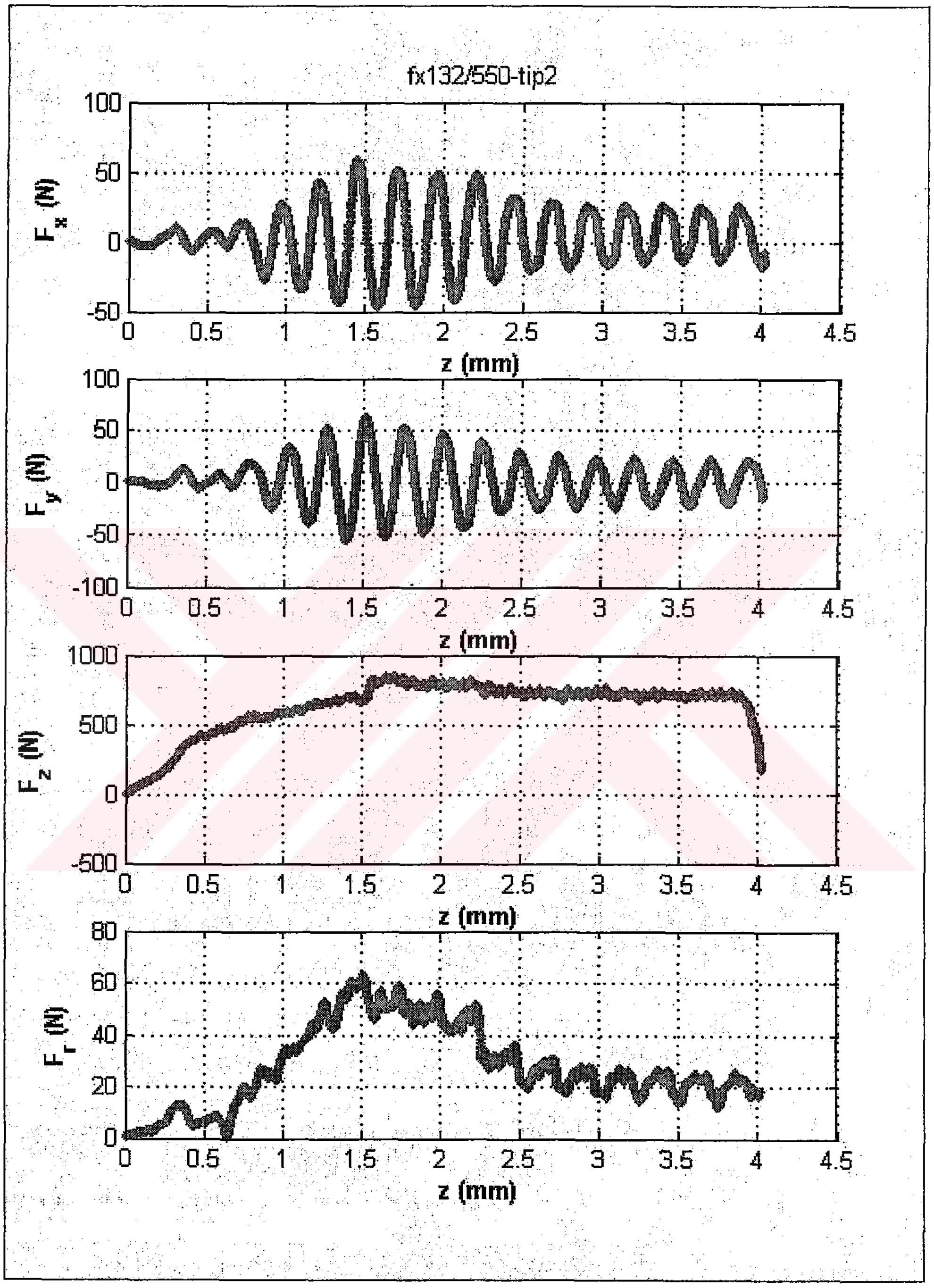

Figure 4.25: Illustration of a measured cutting forces in X, Y, Z and Radial directions of a TIP2 drill for spindle speed of 550 [rpm] and feed rate of 132 [mm/min].

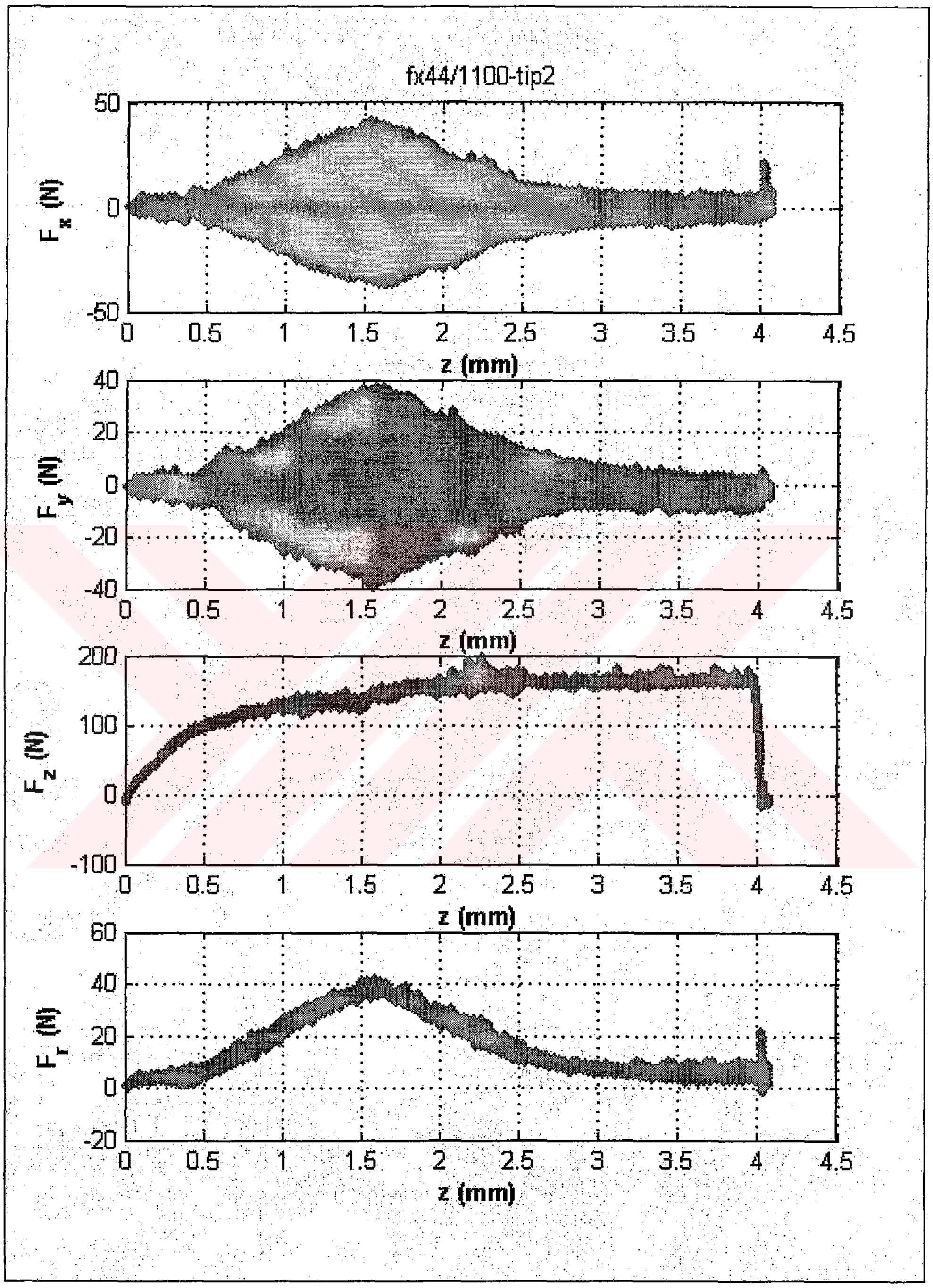

Figure 4.26: Illustration of a measured cutting forces in X, Y, Z and Radial directions of a TIP2 drill for spindle speed of 1100 [rpm] and feed rate of 44 [mm/min].

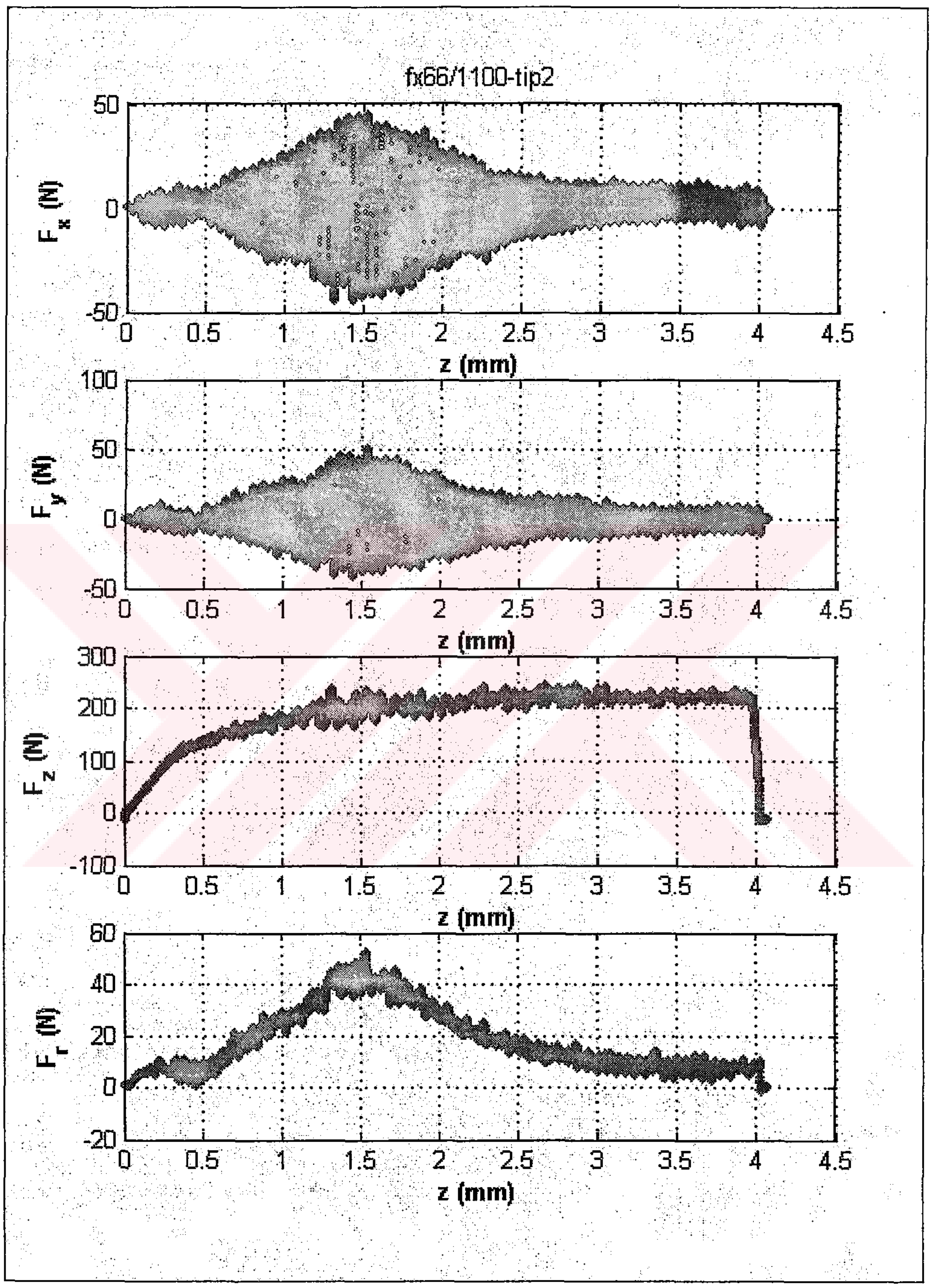

Figure 4.27: Illustration of a measured cutting forces in X, Y, Z and Radial directions of a TIP2 drill for spindle speed of 1100 [rpm] and feed rate of 66 [mm/min].

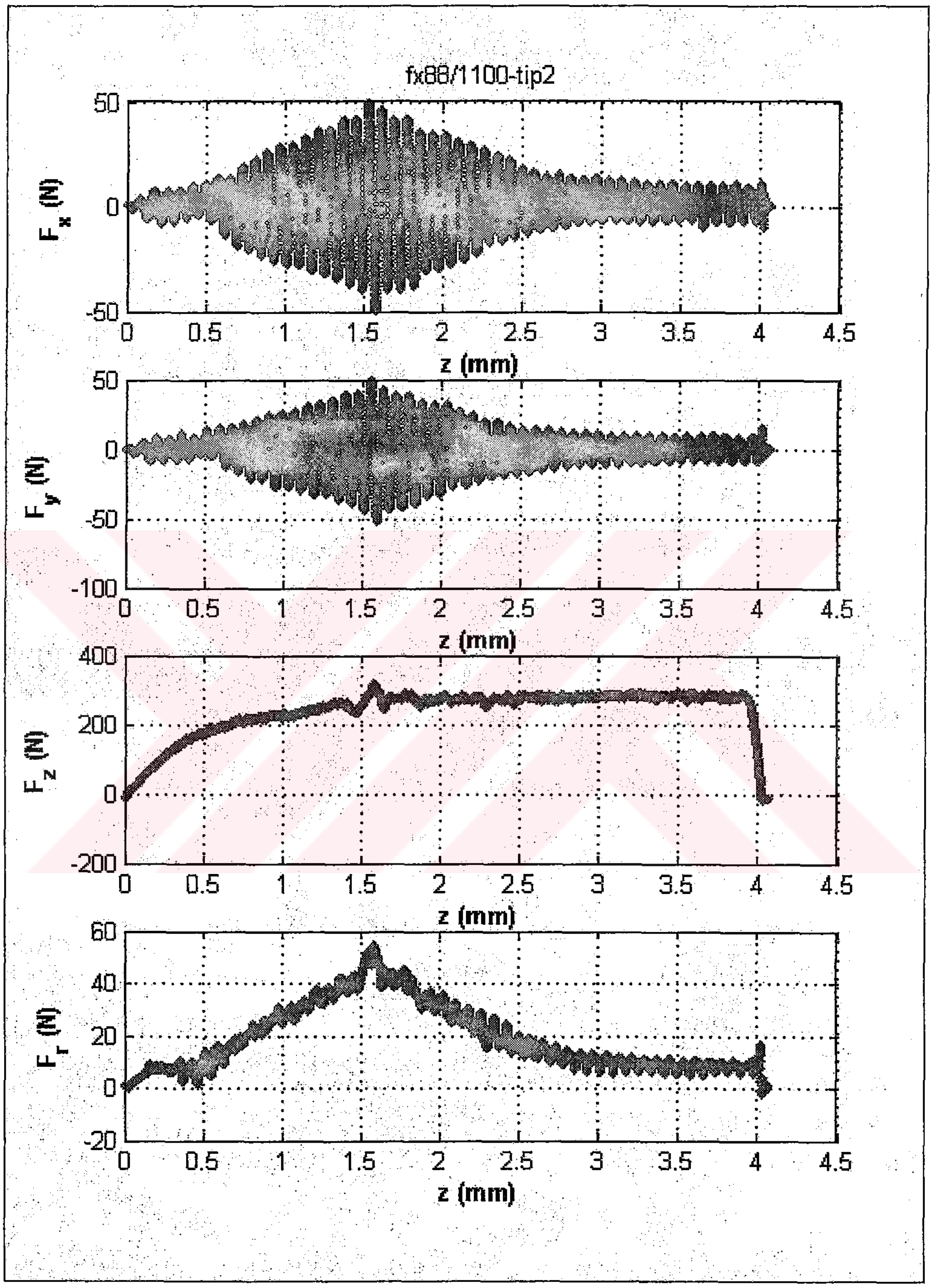

Figure 4.28: Illustration of a measured cutting forces in X, Y, Z and Radial directions of a TIP2 drill for spindle speed of 1100 [rpm] and feed rate of 88 [mm/min].

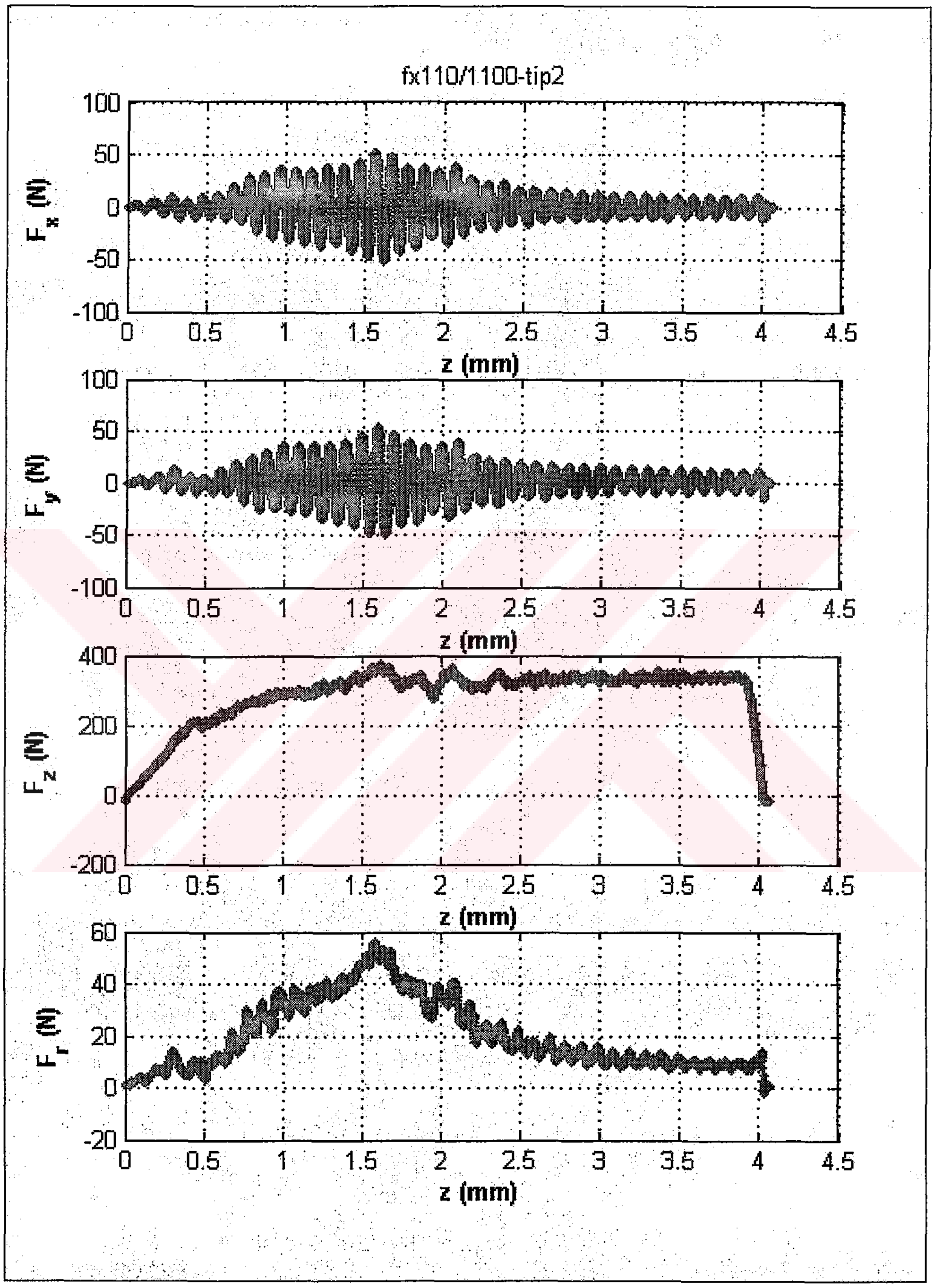

Figure 4.29: Illustration of a measured cutting forces in X, Y, Z and Radial directions of a TIP2 drill for spindle speed of 1100 [rpm] and feed rate of 110 [mm/min].

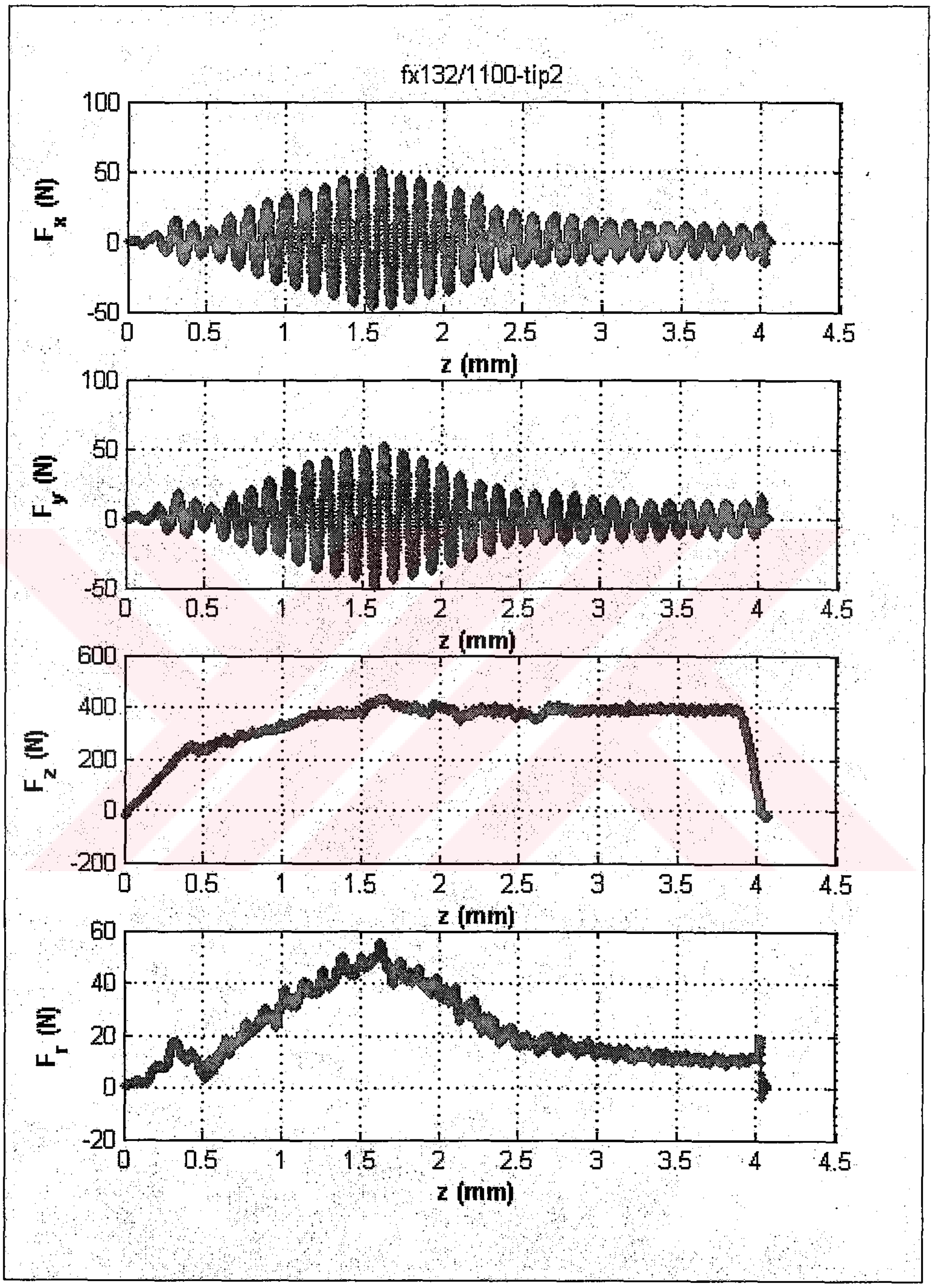

Figure 4.30: Illustration of a measured cutting forces in X, Y, Z and Radial directions of a TIP2 drill for spindle speed of 1100 [rpm] and feed rate of 132 [mm/min].

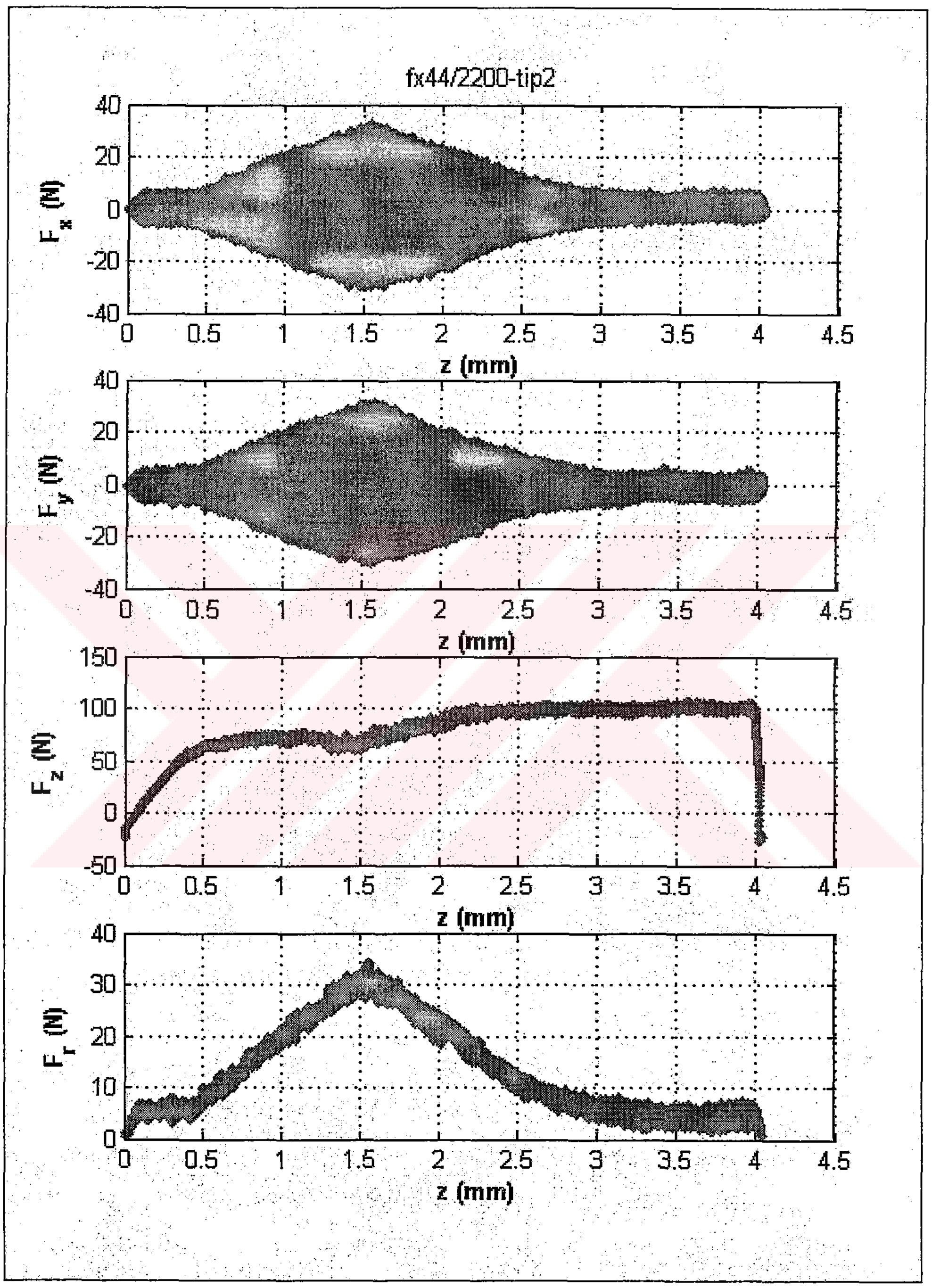

Figure 4.31: Illustration of a measured cutting forces in X, Y, Z and Radial directions of a TIP2 drill for spindle speed of 2200 [rpm] and feed rate of 44 [mm/min].

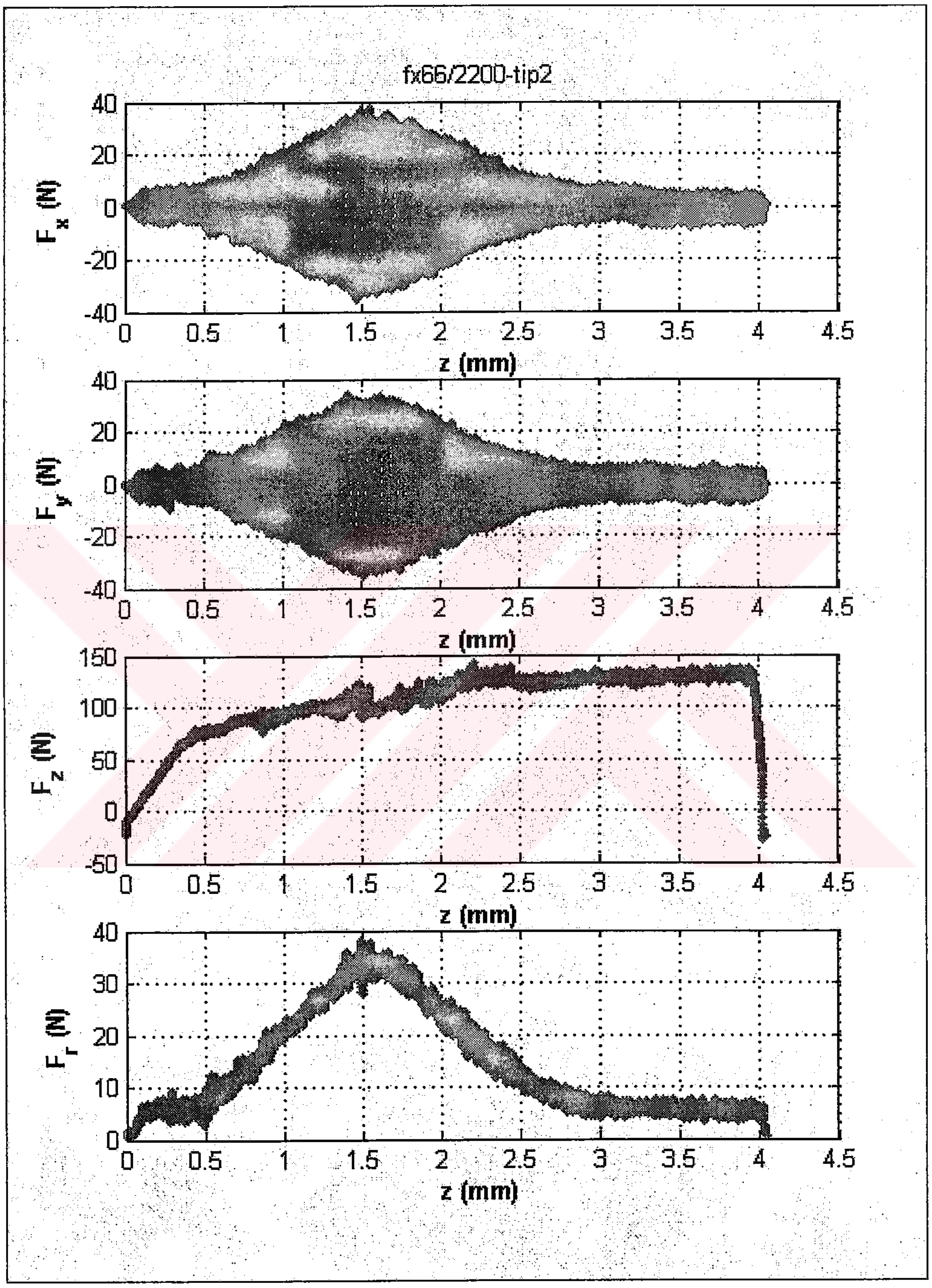

Figure 4.32: Illustration of a measured cutting forces in X, Y, Z and Radial directions of a TIP2 drill for spindle speed of 2200 [rpm] and feed rate of 66 [mm/min].

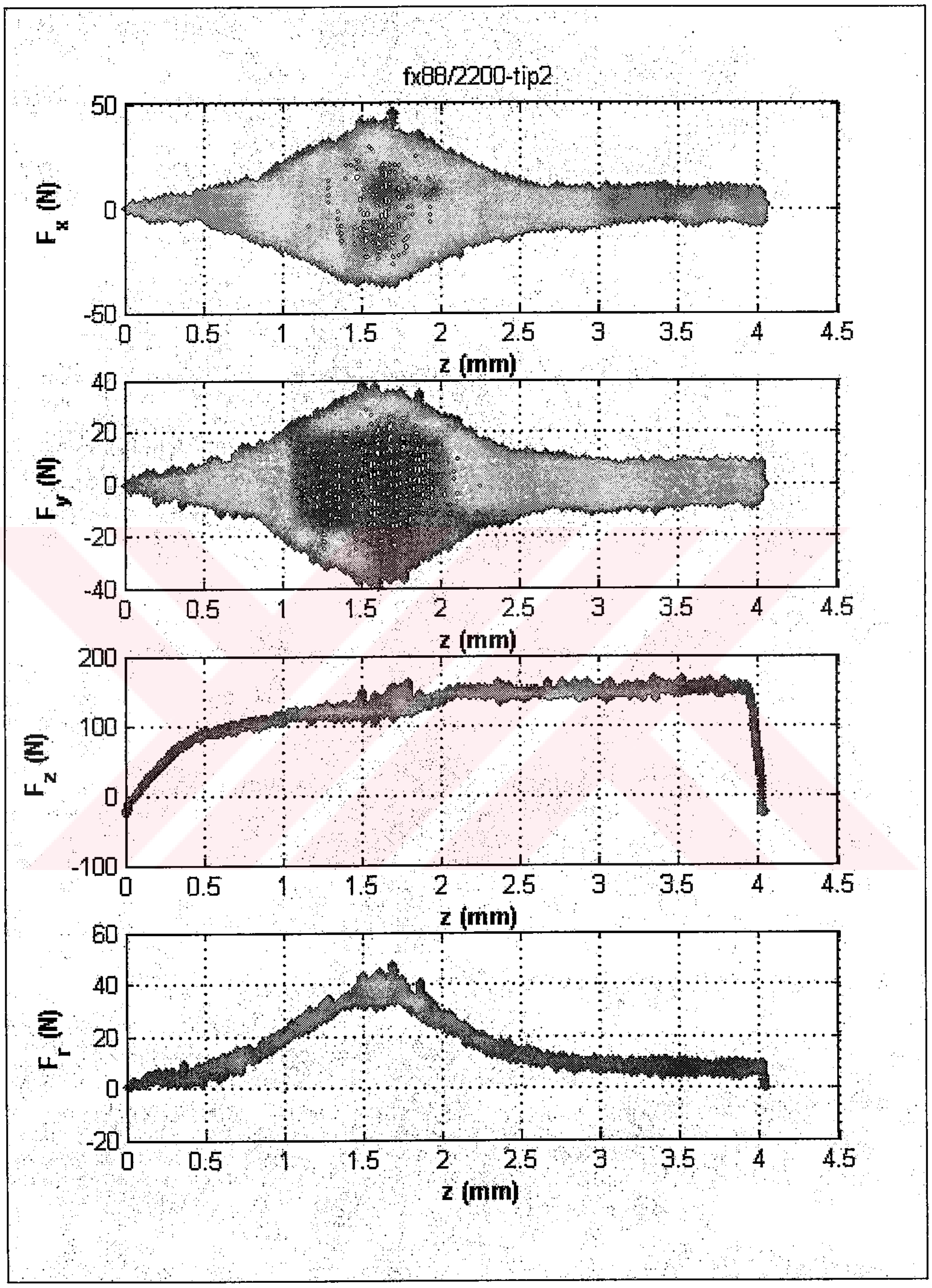

Figure 4.33: Illustration of a measured cutting forces in X, Y, Z and Radial directions of a TIP2 drill for spindle speed of 2200 [rpm] and feed rate of 88 [mm/min].

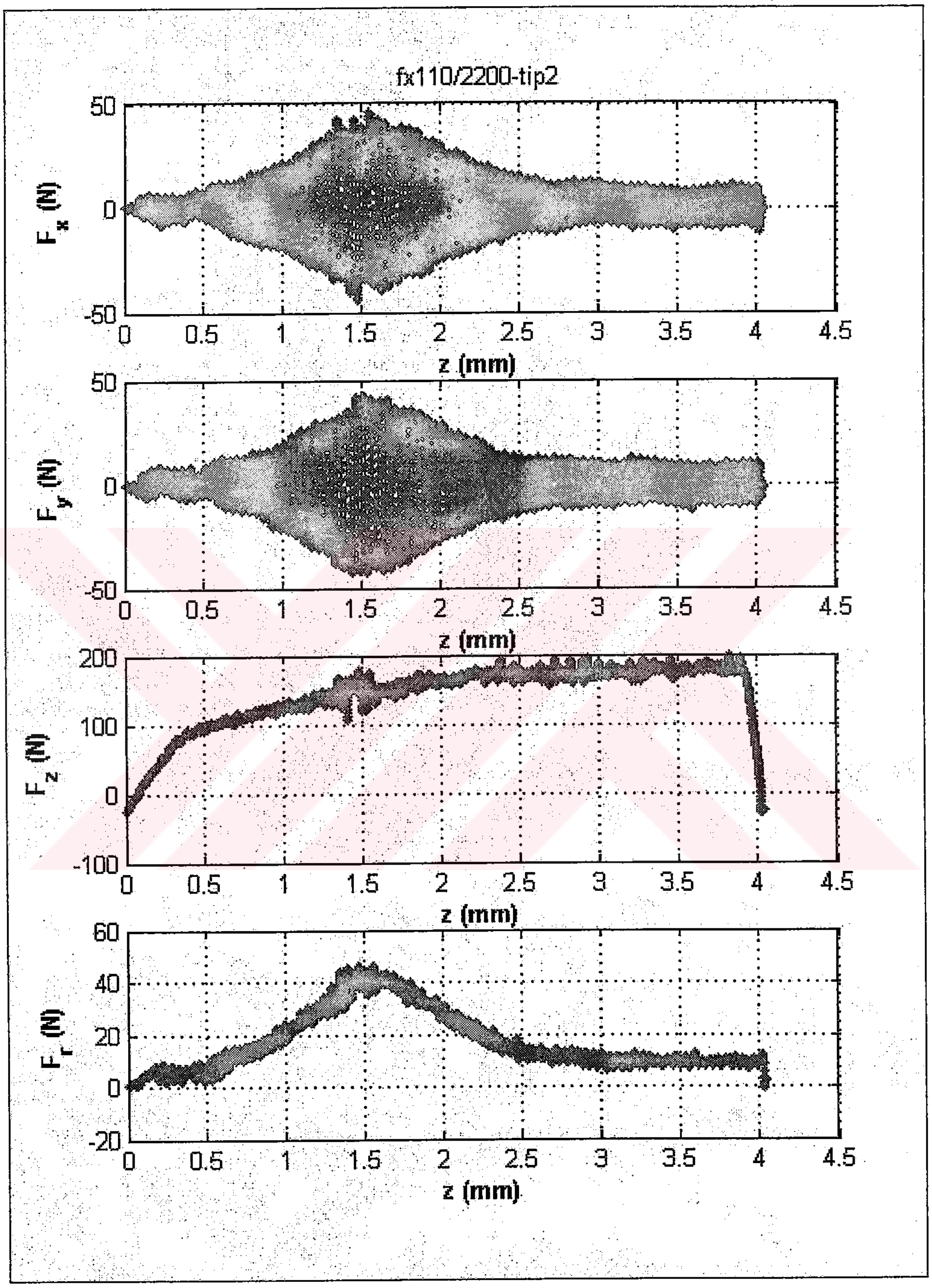

Figure 4.34: Illustration of a measured cutting forces in X, Y, Z and Radial directions of a TIP2 drill for spindle speed of 2200 [rpm] and feed rate of 110 [mm/min].

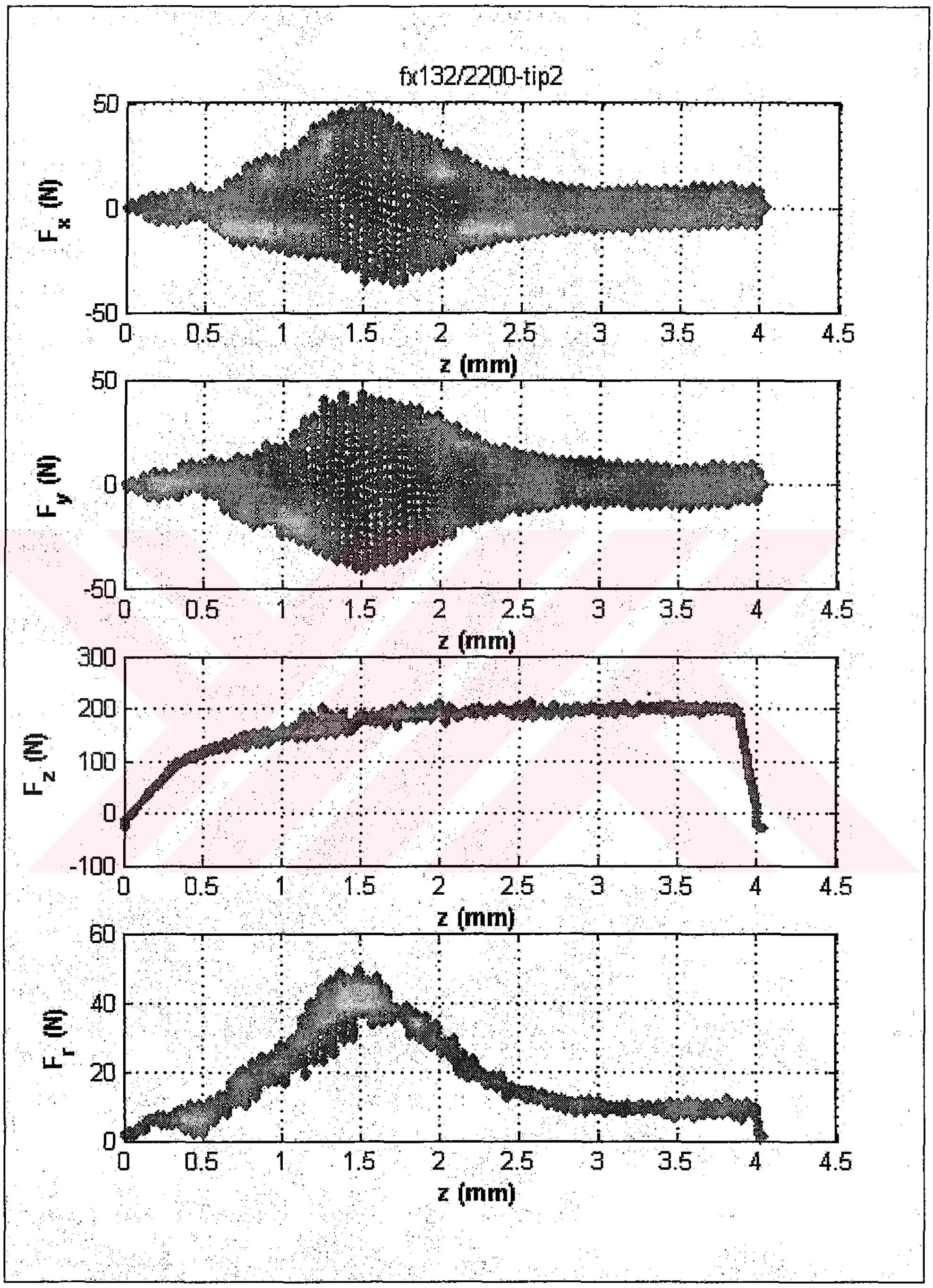

Figure 4.35: Illustration of a measured cutting forces in X, Y, Z and Radial directions of a TIP2 drill for spindle speed of 2200 [rpm] and feed rate of 132 [mm/min].

Table 4.5: The time, depth $\hat{Z}$, $\hat{Z'}$ at which F_x reaches maximum and calculated chipping amount for TIP2 drill, for spindle speed of 550[rpm].

Feed Rate [mm/min]	Time [sec]	$\hat{Z}$ [mm]	$\hat{Z'}$ [mm]	Chipping Calculated [mm]	True Chipping [mm]
44	2.045	1.500	2.918	2.008	2.1
66	1.400	1.540	2.996	2.086	2.1
88	1.095	1.606	3.125	2.215	2.1
110	0.863	1.583	3.080	2.170	2.1
132	0.719	1.582	3.078	2.168	2.1

Table 4.6: The time, depth $\hat{Z}$, $\hat{Z'}$ at which F_x reaches maximum and calculated chipping amount for TIP2 drill, for spindle speed of 1100 [rpm].

Feed Rate [mm/min]	Time [sec]	$\hat{Z}$ [mm]	$\hat{Z'}$ [mm]	Chipping Calculated [mm]	True Chipping [mm]
44	2.093	1.535	2.987	2.077	2.1
66	1.385	1.523	2.963	2.053	2.1
88	1.044	1.531	2.979	2.069	2.1
110	0.855	1.567	3.049	2.139	2.1
132	0.730	1.606	3.125	2.215	2.1

Table 4.7: The time, depth $\hat{Z}$, $\hat{Z'}$ at which F_x reaches maximum and calculated chipping amount for TIP2 drill, spindle speed of 2200 [rpm].

Feed Rate [mm/min]	Time [sec]	$\hat{Z}$ [mm]	$\hat{Z'}$ [mm]	Chipping Calculated [mm]	True Chipping [mm]
44	2.105	1.544	3.004	2.094	2.1
66	1.406	1.547	3.010	2.100	2.1
88	1.072	1.572	3.059	2.149	2.1
110	0.848	1.554	3.024	2.114	2.1
132	0.680	1.495	2.909	1.999	2.1

Table 4.8: Percent Error (%) in calculated chipping amount for spindle speed of 550/1100/2200 [rpm] of TIP2 drill.

Feed Rate [mm/min]	Tip2/550	Tip2/1100	Tip2/2200
44	4.359	1.116	0.282
66	0.653	2.228	0.004
88	5.462	1.486	2.312
110	3.331	1.849	0.645
132	3.220	5.462	4.822

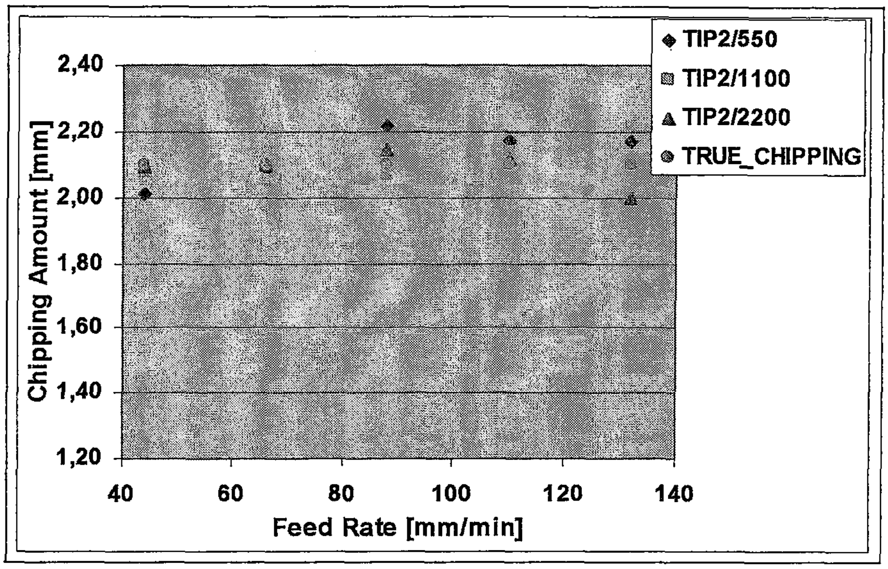

Figure 4.36: Comparison of chipping amount [mm] of TIP2 drill, for spindle speeds 550/1100/2200 [rpm]

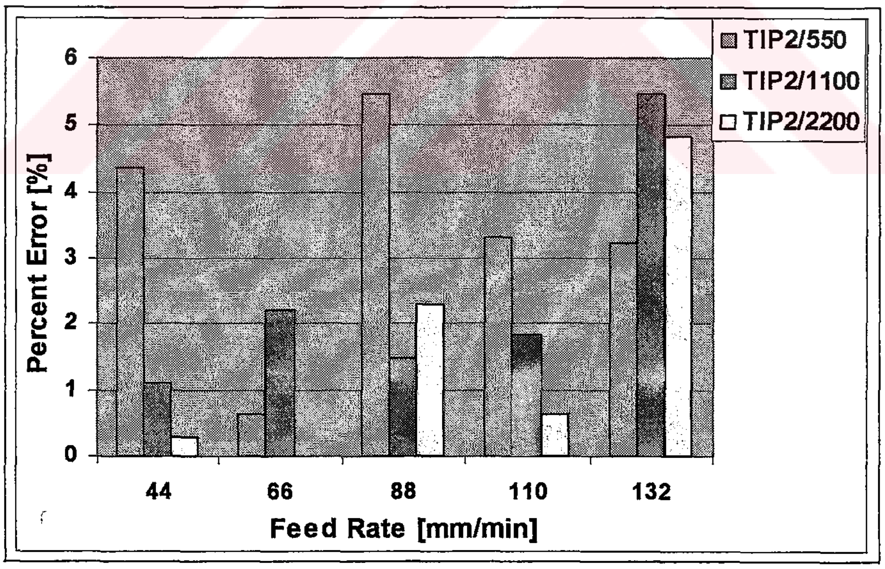

Figure 4.37: Comparison of percent error (%) of TIP2 Drill for spindle speeds 550/1100/2200 [rpm]

4.3 Shank Chipping

Another chipping case is shank chipping case. Shank chipping has a property that it starts from the point where the cutting flute and shank of the drill meet and lying along the cutting edge. As it can be seen from the Figure 4.38, the cutting edge can be analyzed in three sections. First one is chisel edge cutting region, the other one is unchipped portion which starts at the end of chisel edge and lays along the cutting edge to the start of chipping, the last section is chipped portion which starts at the end of unchipped portion and ends as the shank of the drill.

Figure 4.38: Illustration of a drill with a shank chipping induced

The cutting force in X directions can be analyzed in two sections. Section I coincides with chisel edge and unchipped portion of the drill geometrically. As it is seen in the Figure 4.39, first section shows a nearly constant cutting force pattern. Cutting force shows an increasing pattern in Section II This section includes the chipped portion of the drill. Therefore the increase in the cutting force can be explained as one flute will cut the other chipped flute's chip load. There exists an interesting observation that the maximum of the cutting force happens to be at not the full engagement point of the drill but later than that.

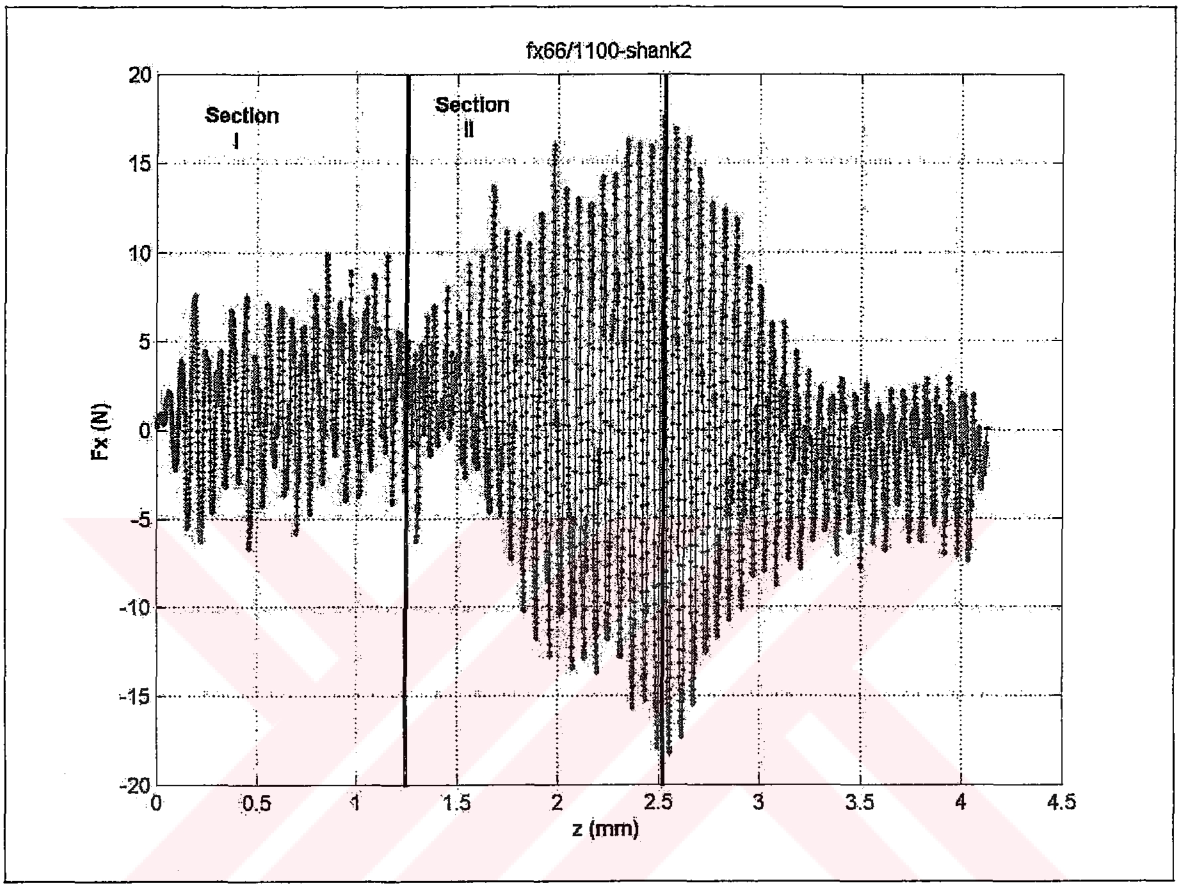

Figure 4.39: Illustration of a measured cutting force in X directions of a SHANK2 Drill for spindle speed of 1100 [rpm] and feed rate 66 [mm/min].

The figures below are the experiment results of the SHANK2 chipping case. The figures are plotted for all cutting force components (F_x, F_y, F_z and F_r) and spindle speeds 550 [rpm], 1100 [rpm] and 2200 [rpm] respectively. Each spindle speed configuration includes feed rates 44-6-88-110-132 [mm/min].

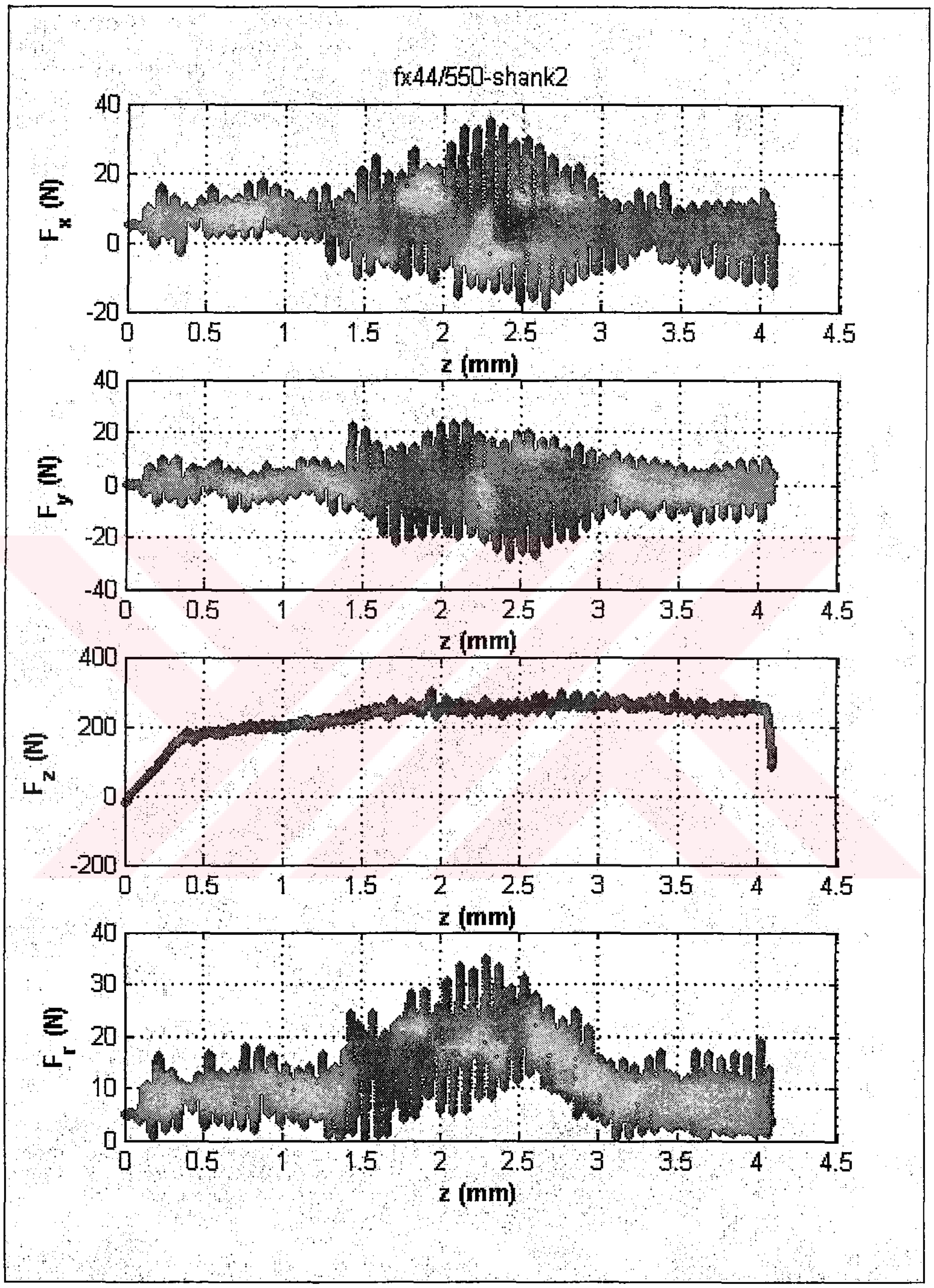

Figure 4.40: Illustration of a measured cutting forces in X, Y, Z and Radial directions of a SHANK2 drill for spindle speed 550 [rpm] and feed rate of 44[mm/min].

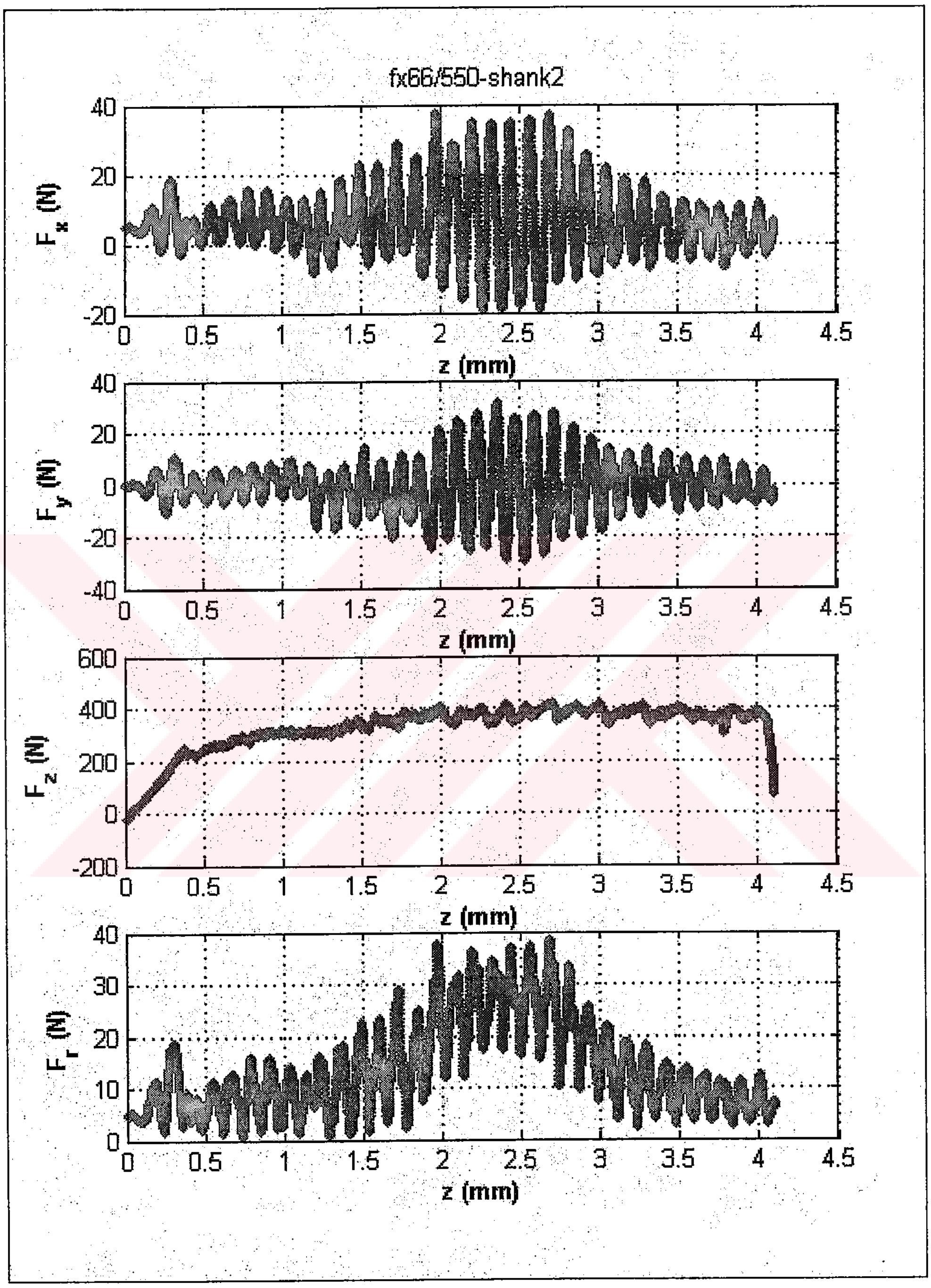

Figure 4.41: Illustration of a measured cutting forces in X, Y, Z and Radial directions of a SHANK2 Drill for spindle speed 550 [rpm] and feed rate of 66 [mm/min].

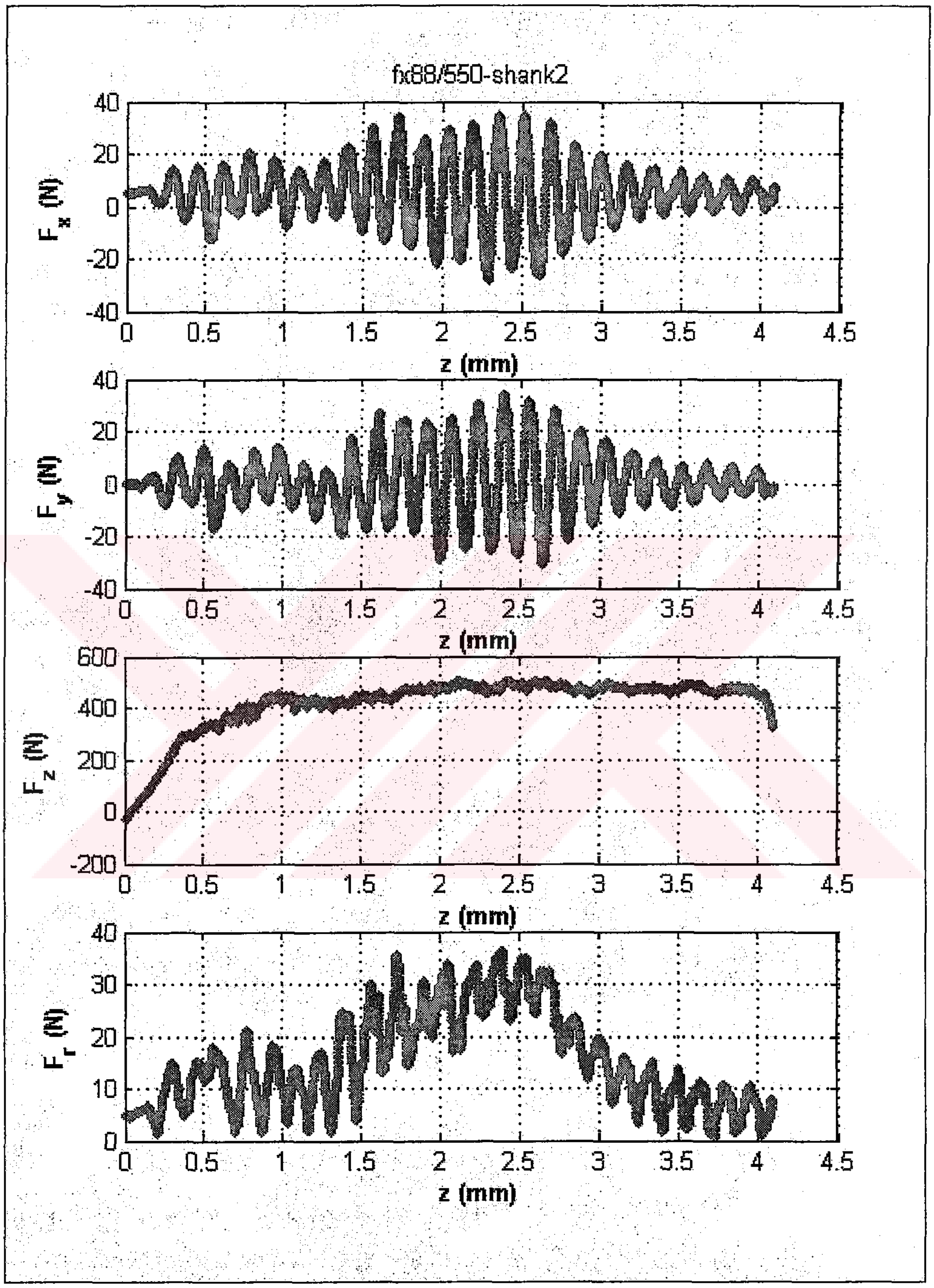

Figure 4.42: Illustration of a measured cutting forces in X, Y, Z and Radial directions of a SHANK2 Drill for spindle speed 550 [rpm] and feed rate of 88 [mm/min].

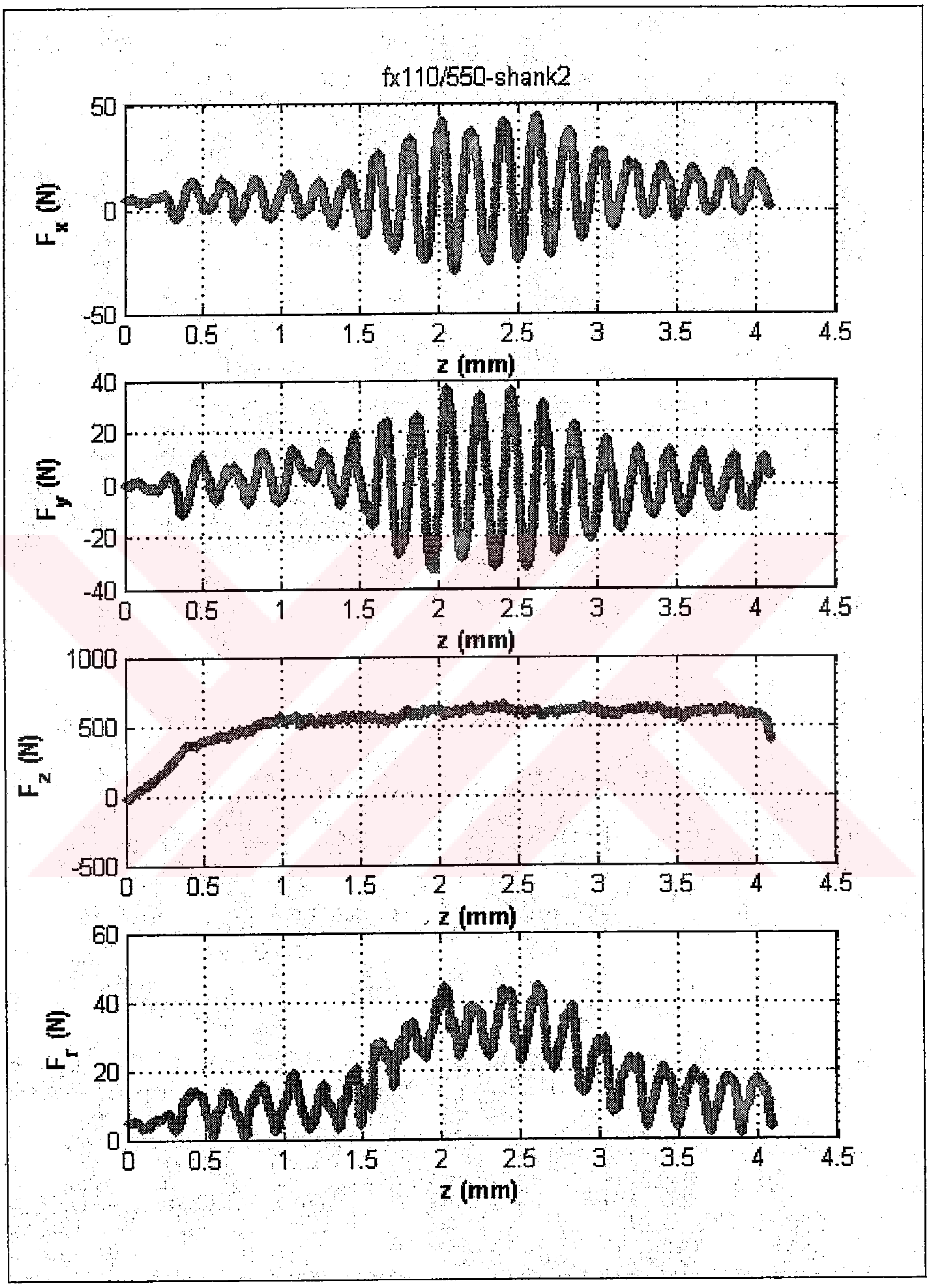

Figure 4.43: Illustration of a measured cutting forces in X, Y, Z and Radial directions of a SHANK2 Drill for spindle speed 550 [rpm] and feed rate of 110 [mm/min].

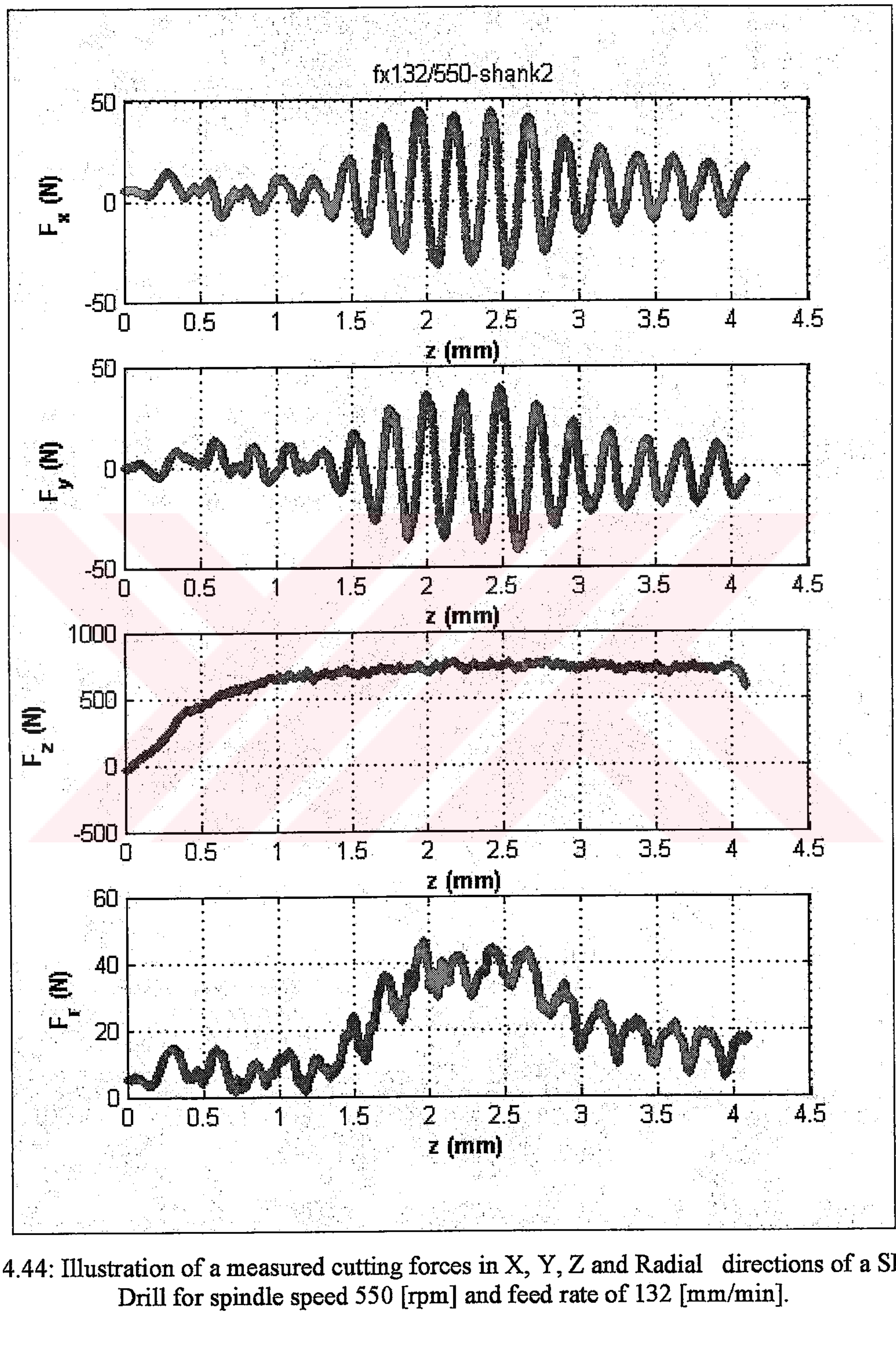

Figure 4.44: Illustration of a measured cutting forces in X, Y, Z and Radial directions of a SHANK2 Drill for spindle speed 550 [rpm] and feed rate of 132 [mm/min].

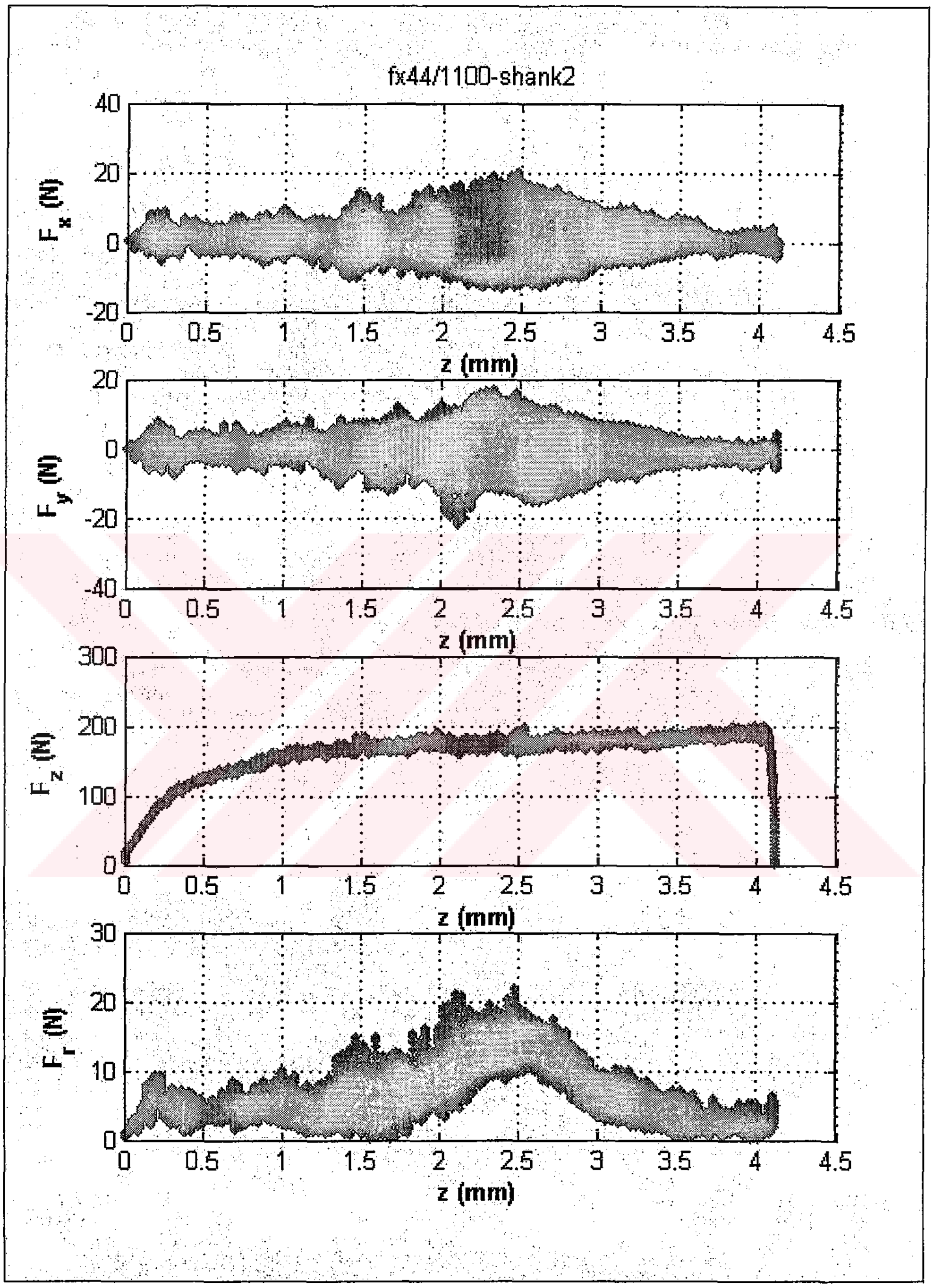

Figure 4.45: Illustration of a measured cutting forces in X, Y, Z and Radial directions of a SHANK2 Drill for spindle speed 1100 [rpm] and feed rate of 44 [mm/min].

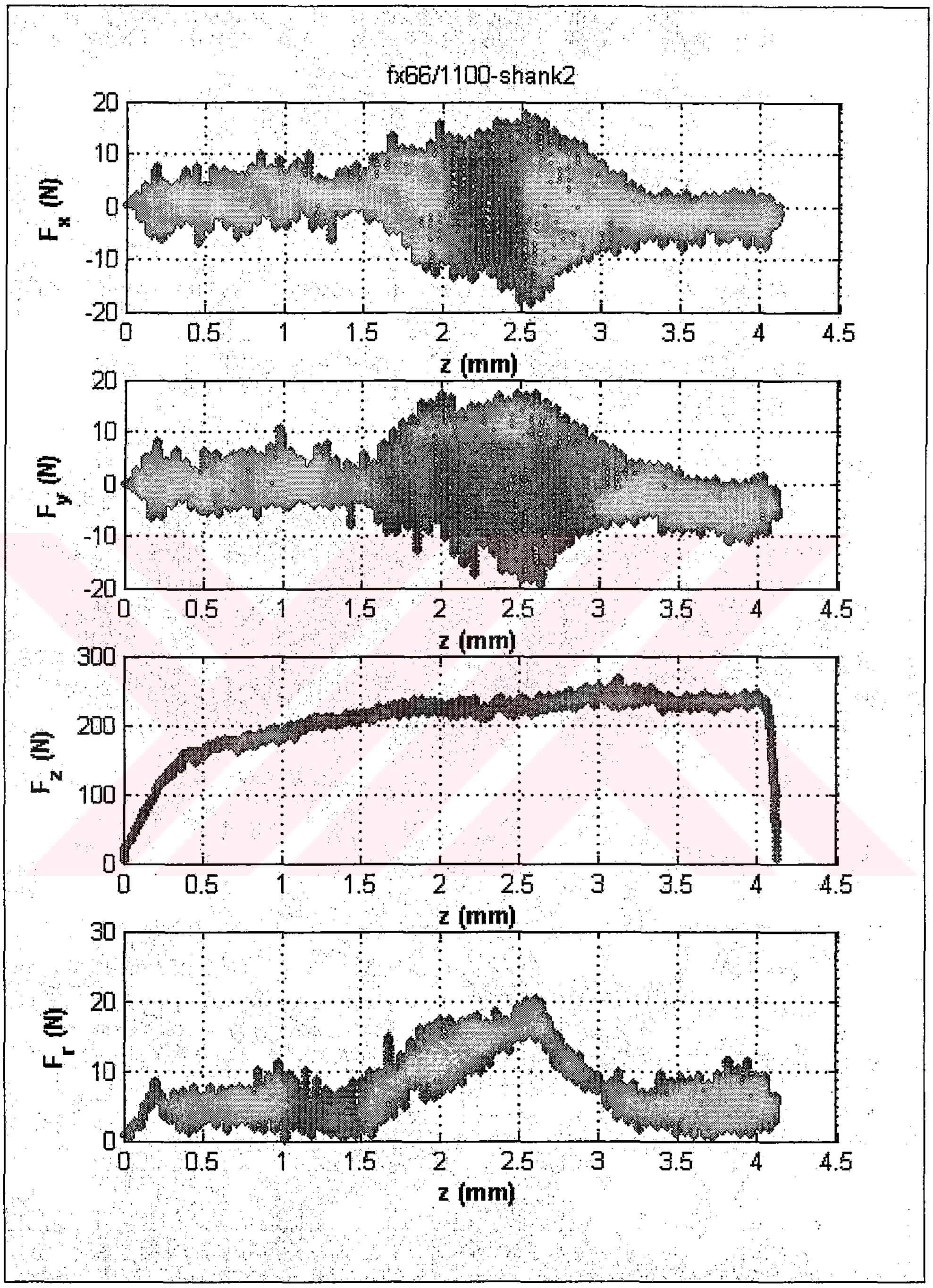

Figure 4.46: Illustration of a measured cutting forces in X, Y, Z and Radial directions of a SHANK2 Drill for spindle speed 1100 [rpm] and feed rate of 66 [mm/min].

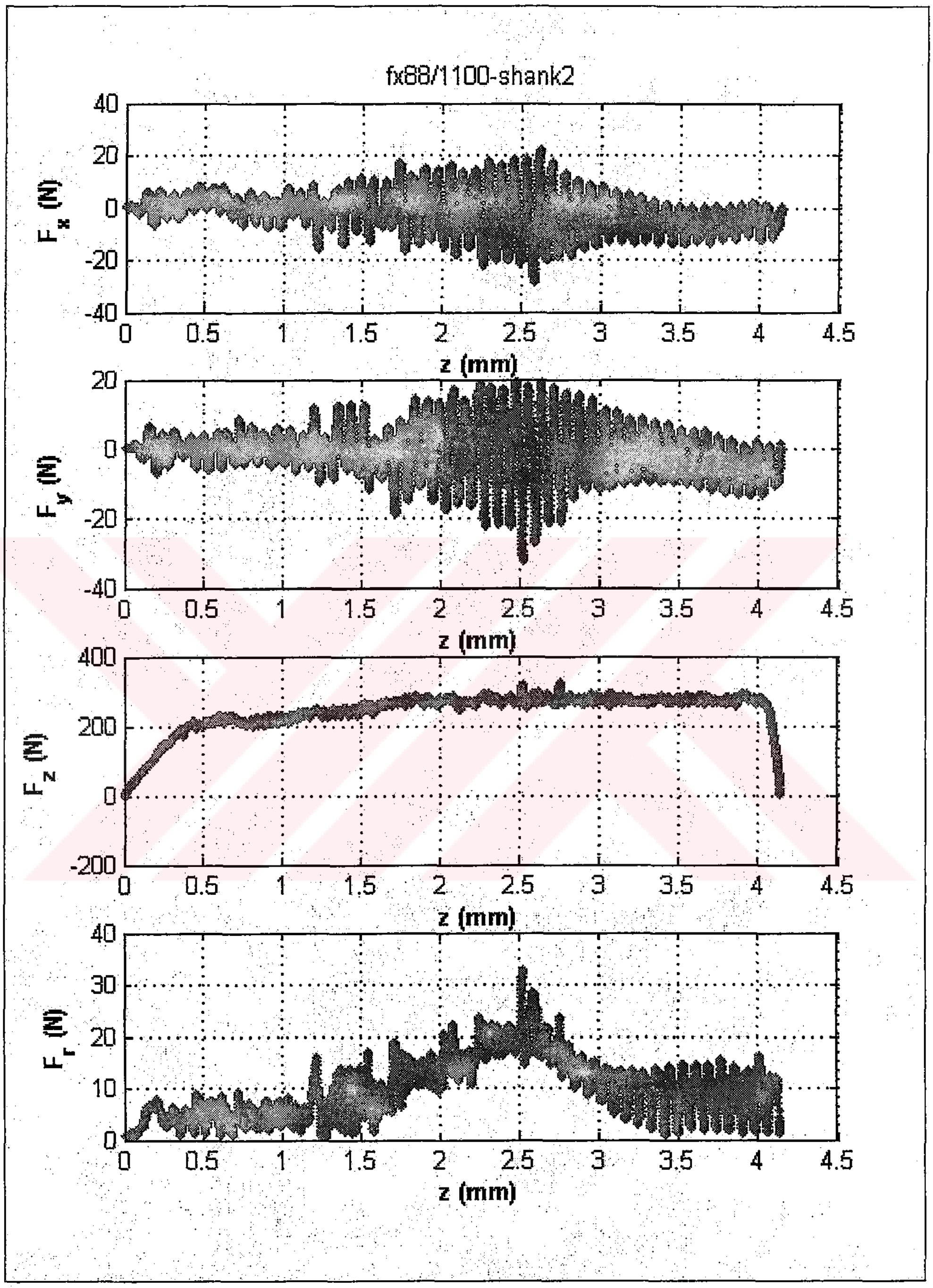

Figure 4.47: Illustration of a measured cutting forces in X, Y, Z and Radial directions of a SHANK2 Drill for spindle speed 1100 [rpm] and feed rate of 88 [mm/min].

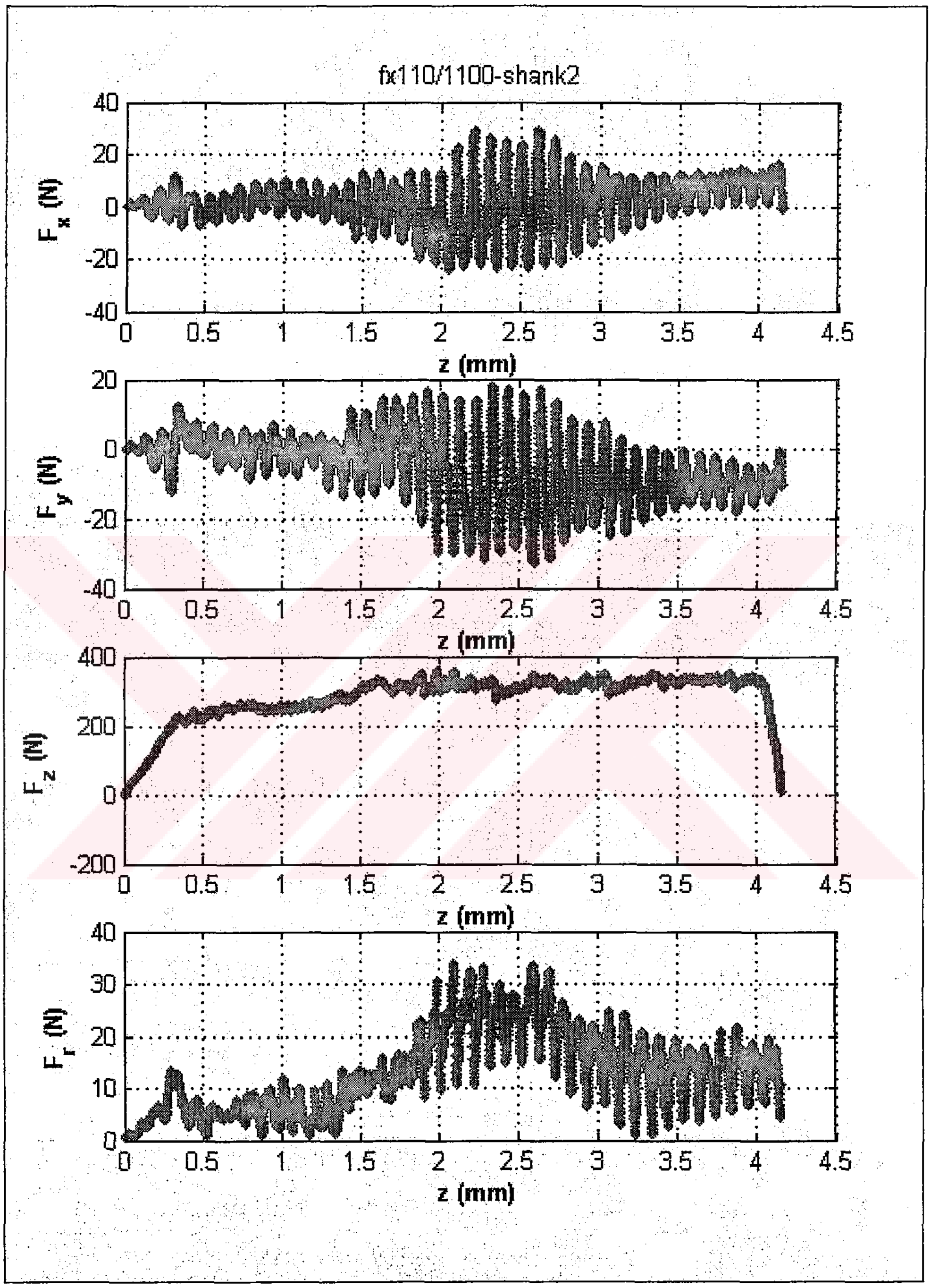

Figure 4.48: Illustration of a measured cutting forces in X, Y, Z and Radial directions of a SHANK2 Drill for spindle speed 1100 [rpm] and feed rate of 110 [mm/min].

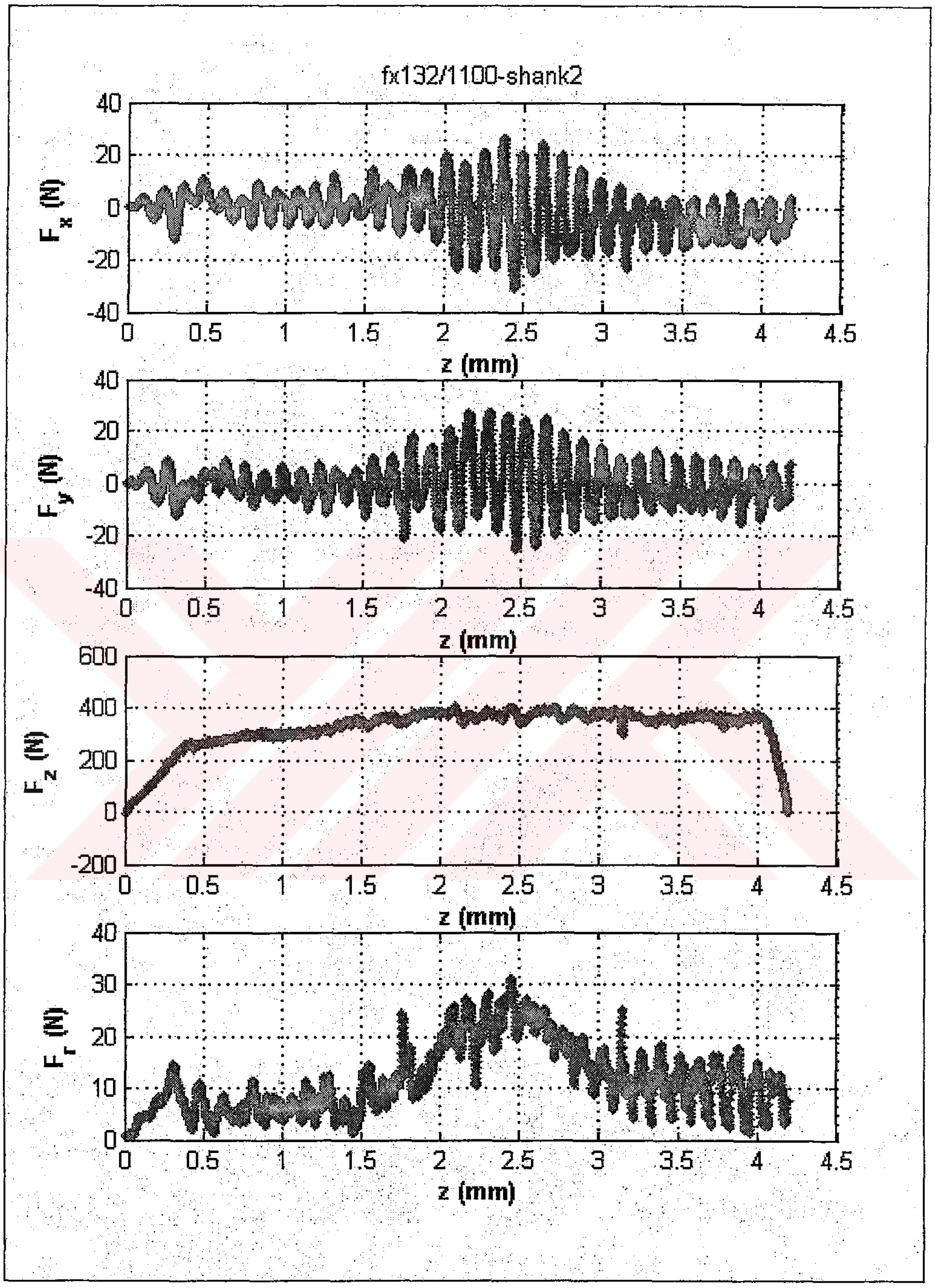

Figure 4.49: Illustration of a measured cutting forces in X, Y, Z and Radial directions of a SHANK2 Drill for spindle speed 1100 [rpm] and feed rate of 132 [mm/min].

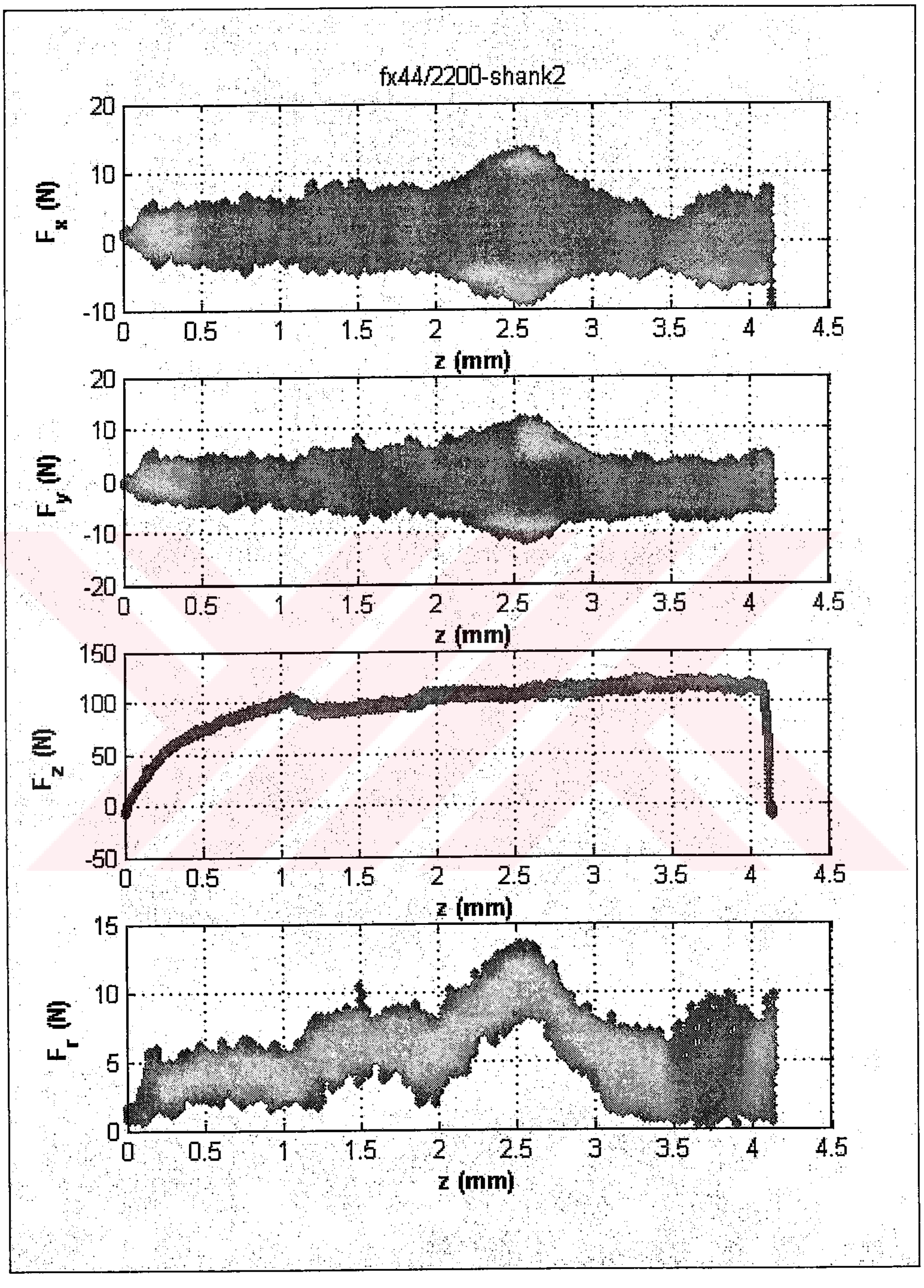

Figure 4.50: Illustration of a measured cutting forces in X, Y, Z and Radial directions of a SHANK2 Drill for spindle speed 2200 [rpm] and feed rate of 44 [mm/min].

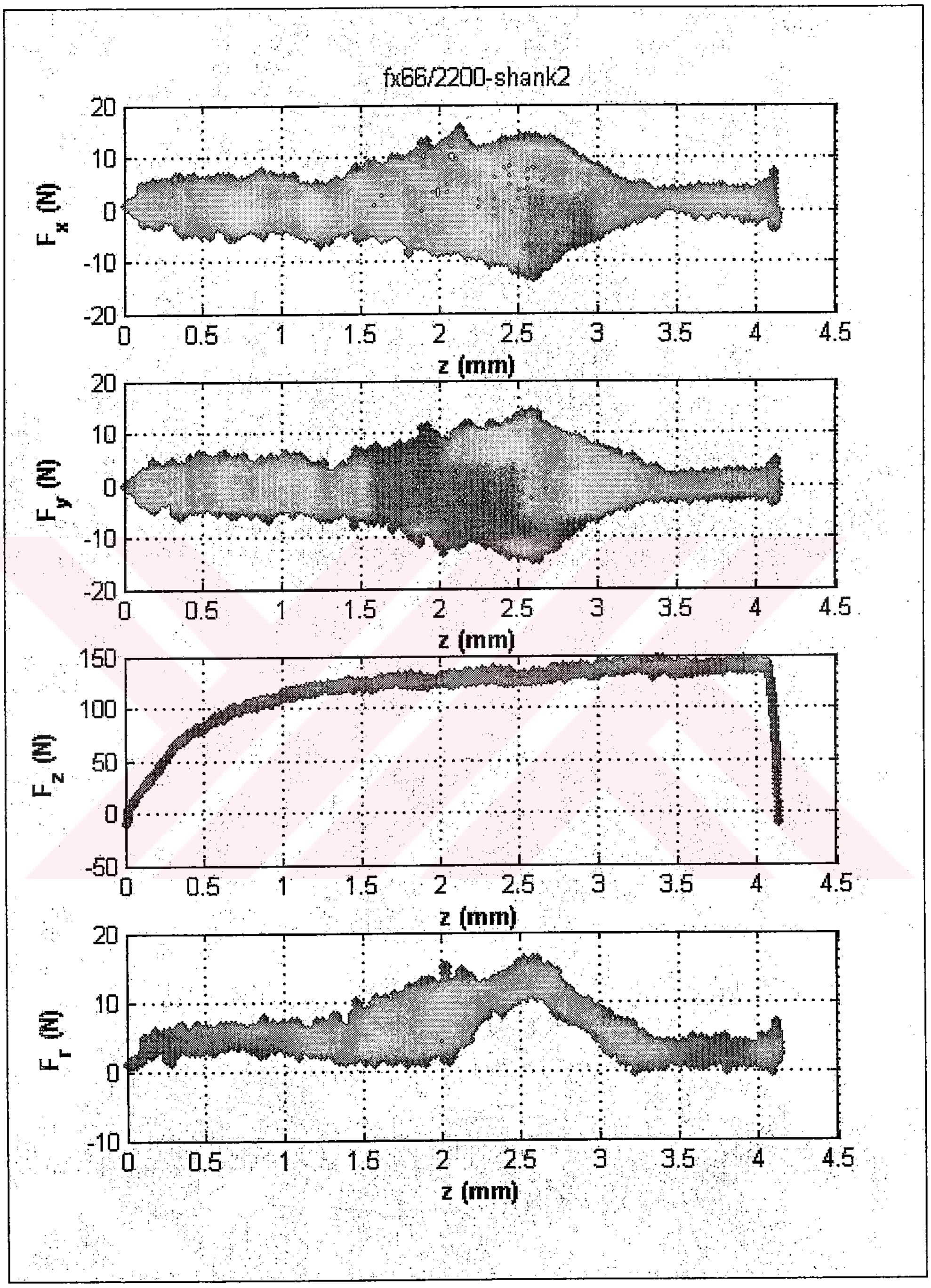

Figure 4.51: Illustration of a measured cutting forces in X, Y, Z and Radial directions of a SHANK2 Drill for spindle speed 2200 [rpm] and feed rate of 66 [mm/min].

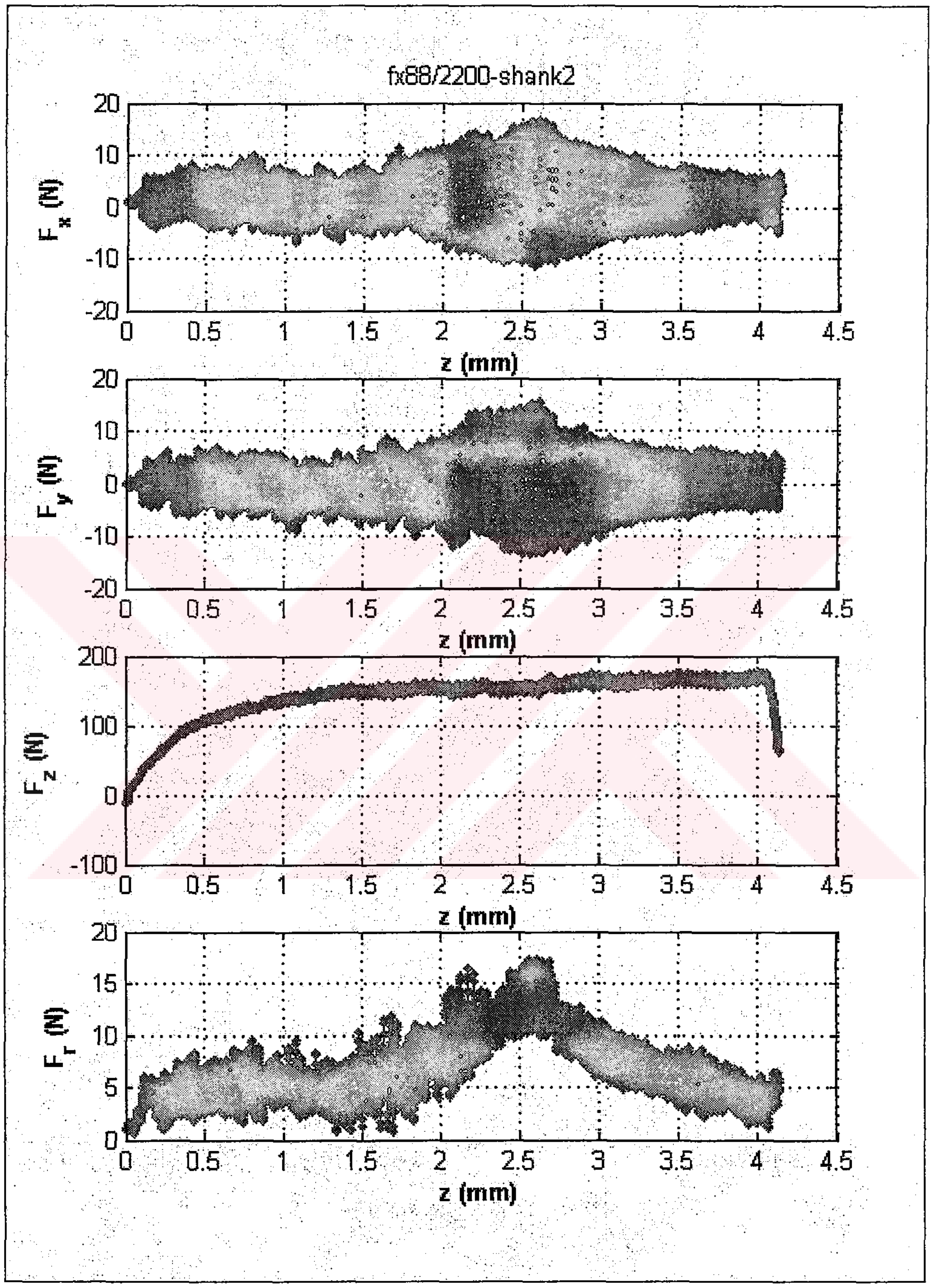

Figure 4.52: Illustration of a measured cutting forces in X, Y, Z and Radial directions of a SHANK2 Drill for spindle speed 2200 [rpm] and feed rate of 88 [mm/min].

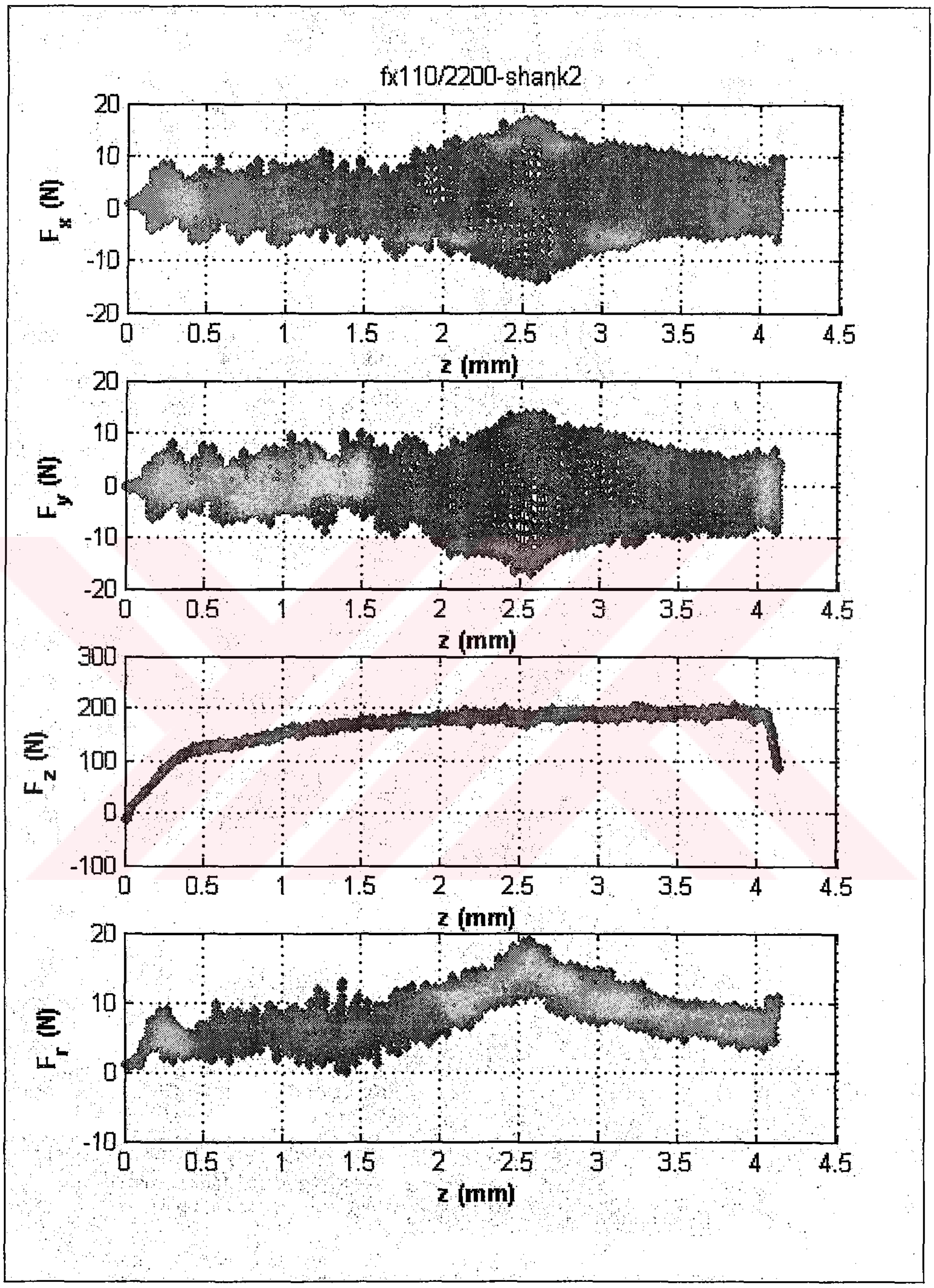

Figure 4.53: Illustration of a measured cutting forces in X, Y, Z and Radial directions of a SHANK2 Drill for spindle speed 2200 [rpm] and feed rate of 110 [mm/min].

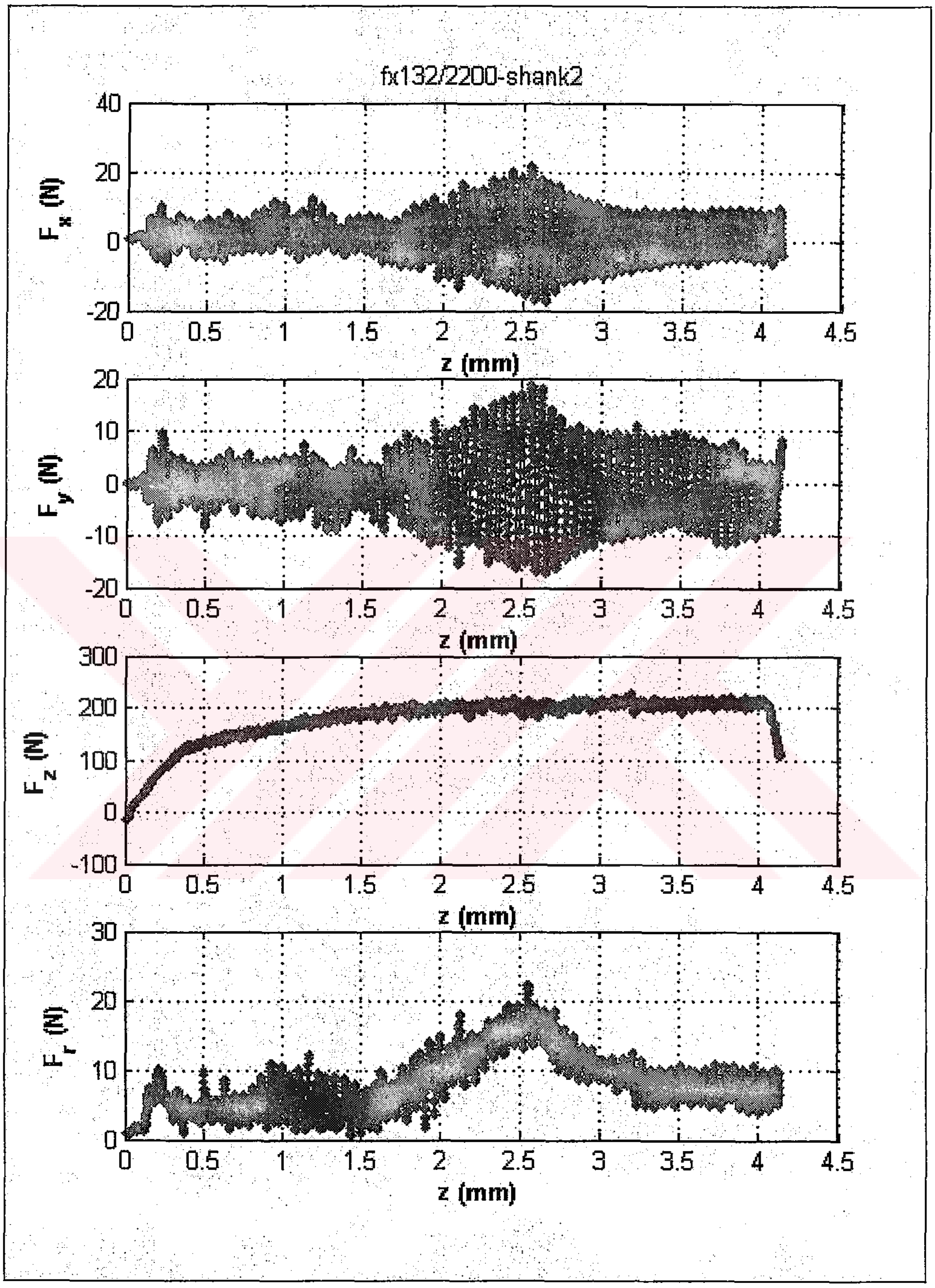

Figure 4.54: Illustration of a measured cutting forces in X, Y, Z and Radial directions of a SHANK2 Drill for spindle speed 2200 [rpm] and feed rate of 132 [mm/min].

Important point in shank chipping case is the transition point between Section I and Section II, if this point is captured than the chipping amount can be calculated easily. However, capturing this point is very difficult in time-domain. In Chapter 5, this trend start will be investigated using wavelet transformation and the point will be captured accurately. The time domain SHANK2 data is only exploited to get the maximum of the cutting force trend.

Table 4.9: Depths at which F_x reaches maximum for SHANK2 Drill for spindle speeds 550/1100/2200 [rpm] and of full engagement

Feed Rate [mm/min]	Zmax/550 [mm]	Zmax/1100 [mm]	Zmax/2200 [mm]	Full Engagement Z [mm]
44	2,291	2,475	2,566	2,32
66	2,266	2,521	2,588	2,32
88	2,287	2,578	2,604	2,32
110	2,090	2,546	2,575	2,32
132	2,479	2,444	2,55	2,32

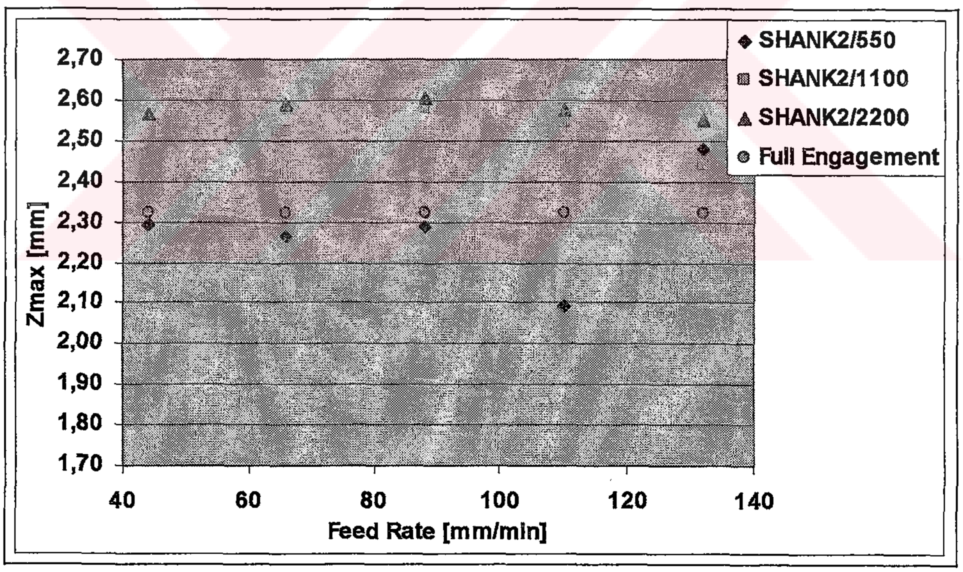

Figure 4.54: Comparison of Depths at which F_x reaches maximum for SHANK2 Drill for spindle speeds 550/1100/2200 rpm

4.4 Comparison of Trust Force

So far, it is investigated that how the cutting force in X directions changes with the chipping types to obtain monitoring features related to them. However, thrust force (force in z directions) also can be a monitoring index for our chipping cases. In this section, thrust force will be utilized to get monitoring features for two type of chipping cases-tip chipping and shank chipping.

As will be seen in the figures below, as the feed rate increases thrust force happens to be a better indicator of chipping. In the figures below, the average of thrust force after full engagement point will be calculated and compared with the other chipping cases and also fresh drill case.

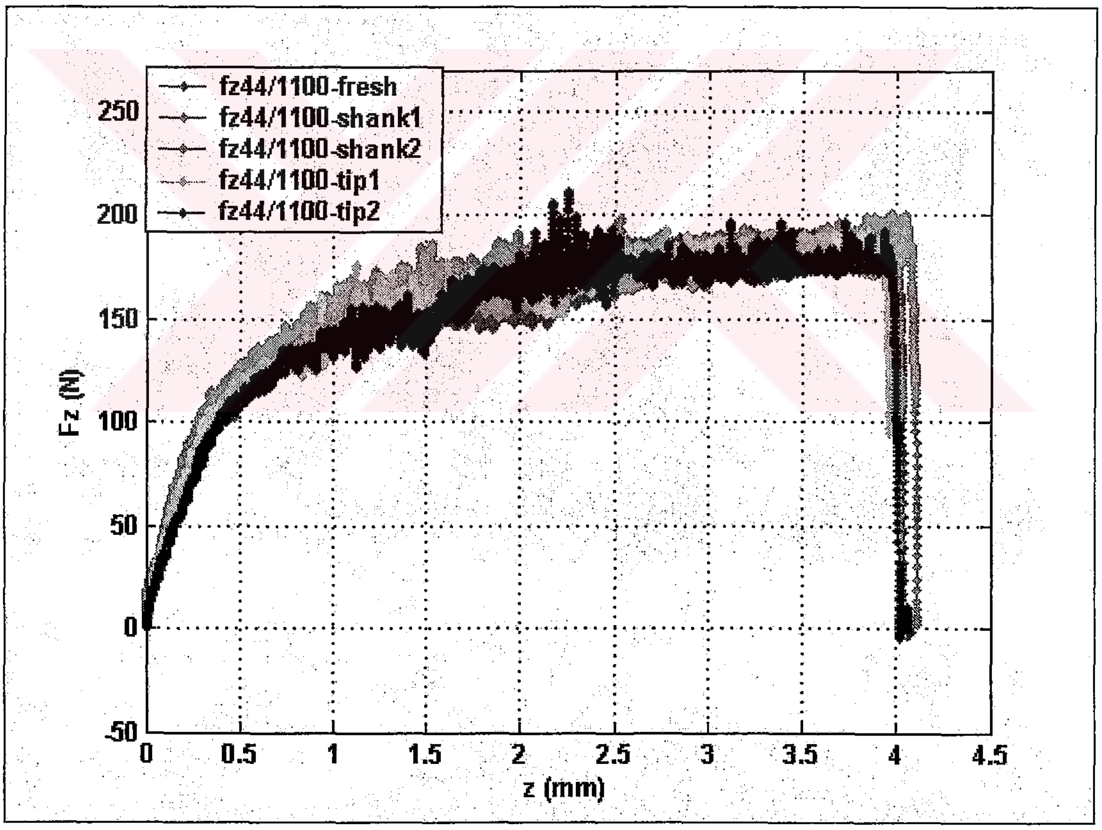

Figure 4.55: Illustration of a measured cutting force in z direction and of Fresh/SHANK1/ SHANK2/TIP1/TIP2 Drills for spindle speed 1100 [rpm] and feed rate of 44 [mm/min].

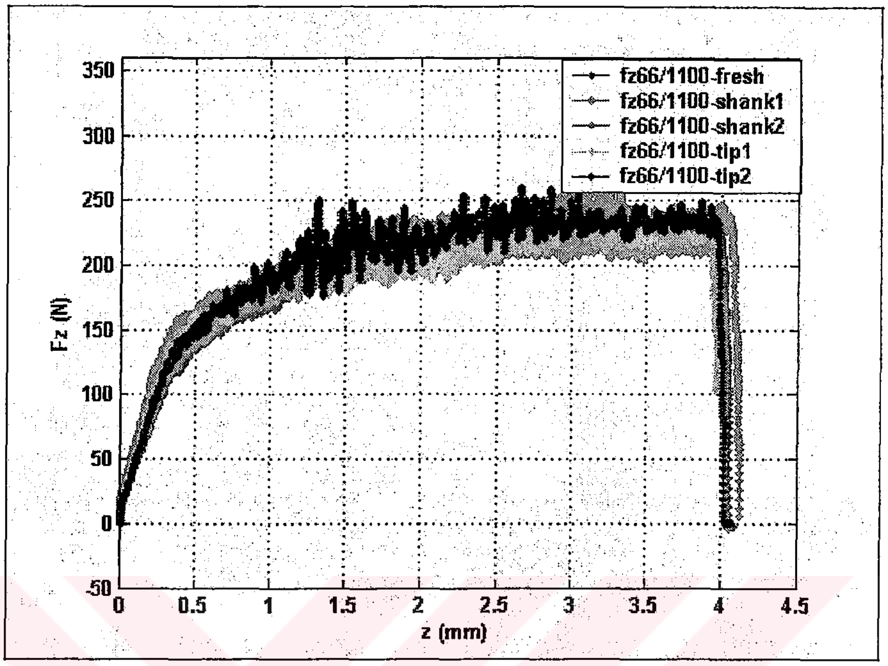

Figure 4.56: Illustration of a measured cutting force in z directions and of Fresh/SHANK1/SHANK2/TIP1/TIP2 Drills for spindle speed 1100 [rpm] and feed rate of 66[mm/min].

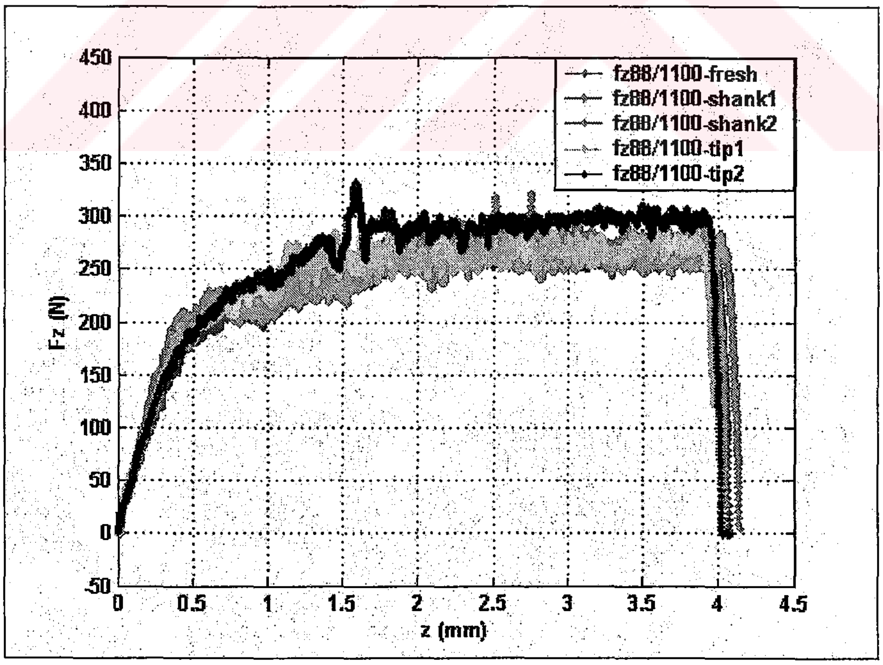

Figure 4.57: Illustration of a measured cutting force in z directions of a Fresh/SHANK1/SHANK2/TIP1/TIP2 Drills for spindle speed 1100 [rpm] and feed rate of 88 [mm/min].

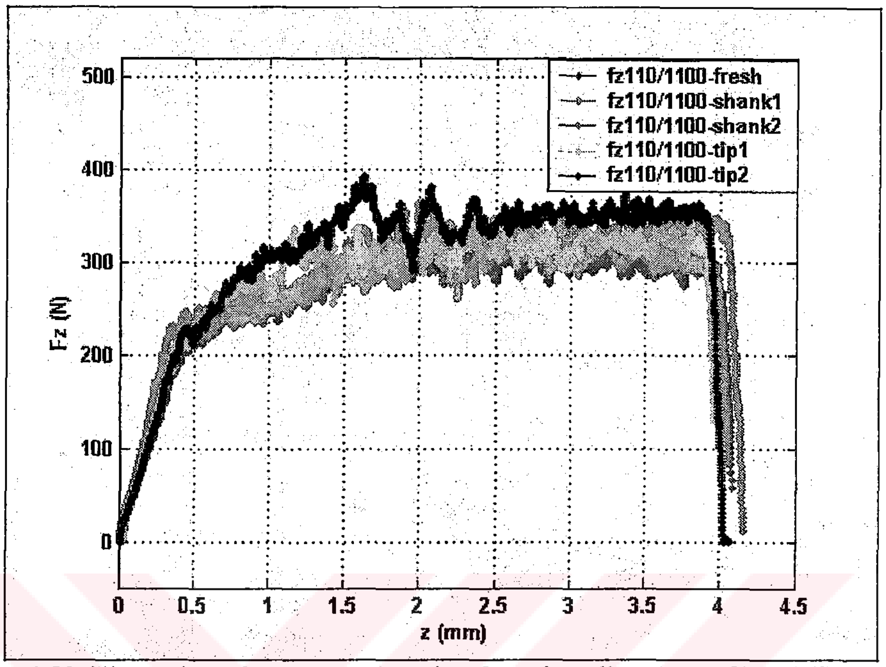

Figure 4.58: Illustration of a measured cutting force in z directions of Fresh/SHANK1/ SHANK2/TIP1/TIP2 Drills for spindle speed 1100 [rpm] and feed rate of 110 [mm/min].

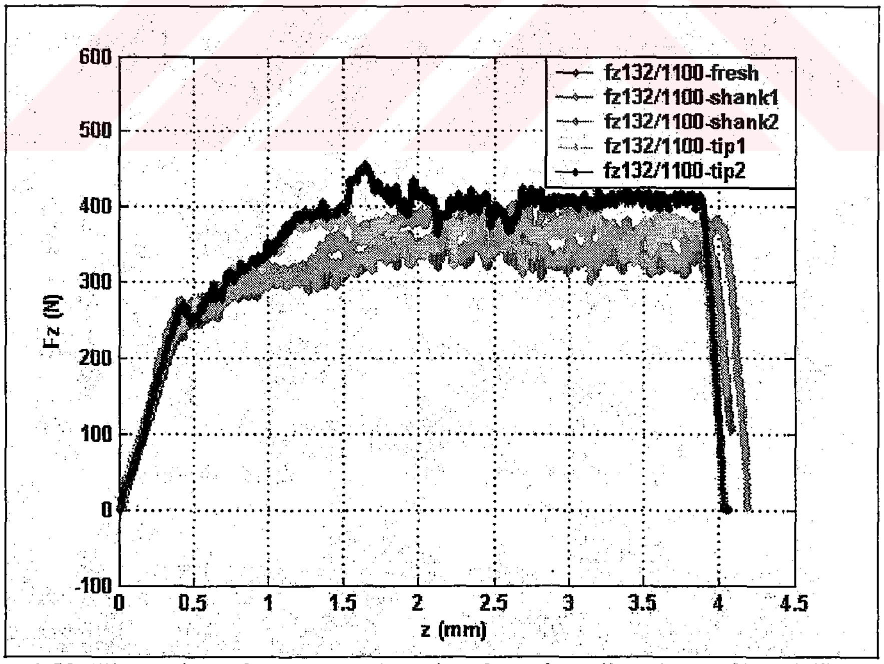

Figure 4.59: Illustration of a measured cutting force in z directions of Fresh/SHANK1/ SHANK2/TIP1/TIP2 Drills for spindle speed 1100 [rpm] and feed rate of 132 [mm/min].

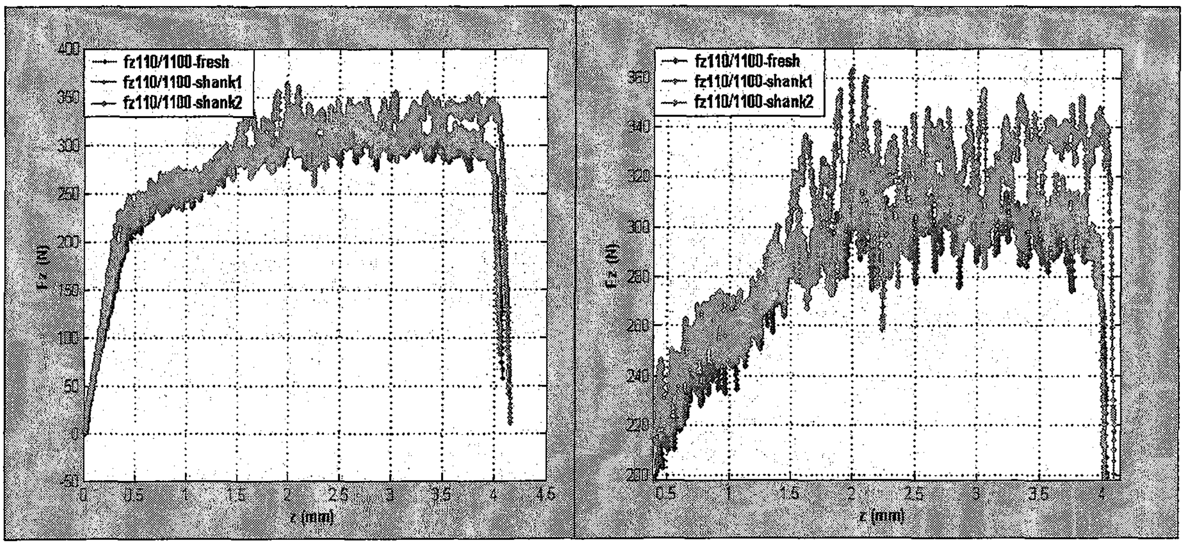

Figure 4.60: Illustration of a measured cutting force in z direction and zoomed version of a Fresh/SHANK1/ SHANK2 Drills for spindle speed 1100 [rpm] and feed rate of 110 [mm/min].

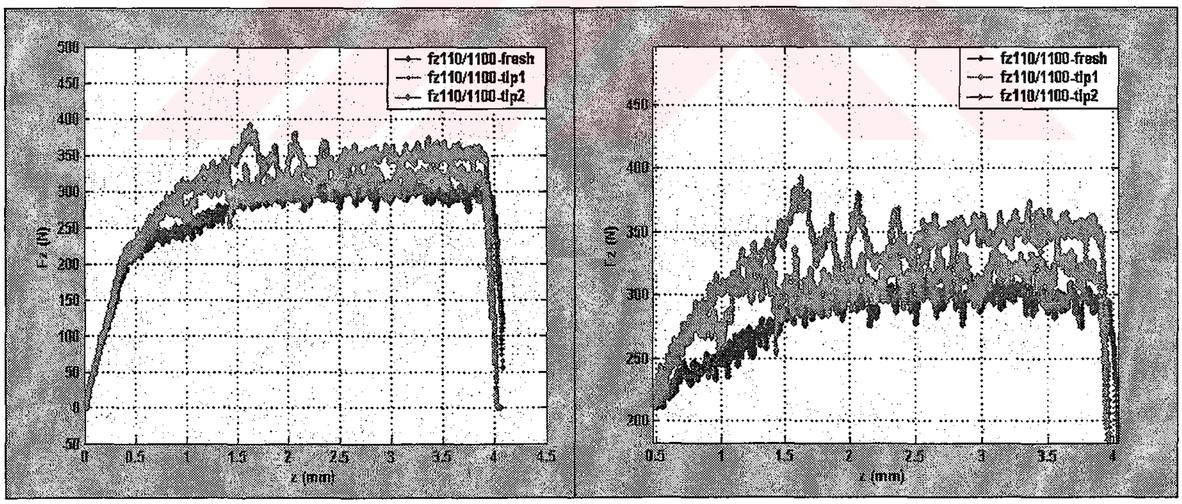

Figure 4.61: Illustration of a measured cutting force in z direction and zoomed version of a Fresh/TIP1/ TIP2 Drills for spindle speed 1100 [rpm] and feed rate of 110 [mm/min].

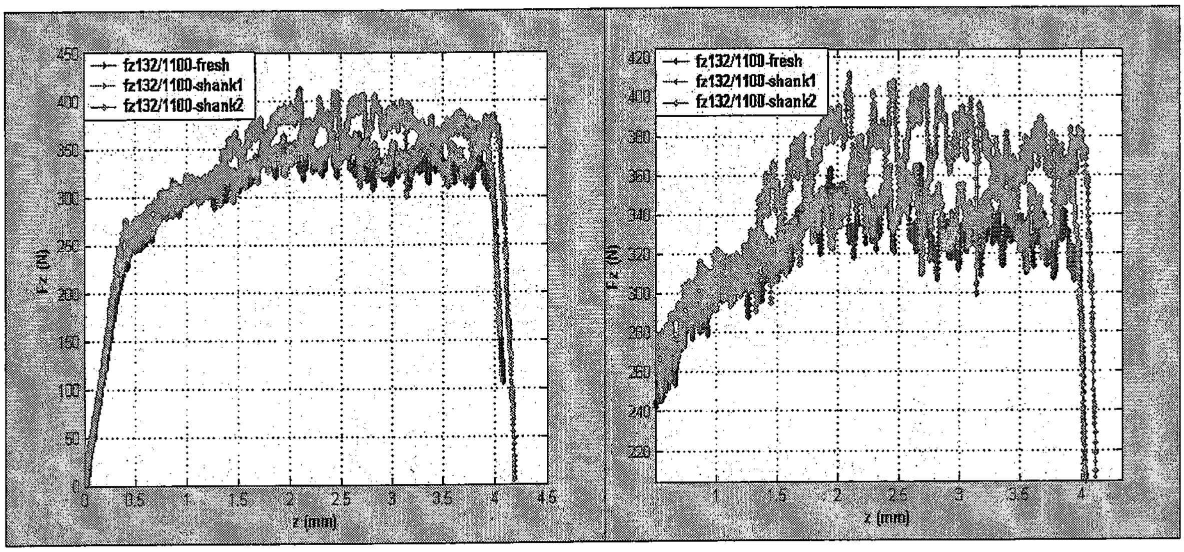

Figure 4.62: Illustration of a measured cutting force in z directions and zoomed version of a Fresh/SHANK1/ SHANK2 Drills for spindle speed 1100 [rpm] and feed rate of 132 [mm/min].

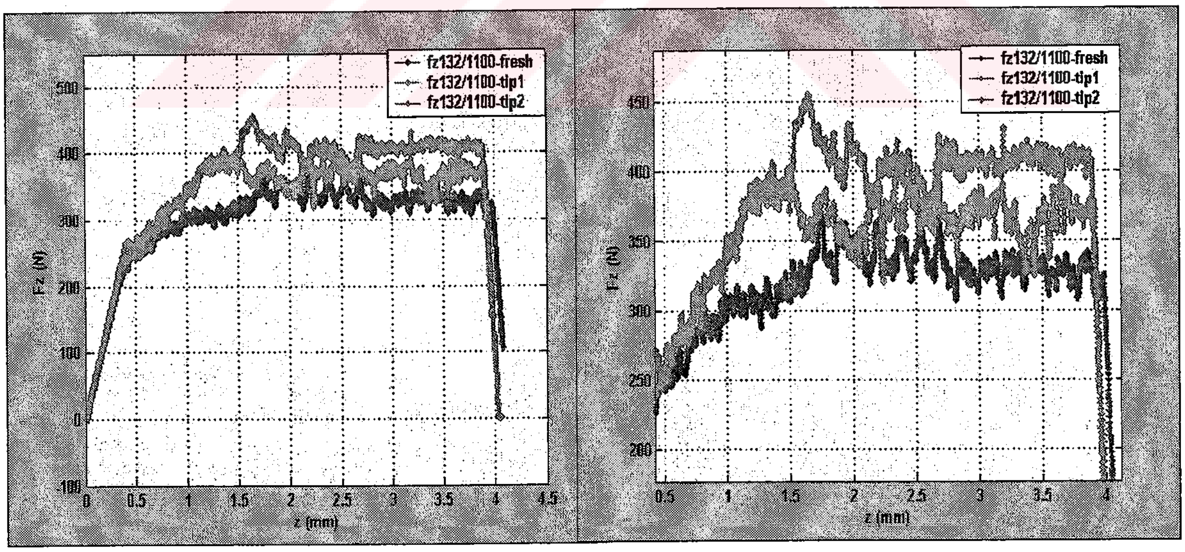

Figure 4.63: Illustration of a measured cutting force in z directions and zoomed version of a Fresh/TIP1/ TIP2 Drills for spindle speed 1100 [rpm] and feed rate of 132 [mm/min].

4.4.1 Comparison of Average Thrust Force

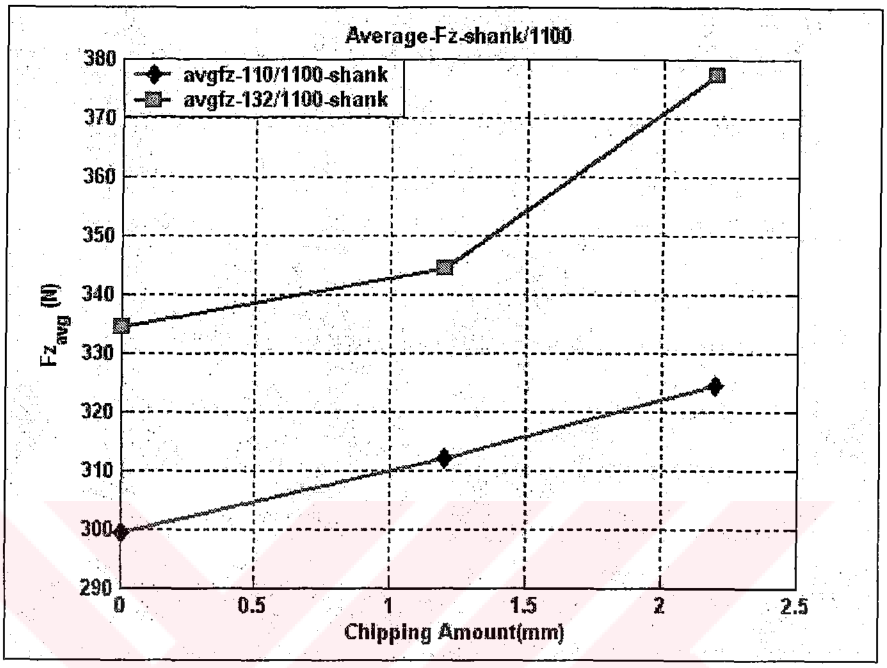

Figure 4.64: Illustration of average thrust force for shank chipping cases for spindle speed 1100 [rpm] and feed rate of 110/132 [mm/min].

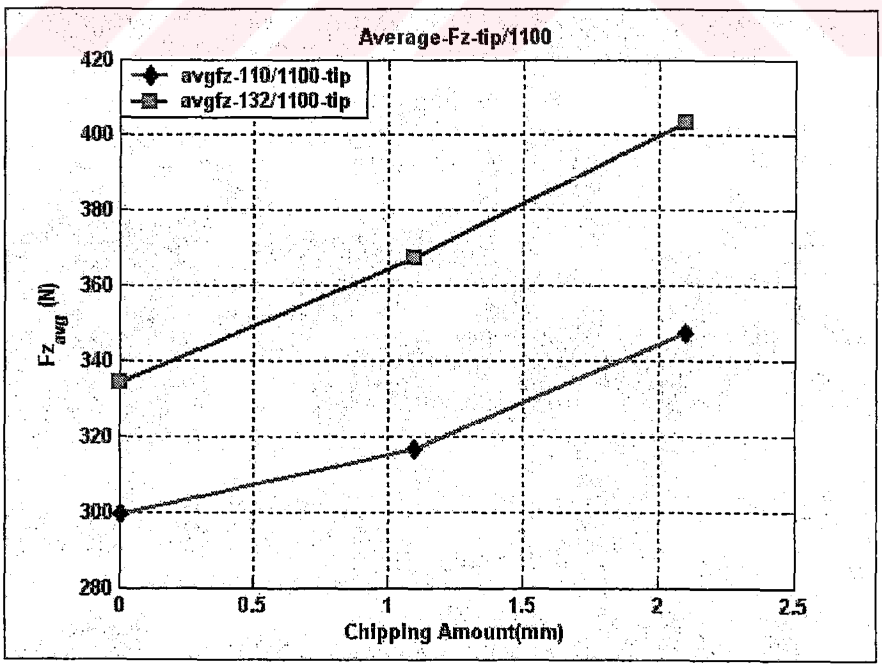

Figure 4.65: Illustration of average thrust force for tip chipping cases for spindle speed 1100 [rpm] and feed rate of 110/132 [mm/min].

4.5 Long Drilling Tests

Up to now, the performed drilling tests are performed to the depth of around 4 mm. However, what if the drilling depth is higher than the 4 mm, how the cutting force pattern will change will be analyzed in this section. In fact the important question is that how a chipped drill behaves after full engagement. To analyze this, two sets of experiments are performed. One for SHANK2 and one for TIP2.

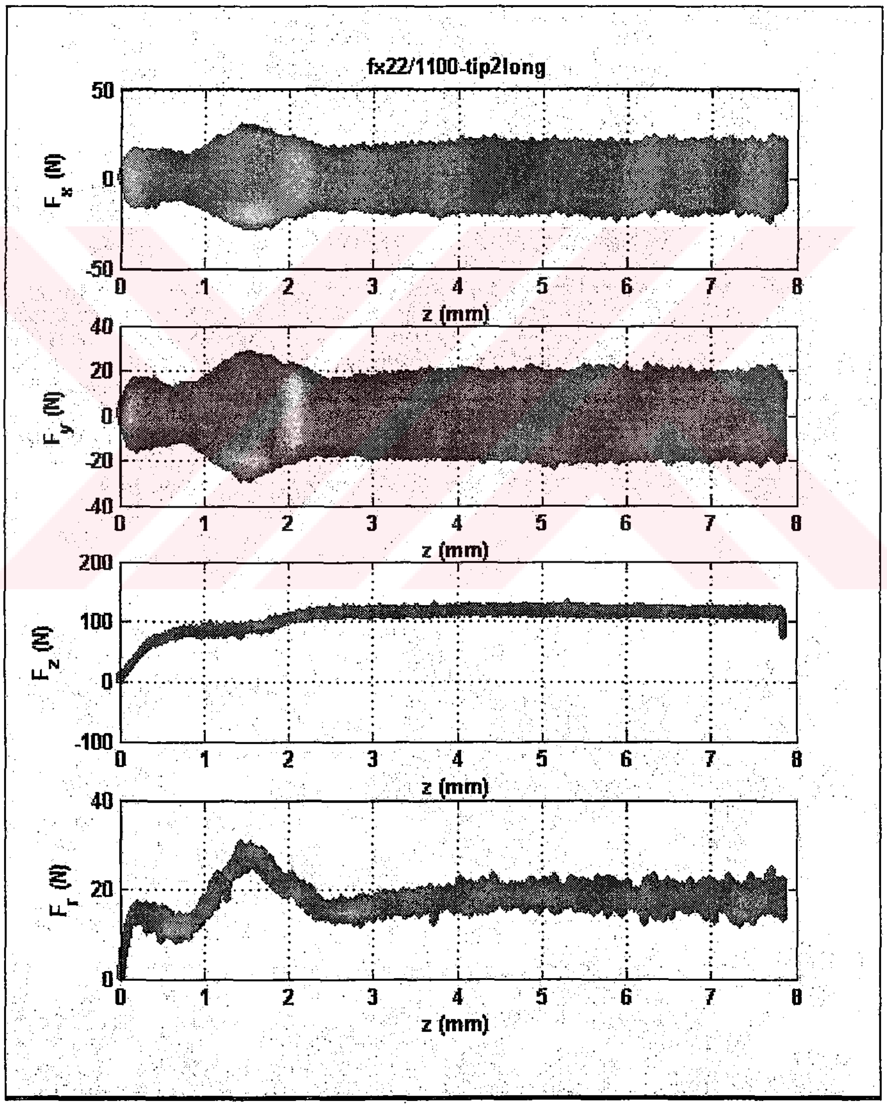

Figure 4.66: Illustration of a measured cutting force components for TIP2 drill, spindle speed of 1100 [rpm], feed rate of 22 [mm/min] and depth of cut 8 [mm]

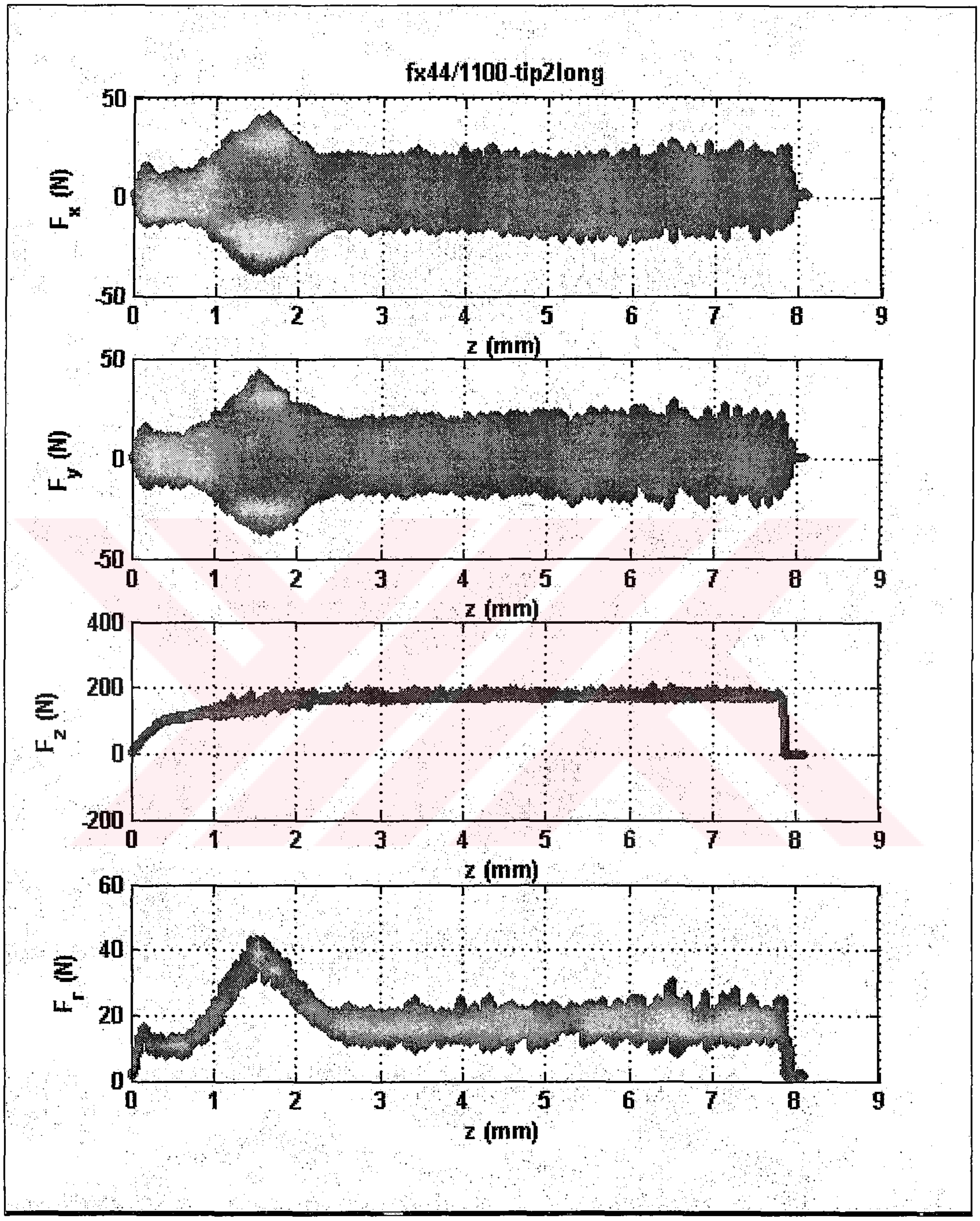

Figure 4.67: Illustration of a measured cutting force components for TIP2 drill, spindle speed of 1100 [rpm], feed rate of 44 [mm/min] and depth of cut 8 [mm]

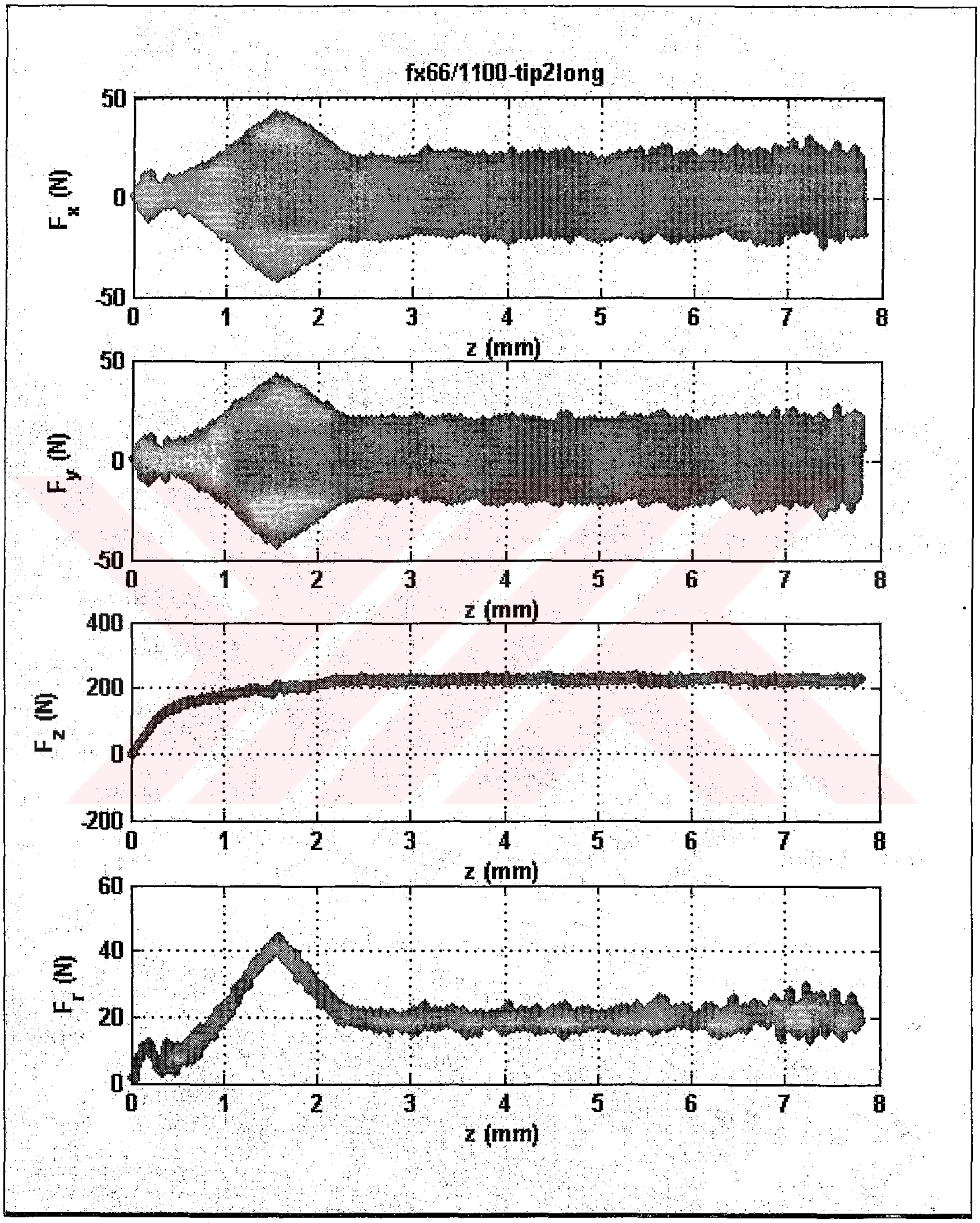

Figure 4.68: Illustration of a measured cutting force components for TIP2 drill, spindle speed of 1100 [rpm], feed rate of 66 [mm/min] and depth of cut 8 [mm]

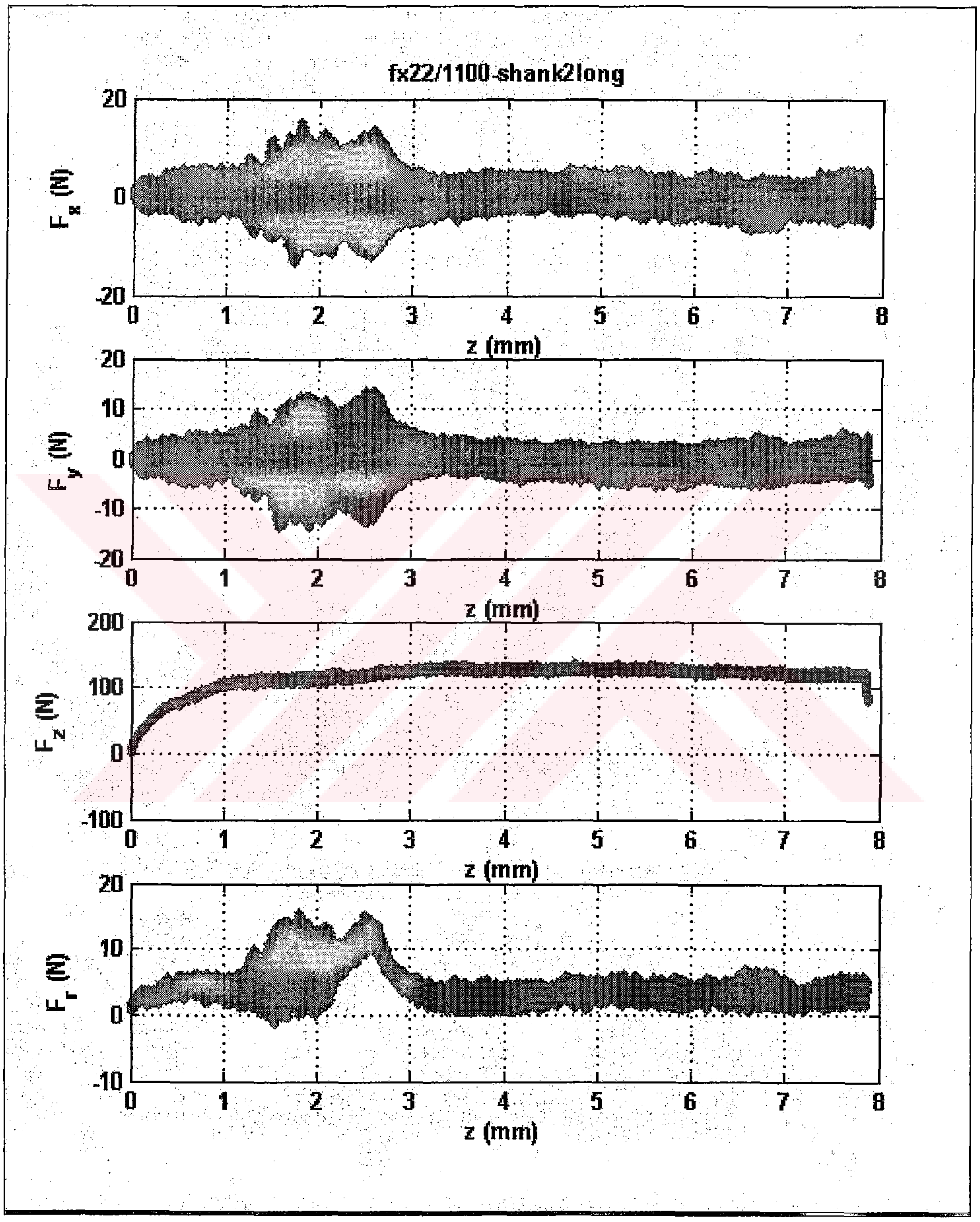

Figure 4.69: Illustration of a measured cutting force components for SHANK2 drill, spindle speed of 1100 [rpm], feed rate of 22 [mm/min] and depth of cut 8 [mm]

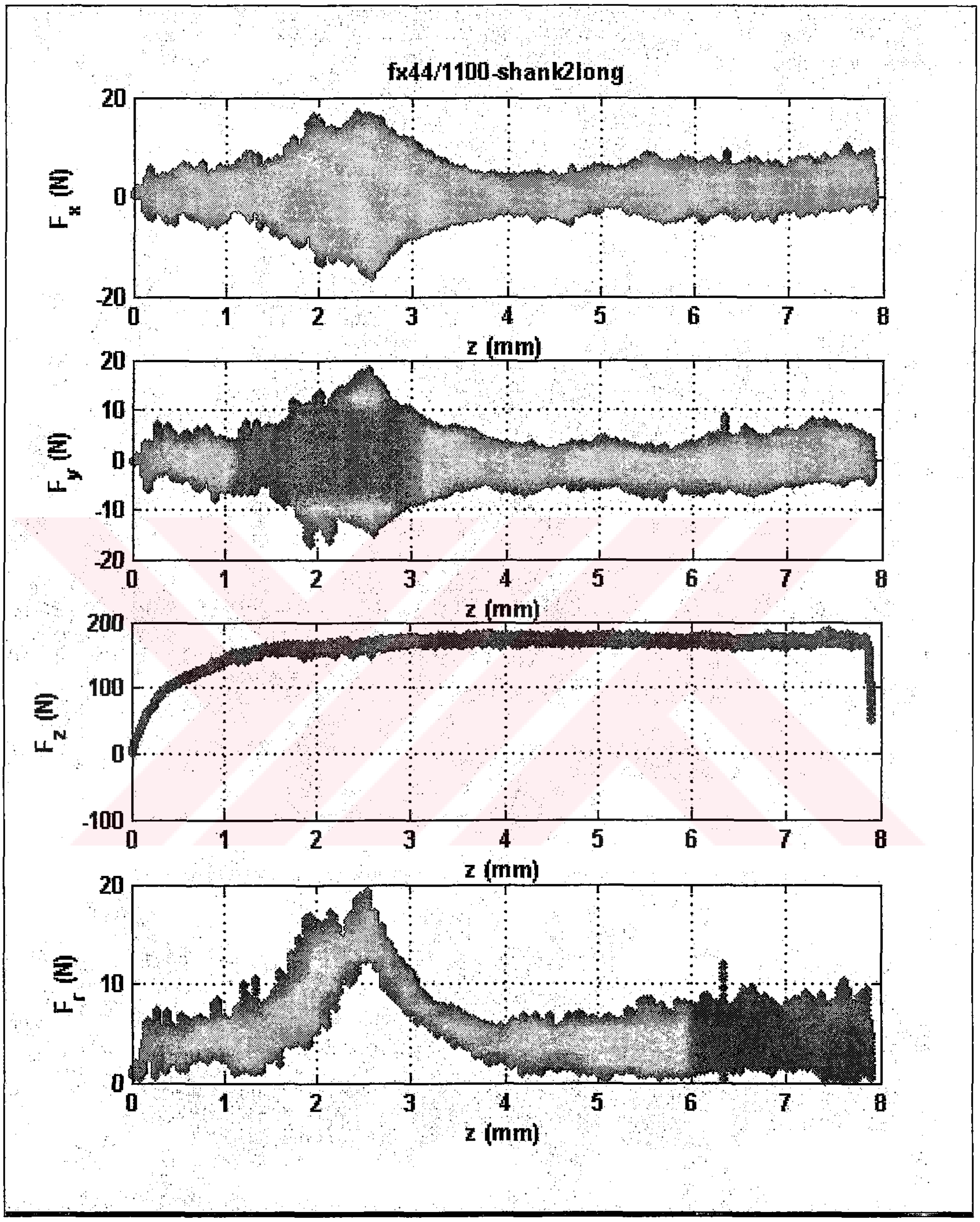

Figure 4.70: Illustration of a measured cutting force components for SHANK2 drill, spindle speed of 1100 [rpm], feed rate of 44 [mm/min] and depth of cut 8 [mm]

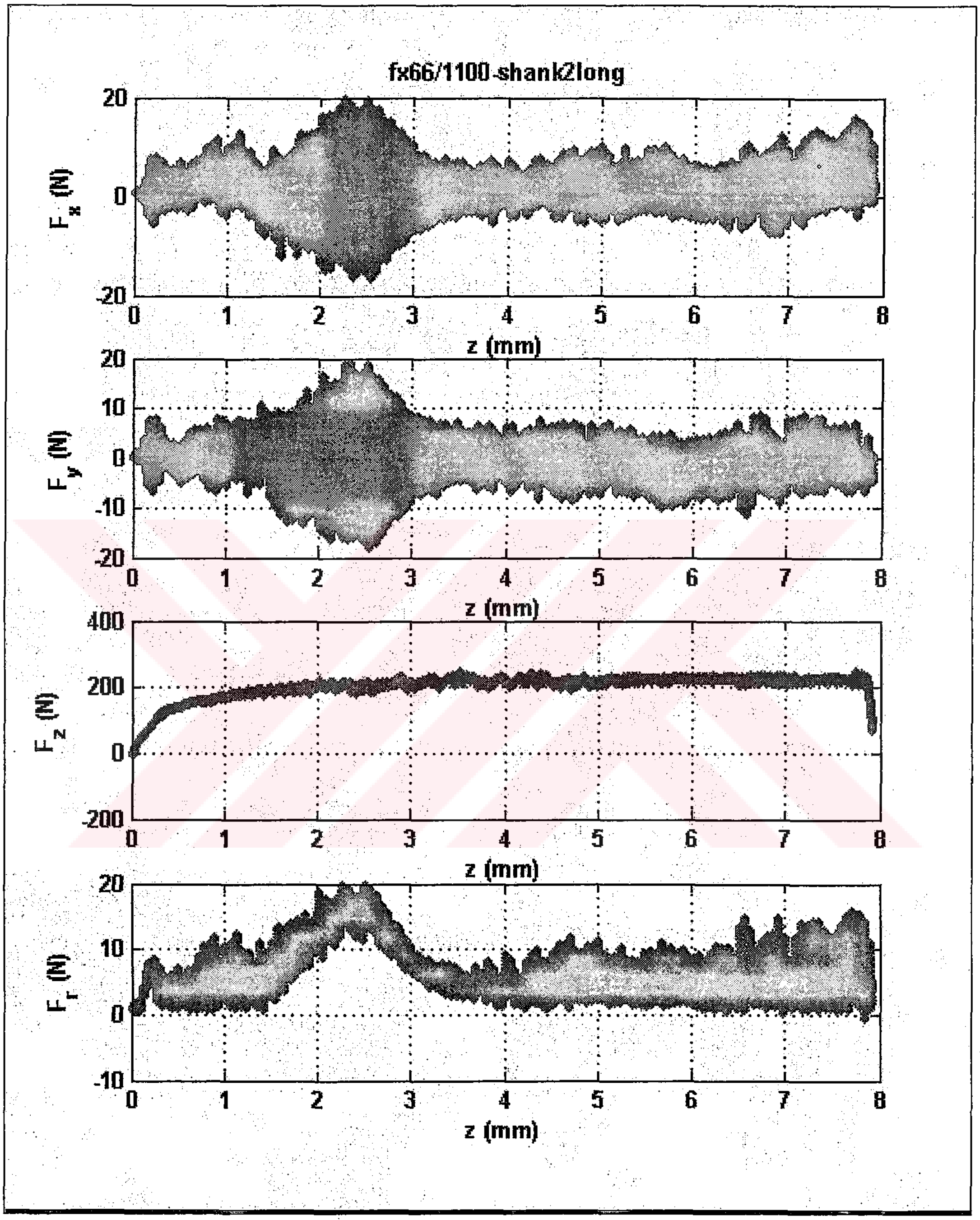

Figure 4.71: Illustration of a measured cutting force components for SHANK2 drill, spindle speed of 1100 [rpm], feed rate of 66 [mm/min] and depth of cut 8 [mm]

4.6 Chapter Discussion/ Conclusion

The conclusions drawn from this chapter are;

- The chipping fault that begins from the chisel edge of the drill can be easily predicted in time domain using cutting force in X and Y directions. The cutting force in X and Y directions are same in drilling process, however the only distinction is the 90° phase difference. Therefore, both of them can be used to get monitoring features, but cutting force in X directions is used throughout the analysis performed in this chapter. As can be seen in the Figures 4.3-18 for TIP1case and Figures 4.22-37 for TIP2 case, feature related to tip chipping is the point where the cutting force reaches maximum in time domain and the beginning of the tip chipping is already known. The deductions made from the experiment for different spindle speed and feed rate of combinations well agree with the measured chipping amounts as can be seen in the Tables 4.1-4 for TIP1 case and Tables 4.5-8 for TIP2 case. However, the general trend for tip chipping cases is that the error between the measured chipping amount and the calculated chipping amount is greater as the spindle speed decreases. For TIP1 case, percent error average is around %20 at spindle speed 500 [rpm] as seen in the Table 4.4. However, at 550 [rpm], TIP2 case is better predicted than TIP1 case. The percent error is around 5 % for this case. Finally, if all the tip chipping conditions are investigated; TIP1 chipping is well predicted for spindle speed 1100[rpm] and 2200[rpm], on the other hand TIP2 chipping is well predicted for all spindle speeds.

- When the shank chipping case is investigated in time domain as seen in the Figures 4.40-55, it is hard to obtain monitoring features related to it. The expected force patterns is a constant regime till the chipping begins and then steady increase in cutting force in X directions until full engagement is reached. The experiment results show that, the expected force regime is logical but the point at which cutting force trend increase occurs is hard to capture in time domain. This point can be better captured by using wavelet transformation. These phenomena will be discussed in chapter 5. Another point is that, the expected cutting force will reach maximum as the drill fully engages with the workpiece, but the reality is not so. The maximum of cutting force happens after full engagement, as it may be seen in the Table 4.9.

The maximum of the cutting force in x directions is nearly same in the same spindle speed and between different spindle speeds.

- Until now, cutting force in X and Y directions is used to get monitoring features related to the chipping cases. However, the cutting force in z direction called as thrust force also gives some monitoring features for chipping cases. The first observation is that the difference in thrust force of all chipping cases becomes more apparent as the feed rate increases as may be seen in Figures 4.55-63. Another observation is that for high feed rate of the average thrust force after full engagement shows nearly a linear pattern. In other words, thrust force increases linearly with the chipping amount as seen in the Figures 4.64-65.

- Drilling tests are performed for TIP2 case and SHANK2 case to the depth of 8 mm to see the steady state behavior of the cutting forces. Long drilling tests and looking the cutting force data after full engagement reveal new features related to chipping cases. Firstly for the TIP2 case, cutting force regime can be stated again as follows: firstly, nearly constant cutting force until chipping starts. Then, as the chipping starts cutting forces begin to increase, cutting forces reaches maximum as the chipped portion of the drill is passed by. After that, until full engagement cutting forces begin to decrease. Finally after full engagement cutting forces remains constant with the same cutting force amplitude as the drill fully engages with the workpiece. One more observation is that the difference between two constant force regimes becomes more significant as the feed rate of increases as seen in the Figures 4.67-69. On the other hand, for the SHANK2 chipping case the long term cutting force behavior shows similar characteristics with TIP2 case. If the cutting force patterns is analyzed from the beginning of the test, it is seen that; cutting forces are nearly constant until the chipped portion of the drill is encountered with the workpiece, as the chipped portion is engages with the workpiece cutting forces begin to increase as seen in the Figures 4.70-73. The increase in the cutting forces continues to a point after which cutting force trend behaves as an decreasing pattern to a point after which cutting forces reaches steady state value and cutting forces keep constant with an amplitude very near to the constant force regime's amplitude which occurs in the beginning of the test. The maximum of the cutting forces and the beginning of the constant regime after full engagement has no physical or geometrical meaning in the Shank 2 case.

- Another observation obtained by analyzing the figures in this chapter is that amplitude gets higher as the chipping amount and /or feed rate of increases and/or spindle speed decreases.

- The approach presented in this chapter is based on trend detection. The trend was observed in all feed rate of and spindle speed combinations. This is the power of this method. For any spindle speed and feed rate of combination, same trend shows off itself and capturing the monitoring features are very easy by using trend detection.

- Finally, the underlying assumption which is the cutting force should increase as the drill is chipped is validated in this chapter.

Chapter 5

Time-Frequency Domain/ Frequency Domain Analysis

5.1 Wavelet Transformation

5.1.1 Introduction

It is well known from Fourier theory that a signal can be expressed as the sum of a, possibly infinite, series of sines and cosines. This sum is also referred to as a Fourier expansion. The big disadvantage of a Fourier expansion, however is that it has only frequency resolution and no time resolution. This means that although we might be able to determine all the frequencies present in a signal, we do not know when they are present. To overcome this problem in the past decades several solutions have been developed which are more or less able to represent a signal in the time and frequency domain at the same time.

5.1.2 Short-Time Fourier Analysis

In an effort to correct this resolution deficiency, Dennis Gabor (1946) adapted the Fourier transform to analyze only a small section of the signal at a time -- a technique called *windowing* the signal. Gabor's adaptation, called the *Short-Time Fourier Transform* (STFT), maps a signal into a two-dimensional function of time and frequency.

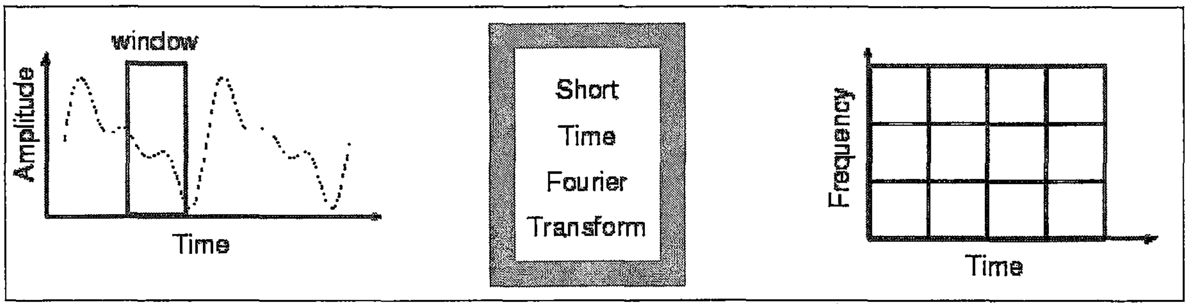

Figure 5.1: Illustration of Short time Fourier Transform (STFT) [24].

The STFT represents a sort of compromise between the time- and frequency-based views of a signal. It provides some information about both when and at what frequencies a signal event occurs. However, you can only obtain this information with limited precision, and that precision is determined by the size of the window. While the STFT compromise between time and frequency information can be useful, the drawback is that once you choose a particular size for the time window, that window is the same for all frequencies. Many signals require a more flexible approach -- one where one can vary the window size to determine more accurately either time or frequency.

5.1.3 Wavelet Analysis

Wavelet analysis represents the next logical step, a windowing technique with variable-sized regions. Wavelet analysis allows the use of long time intervals where more precise low-frequency information is required , and shorter regions where high-frequency information is desired.

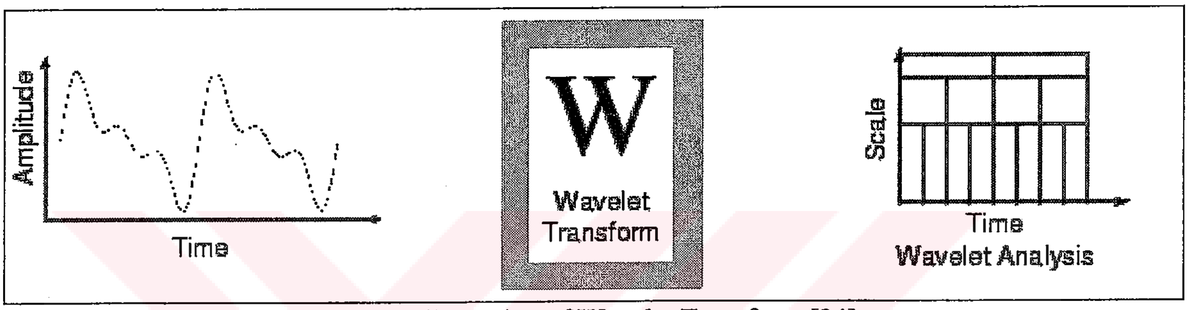

Figure5.2: Illustration of Wavelet Transform [24].

Here's what this looks like in contrast with the time-based, frequency-based, and STFT views of a signal:

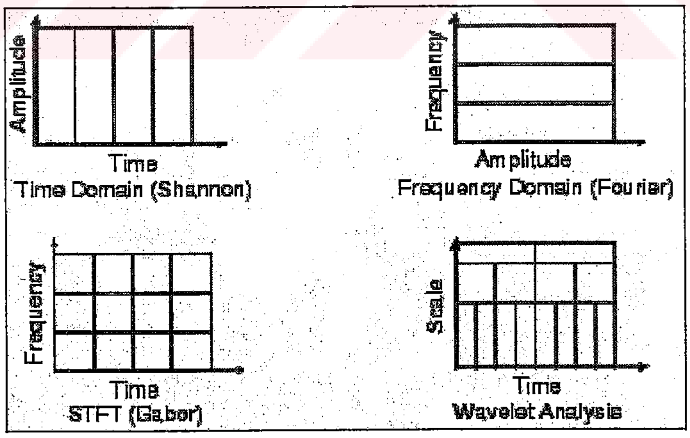

Figure 5.3: Comparison of STFT and Wavelet Analysis [24].

It is worth to notice that wavelet analysis does not use a time-frequency region, but rather a time-*scale* region.

A wavelet is a waveform of effectively limited duration that has an average value of zero. Compare wavelets with sine waves, which are the basis of Fourier analysis. Sinusoids do not have limited duration -- they extend from minus to plus infinity. And where sinusoids are smooth and predictable, wavelets tend to be irregular and asymmetric.

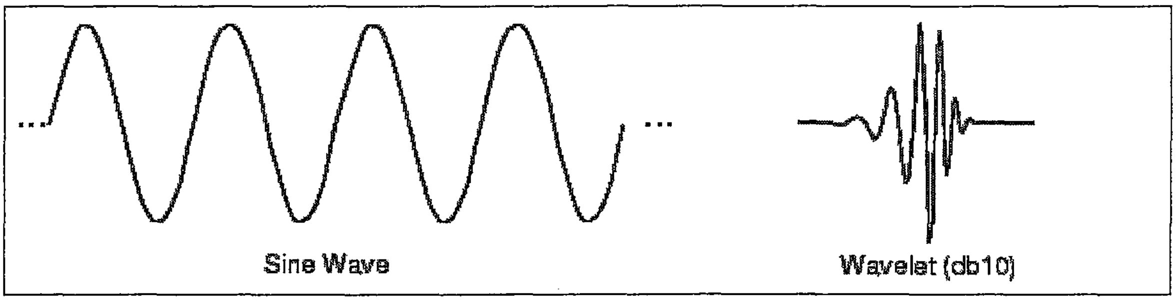

Figure 5.4: Comparison of basis of Fourier Analysis with basis of Wavelet Transform [24].

Fourier analysis consists of breaking up a signal into sine waves of various frequencies. Similarly, wavelet analysis is the breaking up of a signal into shifted and scaled versions of the original (or *mother*) wavelet. Just looking at pictures of wavelets and sine waves, one can see intuitively that signals with sharp changes might be better analyzed with an irregular wavelet than with a smooth sinusoid. It also makes sense that local features can be described better with wavelets that have local extent.

5.1.4 The Continuous Wavelet Transform

Mathematically, the process of Fourier analysis is represented by the *Fourier transform*:

$$F(w) = \int_{-\infty}^{\infty} f(t)e^{-jwt}dt \tag{5.1}$$

Which is the sum over all time of the signal *f(t)* multiplied by a complex exponential. (Recall that a complex exponential can be broken down into real and imaginary sinusoidal components.) The results of the transform are the *Fourier coefficients F(w),* which when multiplied by a sinusoid of frequency (w) yield the constituent sinusoidal components of the original signal. Graphically, the process looks like as below:

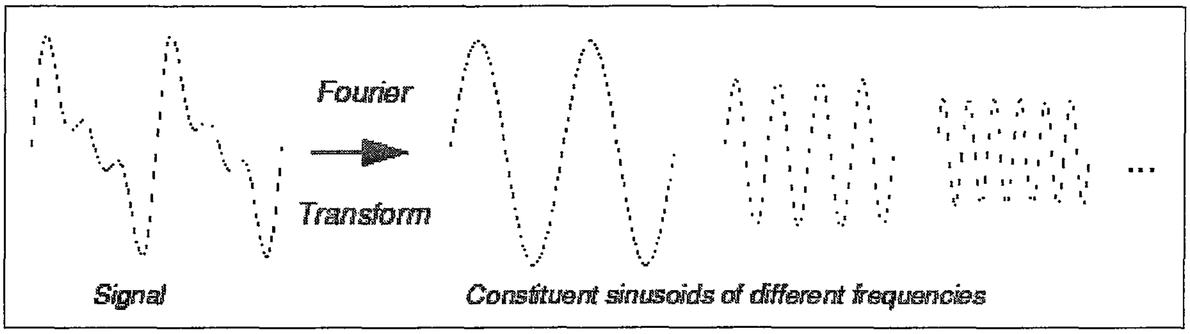

Figure 5.5: Illustration of constituent sinusoids of different frequencies of Fourier Transform [24].

Similarly, the *continuous wavelet transform* (CWT) is defined as the sum over all time of the signal multiplied by scaled, shifted versions of the wavelet function Ψ:

$$C(scale, position) = \int_{-\infty}^{\infty} f(t)\psi(scale, position, t)dt \qquad (5.2)$$

The results of the CWT are many *wavelet coefficients* C, which are a function of scale and position. Multiplying each coefficient by the appropriately scaled and shifted wavelet yields the constituent wavelets of the original signal:

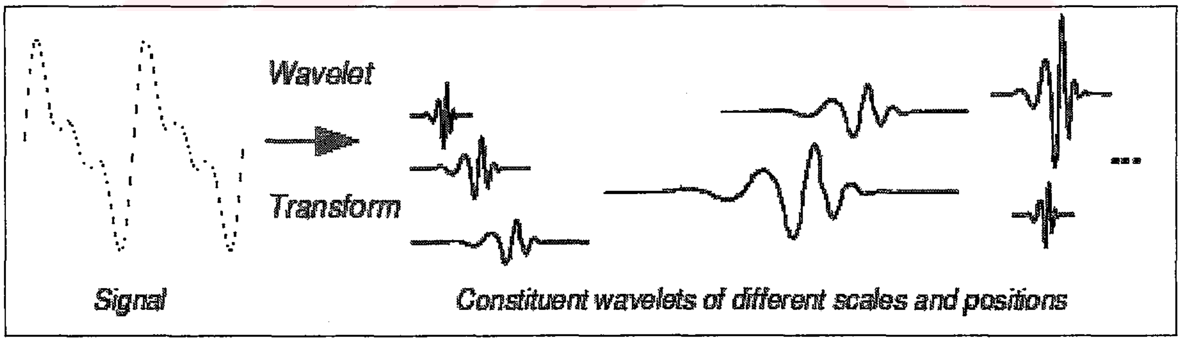

Figure 5.6: Illustration of constituent wavelets of different scales and positions of Wavelet Transform [24].

5.1.4.1 Scaling

Scaling a wavelet simply means stretching (or compressing) it. To go beyond colloquial descriptions such as "stretching," we introduce the *scale factor*, often denoted by the letter *(a)*. The scale factor works exactly the same with wavelets. The smaller the scale factor, the more "compressed" the wavelet.

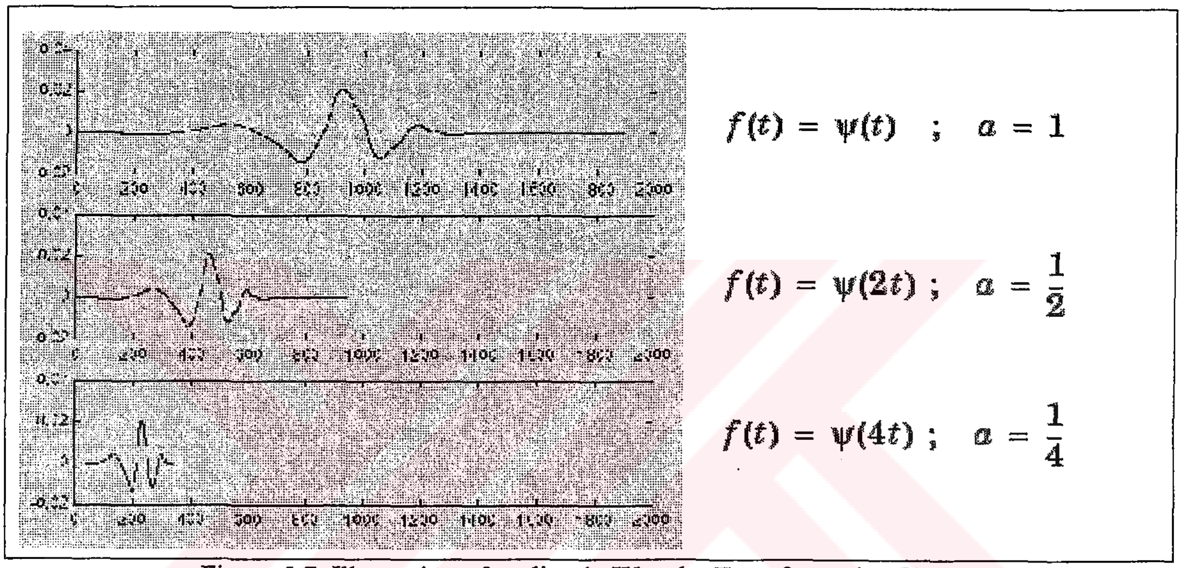

Figure 5.7: Illustration of scaling in Wavelet Transformation [24].

5.1.4.2 Shifting

Shifting a wavelet simply means delaying (or hastening) its onset. Mathematically, delaying a function *f(t)*by *k* is represented by *f(t-k)*:

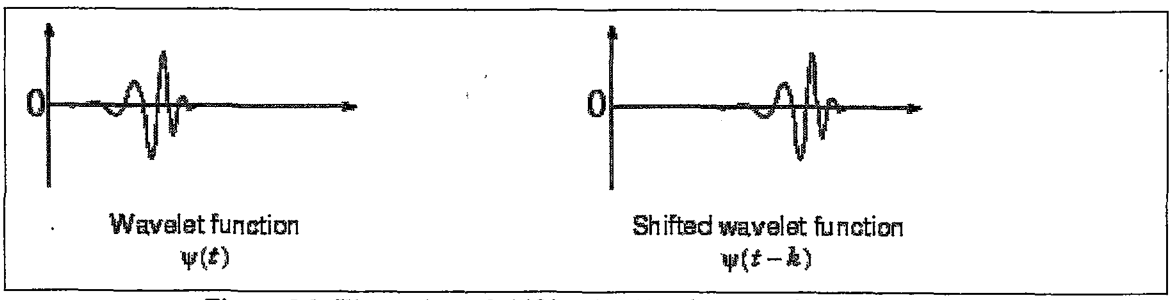

Figure 5.8: Illustration of shifting in Wavelet Transformation [24].

5.1.4.3 Scale and Frequency

Recall that the higher scales correspond to the most "stretched" wavelets. The more stretched the wavelet, the longer the portion of the signal with which it is being compared, and thus the coarser the signal features being measured by the wavelet coefficients.

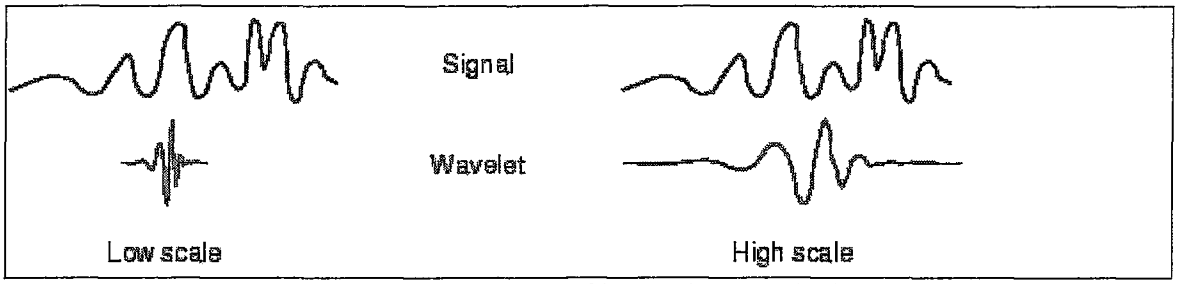

Figure 5.9: Comparison of low scale versus high scale [24]

Thus, there is a correspondence between wavelet scales and frequency as revealed by wavelet analysis:

- Low scale $a \Rightarrow$ Compressed wavelet $\Rightarrow$ Rapidly changing details $\Rightarrow$ High frequency w.
- High scale $a \Rightarrow$ Stretched wavelet $\Rightarrow$ Coarse features $\Rightarrow$ Low frequency w.

5.1.5 Discrete Wavelet Transformation (DWT)

5.1.5.1 One-Stage Filtering: Approximations and Details

For many signals, the low-frequency content is the most important part. It is what gives the signal its identity. The high-frequency content, on the other hand, imparts flavor or nuance. Consider the human voice. If you remove the high-frequency components, the voice sounds different, but you can still tell what's being said. However, if you remove enough of the low-frequency components, you hear gibberish. In wavelet analysis, we often speak of *approximations* and *details*. The approximations are the high-scale, low-frequency components of the signal. The details are the low-scale, high-frequency components. The filtering process, at its most basic level, looks like the following:

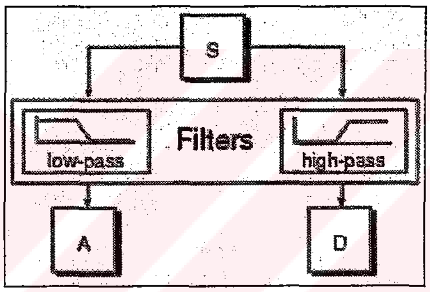

Figure 5.10: Illustration of DWT working principle

The original signal, S, passes through two complementary filters and emerges as two signals. Unfortunately, if we actually perform this operation on a real digital signal, we wind up with twice as much data as we started with. Suppose, for instance, that the original signal S consists of 1000 samples of data. Then the resulting signals will each have 1000 samples, for a total of 2000.

These signals A and D are interesting, but we get 2000 values instead of the 1000 we had. There exists a more subtle way to perform the decomposition using wavelets. By looking carefully at the computation, we may keep only one point out of two in each of the two 2000-length samples to get the complete information. This is the notion of downsampling. We produce two sequences called cA and cD.

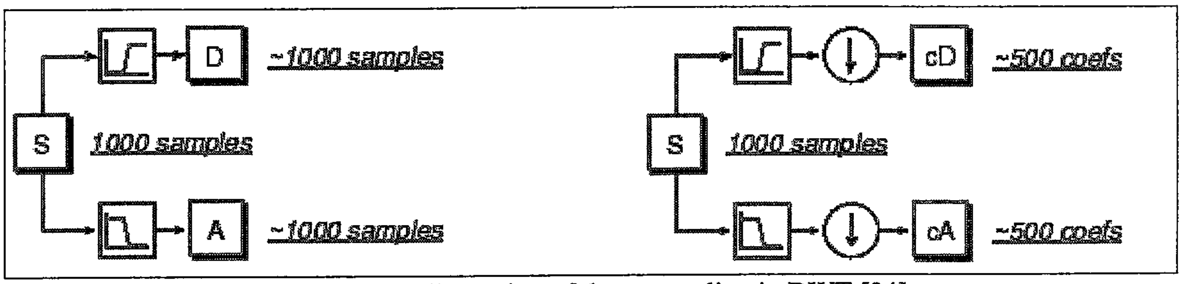

Figure 5.11: Illustration of downsampling in DWT [24].

The process on the right, which includes downsampling, produces DWT coefficients. To gain a better appreciation of this process, let's perform a one-stage discrete wavelet transform of a signal. Our signal will be a pure sinusoid with high-frequency noise added to it. Here is our schematic diagram with real signals inserted into it:

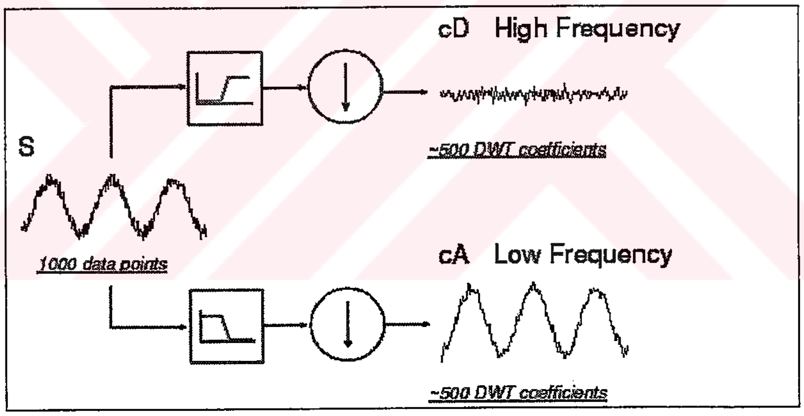

Figure 5.12: Illustration of a real signal example related to DWT [24].

5.1.5.2 Multiple-Level Decomposition

The decomposition process can be iterated, with successive approximations being decomposed in turn, so that one signal is broken down into many lower resolution components. This is called the *wavelet decomposition tree.*

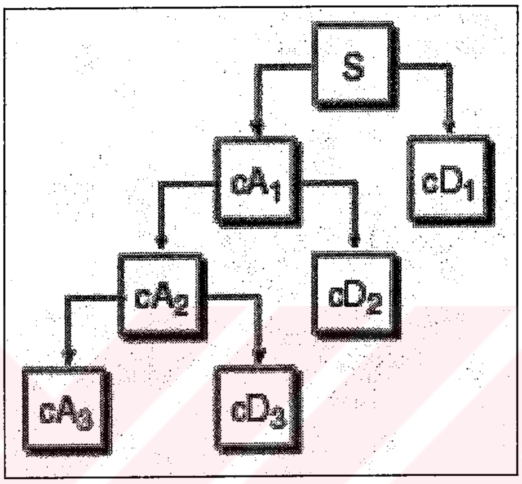

Figure 5.13: Illustration of multi-level decomposition

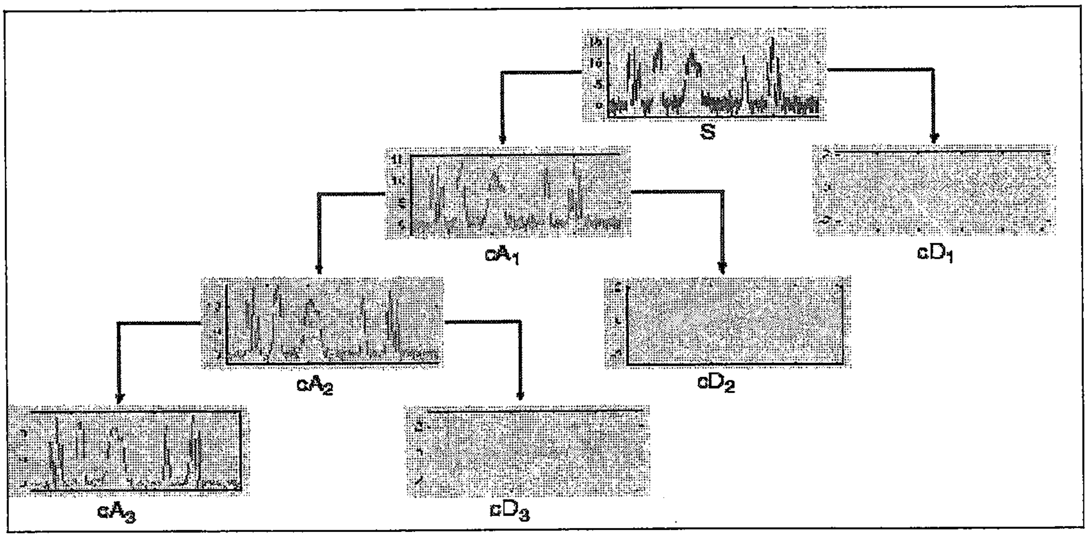

Figure 5.14: Illustration of a real signal multi-level decomposition applied [24].

5.1.6 Mathematics Behind Wavelet Transform:

To consider the continuous wavelet transform, the wavelet corresponding to scale *(a)* and time location *(b)* is

$$\Psi_{a,b} = \frac{1}{\sqrt{|a|}}\Psi\left(\frac{t-b}{a}\right) \quad a,b \in R, \quad a \neq 0 \tag{5.3}$$

where *(a)* and *(b)* are the dilation and translation parameters, respectively. The continuous wavelet transform is then defined as follows:

$$CWT\{x(t); a,b\} = \int x(t)\Psi^{*}_{a,b}(t)\,dt \tag{5.4}$$

where " * " denotes the complex conjugation. When, (1) can be written as $a=2^j$, $b=k2^j$, $j,k \in Z$

$$\Psi_{j,k} = 2^{\frac{-j}{2}}\Psi(2^{-j}t-k) \tag{5.5}$$

The discrete wavelet transform (DWT) is defined as;

$$c_{j,k} = \int f(t)\Psi^{*}_{j,k}(t)\,dt \tag{5.6}$$

where $c_{j,k}$ is called the wavelet coefficient. It may be considered as a time frequency map of the original signal *f(t)*. A multiresolution analysis approach is used in which a discrete scaling function

$$\phi_{j,k} = 2^{\frac{-j}{2}}\phi\left(\frac{t-2^j k}{2^j}\right)2^j \tag{5.7}$$

is defined, together with

$$d_{j,k} = \int f(t)\phi^{*}_{j,k}(t)\,dt \tag{5.8}$$

Where $d_{j,k}$ is called the scaling coefficient which is the sampled version of the original signal[25]. The DWT computes the wavelet coefficients $c_{j,k}$ *and* $d_{j,k}$ $(j=1,\ldots,J)$ given by

$$c_{j,k} = \sum_{n} x[n]h_j[n-2^j k] \tag{5.10}$$

$$d_{j,k} = \sum_n x[n] g_j [n - 2^j k] \tag{5.11}$$

Where $x[n]$ is a discrete-time series. $h_j[n-2^j k]$ is called discrete wavelets, is equivalent to $2^{-j/2}\Psi(2^{-j}(t-2^j k))$. The term $g_j[n-2^j k]$ is called scaling sequence. At the *jth* resolution $c_{j,k}$ and $d_{j,k}$ present the approximation and the detail signal $f(t)$. AT each resolution $j > 0$, the scaling coefficients and the wavelet coefficients are;

$$c_{j+1,k} = \sum_n g[n-2k] d_{j,k} \tag{5.12}$$

$$d_{j+1,k} = \sum_n h[n-2k] d_{j,k} \tag{5.13}$$

5.2 Application of DWT to Chipping Cases

5.2.1 SHANK2 Chipping

SHANK2 chipping case is investigated through the use of DWT in this section. The desired property that is tried to be captured is the start of the increase in the radial cutting force trend. If the trend start point is accurately captured, this point will yield the starting point of the chipping on the drill and the amount of chipping present on the drill.

Different wavelet types are used, and their ability to predict the point of trend starting point is compared. The radial cutting force signal is passed through DWT, approximation and detail coefficients are obtained. Approximation coefficients give the general trend of the signal; on the other hand, detailed coefficients give the high frequency components of the signal which includes highly noise and detail.

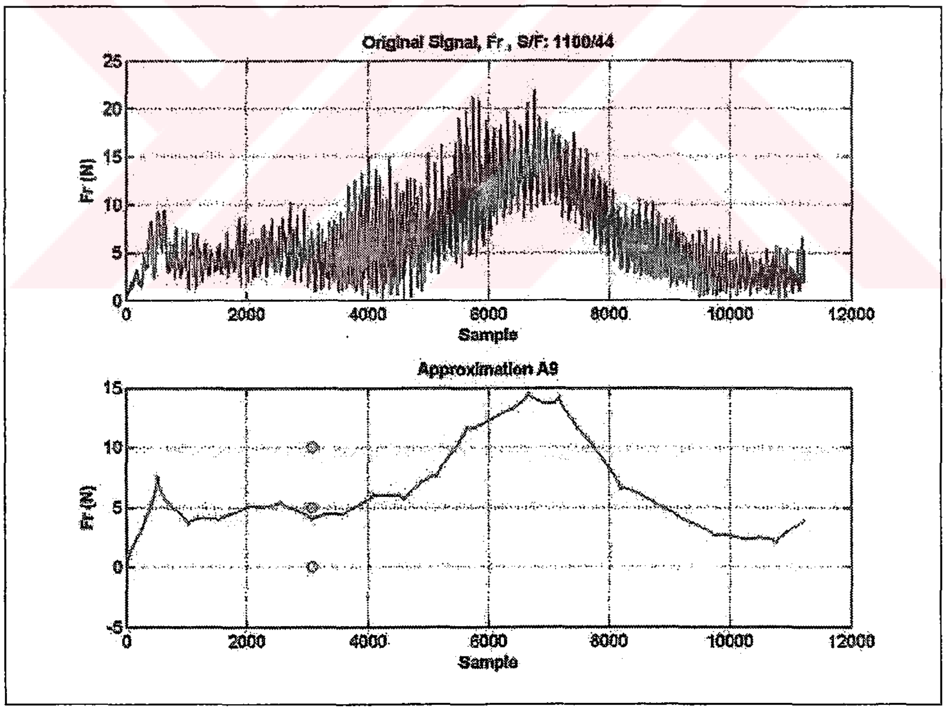

Figure 5.15: Illustration of radial cutting force signal and Approximation at level 9 for SHANK2 case for 1100 [rpm] spindle speed and 44 [mm/min] feed rate using *Coiflet1* as wavelet base of DWT.

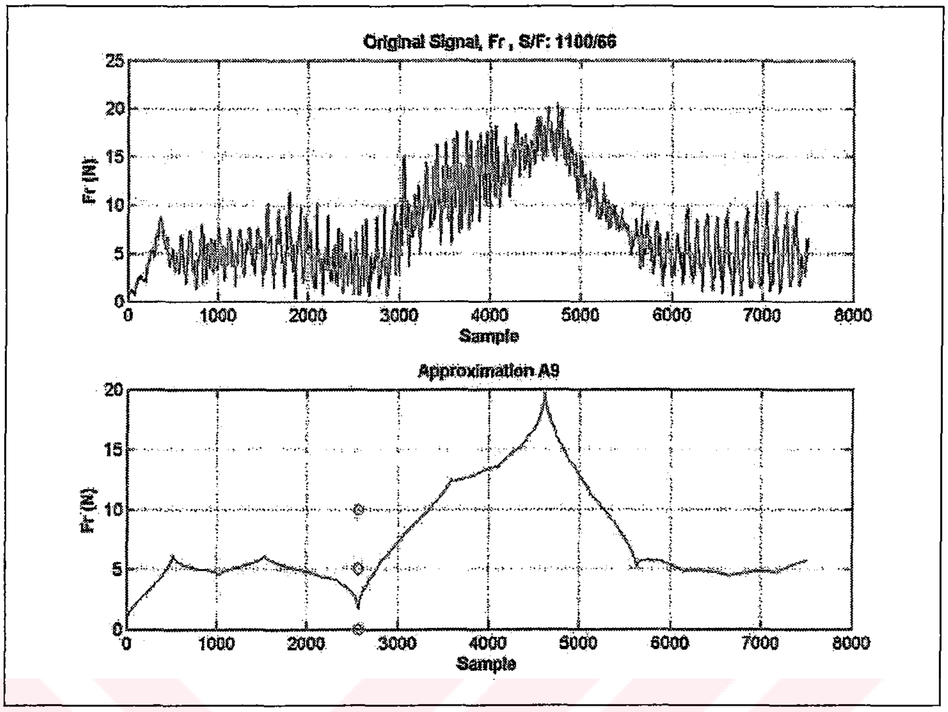

Figure 5.16: Illustration of radial cutting force signal and Approximation at level 9 for SHANK2 case for 1100 [rpm] spindle speed and 66 [mm/min] feed rate using *Coiflet1* as wavelet base of DWT.

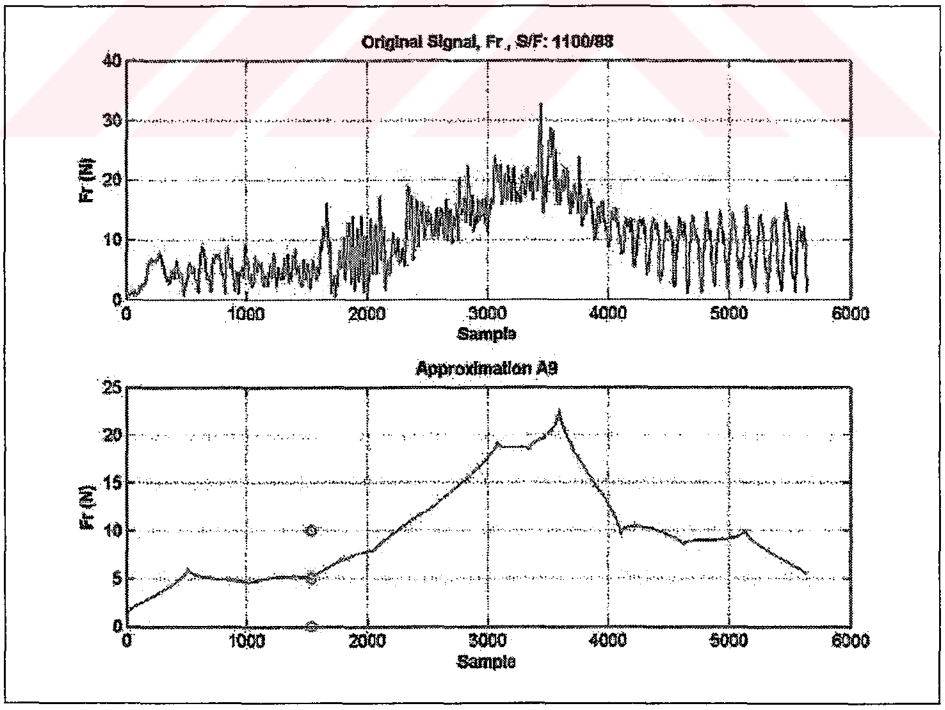

Figure 5.17: Illustration of radial cutting force signal and Approximation at level 9 for SHANK2 case for 1100 [rpm] spindle speed and 88 [mm/min] feed rate using *Coiflet1* as wavelet base of DWT.

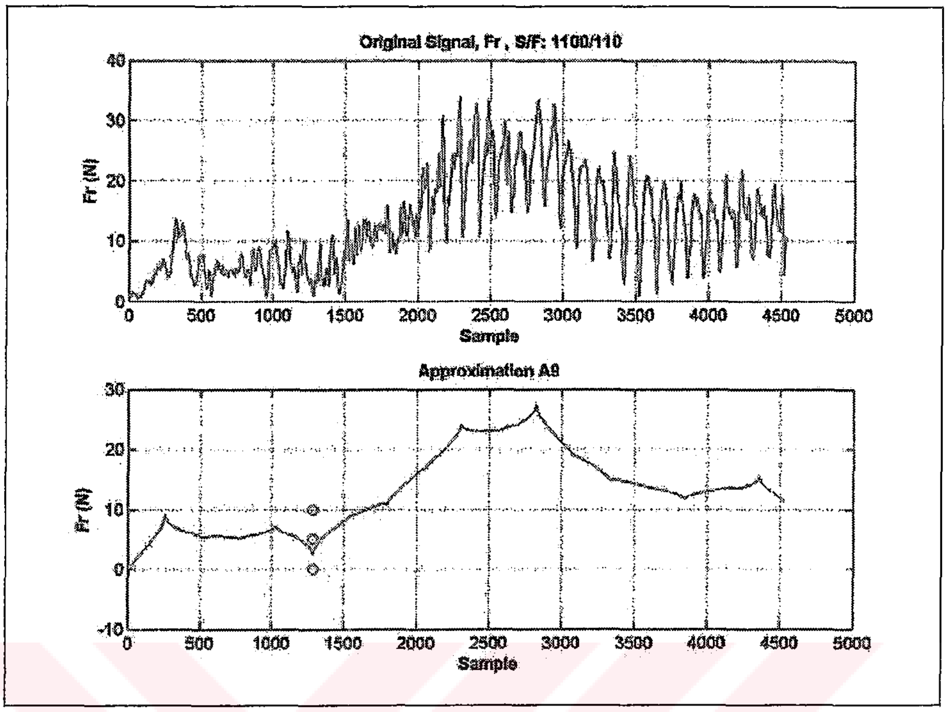

Figure 5.18: Illustration of radial cutting force signal and Approximation at level 9 for SHANK2 case for 1100 [rpm] spindle speed and 110 [mm/min] feedrate using *Coiflet1* as wavelet base of DWT.

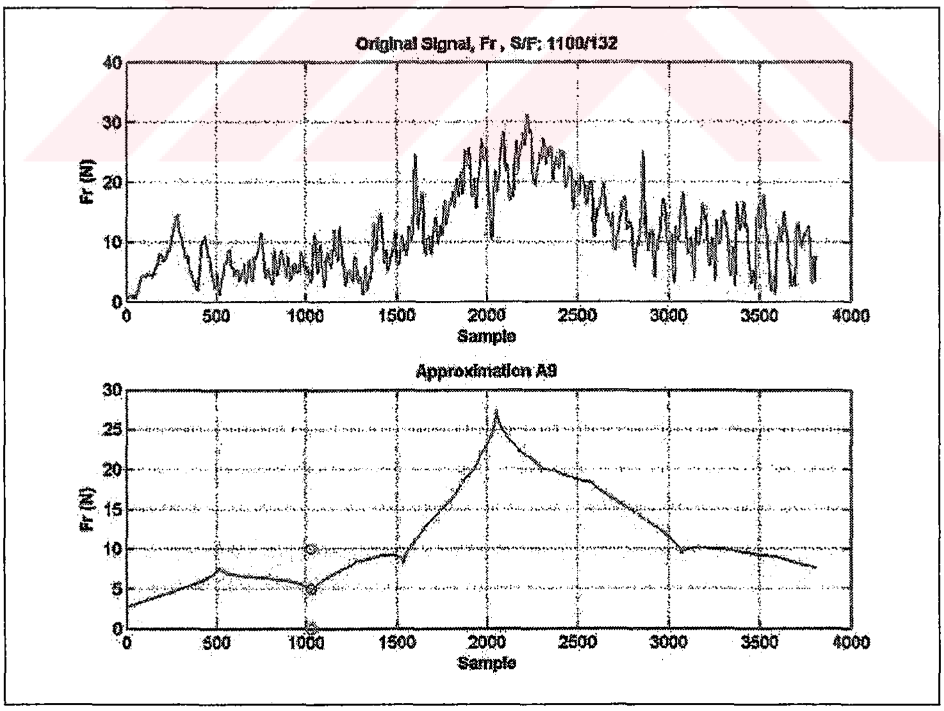

Figure 5.19: Illustration of radial cutting force signal and Approximation at level 9 for SHANK2 case for 1100 [rpm] spindle speed and 132 [mm/min] feed rate using *Coiflet1* as wavelet base of DWT.

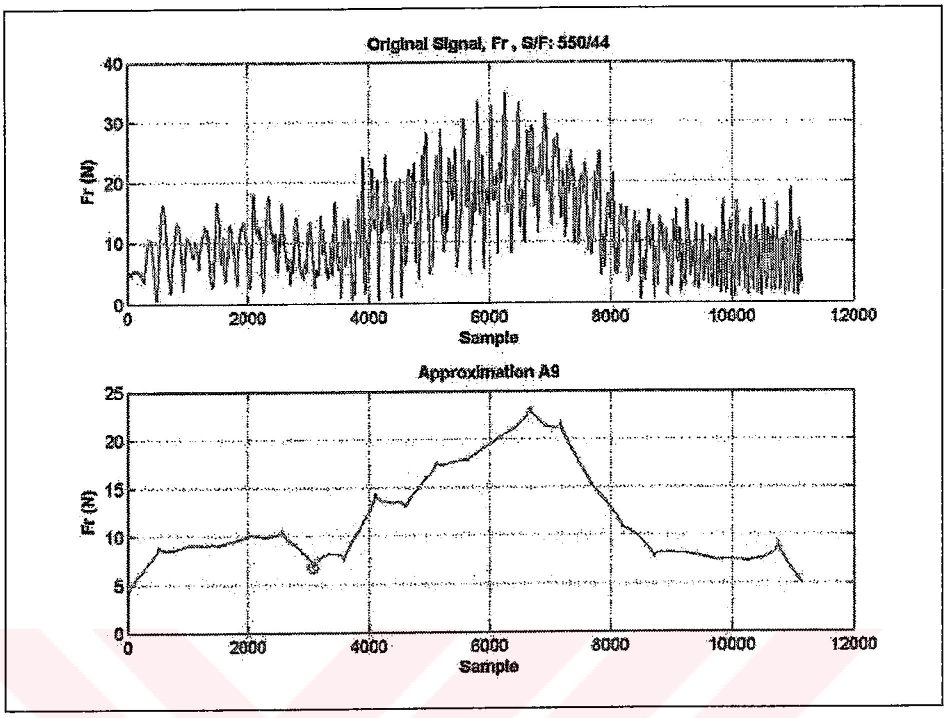

Figure 5.20: Illustration of radial cutting force signal and Approximation at level 9 for SHANK2 case for 550 [rpm] spindle speed and 44 [mm/min] feed rate using *Coiflet1* as wavelet base of DWT.

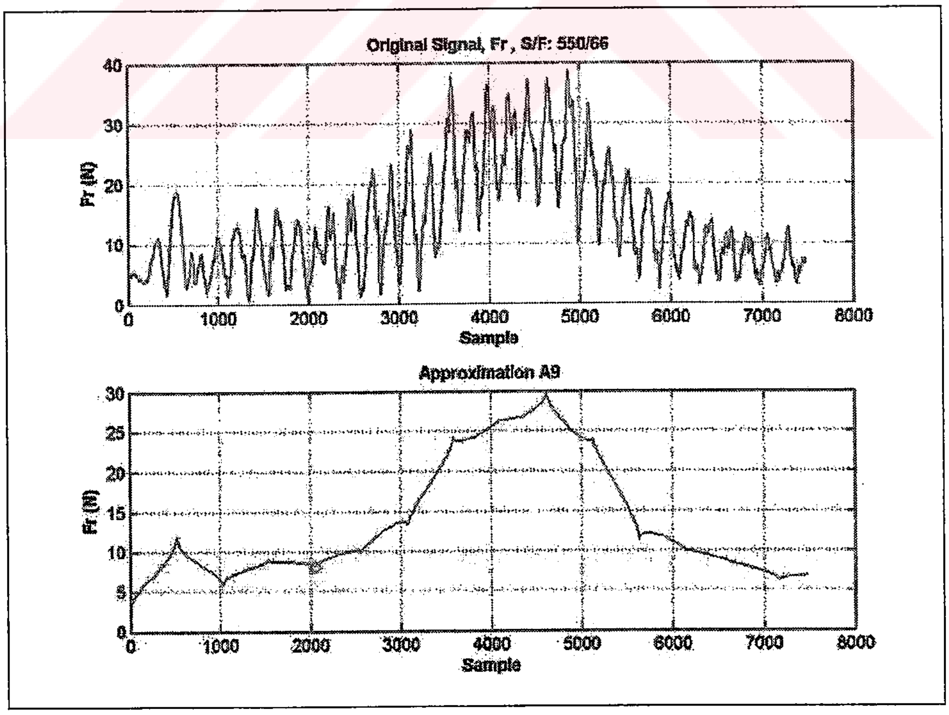

Figure 5.21: Illustration of radial cutting force signal and Approximation at level 9 for SHANK2 case for 550 [rpm] spindle speed and 66 [mm/min] feed rate using *Coiflet1* as wavelet base of DWT.

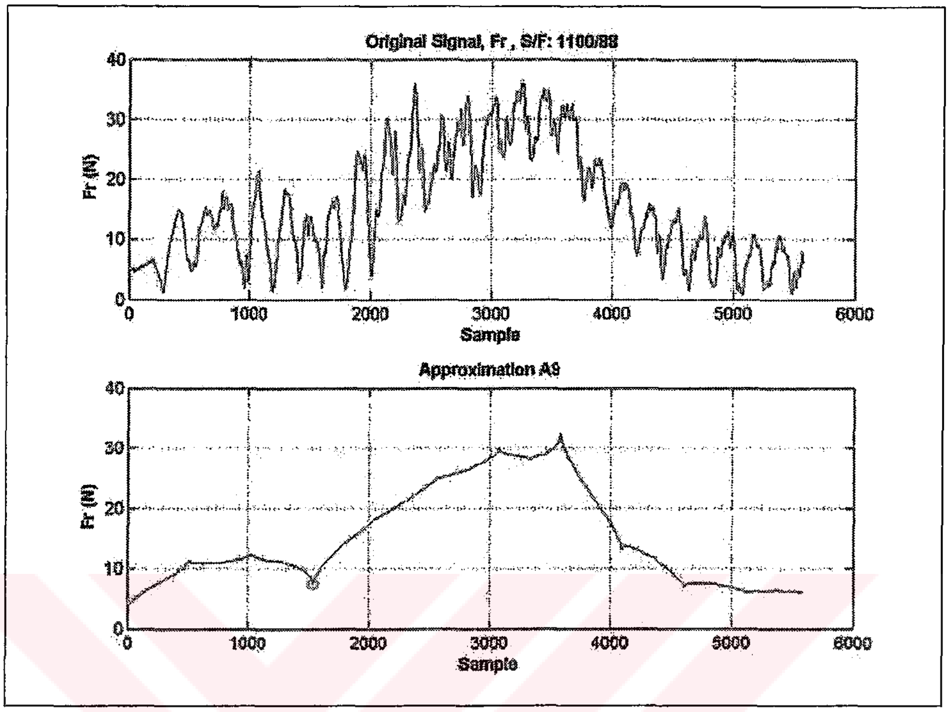

Figure 5.22: Illustration of radial cutting force signal and Approximation at level 9 for SHANK2 case for 550 [rpm] spindle speed and 88 [mm/min] feed rate using *Coiflet1* as wavelet base of DWT.

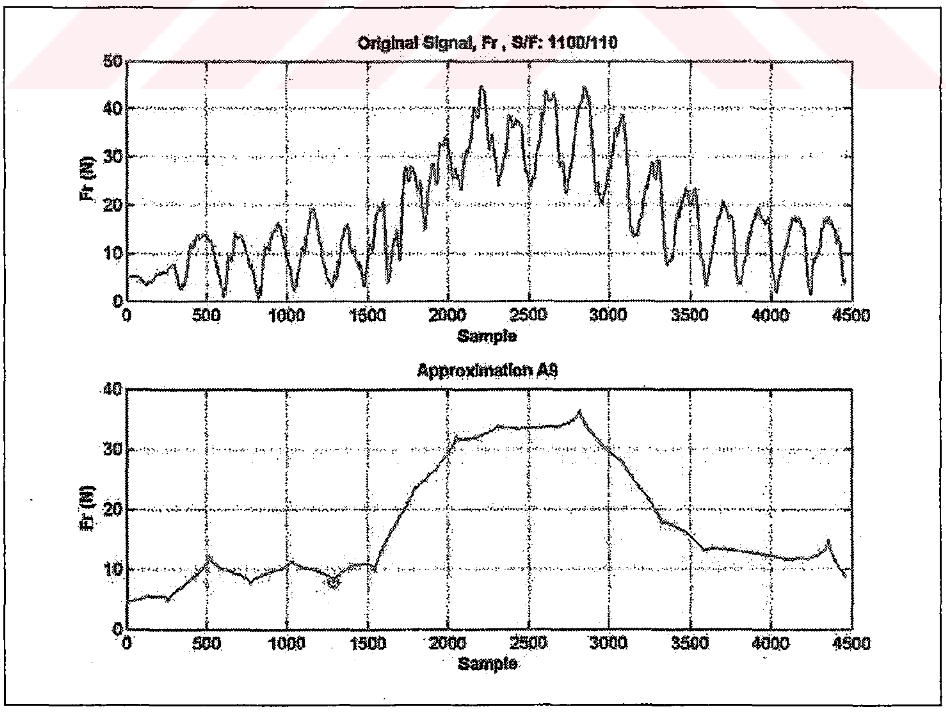

Figure 5.23: Illustration of radial cutting force signal and Approximation at level 9 for SHANK2 case for 550 [rpm] spindle speed and 110 [mm/min] feed rate using *Coiflet1* as wavelet base of DWT.

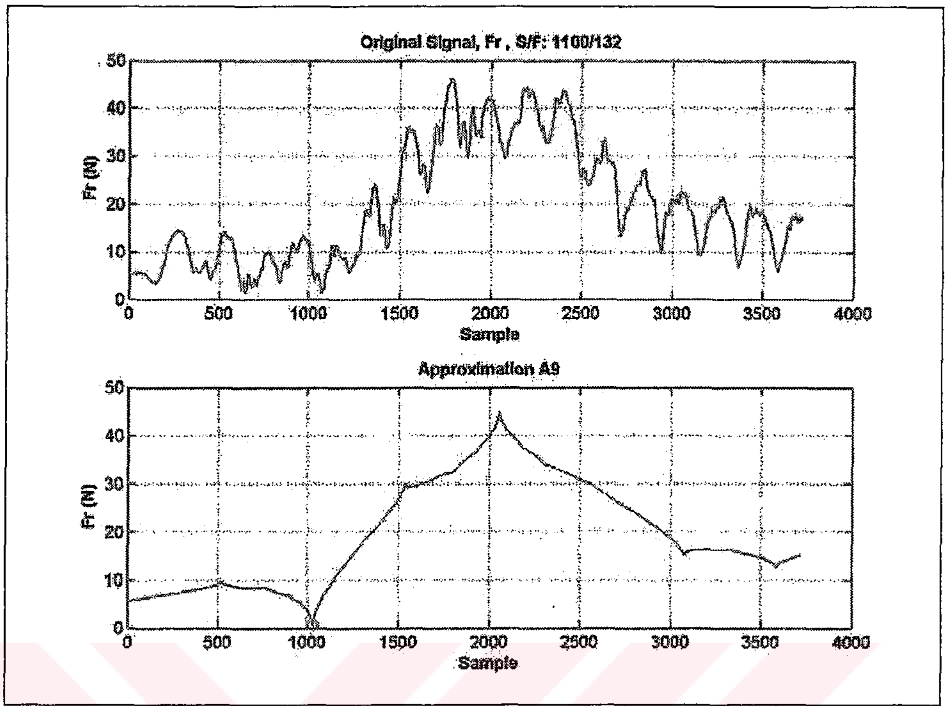

Figure 5.24: Illustration of radial cutting force signal and Approximation at level 9 for SHANK2 case for 550 [rpm] spindle speed and 132 [mm/min] feed rate using *Coiflet1* as wavelet base of DWT.

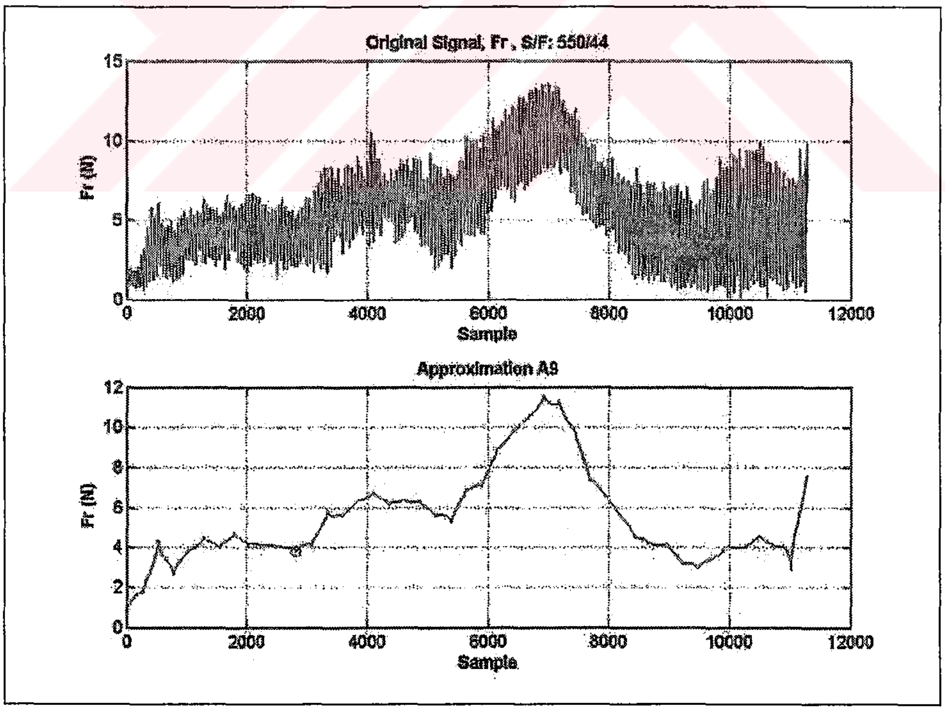

Figure 5.25: Illustration of radial cutting force signal and Approximation at level 9 for SHANK2 case for 2200 [rpm] spindle speed and 44[mm/min] feed rate using *Coiflet1* as wavelet base of DWT.

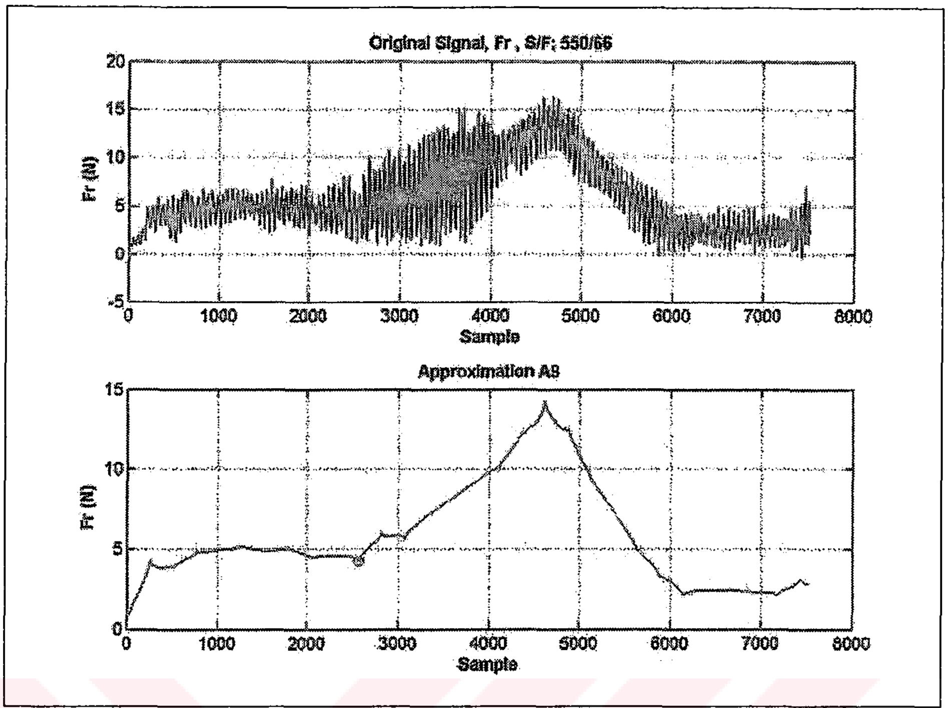

Figure 5.26: Illustration of radial cutting force signal and Approximation at level 9 for SHANK2 case for 2200 [rpm] spindle speed and 66[mm/min] feed rate using *Coiflet1* as wavelet base of DWT.

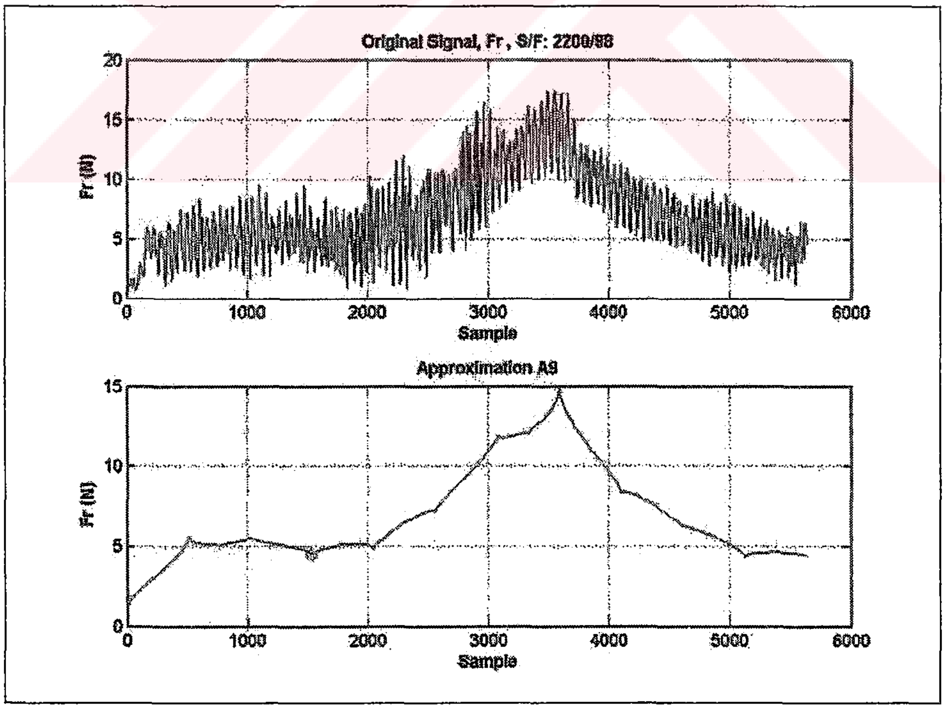

Figure 5.27: Illustration of radial cutting force signal and Approximation at level 9 for SHANK2 case for 2200 [rpm] spindle speed and 88[mm/min] feed rate using *Coiflet1* as wavelet base of DWT.

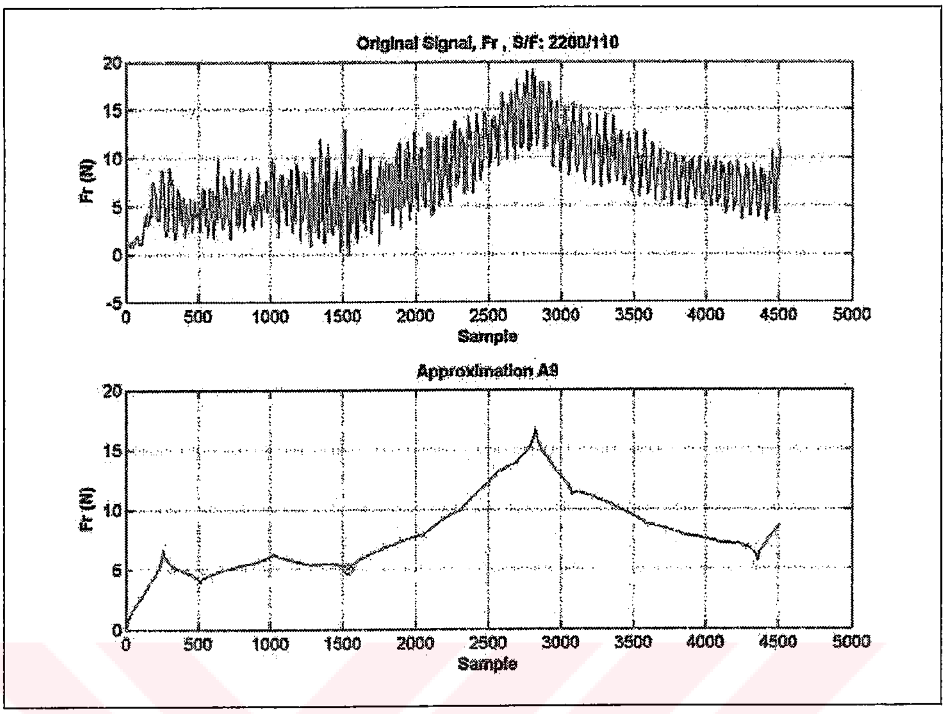

Figure 5.28: Illustration of radial cutting force signal and Approximation at level 9 for SHANK2 case for 2200 [rpm] spindle speed and 110[mm/min] feed rate using *Coiflet1* as wavelet base of DWT.

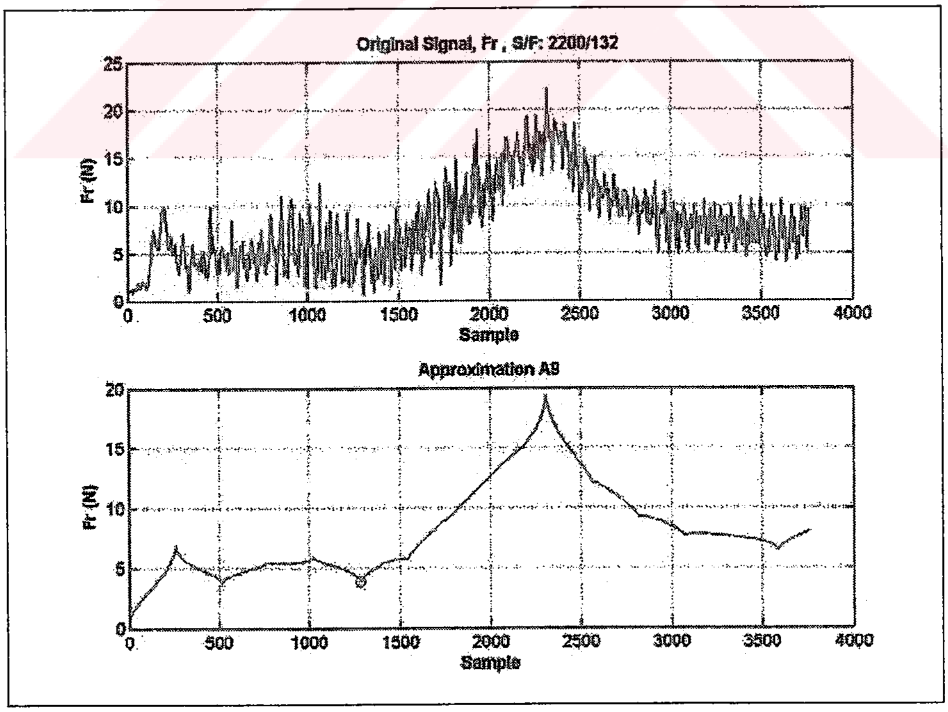

Figure 5.29: Illustration of radial cutting force signal and Approximation at level 9 for SHANK2 case for 2200 [rpm] spindle speed and 132[mm/min] feed rate using *Coiflet1* as wavelet base of DWT.

Table 5.1: Illustration of Z (depth) of starting of increase in radial cutting force trend for spindle speeds 550/1100/2200 [rpm] and feed rates of 44/66/88/110/132 [mm/min] for SHANK2 case using *Coiflet 1* as wavelet base.

Feed Rate [mm/min]	Coif1/550 [mm]	Coif1/1100 [mm]	Coif1/2200 [mm]	True Value [mm]
44	1.133	1.128	1.027	1.180
66	1.125	1.412	1.410	1.180
88	1.133	1.134	1.133	1.180
110	1.180	1.174	1.414	1.180
132	1.133	1.124	1.404	1.180

Table 5.2: Illustration of percent error [%] in Z (depth) of starting of increase in radial cutting force trend for spindle speeds 550/1100/2200 [rpm] and feed rates of 44/66/88/110/132 [mm/min] for SHANK2 case using *Coiflet 1* as wavelet base.

Feed Rate [mm/min]	Coif1/550 [%]	Coif1/1100 [%]	Coif1/2200 [%]
44	4.0	4.4	12.9
66	4.6	19.6	19.5
88	4.0	3.9	4.0
110	0.3	0.5	19.9
132	4.0	4.7	18.9

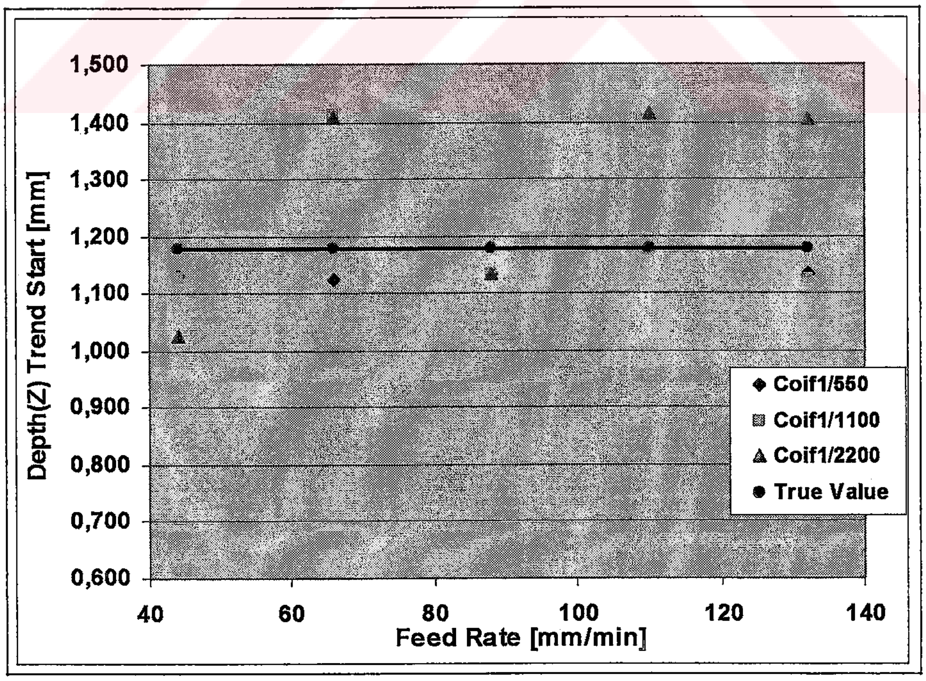

Figure5.30: Illustration of Z (depth) of starting of increase in radial cutting force trend for spindle speeds 550/1100/2200 [rpm] and feed rates of 44/66/88/110/132 [mm/min] for SHANK2 case using *Coiflet 1* as wavelet base.

Same analysis as above is performed done by using different wavelet bases for DWT. The *db3, db8,. dmey* and *sym6* are the wavelet bases used.

Table 5.3: Comparison of Z (depth) of starting of increase in radial cutting force trend for spindle speeds 1100 [rpm] and feed rates of 44/66/88/110/132 [mm/min] for SHANK2 case using *db3, db8. dmey, sym6 and Coiflet 1* as wavelet base.

Feed Rate	db3/1100 [mm]	db8/1100 [mm]	dmey/1100 [mm]	sym6/1100 [mm]	Coif1/1100 [mm]	True [mm]
44	1.140	1.198	1.140	1.198	1.128	1.180
66	1.412	1.400	1.412	1.400	1.412	1.180
88	0.758	0.864	0.758	0.864	1.134	1.180
110	0.938	1.056	0.938	1.056	1.174	1.180
132	1.136	1.148	1.136	1.148	1.124	1.180

Table 5.4: Comparison of percent error in Z (depth) of starting of increase in radial cutting force trend for spindle speeds 1100 [rpm] and feed rates of 44/66/88/110/132 [mm/min] for SHANK2 case using *db3, db8, dmey, sym6 and Coiflet 1* as wavelet base.

Feed Rate	db3/1100	db8/1100	dmey/1100	sym6/1100	Coif1/1100
44	3.4	1.5	3.4	1.5	4.4
66	19.6	18.6	19.6	18.6	19.6
88	35.7	26.8	35.7	26.8	3.9
110	20.5	10.5	20.5	10.5	0.5
132	3.7	2.7	3.7	2.7	4.7

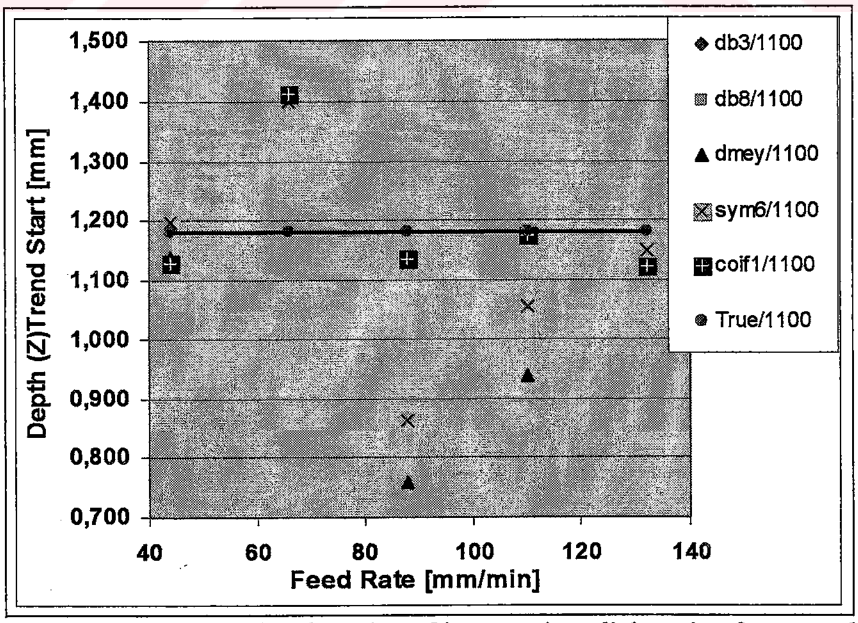

Figure5.31: Illustration of Z (depth) of starting of increase in radial cutting force trend for spindle speeds 1100 [rpm] and feed rates of 44/66/88/110/132 [mm/min] for SHANK2 case using *db3, db, . dmey, sym6 and Coiflet 1* as wavelet base..

5.2.2 Arbitrary Chipping

In this section. arbitrarily given chipping case is investigated using wavelet transform. To do this. different type of wavelet bases are used for DWT to capture the start and end point of arbitrary chipping. Arbitrary chipping case starts and ends along the cutting edge. The expected force increase will begin by the start of the arbitrary chipping end reaches maximum as the arbitrary chipping is fully covered.

Table 5.5: Comparison of Z (depth) of starting of increase and maximum in radial cutting force trend for spindle speeds 1100 [rpm] and feed rates of 44/66/88/110/132 [mm/min] for ARB. Case using *Coiflet 1 and db9* as wavelet base.

	Coif1		db9/A9		db9/A7		TRUE	
Feed Rate [mm/min]	Start	End	Start	End	Start	End	Start	End
44	1.339	1.722	1.192	1.692	1.221	1.751	1.034	1.650
66	1.133	1.692	1.163	1.810	1.133	1.815	1.034	1.650
88	1.133	1.899	1.133	1.781	1.104	1.760	1.034	1.650
110	0.957	1.898	1.045	1.869	1.045	1.663	1.034	1.650
132	1.133	1.693	1.104	1.575	1.075	1.575	1.034	1.650

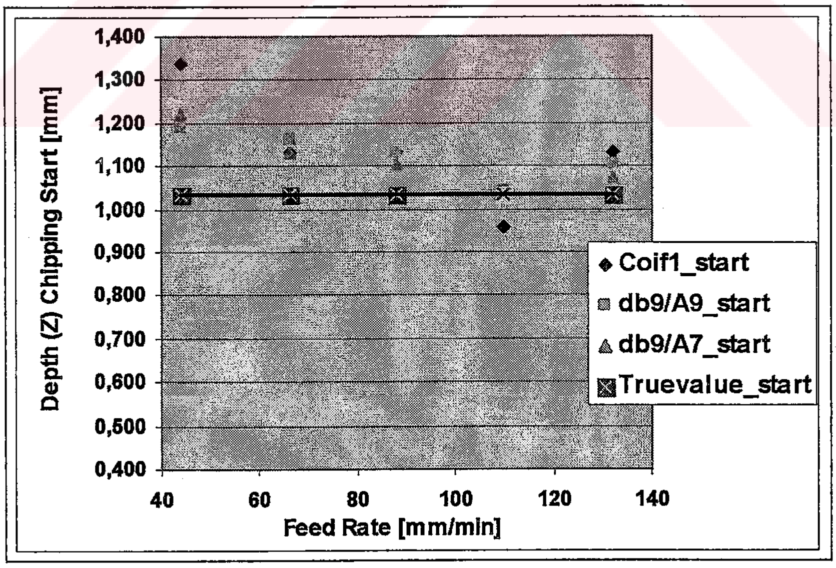

Figure5.32: Illustration of Z (depth) of starting of increase in radial cutting force trend for spindle speeds 1100 [rpm] and feed rates of 44/66/88/110/132 [mm/min] for ARB. Case using *Coiflet 1 and db9* as wavelet base.

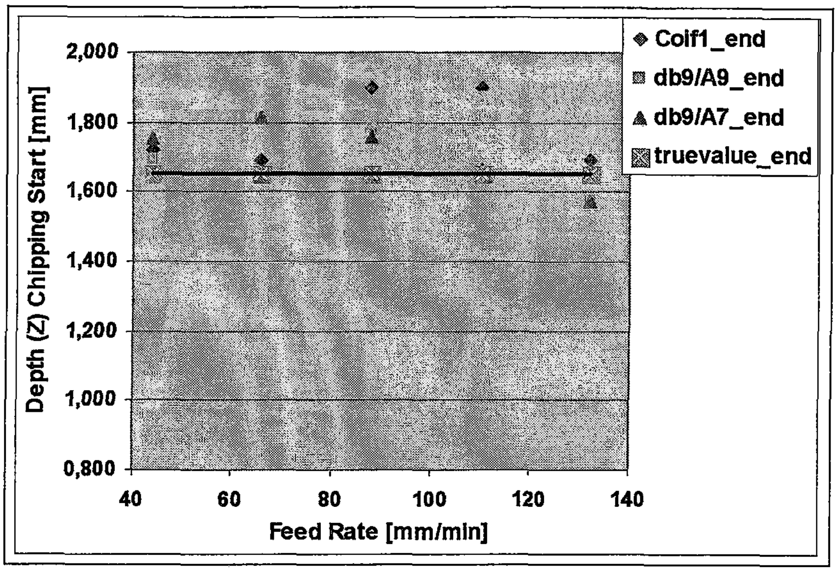

Figure5.33: Illustration of Z (depth) of maximum point of radial cutting force trend for spindle speeds 1100 [rpm] and feed rates of 44/66/88/110/132 [mm/min] for ARB. Case using *Coiflet 1 and db9* as wavelet base.

Table 5.6: Comparison of difference of Z(depth) values for start and end of radial cutting force trend. feed rates 44/66/88/110/132 [mm/min] and spindle speed 1100 [rpm]. ARB case.

Feed Rate [mm/min]	coif1	db9/A9	db9/A7	TRUE
44	0.382	0.500	0.530	0.616
66	0.559	0.647	0.682	0.616
88	0.766	0.648	0.656	0.616
110	0.941	0.824	0.618	0.616
132	0.560	0.471	0.501	0.616

Table 5.7: Comparison of percent error in difference of Z (depth) values for start and end of radial cutting force trend. feed rates 44/66/88/110/132 [mm/min] and spindle speed 1100 [rpm]. ARB case.

Feed Rate [mm/min]	coif1	db9/A9	db9/A7
44	37.9	18.8	14.0
66	9.2	5.1	10.7
88	24.3	5.1	6.5
110	52.8	33.8	0.3
132	9.1	23.6	18.8

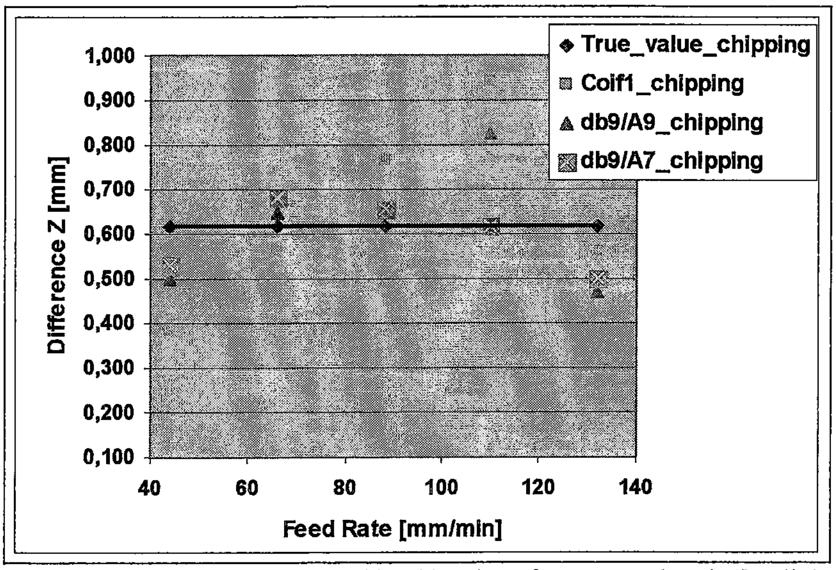

Figure 5.34: Comparison of difference of Z(depth) values for start and end of radial cutting force trend. feed rates 44/66/88/110/132 [mm/min] and spindle speed 1100 [rpm]. ARB case.

5.3 Application of Fast Fourier Transform (FFT) to the Chipping Cases

5.3.1. Introduction to the Fourier Transform

Given a function *h(t)* specified for all *t*. the continuous Fourier transform (FT) of *h(t)* is defined as

$$H(f) = \int_{-\infty}^{+\infty} h(t)\, e^{2\pi i f t}\, dt \qquad (5.14)$$

Frequently. the function *h(t)* is not measured or specified continuously. But rather is measured at fixed intervals of time or sampled. If *h(t)* is measured at the discrete times given by

$$t_n = n\Delta, \quad n = \ldots\text{-}3.\text{-}2.\text{-}1.0.1.2.3\ldots \qquad (5.15)$$

where Δ is known as the sampling interval. We may write

$$h_n = h(t_n) \qquad (5.16)$$

and h_n is a discrete representation of *h(t)*. The sampling theorem is very important and states that a band-limited function *f(t)* is completely specified by the sampled values $f(t_n)$. provided that the sampling interval is no longer than

$$\Delta = \frac{1}{2f_c} \qquad (5.17)$$

The frequency f_c is then known as the Nyquist frequency. for the given sampling interval Δ.
Suppose that the function *h(t)* has been measured only at the discrete times t_k (either at the given times. or averaged over the corresponding time interval) given by

$$t_k = k\Delta \quad k = 0.1.2.\ldots.N\text{-}1 \qquad (5.18)$$

where N is the number of samples. (cases in which N is even and indeed a power of 2 will be considered). The Discrete Fourier Transform (DFT) is then defined as

$$H_n = H(f_n) = \Delta \sum_{k=0}^{N-1} h_k e^{2\pi i k n / N} \qquad (5.19)$$

where the frequencies f_n are given by

$$f_n = \frac{n}{N\Delta} \quad n = -\frac{N}{2}, -\frac{N}{2}+1, \ldots, \frac{N}{2}-1, \frac{N}{2} \tag{5.20}$$

This definition is based on the idea that the sampled function h_k is replicated indefinitely. in the sense that $k_0 = k_N = k_{2N} = \ldots.$ $k_0 = k_{-N} = k_{-2N} = \ldots$ and so forth for all the other elements. There is clearly a close relationship between the DFT and the continuous Fourier integral. The DFT requires the calculation of the sums

$$H(f) = \int_{-\infty}^{+\infty} h(t)\, e^{2\pi i f t}\, dt \tag{5.21}$$

Where $W = exp(2\pi i/N)$. At first sight. This requires at least N^2 multiplications to generate all N of the coefficients H_n. But this is not the case. The summation may be broken into two parts. one over the even-numbered elements (k = 0.2.4....) and the other over the odd-numbered elements (k = 1.3.5...). In turn. Each one of these parts can be broken into *its* even-numbered and odd-numbered parts. And the process can be continued. With careful book-keeping. Until the summation has become divided into 1-point Fourier transforms (which are identity transforms). This repeated dissection of the series into even- and odd-numbered parts can be implemented in the computer by reversing the bit-pattern of the addresses of the data elements. After this is done. the required **N** values of H_n can be generated by making a sequence of 2.4.8....-point summations. The total time for the operation scales not as N^2 but as NlogN, so that for large transforms there is an enormous saving in time.

5.3.2 Application of FFT

In this section, FFT algorithm will be used to obtain the frequency content of the chipped and fresh tools. How the frequency content of the tools is changing according to chipping amount/type, feed rate and spindle speed will be investigated in this section. The change in the frequency content will be used as monitoring features regarding the feed rate, spindle speed and chipping amount/type.

If the FFT result of a typical drilling cutting force in X direction is analyzed, it shows a peak at the spindle speed frequency. The chipped tool shows a variation from the fresh tool as the spindle frequency amplitude is considered. This variation will be depicted in the figures below.

5.3.2.1 FFT Plots:

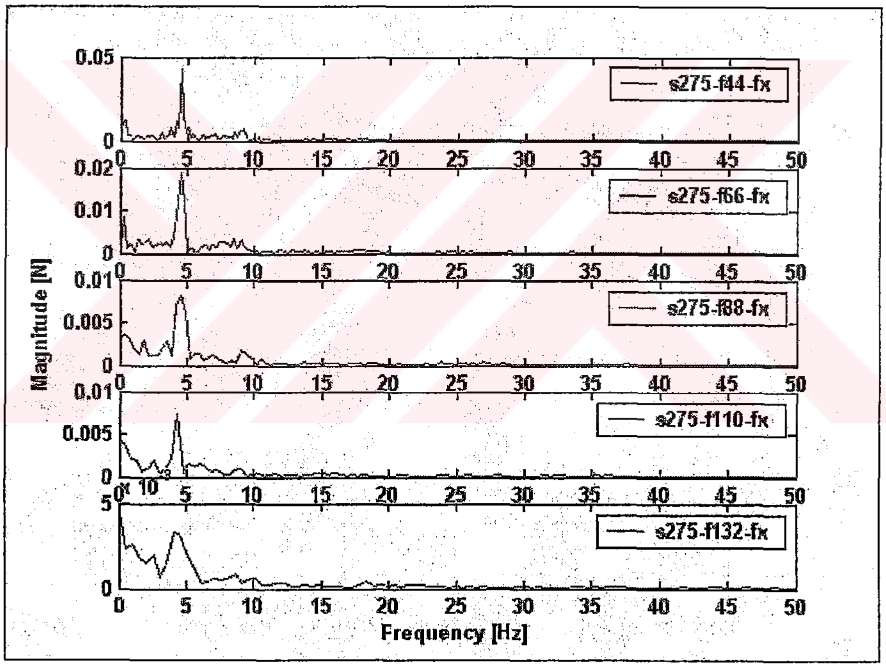

Figure 5.35: Frequency content of cutting force in X direction of Fresh Drill for spindle speed 275 [rpm] and feed rates 44-66-88-110-132 [mm/min].

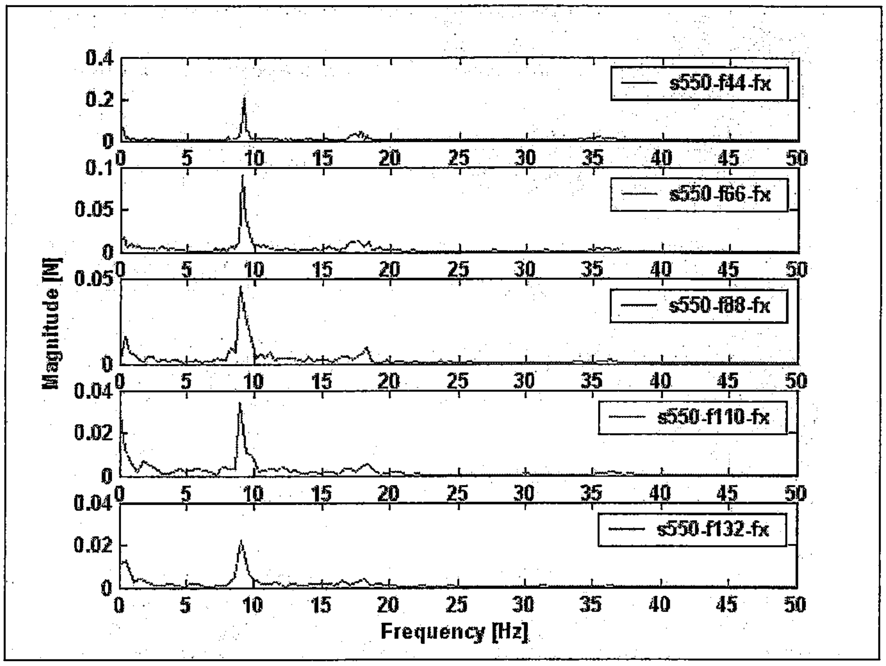

Figure 5.36: Frequency content of cutting force in X direction of Fresh Drill for spindle speed 550 [rpm] and feed rates 44-66-88-110-132 [mm/min].

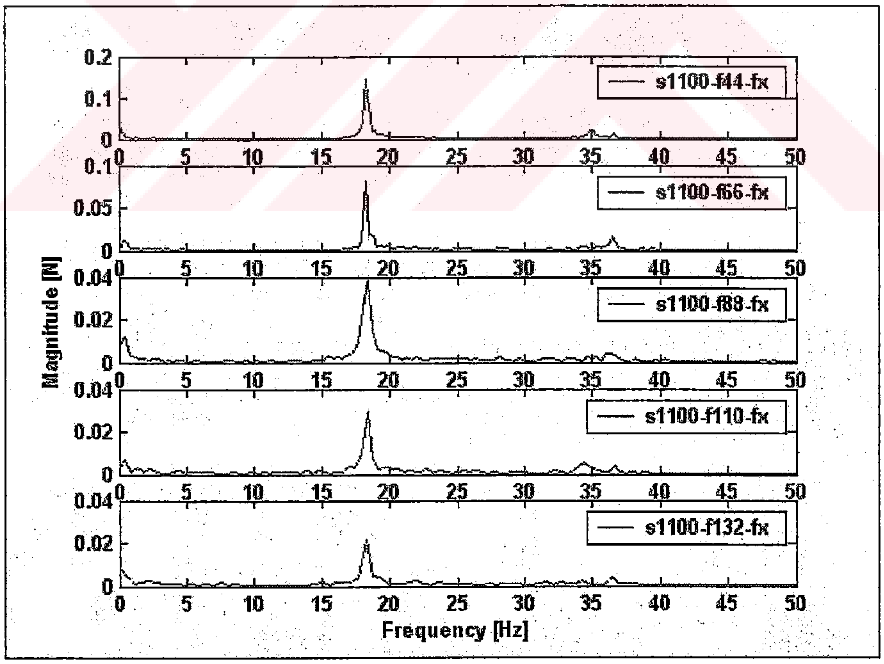

Figure 5.37: Frequency content of cutting force in X direction of Fresh Drill for spindle speed 1100 [rpm] and feed rates 44-66-88-110-132 [mm/min].

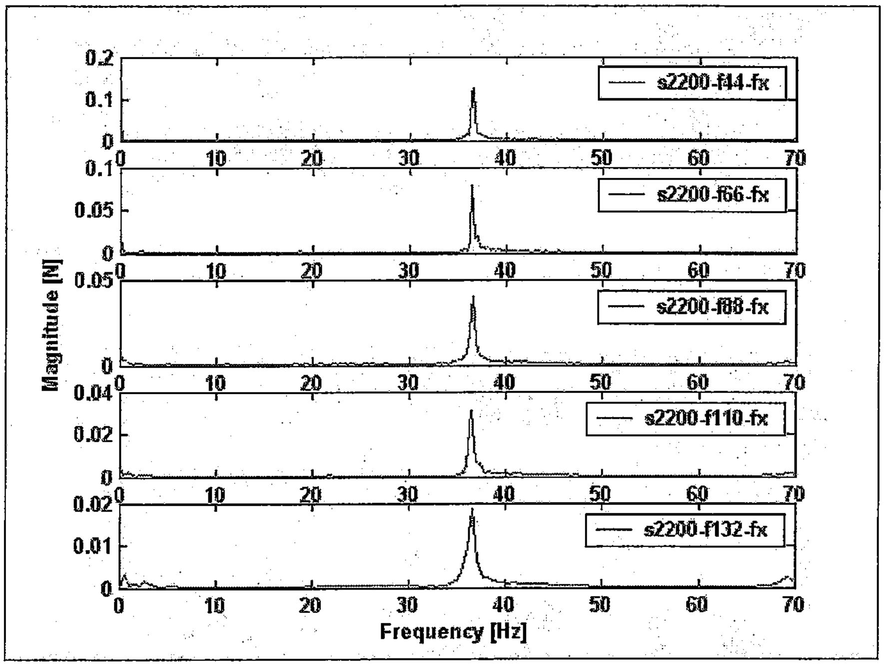

Figure 5.38: Frequency content of cutting force in X direction of Fresh Drill for spindle speed 2200 [rpm] and feed rates 44-66-88-110-132 [mm/min].

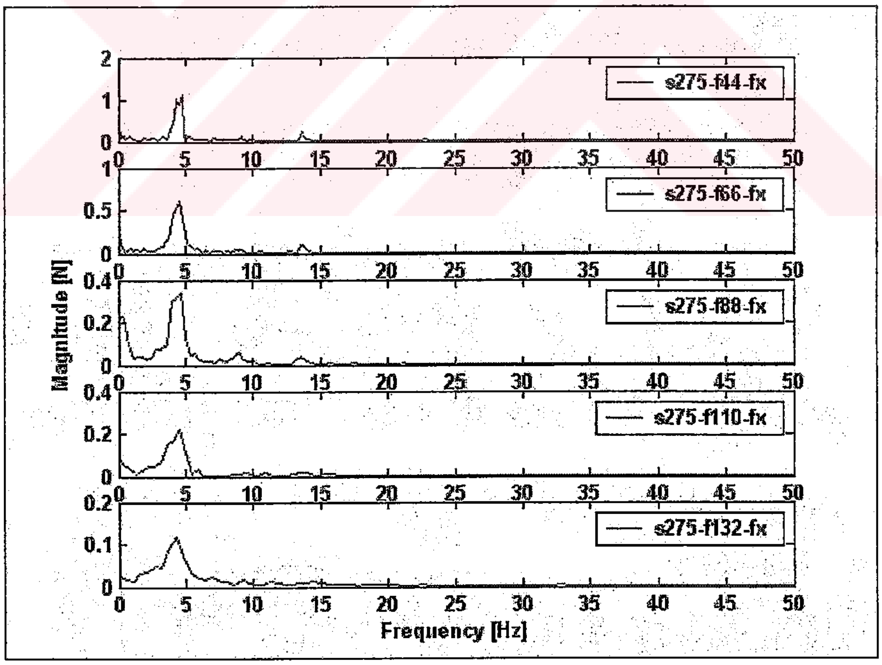

Figure5.39: Frequency content of cutting force in X direction of TIP1 Drill for spindle speed 275 [rpm] and feed rates 44-66-88-110-132 [mm/min].

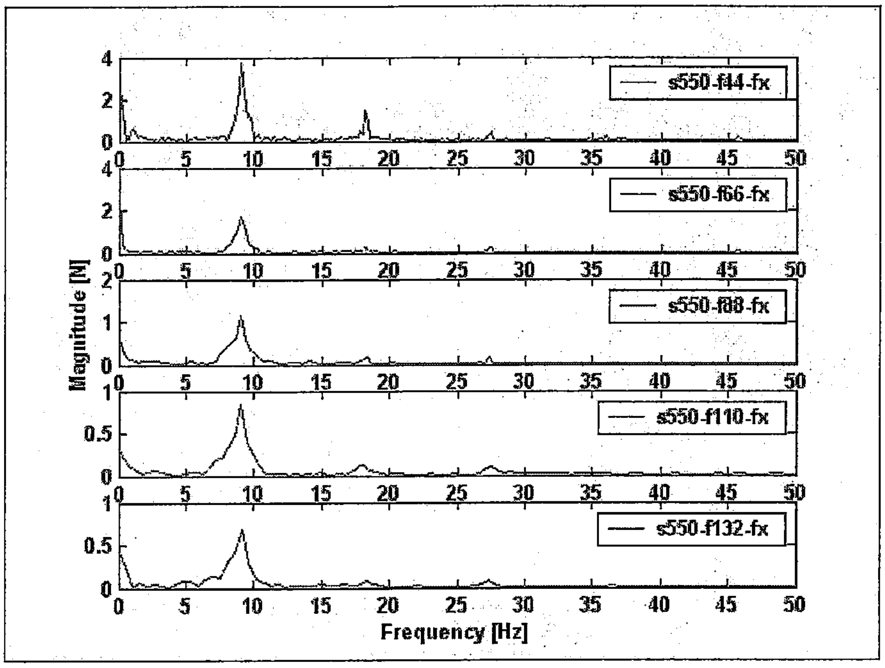

Figure 5.40: Frequency content of cutting force in X direction of TIP1 Drill for spindle speed 550 [rpm] and feed rates 44-66-88-110-132 [mm/min].

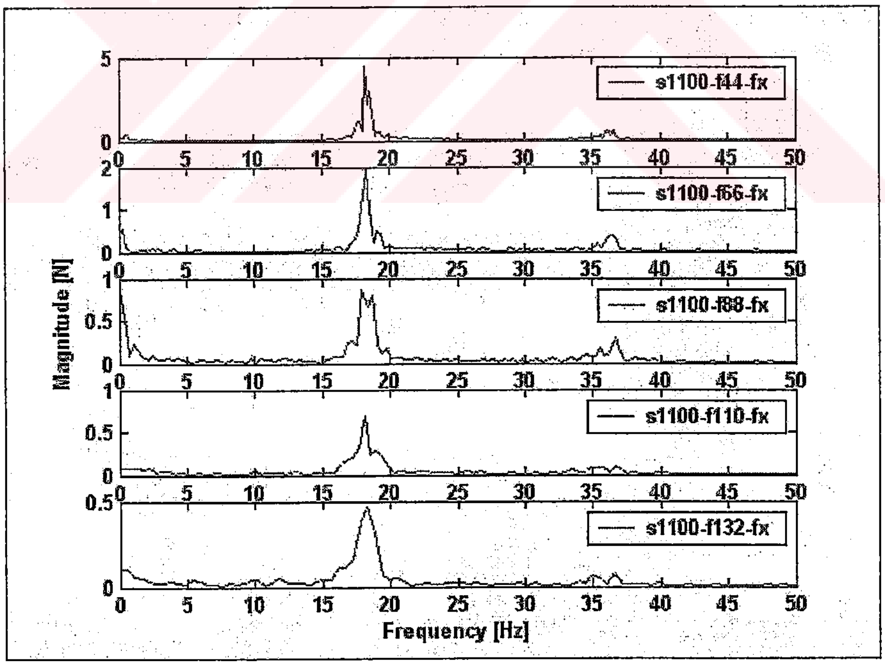

Figure 5.41: Frequency content of cutting force in X direction of TIP1 Drill for spindle speed 1100 [rpm] and feed rates 44-66-88-110-132 [mm/min].

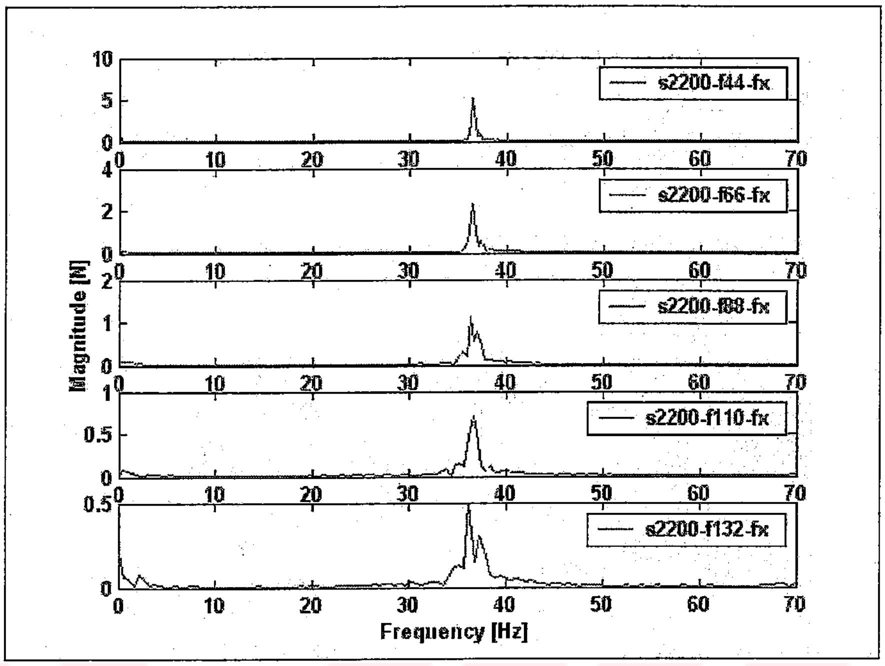

Figure 5.42: Frequency content of cutting force in X direction of TIP1 Drill for spindle speed 2200 [rpm] and feed rates 44-66-88-110-132 [mm/min].

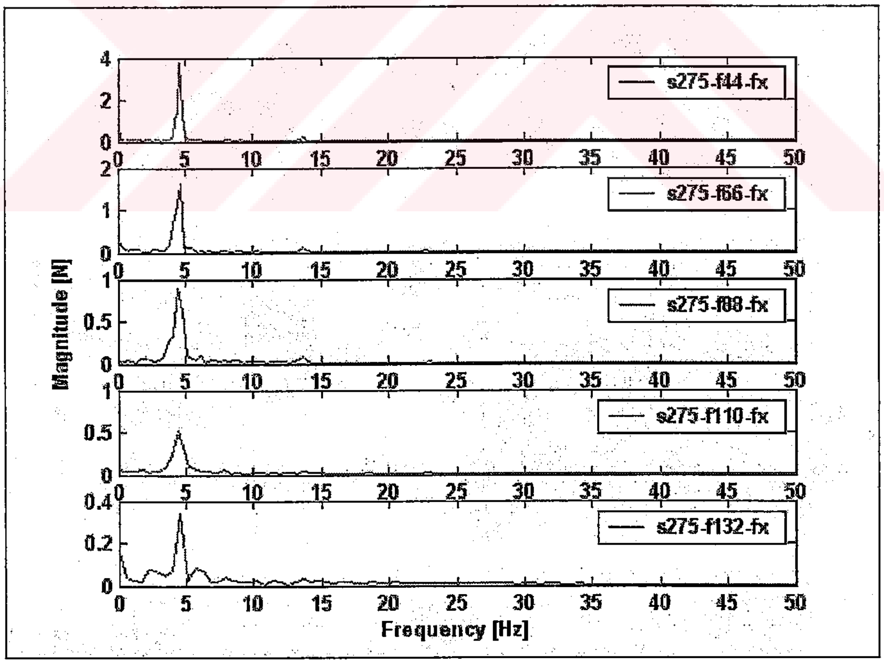

Figure 5.43 Frequency content of cutting force in X direction of TIP2 Drill for spindle speed 275 [rpm] and feed rates 44-66-88-110-132 [mm/min].

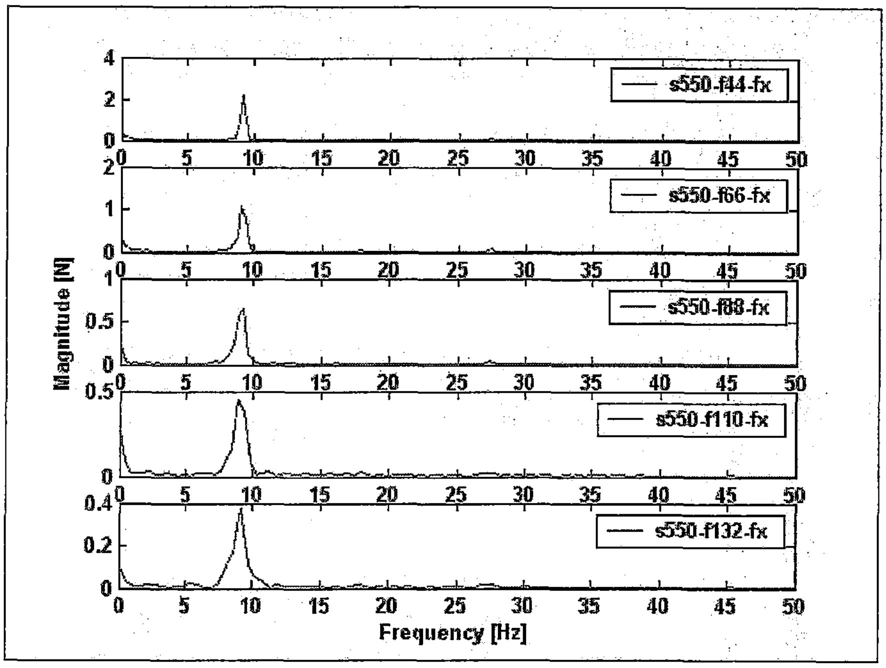

Figure5.44: Frequency content of cutting force in X direction of TIP2 Drill for spindle speed 550 [rpm] and feed rates 44-66-88-110-132 [mm/min].

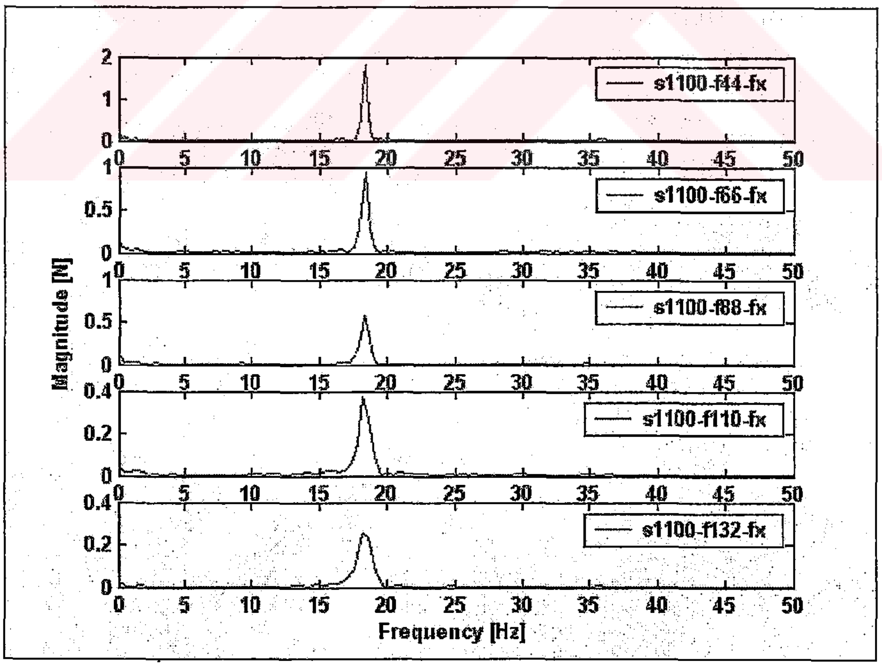

Figure5.45: Frequency content of cutting force in X direction of TIP2 Drill for spindle speed 1100 [rpm] and feed rates 44-66-88-110-132 [mm/min].

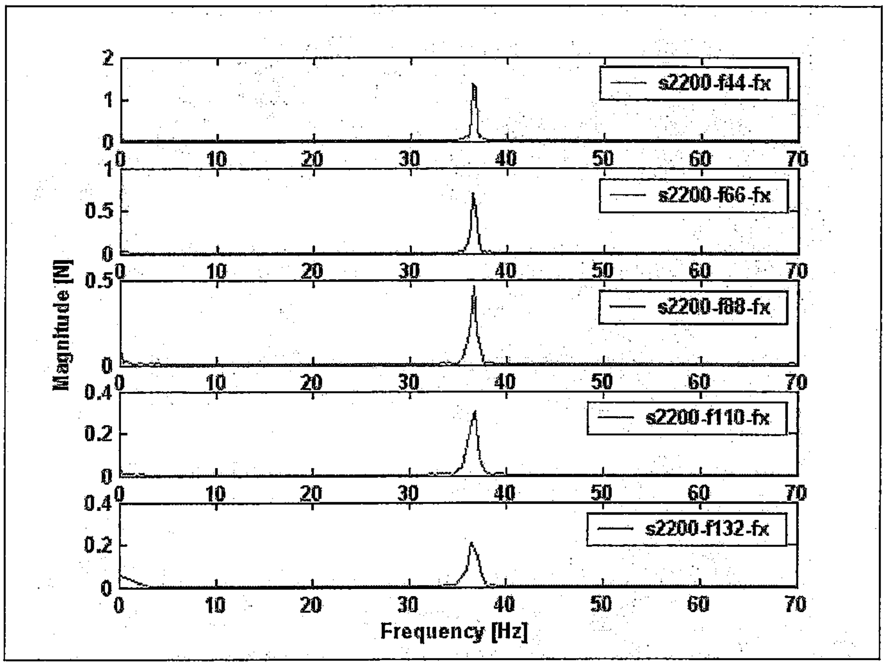

Figure5.46: Frequency content of cutting force in X direction of TIP2 Drill for spindle speed 2200 [rpm] and feed rates 44-66-88-110-132 [mm/min].

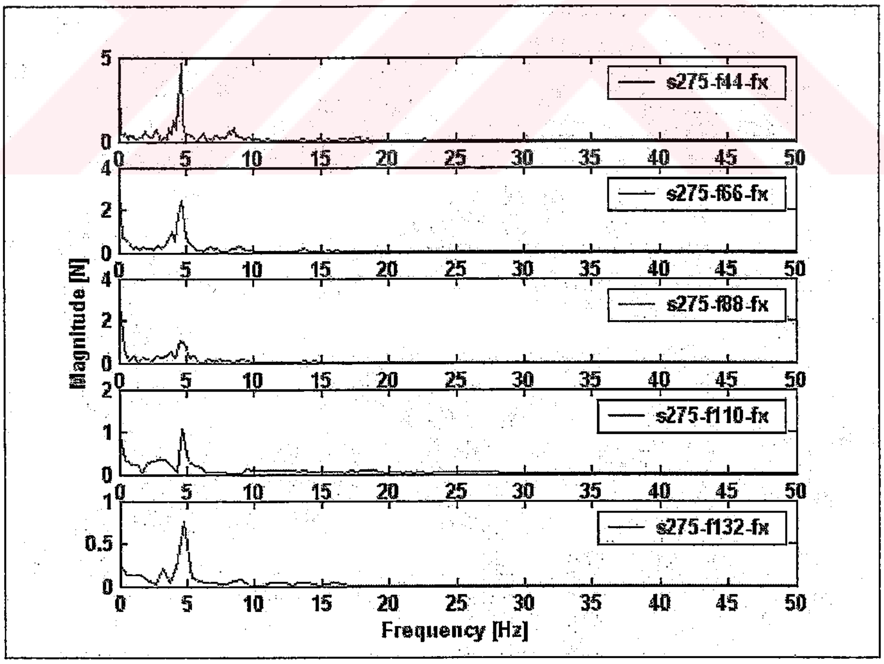

Figure5.47: Frequency content of cutting force in X direction of SHANK1 Drill for spindle speed 275 [rpm] and feed rates 44-66-88-110-132 [mm/min].

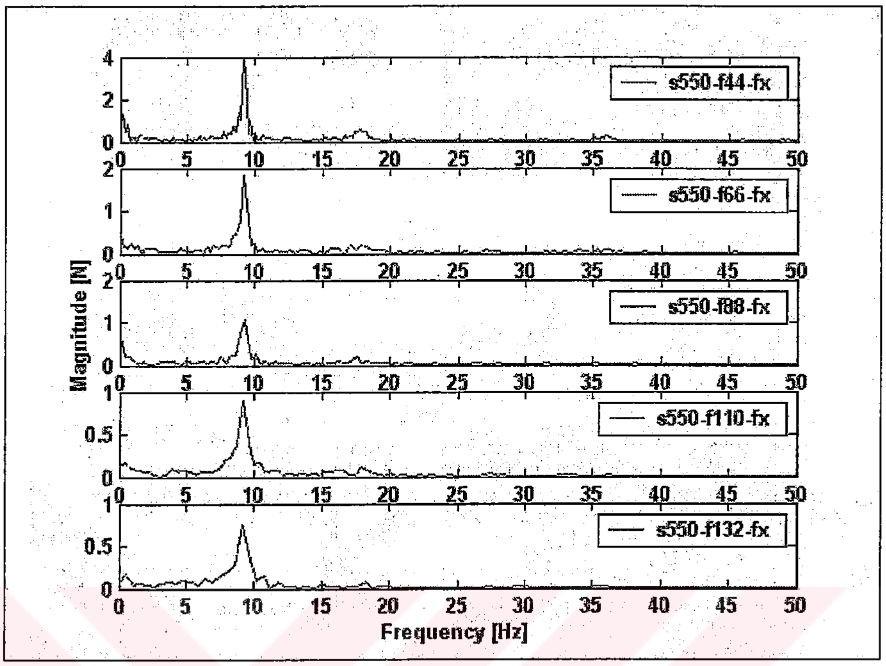

Figure5.48: Frequency content of cutting force in X direction of SHANK1 Drill for spindle speed 550 [rpm] and feed rates 44-66-88-110-132 [mm/min].

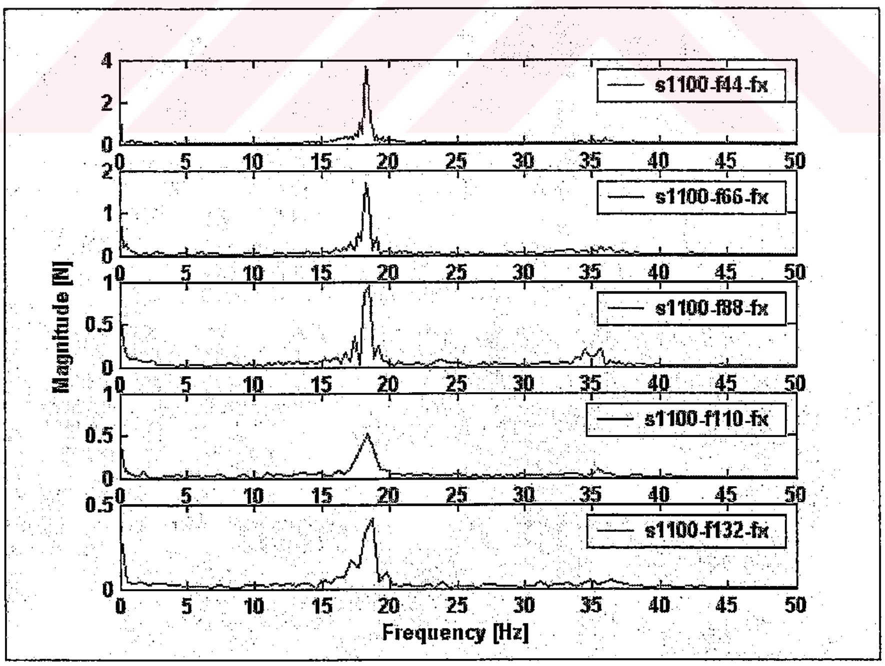

Figure5.49: Frequency content of cutting force in X direction of SHANK1 Drill for spindle speed 1100 [rpm] and feed rates 44-66-88-110-132 [mm/min].

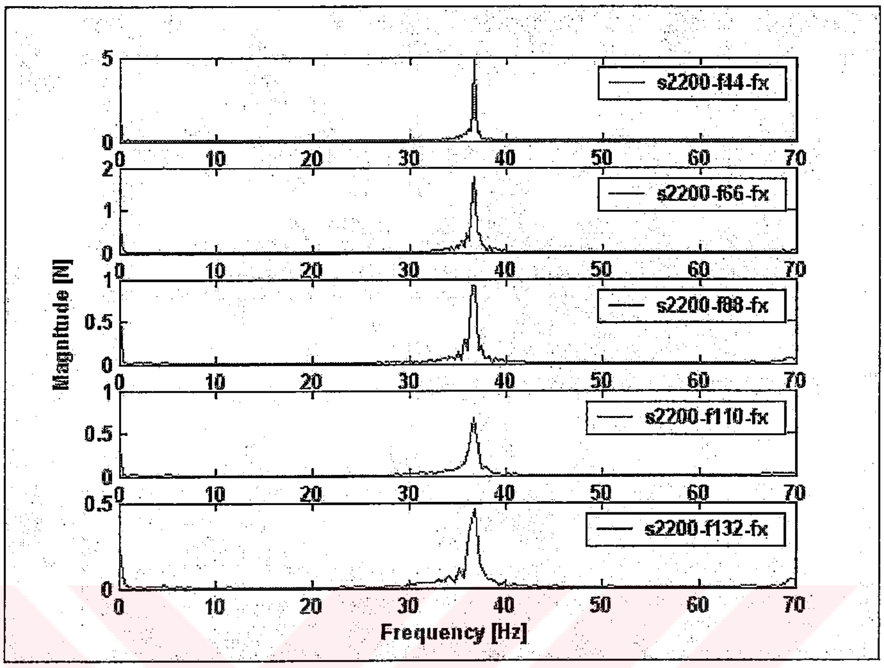

Figure5.50: Frequency content of cutting force in X direction of SHANK1 Drill for spindle speed 2200 [rpm] and feed rates 44-66-88-110-132 [mm/min

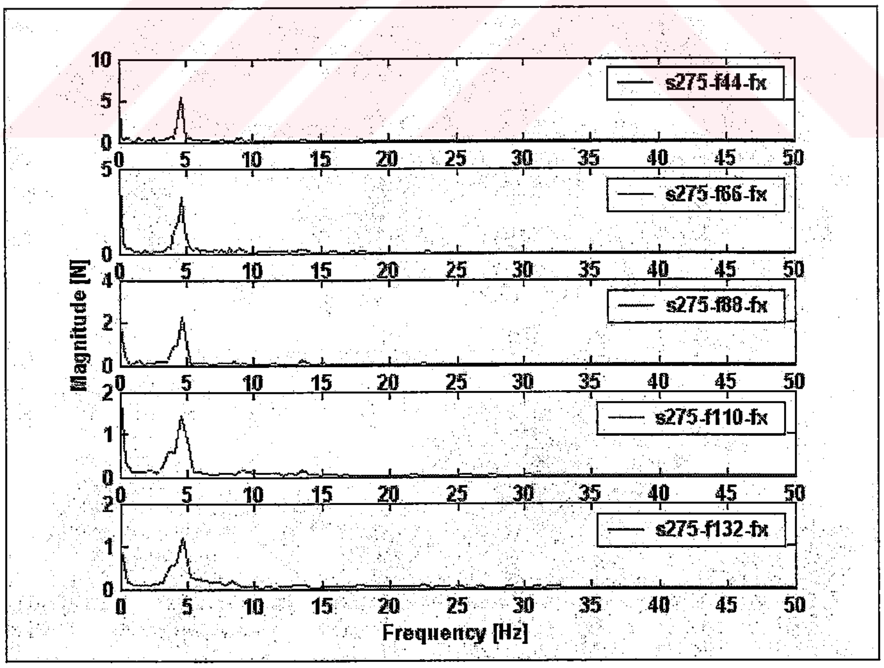

Figure5.51: Frequency content of cutting force in X direction of SHANK2 Drill for spindle speed 275 [rpm] and feed rates 44-66-88-110-132 [mm/min].

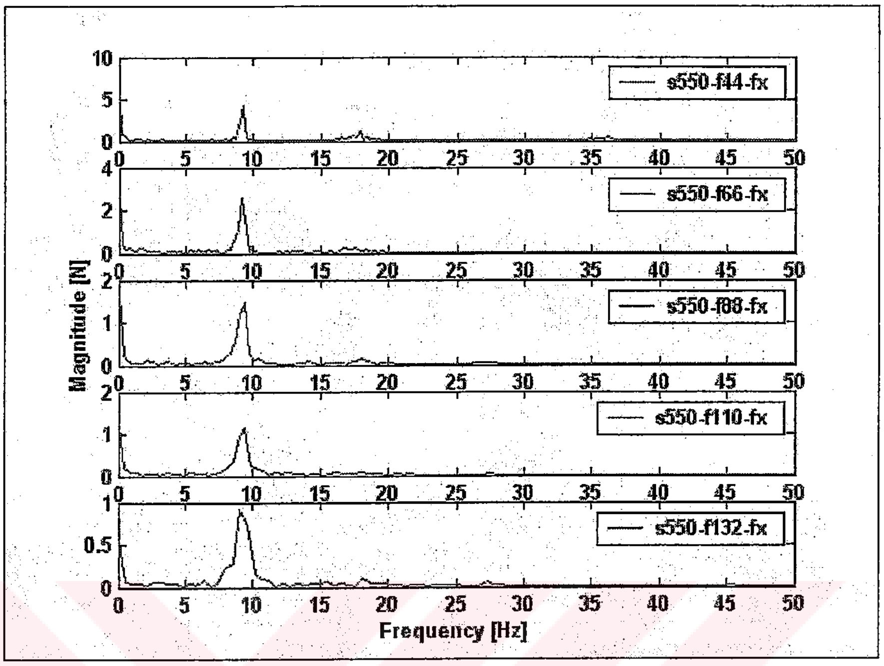

Figure5.52: Frequency content of cutting force in X direction of SHANK2 Drill for spindle speed 550 [rpm] and feed rates 44-66-88-110-132 [mm/min].

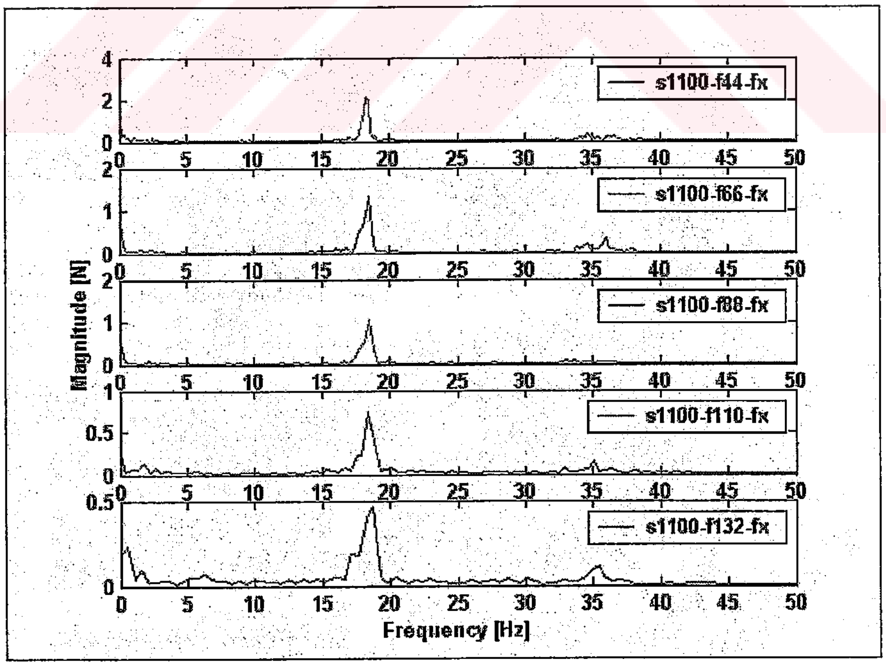

Figure5.53: Frequency content of cutting force in X direction of SHANK2 Drill for spindle speed 1100 [rpm] and feed rates 44-66-88-110-132 [mm/min].

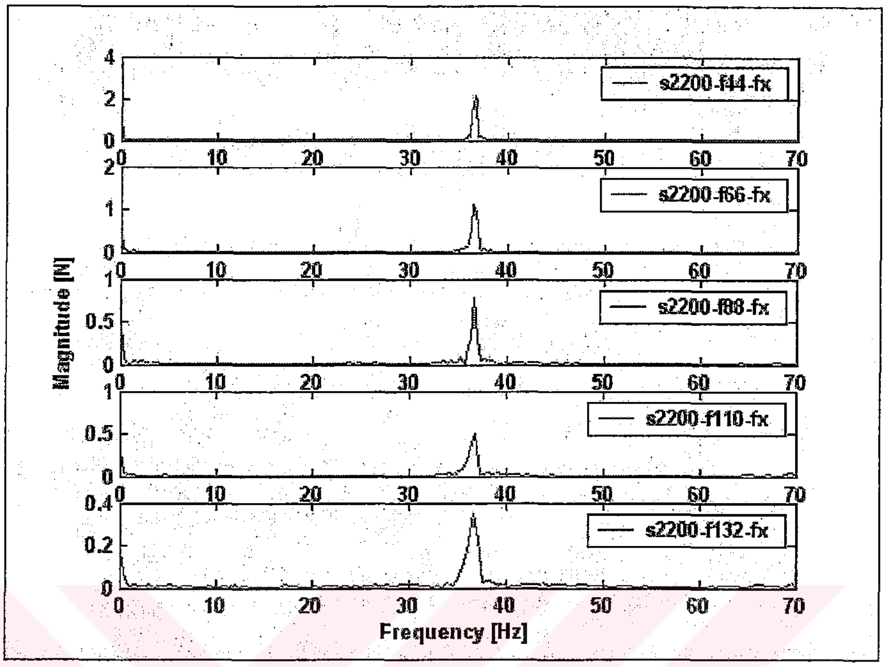

Figure5.54: Frequency content of cutting force in X direction of SHANK2 Drill for spindle speed 2200 [rpm] and feed rates 44-66-88-110-132 [mm/min].

5.3.2.1 Tip chipping cases

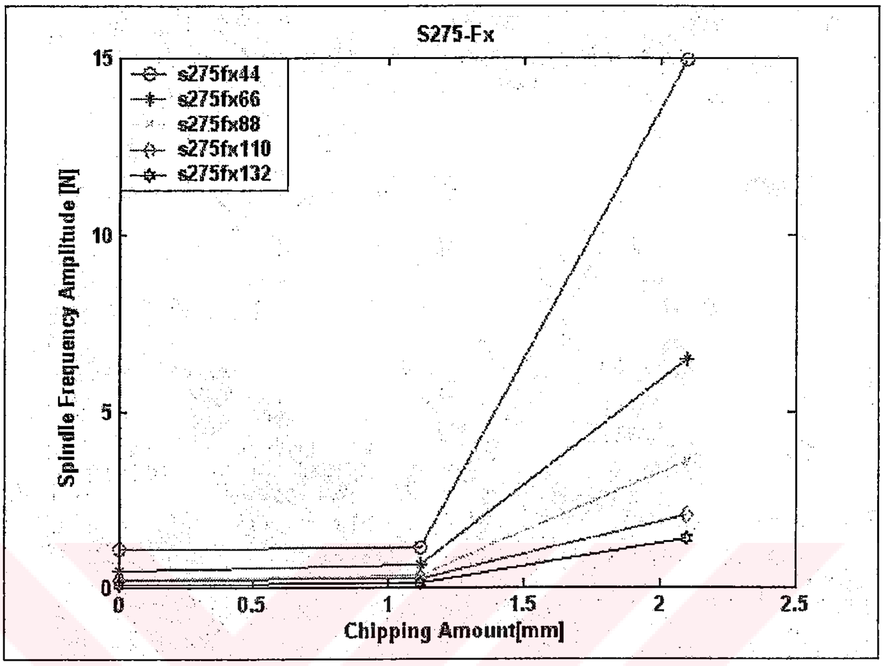

Figure 5.35: Illustration of spindle frequency amplitude [N] for fresh tool. TIP1 tool and TIP2 tool. spindle speed 275 [rpm] and for feed rates 44-66-88-110-132[mm/min]

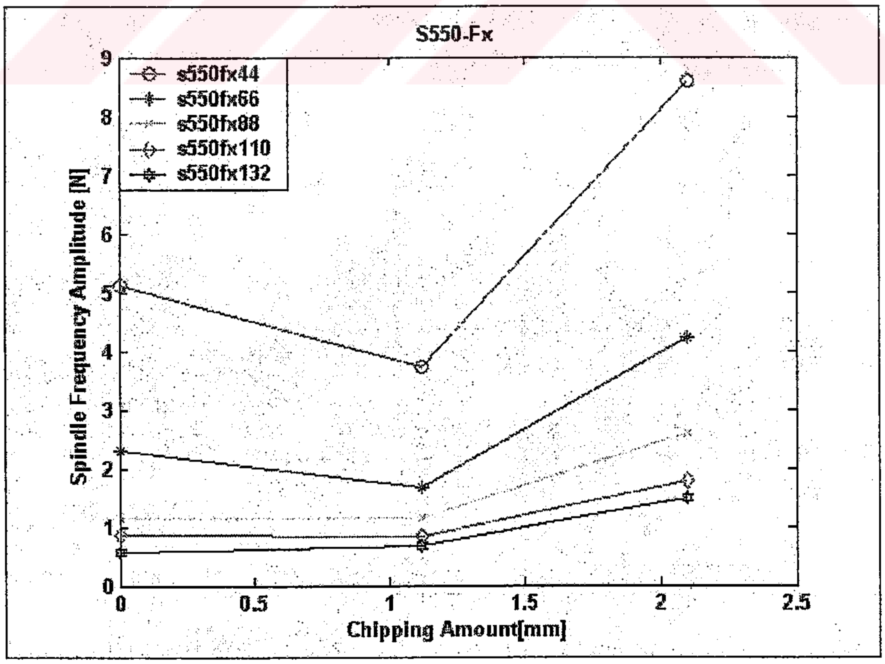

Figure 5.36: Illustration of spindle frequency amplitude [N] for fresh tool. TIP1 tool and TIP2 tool. spindle speed 550 [rpm] and for feed rates 44-66-88-110-132 [mm/min]

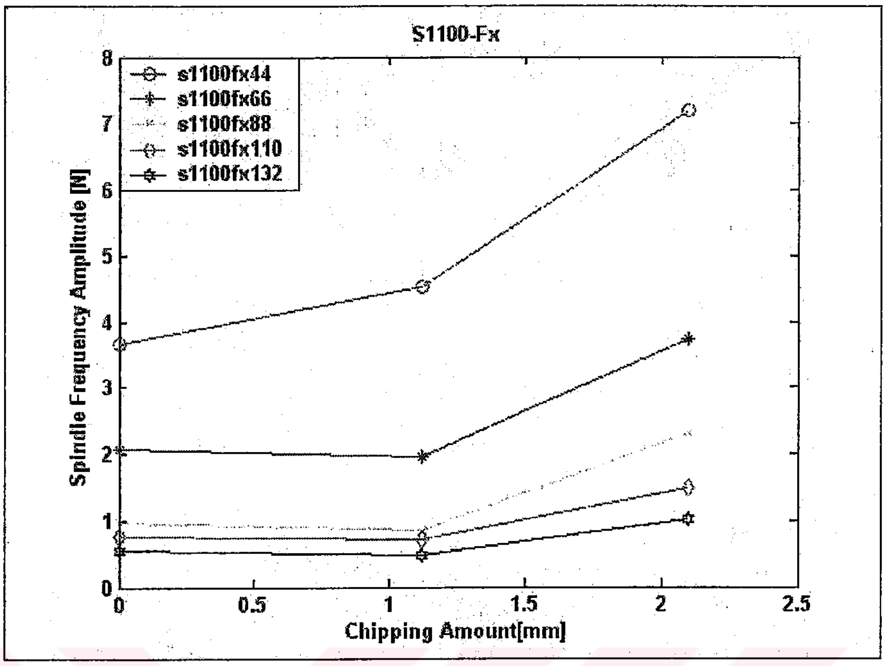

Figure 5.37: Illustration of spindle frequency amplitude [N] for fresh tool. TIP1 tool and TIP2 tool. spindle speed 1100 [rpm] and for feed rates 44-66-88-110-132[mm/min]

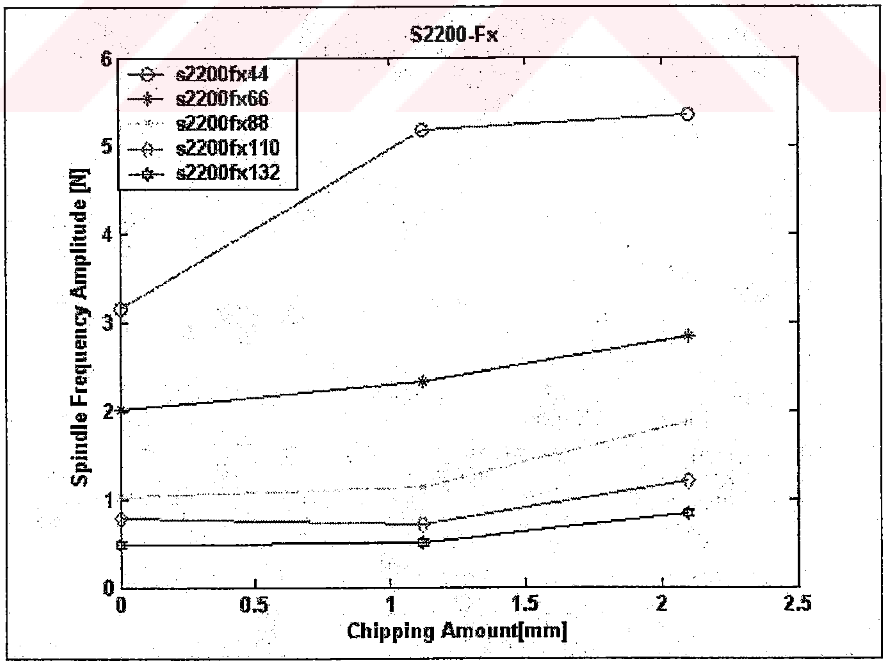

Figure 5.38: Illustration of spindle frequency amplitude [N] for fresh tool. TIP1 tool and TIP2 tool. spindle speed 2200 [rpm] and for feed rates 44-66-88-110-132[mm/min]

5.3.2.2 Shank Chipping Cases

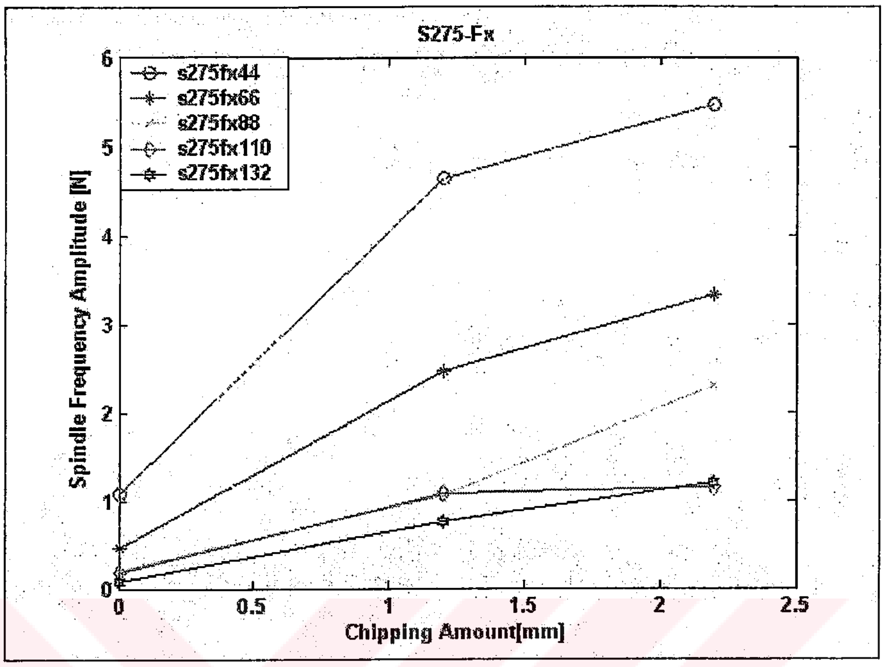

Figure 5.39: Illustration of spindle frequency amplitude [N] for fresh tool. SHANK1 tool and SHANK2 tool. spindle speed 275 [rpm] and for feed rates 44-66-88-110-132[mm/min]

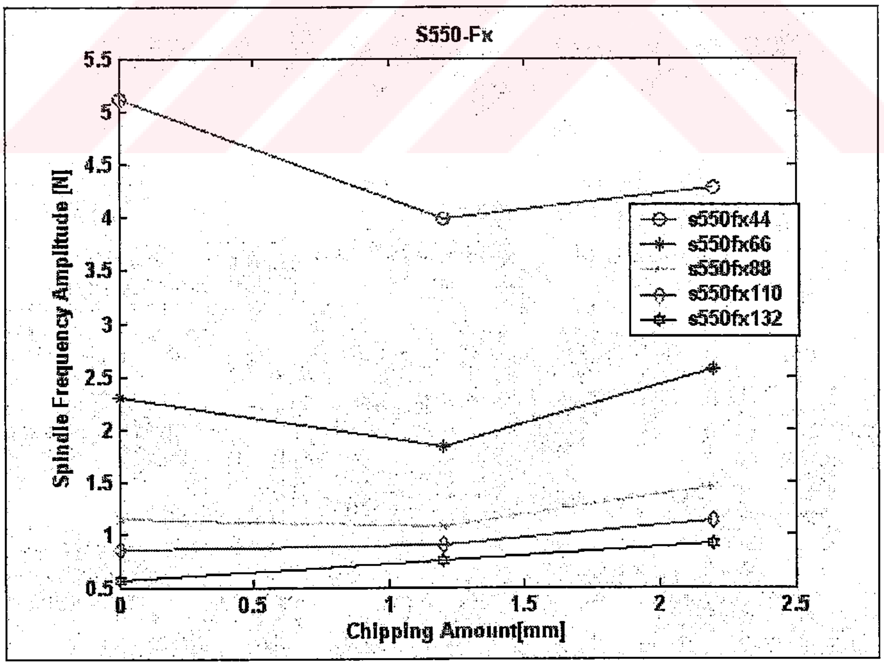

Figure 5.40: Illustration of spindle frequency amplitude [N] for fresh tool. SHANK1 tool and SHANK2 tool. spindle speed 550 [rpm] and for feed rates 44-66-88-110-132[mm/min]

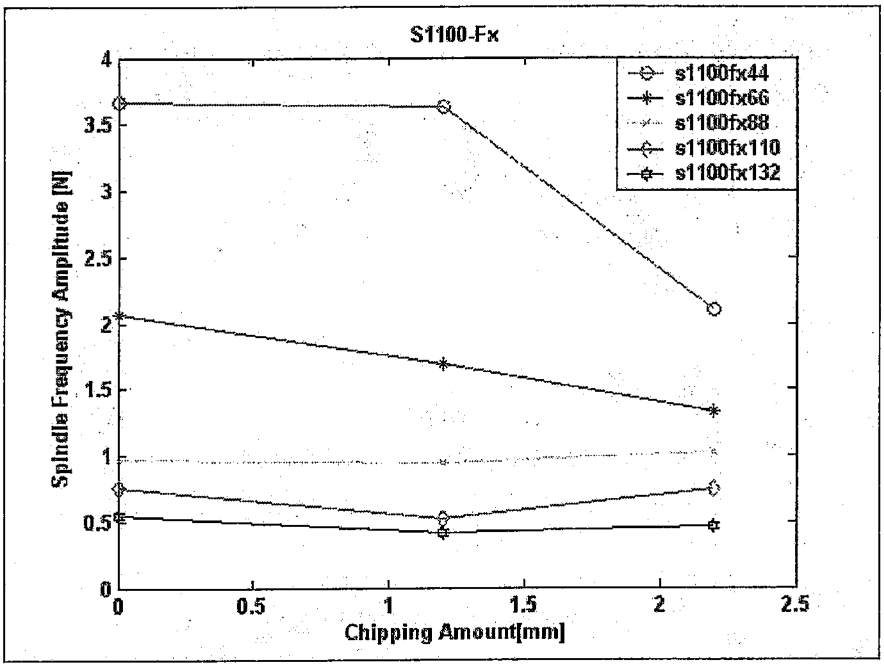

Figure 5.41: Illustration of spindle frequency amplitude [N] for fresh tool. SHANK1 tool and SHANK2 tool. spindle speed 1100 [rpm] and for feed rates 44-66-88-110-132[mm/min]

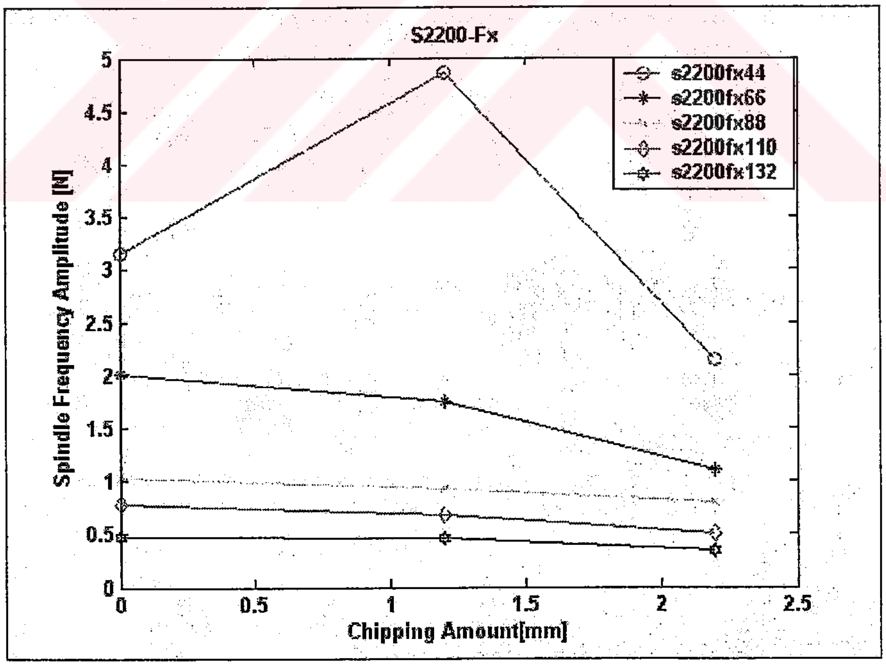

Figure 5.42: Illustration of spindle frequency amplitude [N] for fresh tool. SHANK1 tool and SHANK2 tool. spindle speed 2200 [rpm] and for feed rates 44-66-88-110-132[mm/min]

5.4 Chapter Discussion/ Conclusion

The conclusions drawn from this chapter are;

- In this chapter, radial cutting force is used to obtain monitoring features by the utilization of DWT which decomposes the signal into approximation and detailed coefficients. The related monitoring feature is found in approximation coefficients which show the general trend of the signal. The expected radial cutting force trend shows an inflection at the point where the chipping start. The aim in this chapter is to capture that inflection point which cannot be captured in timed-domain. The shank type of chipping and arbitrary chipping which do not give usable monitoring features is the interest of this chapter.

- When DWT is applied to the SHANK2 type of chipping. most appropriate type of wavelet base is found as *Coiflet1*.The result of DWT using *Coiflet1* well agree with the measured quantity with percent errors less tan 10% as seen in the Table 5.2. The predictions done by using *Coiflet 1* wavelet base show a well agreement with the measured chipping amounts at the lower spindle such as speed 550 [rpm] and predictions get worse at high spindle speeds. The ability of the other wavelet types (*db3, db8, dmey, sym6*) to capture the inflection point is also compared as can be seen in Table 5.3-4. The percent errors for other wavelet bases (*db3, db8, dmey, sym6*) higher than 10%.

- When it comes to arbitrary chipping, same ideology applies as for shank chipping case. The inflection point in radial cutting force signal is the important point to be captured. However,. there is one distinction, the end of chipping portion is not important for shank chipping because chipping ends as the cutting edge meets with the shank of the drill. But for the arbitrary chipping case the end point of the chipping is important because it ends somewhere in the middle of the cutting edge. For this case, different wavelet bases (*Coiflet1*, *db9*) are used to capture the inflection point and their performances are compared as seen in Table 5.6-7. The results are that *db9* type wavelet using the approximation at level 7 can capture the start and end of the trend better than the other wavelet types. Hence, *db9* type wavelet using the approximation at level 7 can predict the chipping amount better than the other types; this can be observed as the percent errors are compared.

- In the second part of this chapter. FFT is utilized to obtain the frequency content of the cutting force signal of the chipped tools in X direction. Frequency of one type of chipping (i.e. tip chipping) is compared with the same type of chipping and the fresh case. This procedure is applied to tip and shank chipping cases separately. The typical FFT plot of cutting force in X direction shows a peak at the spindle frequency as seen in this Figures 5.35-54. This peak is the most distinctive element in the FFT plot. Therefore, it is utilized to obtain monitoring feature related to it. The monitoring feature was the magnitude of the spindle frequency harmonics. This magnitude was obtained for two separate type of chipping cases. Firstly,. for tip chipping case; for all spindle speeds as seen in the Figures 5.35-38, fresh tool and TIP1 tool behave almost same as the magnitude of the spindle frequency is considered. However, TIP2 tool have higher spindle frequency harmonics magnitude than the other two cases. This trend is sometimes linear for some spindle speeds like 2200[rpm] and 1100[rpm]. Another observation for tip chipping is that higher the feed rate higher the magnitude of the spindle frequency harmonics. Secondly, for the shank chipping case as seen in the Figures 5.39-42; as the feed rate increases, magnitude of the spindle frequency harmonics increases observation is valid for shank chipping case. Any apparent observation covering all shank chipping cases can not be found. However, trends are consistent for feed rates of the same spindle speeds. Finally, for all cases one final observation is that spindle frequency magnitudes of high feed rates like 88-110-132 [rpm] are very close to each other.

Chapter 6

CONCLUSION

The objective of the thesis is to analyze the chipping in drilling process experimentally and obtaining monitoring features related to it. Different types of chipping in different amounts are induced artificially to the drills and how the cutting forces were affected from chipping conditions is investigated throughout the thesis. Cutting forces are analyzed in time domain, time-frequency domain and frequency domain. The assumption used throughout this thesis can be stated as follows: cutting force should increase as the chipped portion of the drill is encountered with the workpiece. This assumption is tested for all chipping cases through the thesis.

Tip chipping can be identified successfully from time domain data using the point at which cutting force in X/Y/radial direction reaches maximum. This property is valid for all spindle speed/ feed rate conditions. Shank chipping, on the other hand, is hard to obtain monitoring features using only the time domain data. Thrust force is another parameter that was utilized to obtain monitoring features. Thrust force difference among chipping cases and fresh tool is more apparent as the feed rate increases. Furthermore, thrust force magnitude shows a linear pattern as the chipping amount is changed for same type of chipping. Lastly, long drilling test results show that when cutting force reaches steady state, the cutting force magnitude shows a constant pattern for tip and shank chipping cases. However, the magnitude of the steady state value of the cutting force for tip case is bigger than the constant pattern of same case at the beginning of the cutting process. For shank chipping case, constant cutting force patterns, which occur at the beginning of the cutting and after steady state value are reached, are very close to each other. Finally, long drilling test shows that it is irrelevant to look at the cutting force data after steady state value which occurs after full engagement.

Radial cutting force is used to obtain monitoring features in time-frequency domain by the utilization of DWT which decomposes the cutting force signal into detailed and approximation coefficients. The usable information about chipping is found in approximation coefficients which depicts the general trend of the signal. DWT is utilized for shank and arbitrary chipping conditions whose time domain data do not give usable information about chipping. Start of the increase in the cutting force trend for shank chipping and start/end of the increase in the cutting force trend for arbitrary chipping are the point to capture through the use of DWT.

For shank chipping, Coiflet1 happens to be the most appropriate wavelet base to capture the start of the increase point of the cutting force data among the other wavelet types as db3, db8, dmey, sym6. Through the use of Coiflet1 wavelet base start of increase point is captured successfully.

For arbitrary chipping, start and end of the increase in the cutting force pattern are the interest of DWT analysis. Coiflet1 and db9 type wavelets are utilized for DWT to capture those points. Db9 type wavelet at approximation 7 successfully capture those points better than other alternatives.

FFT is utilized to obtain the frequency content of the cutting force data in X direction. The magnitude of the spindle frequency harmonics are missioned as monitoring features. The tip chipping cases are compared each other and with fresh case considering the magnitude of the spindle frequency harmonics. The TIP1 and fresh cases show similar and lower magnitudes than TIP2 case. Spindle frequency harmonics magnitude gets higher as the feed rate increases for tip and shank chipping cases. Shank chipping cases do not give any apparent observation covering all shank chipping cases but trends are consistent between each for same spindle speeds.

For future work, current sensor can be mounted to the CNC system to measure the current of he feed drive or spindle motor. Same experiments can be done with the current sensor, and the relation can be constructed between cutting force and current. This relationship can be useful, because current sensor is cheap to mount which can be used in industry effectively.

BIBLIOGRAPHY

[1] Erkki Jantuten, A Summary Of Methods Applied To Cool Condition Monitoring In Drilling, International Journal Of Machine Tools & Manufacture, (2002) (42) 997-1010

[2] S.C. Lin, C.J.Ting, Tool Wear Monitoring In Drilling Using Force Signals, Wear, (1995) (180) 53-60

[3] M.A.Mannan, S.Brooms, Monitoring and Adaptive Control Of Cutting Process By Means Of Motor Power and Current Measurements, Annals Of The CIRP, (1989) (38/1) 347-350

[4] A.Thangaraj, P.K.Wright, Computer-Assisted Prediction Of Drill-Failure Using In-process Measurements Of Thrust Force, Journal Of Engineering For Industry, (1988) (110) 192-200

[5] Steven Y.Liang and Rogelio L. Hecker, Robert G.Landers, Machinig Process Monitoring and Control : The State -Of -The-Art, Proceedings of IMECE2002 Asme International Mechanical Engineering Congress & Exposition, (2002) 1-12

[6] R.Teti, A Review Of Tool Condition Monitoring Literature Data Base, Annals Of The CIRP, (1995) (44/2) 659-666

[7] W.König, K.Langhammer, H.-U.Schemmel, Rheinisch-Westfalische TH Aachen, Correlations Between Cutting Force Components And Tool Wear, (19-20)

[8] Dimla E. Dimla Snr, Sensor Signals For Tool-Wear Monitoring in Metal Cutting Operation — A Review Of Methods, International Journal Of Machine Tools & Manufacture, (2000) (40) 1073-1098

[9] Xiaoli Li, Sheng Dong, Zhejun Yuan, Discrete Wavelet Transform For Tool Breakage Monitoring, International Journal Of Machine Tools & Manufacture, (1999) (39) 1935-1944

[10] Xiaoli Li S.K Tso, Drill Water Monitoring Based On Current Signals, Wear (1999) (231) 172-178

[11] H. Y Kim , J.H Ahn , S.H.Kim , S. Takata, Real - time Drill wear Estimation Based On Spindle Motor Power, Journal Of Materials Processing Technology, (2002) (124) 267-273

[12] S.C. Lin, C.J. Ting, Tool wear monitoring in drilling using force signals, Wear 180 (1-2) (1995) 53–60.

[13] I.N. Tansel, C. Mekdeci, Ó. Rodriguez, B. Uragun, Monitoring drill conditions with wavelet based encoding and neural network, International Journal of Machine Tools & Manufacture 33 (4) (1993) 559–575.

[14] E. Jantunen, H. Jokinen, Automated On-line Diagnosis of Cutting Tool Condition (Second version), International Journal of Flexible Automation and Integrated Manufacturing 4 (3-4) (1996) 273–287.

[15] T.I. Liu, K.S. Anantharaman, Intelligent classification and measurement of drill wear, Journal of Engineering for Industry, Transactions of the ASME 116 (1994) 392–397.

[16] T.I. El-Wardany, D. Gao, M.A. Elbestawi, Tool condition monitoring in drilling using vibration signature analysis, International Journal of Machine Tools & Manufacture 36 (6) (1996) 687–711.

[17] A. Noori-Khajavi, Frequency and time domain analyses of sensor signals in a drilling process and their correlation with drill wear, PhD Thesis, Oklahoma State University, Stillwater, OK, 1992.

[18] A. Noori-Khajavi, R. Komanduri, On multisensor approach to drill wear monitoring, Annals of the CIRP 42 (1) (1993) 71–74.

[19] A. Noori-Khajavi, R. Komanduri, Frequency and time domain analyses of sensor signals in drilling, part 1: correlation with drill
wear, International Journal of Machine Tools and Manufacture 35 (6) (1995) 775–793.

[20] X. Li, On-line detection of the breakage of small diameter drills using current signature wavelet transform, International Journal of Machine Tools & Manufacture 39 (1) (1999) 157–164.

[21] A. Noori-Khajavi, R. Komanduri, Frequency and time domain analyses of sensor signals in drilling, part 2: investigation of the problems associated with sensor integration, International Journal of Machine Tools & Manufacture 35 (6) (1995) 795–815.

[22] E. Brinksmeier, Prediction of Tool Fracture in Drilling, 1990

[23] Y. Altintas, Manufacturing Automation: Metal Cutting Mechanics, Machine Tool Vibrations, and CNC Design, Cambridge University Press, 2000.

[24] Matlab® Wavelet Toolbox Help

[25] I. Daubechies, Ten Lectures on Wavelets, Capital City Press, 1992

[26] I. Abu-Mahfouz, Drilling wear detection and classification using vibration signal and artifical neural network, International Journal of Machine Tools & Manufacture 43 (2003) 707-720.

[27] G. Bryne, D. Donfeld, I. Inasaki, G. Ketteler, W. Konig, R. Teti, Tool Condition Monitoring (TCM)-The Status of Research and Industrial Application, Annals Of The CIRP, (1995) (44/2) 541-567

[28] K. Mori, N. Kasashima, J.C. Fu, K. Muto, ,Prediction of Small Drill Bit Breakage by Wavelet Ttransforms and Llinear Discriminant Functions, International Journal of Machine Tools & Manufacture 39 (1999) 1471–1484

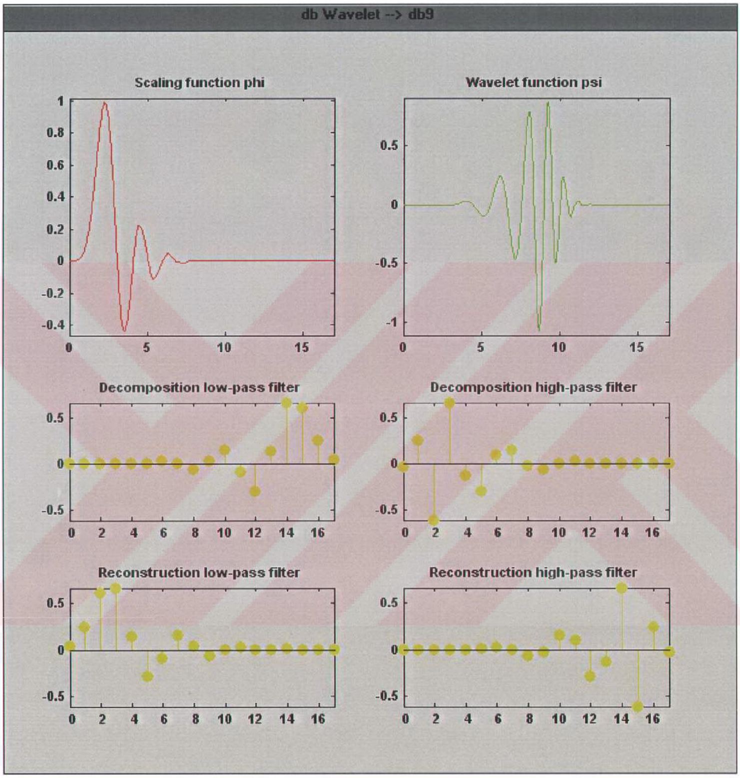

Figure A.1: Db9 wavelet base

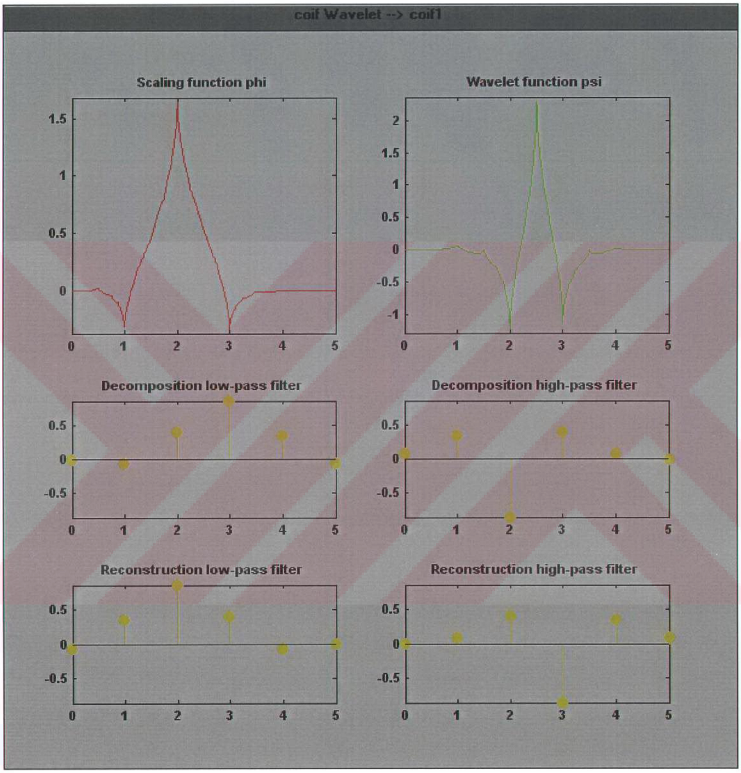

Figure A.2: Coif1 wavelet base

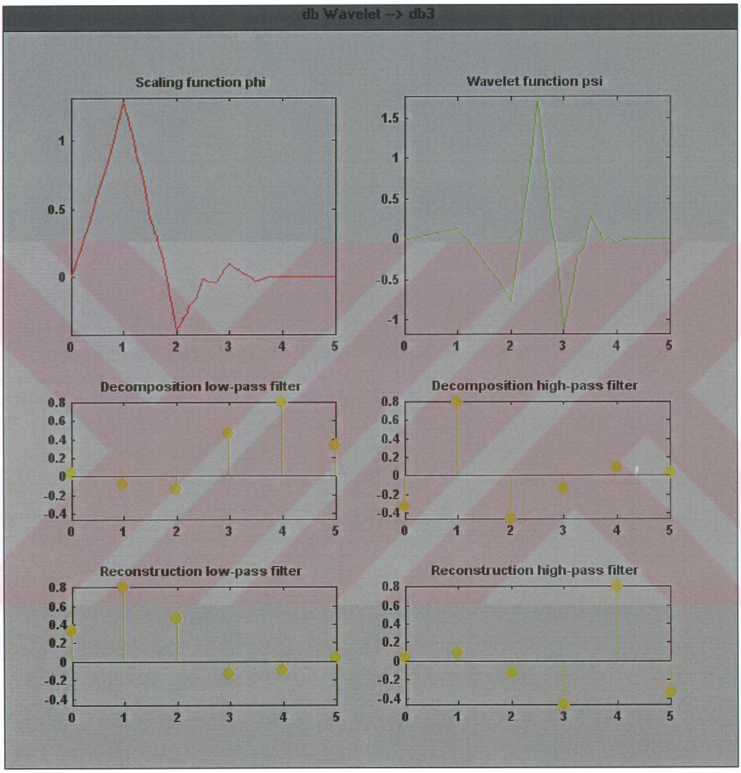

Figure A.3: Db3 wavelet base

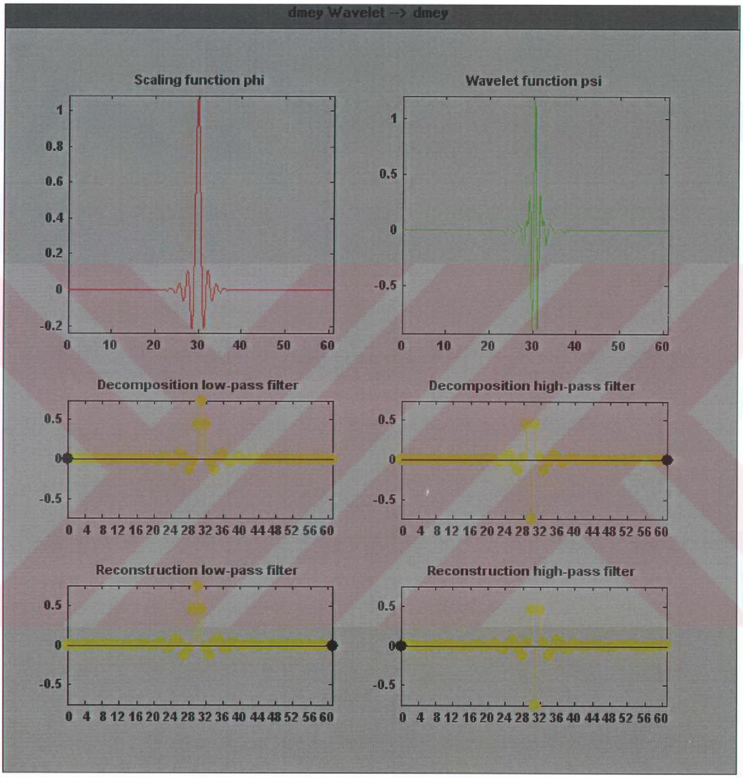

Figure A.4: Dmey wavelet base

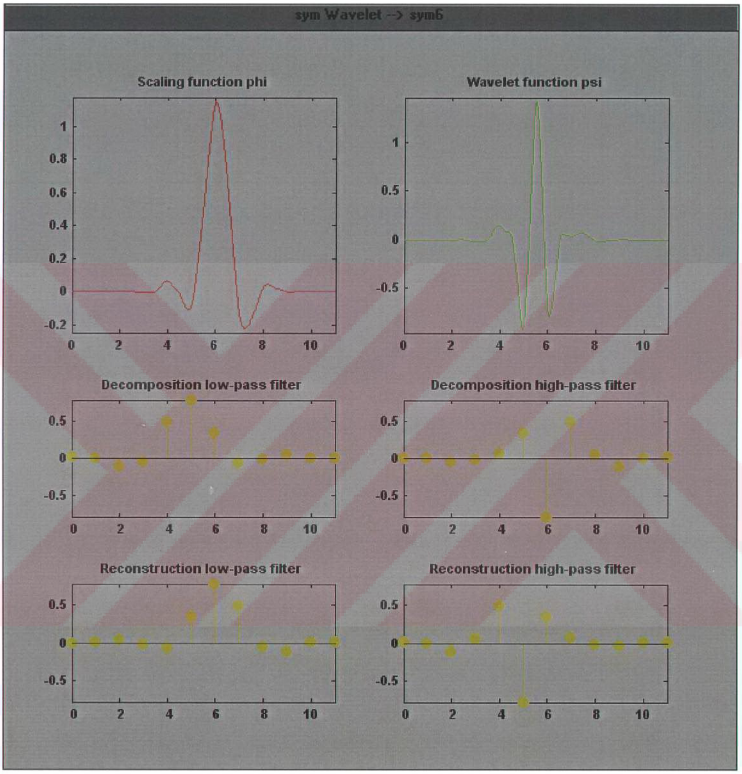

Figure A.5: Sym6 wavelet base

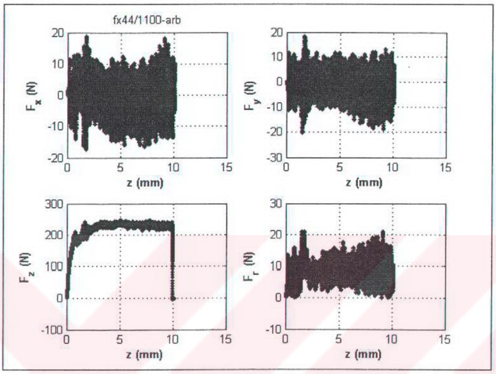

Figure A.6: Illustration of cutting forces in X, Y, Z and radial directions of ARB case for spindle speed 1100 rpm and feed rate of 44 mm/min

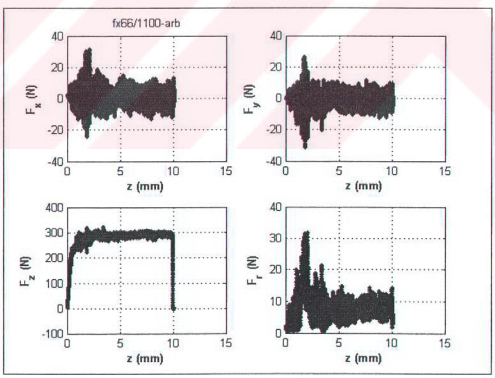

Figure A.7: Illustration of cutting forces in X, Y, Z and radial directions of ARB case for spindle speed 1100 rpm and feed rate of 66 mm/min

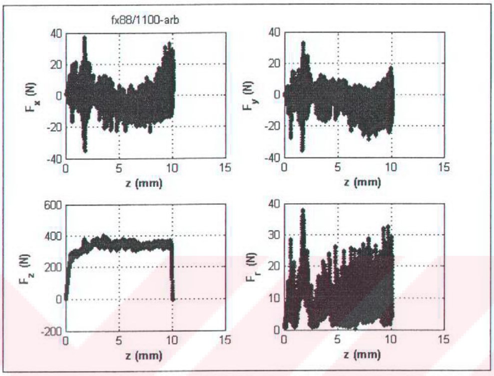

Figure A.8: Illustration of cutting forces in X, Y, Z and radial directions of ARB case for spindle speed 1100 rpm and feed rate of 88 mm/min

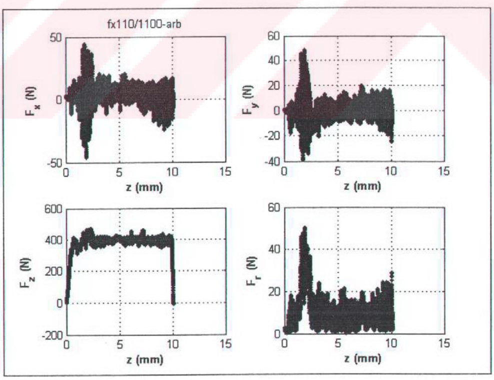

Figure A.9: Illustration of cutting forces in X, Y, Z and radial directions of ARB case for spindle speed 1100 rpm and feed rate of 110 mm/min

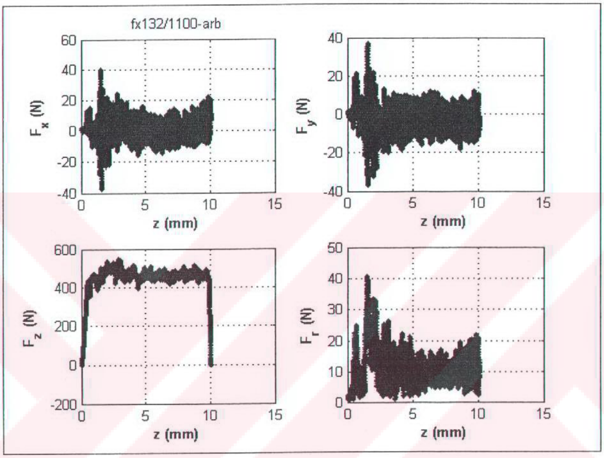

Figure A.10: Illustration of cutting forces in X, Y, Z and radial directions of ARB case for spindle speed 1100 rpm and feed rate of 132 mm/min

VITA

Davut Otar completed the high school in Yalova Lisesi, Yalova, in 1997. He received his B. Sc. Degree in Mechanical Engineering from Boğaziçi University, İstanbul, in 2002. Since 2002, he is in the M.Sc program in Mechanical Engineering at Koc University as a teaching/research assistant.